UNIVERSITY MICROFILMS, INC., ANN ARBOR, MICH.

L. C. Card no. Mic 59- 2155

MILLER, Murray Henri. STUDY OF HIGH-TEMPERATURE ELECTRONS ORIGINATING IN STREAMS FLOWING IN CROSSED D-C ELECTRIC AND MAGNETIC FIELDS.

University of Michigan, Ph. D., 1959
Engineering, electrical

Negative microfilm received from university.

STUDY OF HIGH-TEMPERATURE ELECTRONS ORIGINATING IN STREAMS FLOWING IN CROSSED D-C ELECTRIC AND MAGNETIC FIELDS

by
Murray H. Miller

A dissertation submitted in partial fulfillment
of the requirements for the degree of
Doctor of Philosophy in the
University of Michigan
1958

Doctoral Committee:

Professor William G. Dow, Chairman
Professor Gunnar Hok
Professor Alan B. Macnee
Associate Professor Joseph E. Rowe
Assistant Professor Joseph L. Ullman
Professor Marcellus L. Wiedenbeck

ACKNOWLEDGMENTS

The author wishes to express his appreciation to Professor William G. Dow, chairman of his doctoral committee, and to Professor Gunnar Hok for their encouragement and many stimulating discussions. Professor Joseph E. Rowe and Professor James R. Black also contributed valuable advice. Appreciation is due to Mr. John W. Van Natter who assembled the stream analyzer, and to Miss Priscilla L. Woodhead and the others who have assisted in the preparation of the text.

TABLE OF CONTENTS

	Page
ACKNOWLEDGMENTS	ii
LIST OF FIGURES	v
CHAPTER I. INTRODUCTION	1
1.1 The Problem	1
1.2 An Outline of Previous Studies of the Diocotron Effect	1
1.3 Outline of the Present Investigation	9
CHAPTER II. D-C MOTION OF ELECTRON STREAMS	11
2.1 Summary	11
2.2 D-C Motion of a Single Charged Particle; Electron Ballistics	11
2.3 D-C Motion of Electron Streams; Electron Hydrodynamics	13
2.4 Hamiltonian Formulation of the Equations of Motion for Laminar Streams	23
2.5 D-C Irrotational, Laminar Flow	27
2.6 Magnetically Confined Flow	33
2.7 Nonlaminar Streams	34
2.8 Application of the D-C Stream Models	54
CHAPTER III. WAVE PROPAGATION ON ELECTRON BEAMS	55
3.1 Summary	55
3.2 Equations of Perturbed Laminar Stream Motion	55
3.3 Perturbations of an Electron Plasma	57
3.4 Perturbation of Irrotational Streams	89
3.5 Energy Exchange Mechanisms Between Electrons	114
CHAPTER IV. THE CROSSED-FIELD STREAM ANALYZER	120
4.1 The Purpose of the Crossed-Field Stream Analyzer	120
4.2 Description of the Stream Analyzer and Experimental Setup	120
4.3 Uniformity and Calibration of the Magnetic Field	132
4.4 Geometry of the Interaction Space	133
4.5 Space-Charge-Free Electron Trajectories in the Stream Analyzer	142
CHAPTER V. EXPERIMENTAL INVESTIGATION OF THE DIOCOTRON PHENOMENON	156
5.1 Introduction	156
5.2 Definition of Certain Symbols	157
5.3 D-C Characteristics of the Electron Gun	158
5.4 Gross Characteristics of the Negative-Sole Current	164

TABLE OF CONTENTS (cont.)

		Page
5.5	Distribution of the Sole Current along the Sole	171
5.6	Energy Distribution Measurements	188
5.7	R-F Measurements	197
5.8	Further Interpretation of the Experimental Evidence	202
5.9	Summary	217
5.10	Suggestions for the Continuation of the Investigation	218
BIBLIOGRAPHY		220
LIST OF SYMBOLS		222

LIST OF FIGURES

		Page
Fig. 1.1	Illustration of Electron Stream Motion in a Crossed Electric and Magnetic Field Environment.	2
Fig. 1.2	Geometry of Experimental Trochotron. (After E. D. Aström)	4
Fig. 2.1	Illustration of Multi-Directed Velocity Concept.	16
Fig. 2.2	Vector Diagram Illustrating the Relationship between $\bar{v}$, $\bar{v}_{om}$, and $\bar{u}$.	18
Fig. 2.3	Representation of the Velocity Distribution Function $Fd\bar{v}$.	20
Fig. 2.4	Illustrations of Special Velocity Distribution Functions.	21
Fig. 2.5	Coordinate System for Rectilinear Nonlaminar Flow Model.	37
Fig. 2.6	Particle Motion in Rectilinear Nonlaminar Stream Model.	42
Fig. 2.7	Geometry of Annular Axial Nonlaminar Flow.	43
Fig. 2.8	Uniform Symmetrical Distribution Function for Nonlaminar Rectilinear Stream Model.	49
Fig. 3.1	Geometry of Plasma Perturbation Described in Section 3.2.2.	62
Fig. 3.2	Sketch of Boundary Perturbation for Stream of Fig. 3.1.	63
Fig. 3.3	Illustration of Plasma Configurations for the Two Types of Wave Propagation.	68
Fig. 3.4	Sketch of Function Discussed in Relation to Equation 3.41a.	71
Fig. 3.5	Gain Characteristic for Space-Charge Wave Coupling in a Binary Plasma System.	75
Fig. 3.6	Dispersion Relation for Propagation of Space-Charge Waves in a Magnetic Field, Eq. 3.63a.	79
Fig. 3.7	Dispersion Relation for Propagation of Solenoidal Waves in a Magnetic Field, Eq. 3.67.	81

LIST OF FIGURES (cont.)

		Page
Fig. 3.8	Geometry Used in Discussion of Plasma Coupling in a Magnetic Field, Section 3.2.5.	87
Fig. 3.9	Geometry of Axially Symmetric Hollow-Stream Flow Discussed in Section 3.3.2.	94
Fig. 3.10	Perturbation of a "Thin" Axially Symmetric Hollow Stream.	99
Fig. 3.11	Geometry of Circular Brillouin Flow.	103
Fig. 3.12	Gain vs. Frequency for an Unconfined Slipping Stream. ($m = 0.25$)	110
Fig. 3.13	Geometry of "Thin" Stream Rectilinear Flow Model.	111
Fig. 4.1	Crossed-Field Stream Analyzer, Assembly Drawing.	121
Fig. 4.2	Stream Analyzer Anode Subassembly.	123
Fig. 4.3	Sole Segment Subassembly.	124
Fig. 4.4	Cross Section of Stream Analyzer Geometry.	125
Fig. 4.5	Crossed-Field Stream Analyzer.	126
Fig. 4.6	Cathode Block and Filament Assembly.	127
Fig. 4.7	Stream Analyzer Components.	129
Fig. 4.8	Stream Analyzer Experimental Setup.	130
Fig. 4.9	Experimental Test Setup.	131
Fig. 4.10	Dimensioning of Plate-Sole Space and Cathode Region.	134
Fig. 4.11	Cycloidal Motion in Uniform Crossed Fields.	135
Fig. 4.12	Idealized Electron Stream Injection System.	139
Fig. 4.13	Trochoidal Stream Focussing.	141
Fig. 4.14	Sketch Illustrating the Nature of Space-Charge-Free Trajectories and Equipotentials in the Stream Analyzer.	143

LIST OF FIGURES (cont.)

		Page
Fig. 4.15	Space-Charge-Free Electron Trajectories in Stream Analyzer Geometry.	147
Fig. 4.16	Space-Charge-Free Electron Trajectories in Stream Analyzer Geometry.	148
Fig. 4.17	Space-Charge-Free Electron Trajectories in Stream Analyzer Geometry.	149
Fig. 4.18	Space-Charge-Free Electron Trajectories in Stream Analyzer Geometry.	150
Fig. 4.19	Space-Charge-Free Electron Trajectories in Stream Analyzer Geometry.	151
Fig. 4.20	Space-Charge-Free Electron Trajectories in Stream Analyzer Geometry.	152
Fig. 4.21	Space-Charge-Free Electron Trajectories in Stream Analyzer Geometry.	153
Fig. 4.22	Space-Charge-Free Electron Trajectories in Stream Analyzer Geometry.	154
Fig. 4.23	Space-Charge-Free Electron Trajectories in Stream Analyzer Geometry.	155
Fig. 5.1	Schematic of Measuring Circuitry and Definition of Symbols.	159
Fig. 5.2	Perveance of Stream Analyzer Electron Gun. (ϕ_{os} = 0. Cathode No. 1)	161
Fig. 5.3	Perveance of Stream Analyzer Electron Gun. (Cathode No. 2)	163
Fig. 5.4	Volt-Ampere Characteristic of Stream Analyzer Electron Gun. (ϕ_{os} = 0. Cathode No. 1)	165
Fig. 5.5	Gross Sole Current Characteristic. (Cathode No. 1)	167
Fig. 5.6	Gross Sole Current Characteristic. (Cathode No. 2)	168
Fig. 5.7	Gross Sole Current Characteristic, C.S.F. data.	169

LIST OF FIGURES (cont.)

		Page
Fig. 5.8	Distribution of Sole Current along the Sole. (ϕ_{oa} = 800 volts, B_o = 1000 gauss, ϕ_{oa}/B_o^2 = 0.8 x 10^{-3} volts/gauss^2. Cathode No. 2)	173
Fig. 5.9	Distribution of Sole Current along the Sole. (ϕ_{oa} = 1000 volts, B_o = 1000 gauss, ϕ_{oa}/B_o^2 = 1.0 x 10^{-3} volts/gauss^2. Cathode No. 2)	174
Fig. 5.10	Distribution of Sole Current along the Sole. (ϕ_{oa} = 1300 volts, B_o = 1000 gauss, ϕ_{oa}/B_o^2 = 1.3 x 10^{-3} volts/gauss^2. Cathode No. 2)	175
Fig. 5.11	Distribution of Sole Current along the Sole. (ϕ_{oa} = 500 volts, B_o = 500 gauss, ϕ_{oa}/B_o^2 = 2.0 x 10^{-3} volts/gauss^2. Cathode No. 2)	176
Fig. 5.12	Distribution of Sole Current along the Sole. (ϕ_{oa} = 600 volts, B_o = 500 gauss, ϕ_{oa}/B_o^2 = 2.4 x 10^{-3} volts/gauss^2. Cathode No. 2)	177
Fig. 5.13	Distribution of Sole Current along the Sole. (ϕ_{oa} = 700 volts, B_o = 500 gauss, ϕ_{oa}/B_o^2 = 2.8 x 10^{-3} volts/gauss^2. Cathode No. 2)	178
Fig. 5.14	Distribution of Sole Current along the Sole. (ϕ_{oa} = 800 volts, B_o = 500 gauss, ϕ_{oa}/B_o^2 = 3.2 x 10^{-3} volts/gauss^2. Cathode No. 2)	179
Fig. 5.15	Distribution of Sole Current along the Sole. (ϕ_{oa} = 900 volts, B_o = 500 gauss, ϕ_{oa}/B_o^2 = 3.6 x 10^{-3} volts/gauss^2. Cathode No. 2)	180
Fig. 5.16	Distribution of Sole Current along the Sole. (ϕ_{oa} = 1000 volts, B_o = 500 gauss, ϕ_{oa}/B_o^2 = 4.0 x 10^{-3} volts/gauss^2. Cathode No. 2)	181
Fig. 5.17	Distribution of Sole Current along the Sole. (ϕ_{oa} = 720 volts, B_o = 400 gauss, ϕ_{oa}/B_o^2 = 4.5 x 10^{-3} volts/gauss^2. Cathode No. 2)	182
Fig. 5.18	Distribution of Sole Current along the Sole. (ϕ_{oa} = 800 volts, B_o = 400 gauss, ϕ_{oa}/B_o^2 = 5.0 x 10^{-3} volts/gauss^2. Cathode No. 2)	183
Fig. 5.19	Distribution of Sole Current along the Sole. (ϕ_{oa}= 960 volts, B_o = 400 gauss, ϕ_{oa}/B_o^2 = 6.0 x 10^{-3} volts/gauss^2. Cathode No. 2)	184

LIST OF FIGURES (cont.)

		Page
Fig. 5.20	Distribution of Sole Current along the Sole. (ϕ_{oa} = 630 volts, B_o = 300 gauss, ϕ_{oa}/B_o^2 = 7.0 x 10^{-3} volts/gauss^2. Cathode No. 2)	185
Fig. 5.21	Distribution of Sole Current along the Sole. (ϕ_{oa} = 720 volts, B_o = 300 gauss, ϕ_{oa}/B_o^2 = 8.0 x 10^{-3} volts/gauss^2. Cathode No. 2)	186
Fig. 5.22	Energy Distribution Curves, Sole Segment No. 4. (Cathode No. 1)	189
Fig. 5.23	Energy Distribution Curves, Sole Segment No. 7. (Cathode No. 1)	190
Fig. 5.24	Energy Distribution Curves, Sole Segment No. 13. (Cathode No. 1)	191
Fig. 5.25	Energy Distribution Curves, Sole Segment No. 4. (Cathode No. 2)	192
Fig. 5.26	Energy Distribution Curves, Sole Segment No. 7. (Cathode No. 2)	193
Fig. 5.27	Energy Distribution Curves, Sole Segments 1, 2, 3, 15, 16, 17, 18, 29, 30. (Cathode No. 1)	196
Fig. 5.28	Energy Distribution Curves, Sole Segment No. 7. (Cathode No. 2)	198
Fig. 5.29	Location of R-F Probe in the Cathode Region.	200
Fig. 5.30	Spectrum of Observed R-F Signal. (ϕ_{oa} = 700 volts, ϕ_{os} = -35.5 volts, B_o = 500 gauss, ϕ_{oa}/B_o^2 = 2.8 x 10^{-3} volts/gauss^2, Cathode No. 2)	203

CHAPTER I. INTRODUCTION

1.1 The Problem

The subject matter with which this dissertation is concerned is the investigation of the phenomenon known widely as the diocotron effect.

Figure 1.1 is a sketch useful in describing the phenomenon. An electrostatic field is maintained between two plane electrodes (plate and sole, respectively) and directed toward the sole. A uniform magnetic field, directed into the page, completes the establishment of a crossed d-c electric and magnetic field environment within the structure. An electron stream, launched from a zero-reference-potential cathode along a trochoid-like arc, is injected into the plate-sole space and continues along a trajectory corresponding more or less to rectilinear Brillouin flow. The stream terminates, after traversing the plate-sole space, on a collector.

The term diocotron effect has been applied to the observation of a current to the sole even though that electrode may be at a considerably negative potential relative to the cathode. The negative-sole current is indicative of electrons gaining energy in excess of that which would correspond to d-c motion in the electrostatic field. This excess energy is too great to be attributable to such diverse effects as initial thermal emission energy or contact difference of potential.

1.2 An Outline of Previous Studies of the Diocotron Effect

1.2.1 The Measurements of Åström. The earliest observation of the diocotron effect, per se, was noted in a collection of papers on the

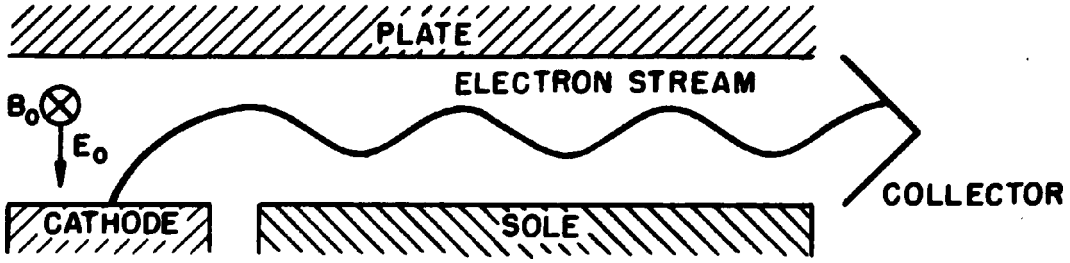


FIG. 1.1 ILLUSTRATION OF ELECTRON STREAM MOTION IN A CROSSED ELECTRIC AND MAGNETIC FIELD ENVIRONMENT.

theory and applications of trochotrons[1*]. Trochotron is a generic name for a multi-channel electronic switching tube utilizing the trochoidal motion of electrons in crossed electric and magnetic field environments such as that illustrated by Fig. 1.1. In the course of studying the trochotron a negative-sole current was noted, and a number of measurements of the phenomenon were reported by Åström in the papers cited above. The geometry of the experimental tube used by Åström is illustrated in Fig. 1.2. It is similar to that shown in Fig. 1.1 except for the location of the cathode and the division of the sole into seventeen electrically insulated segments. The cathode was located midway between the plate and sole; the plate-sole spacing was 10 mm. Sixteen of the sole segments were 5 mm long, and the seventeenth, located beneath the cathode, was longer (see Fig. 1.2).

For one experiment the plate was operated at 400 volts and the cathode and sole at zero potential. A magnetic field of 640 gauss was used to focus the stream. Cathode emission was controlled by temperature-limiting the oxide-coated nickel cathode ribbon. Measurements were taken, for various cathode currents, of the current to each sole segment. Each segment current, as a function of cathode current, first increased, reached a maximum, and then decreased fairly slowly. The greater the distance from the segment to the cathode, the smaller the maximum current, and the further it was displaced towards smaller cathode emission.

When, on the other hand, the cathode current was kept constant and the sole current distribution along the sole was measured, it was found that the sole current first increased with distance from the cathode, reached a maximum, and then decreased. The maximum sole current increased

*Superscript numbers refer to references listed in the bibliography.

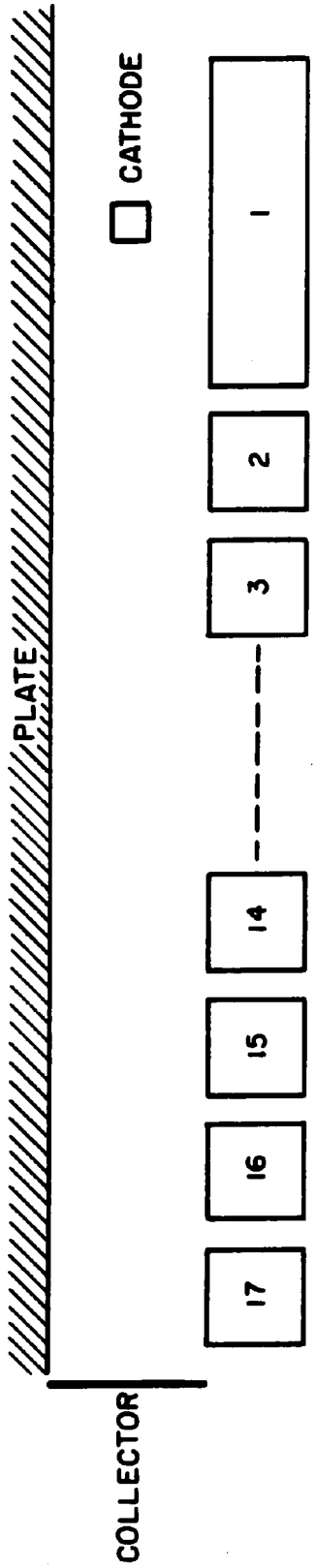


FIG. I.2 GEOMETRY OF EXPERIMENTAL TROCHOTRON. (AFTER E.D. ÅSTRÖM)

more than linearly with an increase of cathode current, and was displaced toward the cathode for increasing emission.

A similar set of measurements was also obtained with the cathode potential raised to 100 volts and the magnetic field increased to 1130 gauss. The sole current as a whole decreased considerably. The segment currents increased rapidly as a function of the cathode emission, reached a maximum toward the end of the tube and then decreased. The sole current also increased very rapidly with distance from the cathode before a maximum was obtained.

Åström concluded from these measurements that the process causing the sole current took place in the electron stream during the traversal of the plate-sole space and not at all, or only partially, near the cathode. This conclusion is contradicted by the results of the investigation described subsequently in this dissertation.

Åström's experiment is certainly indicative of a diocotron effect inasmuch as about two percent of the cathode current reached the sole when it was 100 volts below cathode potential. The anode potential, it will be noted, was only 300 volts above cathode potential. However, a number of characteristics of the measured data leave open to question the conclusion noted above, that the process causing the sole current occurs in a region remote from the cathode. As background for this questioning, we note that the stream trajectory would follow, approximately, an equipotential line. We can use the space-charge-free cycloidal trajectory of a single electron in the same fields as above as an approximate measure of the actual stream trajectory[2]. The period of such a trajectory in the given fields is of the order of 1 mm and the height of such a trajectory is of the order of 0.1 mm. The equipotential on which the stream "rolls" would then be at about the cathode potential.

The stream would therefore follow a path which would be midway between the sole and plate in the immediate vicinity of the cathode and move down to approximately one-quarter of the plate-sole spacing above the sole.

The fact that current reached the sole at all bespeaks a large energy exchange between electrons. Even more spectacular is the fact that there was a significant current to the first few segments near the cathode. This would seem to indicate a rather large energy exchange in the immediate vicinity of the cathode, contradicting Åström's conclusion mentioned above. The fact that the current distribution along the sole reaches a maximum also casts doubt on his conclusion. The total current drawn to the sole is a small fraction of the stream current. It is, therefore, difficult to see why any process occurring in the uniform plate-sole region should suddenly alter its characteristics in that region.

Similar questions can be raised concerning the data taken with the sole and cathode at the same potential.

Another interesting experiment described in Åström's paper was a measurement of sole-current characteristics of three tubes having dimensions in the ratio of 1:4:16. The voltages on each of these tubes were the same but the magnetic fields used were inversely proportional to the tube dimensions. The fraction of the cathode current going to the sole was essentially the same for all three tubes, suggesting the applicability of scaling rules to the diocotron phenomenon.

Measurements were also made on the noise characteristics of the electron stream. The measurements indicated that, above a certain level of stream current, the noise level increased quite rapidly. It was noted that nothing particularly remarkable happened to the frequency spectrum of the noise in the neighborhood of the cyclotron frequency.

Unfortunately, the main concern of the paper related to the performance characteristics of trochotrons and the data covered only a small range of parameters pertinent to the diocotron effect.

1.2.2 The Measurements of Guenard and Huber. The diocotron effect was subsequently noted in the course of a study of carcinotrons, which are nonre-entrant magnetron-type oscillators. In a paper by Warnecke, Huber, Guenard, and Doehler[3] the negative-sole current is explained as a manifestation of a growing-wave electron interaction (described in Chapter III). A measurement is described on two tubes having a geometry similar to that illustrated in Fig. 1.1 except that the smooth plate is modified. In one of the tubes the plate was modified by the introduction of two short lengths of slow-wave structure (interdigital lines) at either end to provide an r-f signal input and output. The second tube was identical to the first except that the smooth plate was removed and the slow-wave structures brought together. Comparison of the signal gains of the two tubes under the same operating conditions then provided a measure of the effect of the stream traversal under the smooth plate. It was observed that an additional gain of the order of 10 to 20 db could be obtained in the tube having the central smooth plate. It is in this paper that the term diocotron (from the Greek word διωκειν, to pursue) is applied to one cause of a growing-wave phenomenon. The application of this term to the observation of a negative-sole current, while of common usage, will be shown to convey an erroneous suggestion of a cause-effect relationship.

The experiment above, and others, were later amplified in a paper by Guenard and Huber[4]. In this latter paper, measurements of the negative-sole current are also presented. These measurements were also made on a tube of the same general geometry as illustrated in Fig. 1.1 except

that the smooth plate was replaced by an interdigital line. However, the line was made highly lossy (more than 50 db at a wavelength of 25 cm) by a lossy coating covering all of the digits except the part seen by the stream. In addition, the sole had a single electrically insulated segment inserted approximately halfway down its length. Measurements were taken of the current to this sole segment as a function of its potential; all other operating parameters of the tube were held fixed during each such measurement. A semi-log plot of segment current against its potential turned out to be linear, indicating a Maxwellian energy distribution for the segment current. Depending on particular operating conditions, the average energy of the energy distribution was from 10 to 40 electron volts. If the negative-sole current maintained an average energy of this order of magnitude over the entire sole, then, for some operating conditions described, a power of about one watt was delivered to the sole by the negative-sole current! This is rather difficult to explain in terms of gains of 10 to 20 db due to growing-wave amplification.

1.2.3 Associated Phenomena. There are a number of phenomena which appear likely to be different manifestations of the same general process of which the negative-sole current is one indication. It has been observed, for example, that the anode current in a preoscillating cylindrical magnetron does not cease abruptly at a certain critical magnetic field as simple theory predicts[4,5]. The cutoff occurs at a higher value of magnetic field than is predicted and is neither abrupt nor complete. The "backheating" effect in magnetrons, where cathode-emitted electrons return to the cathode with rather large energies, also bespeaks an energy exchange process. Measurements of the space-charge density distribution in preoscillating magnetrons have indicated substantial space charge in

regions where simple theory provides no explanation of their presence. The study of these phenomena is, however, somewhat different from that of the diocotron phenomena because of the re-entrant nature of the electron streams and slow-wave structures. For re-entrant crossed-field devices, electrons, in general, spend rather long times in the device, whereas for nonre-entrant devices the electron trajectory is generally such as to remove the electron from the system in a relatively short time. Consequently, cumulative small effects which are of importance in re-entrant devices are negligible in nonre-entrant devices.

The recent observations of the breakup of hollow electron streams, focused by a longitudinal magnetic field, into a discrete set of vortex filaments has been generally ascribed to the same cause as the diocotron effect[6]. However, as is subsequently pointed out, this phenomenon is caused neither by the same mechanism as causes the negative-sole current nor even by a "slipping stream" amplification.

1.3 Outline of the Present Investigation

To provide a background for the interpretation of the investigation described in this dissertation, the next two chapters present a theoretical study of the motion of electrons in electric and magnetic force fields.

Chapter II is a discussion of the time invariant motion of charged particles. A number of d-c stream models, having relatively simple mathematical characteristics, are described in detail.

After the establishment of these several stream models, Chapter III presents a description of the propagation of electromagnetic fluctuations on these models in terms of the well-known "small-signal" perturbation procedures. Particular emphasis is applied to a description of the propagation of electromagnetic waves along an electron stream in crossed d-c electric and magnetic fields.

To provide more detailed and more extensive data on the diocotron effect, a crossed-field stream analyzer was designed and constructed. Chapter IV describes the device and the associated measuring circuitry. In addition, the results of a study of the motion of a single electron in the geometry of the stream analyzer are presented. This study is subsequently useful in the interpretation of the experimental data.

Chapter V presents and interprets the experimental data obtained from the stream analyzer. It is shown that the common belief that negative-sole current is caused primarily by a "slipping stream" type of amplification is incorrect. A more plausible mechanism to account for the phenomenon is described and related to supporting experimental evidence. Also, several suggestions for the continuation of the investigation are presented.

CHAPTER II. D-C MOTION OF ELECTRON STREAMS

2.1 Summary

The d-c motion ($\partial/\partial t = 0$) of a single charged particle in given electric and magnetic force fields has been understood for some time. The simultaneous d-c motion of large numbers of charged particles in given electric and magnetic force fields has likewise been long understood, although to a somewhat lesser extent. The following discussion reviews and extends a portion of the understanding of the d-c motion of charged particles pertinent to the subsequent development of the dissertation.

2.2 D-C Motion of a Single Charged Particle; Electron Ballistics[2,7,8,9,10]

The familiar Lorentz force and Newton's laws of motion describe the motion of a single nonrelativistic charged particle in the region of an electric and magnetic force field by the equation

$$-q[\bar{E} + \bar{v} \times \bar{B}] = m \frac{d\bar{v}}{dt} \quad , \tag{2.1}$$

where $\bar{E}$ = electric intensity vector,*

$\bar{B}$ = magnetic density vector,

$\bar{v}$ = particle velocity vector,

m = particle mass, and

$-q$ = particle charge (a negative quantity for electrons).

For time invariant motion ($\partial/\partial t = 0$) the scalar product of the equation of motion, Eq. 2.1, with $\bar{v}$ leads to the statement of the conservation of energy

$$\nabla\left(-q\,\phi + \frac{m}{2}\,\bar{v} \cdot \bar{v}\right) = 0 \quad , \tag{2.2}$$

*A bar over a quantity indicates a vector.

where the electric field potential ϕ is defined from

$$\bar{E} = -\nabla\phi \quad . \tag{2.3}$$

Some simple solutions of the equation of motion (Eq. 2.1) are well known:

a). If the electric field is a constant and the magnetic field vanishes, the charged particle undergoes uniformly accelerated motion.

b). If the magnetic field is constant and the electric field vanishes, the charged particle follows a helical trajectory. The component of the velocity parallel to the magnetic field is unaffected by the field. The velocity component normal to the magnetic field causes an acceleration normal to itself, leading to a circular component of motion with an angular velocity equal to the cyclotron frequency $q\bar{B}/m$. An important property of the motion, characteristic of the spatial asymmetry produced by the magnetic field, is that the motion is not reversible.

c). If both the electric and magnetic fields are constant and non-vanishing the trajectory is trochoidal in nature. If the frame of reference for the motion is shifted to one advancing with the velocity $\bar{E} \times \bar{B}/\bar{B}\cdot\bar{B}$, the description of the motion becomes

$$-q\bar{v}' \times \bar{B} = m\frac{d\bar{v}'}{dt} \quad , \tag{2.4}$$

where $\bar{v}'$, the velocity as seen in the advancing frame of reference, is

$$\bar{v}' = \bar{v} - \frac{\bar{E} \times \bar{B}}{\bar{B} \cdot \bar{B}} \quad . \tag{2.5}$$

Equation 2.4 corresponds to a helical trajectory in the advancing frame of reference. The motion in the stationary reference frame is therefore a superposition of a linear trajectory normal to the electric and magnetic fields and a helical motion about the magnetic flux lines. The characteristic velocity $\bar{E} \times \bar{B}/\bar{B}\cdot\bar{B}$ corresponds to that electron velocity which results in a uniform rectilinear trajectory ($\bar{v}' = 0$).

In general the motion of a single charged particle in a specified force field of more complex form than illustrated above can be obtained in a straightforward manner, analytically in some cases, and by numerical or machine computation of as great an accuracy as desired in less tractable cases.

The analogy between the motion of charged particles in electric and magnetic force fields and the ballistic motion of projectiles has led to referring to the former as "electron ballistics." While the analogy is somewhat strained by the introduction of magnetic forces (corresponding, after a fashion, to a Coriolis force), its usage is sanctioned by custom.

2.3 D-C Motion of Electron Streams; Electron Hydrodynamics[11,12,13,14]

When the Coulomb interaction forces between charged particles can be neglected the motion of a stream of particles can be described by a multiplicity of ballistic trajectories with varying initial conditions; such an approximation has been usefully applied to beam dynamics in cathode ray tubes, for example. However, the long-range effect of the Coulomb forces, the presence of different types of charged or neutral particles, and the scattering due to the discrete nature of the particles are often important characteristics of electron streams. The detailed description

of the d-c motion of a number of charged particles, accounting for inverse-square law Coulomb forces depending on the instantaneous positions of the particles, is enormously complicated compared to that for a single particle. It is often found, however, that the particles are sufficiently numerous that an averaged motion of the particle stream, rather than a detailed accounting of each trajectory, provides an adequate description of the motion. Under certain conditions, then, the net effect of the complex interparticle interaction can be replaced by a statistical average interaction.

A situation of particular interest here occurs when the momentum transfer due to close collisions is negligible compared to the net momentum interchange due to the simultaneous interaction of a particle with all the other particles through the long-range nature of the Coulomb forces. Ignoring the infrequent large fluctuations associated with close collisions, the cumulative effect of the long-range interactions is replaced by a space-averaged momentum transfer. In less esoteric language, the discrete superposition of Coulomb's law is replaced by the "smoothed-out" behavior described by Poisson's law. In what follows the particle flow will be supposed to be satisfactorily described in terms of only the smoothed-out forces.

To simplify a complex problem further it will be assumed that all the charged particles originate from a zero-potential surface with zero velocity. For d-c motion under these conditions, the statement of the conservation of energy, Eq. 2.2, becomes simply

$$-q\,\phi + \frac{m}{2}\,\bar{v}\cdot\bar{v} = 0 \quad . \tag{2.6}$$

Since the potential ϕ is, in general, a function of position, the individual particle velocities are also functions of position. Moreover,

Eq. 2.6 requires, to a first-order approximation, that all particles occupying an infinitesimal volume element have the same magnitude of velocity. There is, however, no restriction implied by Eq. 2.6 as to direction of the various particle velocities, i.e., no information is conveyed by Eq. 2.6 about the components of the velocity vectors. It is, therefore, possible that a number of different velocity directions might be associated with a given magnitude of velocity in a volume element of the stream.

Figure 2.1 illustrates the nature of the multi-directed velocity concept, described above, in a particular case. The sketch in Fig. 2.1 represents a portion of an electron stream flowing in d-c electric and magnetic fields (not shown). The stream boundaries are indicated and possible trajectories are shown for two of the electrons comprising the stream. In general, all the electrons follow some sort of trochoid-like trajectory similar to those shown. A volume element containing a portion of both trajectories is also shown. The size of the volume element is chosen so that there is no first-order potential variation within its boundaries. Hence Eq. 2.6 requires both electrons to have the same magnitude of velocity within the volume element. However, as Fig. 2.1 illustrates, the direction of motion of the two electrons need not be the same. This dispersion of direction of travel can come about, for example, because the electrons experience different forces along their trajectories.

The usual way of describing a velocity distribution, such as that above, associated with an infinitesimal volume element located by a coordinate reference vector $\bar{r}$, is by means of a distribution function, $F(\bar{v},\bar{r},t)\, d\bar{v}$. A convenient definition of such a distribution function is

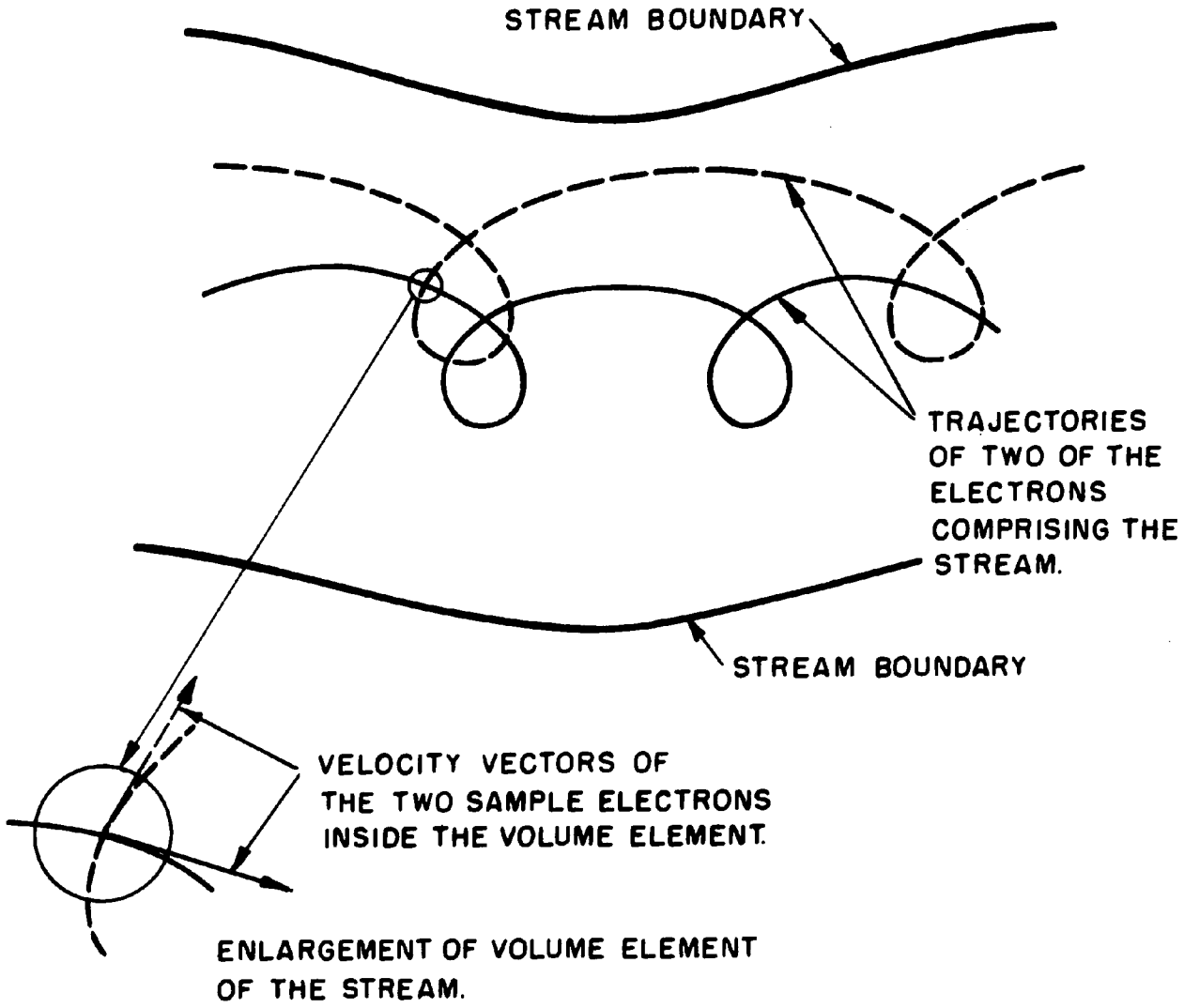


FIG. 2.1 ILLUSTRATION OF MULTI-DIRECTED VELOCITY CONCEPT.

$F(\bar{v},\bar{r},t)\, d\bar{v}$ = the electric charge density associated with the particles in the volume element at $\bar{r}$, at time t, which have a velocity in the range between $\bar{v}$ and $\bar{v} + d\bar{v}$. (F is a negative quantity for electrons.) (2.7)

Since all the particles have some velocity we require

$$\int F\, d\bar{v} = \rho_o \quad , \tag{2.8}$$

where ρ_o is the total charge density associated with the volume element at $\bar{r}$. The integration is to be performed over all possible velocity directions. For a sufficiently high particle density, the distribution function provides a statistically definite and continuous description of the velocity distribution. It is convenient for the following discussion to define the following velocity parameters:

The mean velocity associated with a given volume element is

$$\bar{v}_{om} = \frac{1}{\rho_o} \int \bar{v}\, F\, d\bar{v} \quad ; \tag{2.9}$$

The deviation of a particular particle velocity from the mean velocity $\bar{v}_{om}$ is denoted by $\bar{u}$, i.e.,

$$\bar{u} = \bar{v} - \bar{v}_{om} \quad . \tag{2.10}$$

The mean value of $\bar{u}$ is, using Eq. 2.9, zero. Figure 2.2 is a vector diagram illustrating the relations between the various velocities for the electrons in a given volume element. The average velocity $\bar{v}_{om}$ is used as a reference vector. The individual particle velocity vectors $\bar{v}$ lie on a locus which is a circle whose radius is found from Eq. 2.6 evaluated in the volume element. For convenience, Fig. 2.2 illustrates a two-dimensional flow. The difference between an individual particle velocity and the average velocity, $\bar{u}$, is the vector difference between

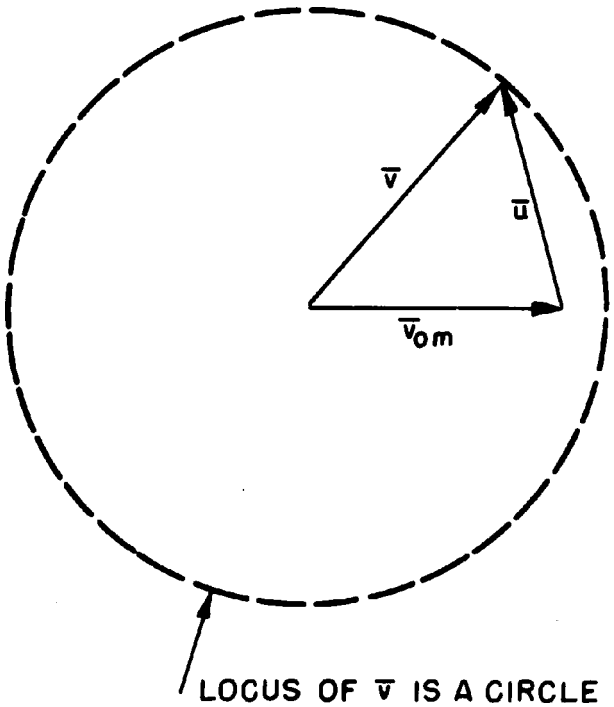


FIG. 2.2 VECTOR DIAGRAM ILLUSTRATING THE RELATIONSHIP BETWEEN $\bar{v}$, $\bar{v}_{om}$, AND $\bar{u}$

$\bar{v}$ and $\bar{v}_{om}$. It should be noted that, since

$$|\bar{v}| \geq |\bar{v}_{om}| \ , \tag{2.11}$$

the average velocity vector never extends outside the circle. Figure 2.2 indicates that $\bar{u}$ assumes its maximum and minimum magnitudes when it is antiparallel and parallel, respectively, to $\bar{v}_{om}$.

The representation of Fig. 2.2 suggests a convenient method of indicating the velocity distribution function $F\, d\bar{v}$. This method is shown in Fig. 2.3. The charge density associated with a given velocity range is indicated by the radial height of the curve labeled F above the locus circle of the particle velocities.

The representation of the distribution function in Fig. 2.3 suggests expressing $F\, d\bar{v}$ in a polar form as a function of the angle ψ which a given velocity $\bar{v}$ makes with the average velocity in the volume element, $\bar{v}_{om}$. Accordingly, we have the following paraphrasing of the definition Eq. 2.7:

$$\begin{aligned} F(\bar{r},\psi,t)\, d\psi &= F(\bar{r},\bar{v},t)\, d\bar{v} \\ &= \text{the electric charge density associated with the particles in the volume element at } \bar{r}, \text{ at time t, which have a velocity in the angular range between } \psi \text{ and } \psi + d\psi. \end{aligned} \tag{2.12}$$

In general, the velocity distribution function can have any shape. Two special cases which produce simplifications in the mathematics can be noted. If the distribution function is symmetrical about some velocity, the average velocity is parallel to that velocity. This can be readily shown by interpreting the distribution function as a function of ψ rather than $\bar{v}$. An example of a symmetrical distribution function is illustrated in Fig. 2.4a.

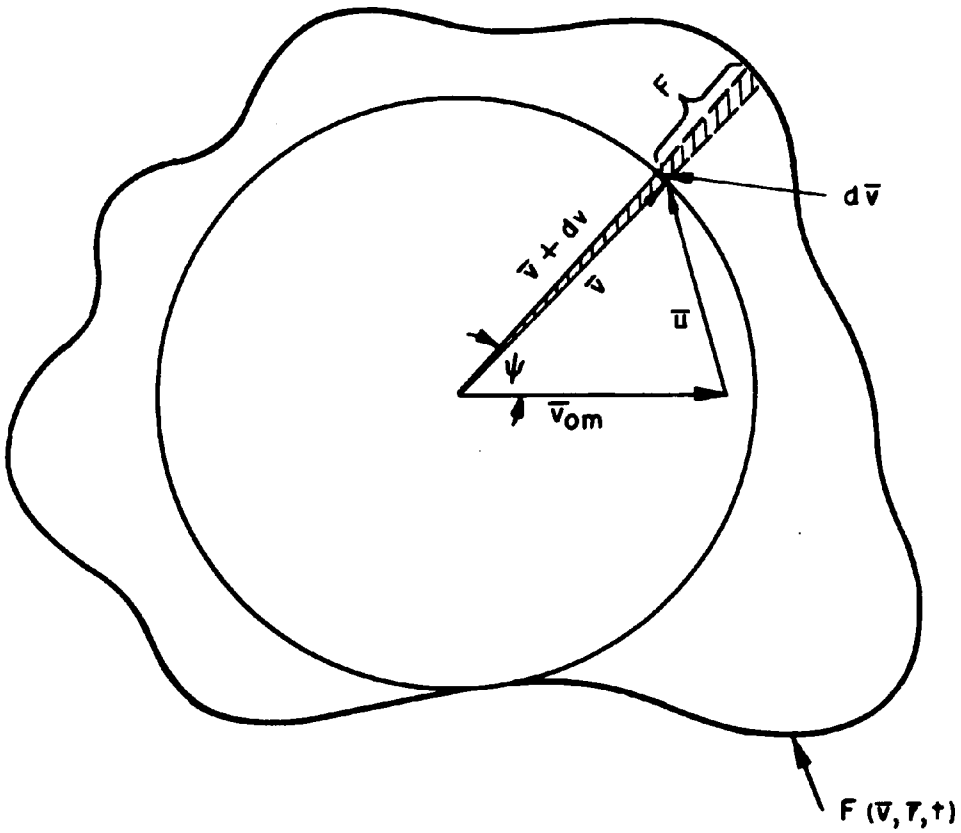
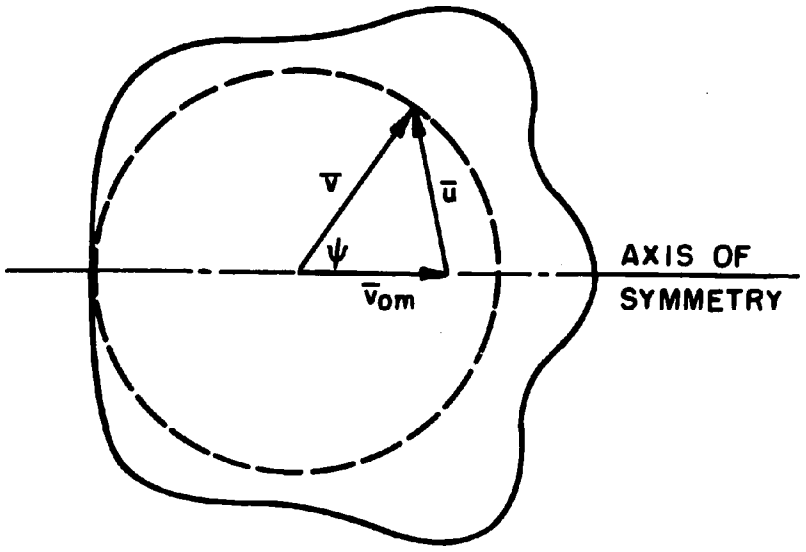
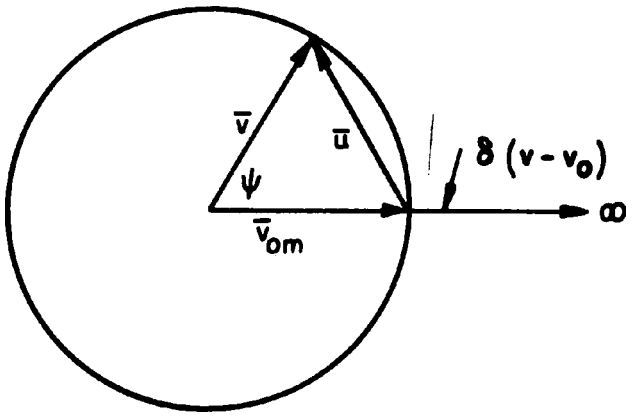


FIG. 2.3 REPRESENTATION OF THE VELOCITY DISTRIBUTION FUNCTION $F d\bar{v}$.



a. SYMMETRICAL DISTRIBUTION.



b. LAMINAR FLOW.

FIG. 2.4 ILLUSTRATIONS OF SPECIAL VELOCITY DISTRIBUTION FUNCTIONS.

If the electron velocity is required to be a single-valued function of position, so that all particles associated with a given volume element have the same vector velocity, the flow is said to be laminar. For laminar flow, electron trajectories do not cross, and $\bar{u}$ is identically zero for all the electrons. The distribution function consists in this case of a single "spike" (δ function) located at the average velocity. Figure 2.4b illustrates such a distribution function. It can be noted that the distribution function can consist of a number of "spikes" as contrasted with the continuous distribution illustrated in Fig. 2.4a. This might be the case in, for example, a two-stream electron tube of the Haeff type[15].

The equation describing the average motion of the stream is obtained in exactly the same manner as the equation of conservation of momentum is obtained from the Boltzmann transport equation[11]. The resulting equation is

$$\frac{-q}{m}\left[\bar{E} + \bar{v}_{om} \times \bar{B}\right] = \frac{d\bar{v}_{om}}{dt} \quad \frac{\nabla\cdot(\rho_o \tilde{P})}{\rho_o} \quad , \qquad (2.13)$$

where the electric intensity $\bar{E}$ includes the smoothed-out Coulomb forces, and $\tilde{P}$ is defined below. In deriving Eq. 2.13, it should be noted that the vector components of the velocity of each electron are independent of position in the stream. The average velocity, $\bar{v}_{om}$, associated with a volume element, on the other hand, is a function of position and hence so is the relationship between $\bar{u}$ and $\bar{v}_{om}$. The quantity $\tilde{P}$ appearing in Eq. 2.13 is a symmetric tensor having components in an orthogonal coordinate system (coordinates α, β, γ),

$$\tilde{P} \triangleq \begin{bmatrix} \widehat{u_\alpha u_\alpha} & \widehat{u_\alpha u_\beta} & \widehat{u_\alpha u_\gamma} \\ \widehat{u_\beta u_\alpha} & \widehat{u_\beta u_\beta} & \widehat{u_\beta u_\gamma} \\ \widehat{u_\gamma u_\alpha} & \widehat{u_\gamma u_\beta} & \widehat{u_\gamma u_\gamma} \end{bmatrix} ; \qquad (2.14)$$

where

$$\widehat{u_\alpha u_\beta} = \frac{1}{\rho_o} \int u_\alpha u_\beta F \, d\bar{u} \quad . \qquad (2.15)$$

The integration is carried out over all values of $\bar{u}$. The other components of $\tilde{P}$ are defined by appropriate substitution of subscripts. The term containing $\tilde{P}$ in Eq. 2.13 represents a contribution to the average momentum change in moving out of the volume element due to change in the distribution function $F \, d\bar{v}$, i.e., to a change in the number of electrons which have a given velocity $\bar{v}$. Equation 2.13, suitably interpreted, is identical to the hydrodynamic equation of flow; the contribution of the tensor $\tilde{P}$ is analogous to a fluid pressure tensor. Because of this formal identity in mathematical description, the study of electron streams is often referred to as electron hydrodynamics.

For laminar flow the stream velocity is single-valued and the pressure tensor is identically zero. Equation 2.13 can be reduced to the same form as Eq. 2.1 except that the electric field includes the space-charge forces. In the following sections laminar streams are considered first, and subsequently, nonlaminar streams.

2.4 Hamiltonian Formulation of the Equations of Motion for Laminar Streams

The equations of motion in the Newtonian form of Eq. 2.1 can advantageously be transformed, through the use of a different set of variables, in a manner corresponding to the Hamiltonian formulation of classical mechanics.

The electric and magnetic fields can be described in terms of a scalar and vector potential, ϕ and $\bar{A}$ respectively, defined conventionally by

$$\nabla \times \bar{A} = \bar{B} \tag{2.16a}$$

$$-\nabla\phi = \bar{E} + \frac{\partial \bar{A}}{\partial t} \cdot \quad [\phi \text{ is generalized from Eq. 2.3 to include time varying motion.}] \tag{2.16b}$$

On substituting the expansion

$$\frac{d\bar{A}}{dt} = \frac{\partial \bar{A}}{\partial t} + (\bar{v} \cdot \nabla)\, \bar{A} \,, \tag{2.17}$$

into Eq. 2.1, the following expression is obtained;

$$\begin{aligned} -q[-\nabla\phi + (v \cdot \nabla)\, \bar{A} + \bar{v} \times (\nabla \times \bar{A})] \\ = \frac{d}{dt}\,(m\bar{v} - q\bar{A}) \\ = \frac{d\bar{p}}{dt} \,, \end{aligned} \tag{2.18}$$

where $\bar{p} = m\bar{v} - q\bar{A}$ is the electromagnetic "total" momentum.

Consider a function H, known classically as a Hamiltonian function, defined as

$$\begin{aligned} H &= \frac{m}{2}\,\bar{v} \cdot \bar{v} - q\phi \\ &= \frac{1}{2m}\,[\bar{p} + q\bar{A}] \cdot [\bar{p} + q\bar{A}] - q\phi \,. \end{aligned} \tag{2.19}$$

It should be noted that, while the Hamiltonian has the same <u>value</u> whether expressed in terms of $\bar{p}$ or $\bar{v}$, it is a different <u>function</u> in the two expressions. We can choose not only to regard the spatial coordinates of the stream as independent variables but also to elevate the electromagnetic momentum to this special status. By so doing we change the

description of the motion from a set of second-order differential equations to a set of twice as many first-order equations. Considering the Hamiltonian as a function of both $\bar{p}$ and position we have

$$\nabla H = \frac{1}{2m}[(\bar{p} + q\bar{A})\cdot\nabla](q\bar{A}) - q\nabla\phi \quad . \tag{2.20}$$

Equation 2.20 may be evaluated in terms of $\bar{v}$ and position as

$$\nabla H \equiv (\bar{v}\cdot\nabla)\, q\bar{A} + \bar{v} \times (\nabla \times q\bar{A}) - q\nabla\phi \quad . \tag{2.21}$$

Comparison of Eq. 2.21 with Eq. 2.18 indicates that the latter may be simplified to

$$-\nabla H = \frac{d\bar{p}}{dt} \quad . \tag{2.22}$$

The companion set of equations, obtained directly from the definition of the Hamiltonian function, is

$$\nabla_{\bar{p}} H = \bar{v} \quad , \tag{2.23}$$

where $\nabla_{\bar{p}}$ is a momentum gradient operator in momentum space corresponding to the familiar gradient operator in configuration space. (In rectangular coordinates, $\nabla_{\bar{p}} = \partial/\partial p_x\, \bar{x} + \partial/\partial p_y\, \bar{y} + \partial/\partial p_z\, \bar{z}$.) The function $\bar{v}$ should properly be regarded as the time derivative of the configuration variables, thus emphasizing the symmetry of Eqs. 2.22 and 2.23. It is worthwhile emphasizing that Eq. 2.22 and 2.23 describe the stream motion in a six-dimensional phase space with both position and momentum as independent coordinates.

Equation 2.22 leads directly to an invariant of the motion, known as Lagrange's invariant. Taking the curl of this equation we have

$$
\begin{aligned}
-\nabla \times \nabla H &= \nabla \times \frac{d\bar{p}}{dt} \\
&= \nabla \times \left[\frac{\partial \bar{p}}{\partial t} + (\bar{v}\cdot \nabla)\bar{p}\right] \\
&= \nabla \times \left[\frac{\partial \bar{p}}{\partial t} - \bar{v} \times (\nabla \times \bar{p})\right] \\
&= 0 \quad . \qquad (2.24)
\end{aligned}
$$

Use has been made of the vector identity

$$(\bar{v}\cdot\nabla)\,\bar{p} + \bar{v} \times (\nabla \times \bar{p}) = 0 \quad , \qquad (2.25)$$

obtained by recognizing that $\bar{p}$ is independent of the positional coordinates in the Hamiltonian formulation. Stoke's Theorem leads to the representation of Eq. 2.24 in the integral form

$$\frac{d}{dt} \oint p\cdot d\bar{s} = 0 \quad , \qquad (2.26)$$

where $d\bar{s}$ is a differential element of any closed-configuration contour of the stream. As applied to cylindrically symmetrical electron streams, Lagrange's invariant is known in the study of electron stream focusing as Busch's Theorem. Lagrange's invariant is applicable to any stream for which the stream velocity is a single-valued function of position, i.e., a laminar flow.

Another useful invariant of the stream motion, known as Liouville's invariant, expresses the conservation of volume in phase space,

$$\frac{d}{dt} \oint d\bar{p}\, d\bar{r} = 0 \quad , \qquad (2.27)$$

where $d\bar{p}\, d\bar{r}$ is a differential volume element in phase space (in rectangular coordinates $d\bar{p}\, d\bar{r} = dp_x\, dp_y\, dp_z\, dx\, dy\, dz$). The integration is over any volume of phase space. Equation 2.27 follows on noting that

$$\frac{d}{dt}\oint d\bar{p}\, d\bar{r} = \oint \left[\nabla_{\bar{p}} \cdot \frac{d\bar{p}}{dt} + \nabla \cdot \frac{d\bar{r}}{dt}\right] d\bar{p}\, d\bar{r}$$

$$= \oint \left[\nabla_{\bar{p}} \cdot (-\nabla H) + \nabla \cdot (\nabla_{\bar{p}} H)\right] d\bar{p}\, d\bar{r}$$

$$= 0 \quad . \tag{2.28}$$

2.5 D-C Irrotational, Laminar Flow

The d-c characteristics of an electron stream are of considerable importance in the analysis of r-f propagation along the stream if only for the reason that essentially all the analyses appearing in the literature take the form of a first-order perturbation of the d-c stream.

Under the assumption of d-c flow, the Hamiltonian becomes the total energy of the system and, assuming the stream originates with zero velocity from a zero-potential surface, is conveniently equal to zero. Lagrange's invariant, which is an alternative statement of the conservation of energy, reduces to

$$\bar{v}_o \times (\nabla \times \bar{p}_o) = 0. \tag{2.29}$$

The particular case where Eq. 2.29 is satisfied by

$$\nabla \times \bar{p}_o = 0 \tag{2.30}$$

is of special importance. Streams for which this condition is satisfied are said to be irrotational. It can be shown that the stream will be irrotational if there is no magnetic flux normal to the unipotential cathode where the stream originates[13]. The sufficiency of this condition follows from the integral form of Lagrange's invariant, Eq. 2.26. If the integral vanishes anywhere, it then necessarily vanishes everywhere, and, since the contour of integration is arbitrary, Eq. 2.30

follows. The validity of Eq. 2.30 at the stream cathode under the conditions stated above is established by assuming a finite non-zero velocity of emission normal to the cathode surface and noting that Eq. 2.30 requires that the component of $\nabla \times \bar{p}_o$ parallel to the cathode surface vanish. The velocity of emission can then be made arbitrarily small so that $\nabla \times \bar{v}_o$ vanishes on the cathode surface. The validity of Eq. 2.30 under the specified conditions follows directly.

The importance of this special case is due to the fact that many electronic devices satisfy this condition.

The irrotational condition of Eq. 2.30 can be expanded to

$$\nabla \times \bar{v}_o = \frac{q}{m} \bar{B}_o \quad , \tag{2.31}$$

and separated into transverse (subscript t) and axial (subscript z) components in an axial coordinate system, i.e.,

$$\underline{\bar{z}} \cdot \nabla \times \bar{v}_o = \nabla \cdot (\bar{v}_o \times \underline{\bar{z}}) = \frac{q}{m} B_{oz} \quad , \tag{2.32a}$$

$$\begin{aligned} (\nabla \times \bar{v}_o)_t &= [\underline{\bar{z}} \times (\nabla \times \bar{v}_o)] \times \underline{\bar{z}} \\ &= \left[\nabla v_{oz} - \frac{\partial \bar{v}_o}{\partial z} \right] \times \underline{\bar{z}} \\ &= \frac{q}{m} \bar{B}_{ot} \quad . \end{aligned} \tag{2.32b}$$

2.5.1 Rectilinear, Irrotational, Laminar Flow. The only laminar irrotational rectilinear flow is the familiar Brillouin flow. Assuming no variations parallel to a $\underline{\bar{z}}$-directed uniform magnetic field and a uniform velocity normal to the magnetic field ($\underline{\bar{x}}$-directed), we have from Eq. 2.32

$$\frac{\partial v_{ox}}{\partial y} = \omega_c \quad , \tag{2.33}$$

where the cyclotron frequency ω_c is defined as

$$\omega_c = \frac{q}{m} B_{oz} \quad . \tag{2.34}$$

The space-charge density ρ_o can be obtained from Poisson's equation, or, for convenience, from the form of Poisson's equation obtained by taking the divergence of Eq. 2.1,

$$\nabla^2(\bar{v}_o \cdot \bar{v}_o) = \frac{-2\, q\rho_o}{m\epsilon_o} = 2\,\omega_p^2 \quad , \tag{2.35}$$

where ω_p^2 is the electron density (plasma) radian frequency. Substituting Eq. 2.33 into Eq. 2.35, we obtain

$$\omega_p^2 = \omega_c^2 \quad . \tag{2.36}$$

The flow may be made skew to the magnetic field, by adding a constant velocity component parallel to the magnetic field, without altering the above conclusions.

A transverse electric field normal to the magnetic field is required to balance the magnetic and space-charge forces. This type of flow will be discussed in further detail subsequently in connection with the design of a crossed electric and magnetic field stream analyzer.

2.5.2 Axially Symmetric, Irrotational, Laminar Flow. In this instance we apply Eq. 2.30 to cylindrically symmetrical axial flow (coordinates r, θ, z), assuming no variation of velocity and space-charge density parallel to a uniform axial magnetic field. The magnetic field must, of course, be so oriented or shielded with respect to the cathode as to establish the irrotational character of the flow.

From Eq. 2.32a we have

$$\frac{1}{r} \frac{\partial(rv_{o\theta})}{\partial r} = \omega_c \quad , \tag{2.37}$$

where ω_c is redefined, analogously to Eq. 2.34, as

$$\omega_c = \frac{q}{m} B_{oz} \quad . \tag{2.38}$$

Integration of Eq. 2.37 yields

$$v_{o\theta} = \frac{\omega_c}{2} r + \frac{C}{r} \quad , \tag{2.39}$$

where C is a constant of integration. The information obtained from Eq. 2.32b,

$$\frac{\partial v_{oz}}{\partial r} - \frac{\partial v_{or}}{\partial z} = 0 \quad , \tag{2.40a}$$

$$\frac{\partial v_{o\theta}}{\partial z} = 0 \quad , \tag{2.40b}$$

shows the constant of integration C to be independent of z.

Substitution of the above equations into Poisson's equation, Eq. 2.35, gives

$$\frac{1}{r}\left[r \frac{\partial}{\partial r} (v_{or}^2 + v_{oz}^2)\right] + \frac{\partial^2}{\partial z^2} (v_{or}^2 + v_{oz}^2) = 2\omega_p^2 - \omega_c^2 - \frac{4C^2}{r^4} \quad . \tag{2.41}$$

Several special cases of Eqs. 2.39, 2.40, and 2.41, of particular importance, involve the assumption of no radial velocity. Equation 2.40 indicates that if the radial velocity vanishes, the axial velocity is independent of transverse dimensions, and, since we have assumed axial uniformity, is therefore simply a constant. Equation 2.41 reduces, for the condition of zero radial velocity, to

$$2\,\omega_p^2 - \omega_c^2 - \frac{4C^2}{r^4} = 0 \quad . \tag{2.42}$$

An additional boundary condition, necessary to determine the constant of integration C, differentiates various types of irrotational, axially symmetric, laminar flows.

A familiar special case is that for which the constant C is zero. Such a condition is necessary, for example, for a stream whose interior includes the axis in order to maintain a finite kinetic energy; this is indicated by Eq. 2.39. If the axial velocity is not zero, the flow is called axial Brillouin flow. From Eq. 2.42 we obtain the well-known relation between the magnetic field and the space-charge density for this type of flow,

$$2\,\omega_p^2 = \omega_c^2 \quad . \tag{2.43}$$

It is, of course, not necessary that the stream include the axis; various types of hollow-stream flow are possible. One hollow-stream flow occurs when the stream is launched in such a manner as to maintain the constant C zero. Such a flow is a circumferential counterpart of rectilinear Brillouin flow. This relationship is particularly evident if the axial velocity, for which no restrictions other than that it is constant have been made as yet, is chosen to be zero.

Another hollow-stream flow of some interest occurs if the circumferential velocity is supposed to be zero on a cylinder bounded by radius r_k. Within the stream the angular velocity at an arbitrary radius r is then given by

$$\frac{v_{o\theta}}{r} = \frac{\omega_c}{2}\left(1 - \frac{r_k^2}{r^2}\right) ,$$

where

$$r \geq r_k \quad . \tag{2.44}$$

The relationship between the magnetic field and the space-charge density is

$$2\,\omega_p^2 = \omega_c^2 \left(1 + \frac{r_k^4}{r^4}\right) \quad . \tag{2.45}$$

These relationships reduce to those for axial Brillouin flow if the radius r_k becomes zero.

If the axial velocity for the above flow is zero it is known as single-stream magnetron flow. The radius r_k corresponds to the inner of two cylinders between which the flow takes place. The vanishing of the circumferential velocity at this radius represents a statement of the conservation of energy requirement on the magnetron cathode which forms the inner cylinder.

A special limiting case of Eqs. 2.45 and 2.46 occurs when the stream is confined between two cylinders whose radii approach infinity concurrently. The circumferential Brillouin flow approaches rectilinear Brillouin flow in this limiting case.

The laminar irrotational flow is also possible if the magnetic field vanishes. In this case the constant C is necessarily non-zero. The space-charge density is not constant over the cross section of the flow but varies, as seen from Eq. 2.42, as

$$\omega_p^2 = \frac{2C^2}{r^4} \quad . \tag{2.46}$$

The space-charge repulsive forces are balanced by the centrifugal force of the stream rotation. If the axial velocity is not zero, this type of flow is known as Harris flow. If the axial velocity vanishes, the flow is one which has been discussed in the literature under the designation E flow. A radial electric field is necessary to supply the energy for this motion.

The laminar irrotational streams considered above are useful in analyzing microwave interaction with electron streams because of the relative simplicity of the motion. In practice, however, the realization of laminar motion is a difficult matter involving the launching of the stream in a particular precise manner. Ordinarily one is satisfied with the focusing of the stream if the perturbation, or scalloping, of the stream is within acceptable limits.

2.6 Magnetically Confined Flow

Axial Brillouin flow, discussed above, involves the balancing of space-charge forces by a combination of centrifugal force and magnetic force. A magnetic field can also be used to focus an axial flow by limiting the energy available to the nonaxial motion. The stream flow is no longer irrotational; rather, some magnetic flux is allowed to pass through the cathode surface. Applying Lagrange's invariant, Eq. 2.26, to a circular contour transverse to the axis of symmetry we have

$$\frac{v_{o\theta}}{r} = \frac{1}{2}\left(\omega_{ck}\frac{r_k^2}{r^2} - \omega_c\right) , \qquad (2.47)$$

where $v_{o\theta}/r$ is the angular velocity acquired by an electron at radius r and the subscript k indicates a quantity is to be evaluated at the cathode for the same electron. If no flux links the cathode we have, of course, the irrotational flow previously discussed, in which the stream rotates with a constant angular velocity. If magnetic flux links the cathode, however, the constancy of the angular velocity necessary for uniform flow is not obtained and a radial perturbation of the stream ensues. The radial perturbations are bounded, however, as follows. From Eq. 2.48 it is noted that the kinetic energy of rotation increases indefinitely as the radial position of a stream particle either increases

or decreases. Since the total energy is limited there must be an upper and a lower bound to the radial perturbation. For small perturbations the axial space-charge forces due to the axial irregularity of the stream can be neglected, and hence the action of the magnetic field taken to be that of interchanging radial and angular kinetic energy. Increasing the magnetic field enhances the rate of energy interchange and hence reduces the extent of the radial perturbations. It is evident that the radial perturbations cannot completely vanish as they form a necessary part of the focusing mechanism.

2.7 Nonlaminar Streams

The laminar stream models discussed above are, of course, idealizations of practically obtainable streams. The rather critical conditions necessary to launch and maintain these streams are much too onerous to be met exactly in engineering devices. It is therefore pertinent to examine the effects of modifications of the idealized stream models. One type of modification can be described as an environmental change. This can be illustrated by the substitution of periodic electric and magnetic fields for uniform focussing fields. The general description of the stream model is not changed by this substitution; i.e., the stream is assumed to remain laminar. Another type of modification which retains a laminar description of the model can be described as a relaxation of constraints. The previous discussion of magnetically confined flow is an example of this modification; a radial motion is permitted, as contrasted with the radially invariant motion of an axial Brillouin stream. A more fundamental stream model modification, requiring a modification in the mathematical description of the model, is typified by the multi-directed velocity streams suggested by the discussion in section 2.3.

In the following sections the multi-directed velocity concept is expanded and stream models involving this concept are described.

2.7.1 The Design of Nonlaminar Stream Models. It is often true that many gross external characteristics of an electron stream are not critically dependent on the detailed internal structure of the model. Unfortunately, the inverse is also, all too often, true. In the case of electron streams flowing in crossed electric and magnetic fields it is the latter situation which must be considered.

To discuss nonlaminar flows we make use of the complete hydrodynamic equation of motion, which is repeated below,

$$\frac{-q}{m}\left[\bar{E} + \bar{v}_o \times \bar{B}\right] = \frac{dv_o}{dt} + \frac{\nabla \cdot (\rho_o \tilde{P})}{\rho_o} \quad . \qquad (2.13)$$

In order to deal with Eq. 2.13 it is necessary to have some sort of information about the pressure tensor.

To determine the pressure tensor directly would require a detailed knowledge of the motion of the particles comprising the stream and is, in general, a formidable undertaking. However it is possible to circumvent this difficulty in special cases in two related ways.

One procedure which can be used is to assume, more or less arbitrarily, a distribution function $F\bar{dv}$ and determine from Eq. 2.13 a stream model compatible with this assumption. The initial assumption can be developed either on the basis of experimental measurements or from purely heuristic considerations. The effects of various general types of multi-directional velocity distributions can be examined for the purpose of obtaining at least a qualitative picture of the effects of similar distributions in actual streams.

On the other hand, we can more or less arbitrarily assume a stream model having certain parameters describing its average motion. The relations between these various stream parameters can then be established using Eq. 2.13. In the first procedure described above, we start out with a knowledge of the details of the motion of each electron, and calculate the average motion of the stream. In this second method, we determine if a stream model, whose average motion is postulated, is compatible with physical laws.

In the following sections both procedures are illustrated for electron streams flowing in crossed electric and magnetic force fields.

2.7.2 Rectilinear, Nonlaminar, Stream Model. In this section the method used is the one wherein the general character of the model is postulated and the various stream parameters then determined from the laws of nature and Eq. 2.13. The first model considered describes rectilinear nonlaminar flow in crossed electric and magnetic fields.

Figure 2.5 relates a Cartesian coordinate system to the stream model to be analyzed. An electron stream confined within plane boundaries $y = a, b$ $(a \leq b)$ has an average motion v_{ox} in the positive $\bar{x}$ direction only. A uniform magnetic field B_o is directed in the negative $\bar{z}$ direction, and plane electrodes not shown supply the necessary transverse electric field E_o. The average stream motion is assumed invariant in the $\bar{x}$ and $\bar{z}$ directions $(\partial/\partial x = \partial/\partial z = 0)$. The average space-charge density is assumed uniform across the stream.

The model described above is often used in the literature, although without the detailed nonlaminar study, which is presented here. The analysis will show the impropriety of assumptions which are sometimes made about various stream parameters.

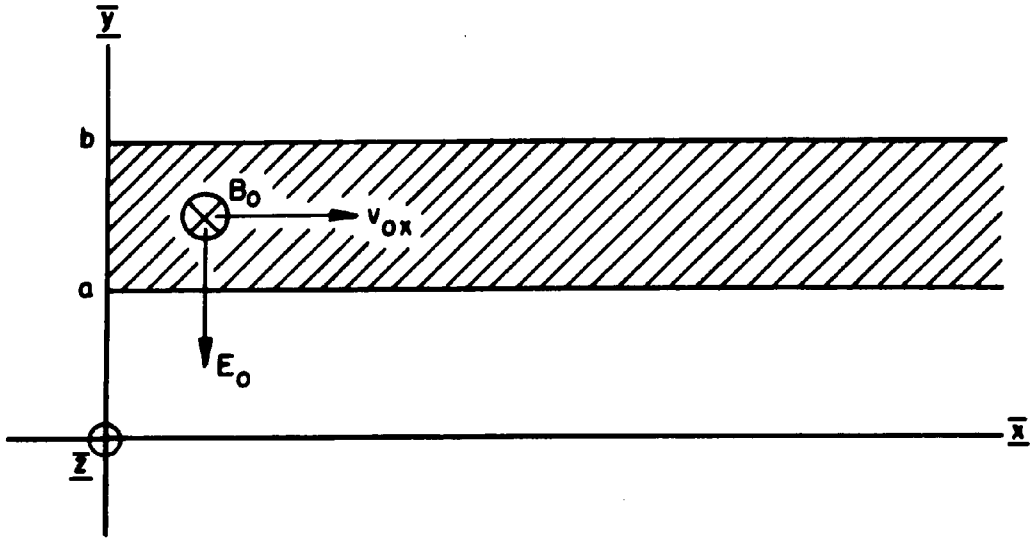


FIG. 2.5 COORDINATE SYSTEM FOR RECTILINEAR NONLAMINAR FLOW MODEL.

For the model described above, the components of Eq. 2.13 are:

$$\frac{\partial}{\partial y} \left(\widehat{u_x u_y}\right) = 0 \quad , \quad \bar{x} \text{ component;} \tag{2.48a}$$

$$\frac{-q}{m} \left[E_o + v_{ox} B_o\right] - \frac{\partial}{\partial y} \left(\widehat{u_y^2}\right) = 0 \quad , \quad \bar{y} \text{ component.} \tag{2.48b}$$

Since all particles have identical vector velocities at the stream boundaries it follows that, at y = a, b,

$$u_x = u_y = \widehat{u_x^2} = \widehat{u_y^2} = \widehat{u_x u_y} = 0 \quad . \tag{2.49}$$

These boundary conditions, together with Eq. 2.48a, require $\widehat{u_x u_y}$ to be identically zero.

It is convenient to make use of Poisson's equation,

$$\frac{\partial E_o}{\partial y} = \frac{\rho_o}{\epsilon_o} \quad , \tag{2.50}$$

to put Eq. 2.48b into the form

$$\omega_p^2 - \omega_c \frac{\partial v_{ox}}{\partial y} = \frac{\partial^2 \widehat{u_y^2}}{\partial y^2} \quad , \tag{2.51}$$

where, as before,

$$\omega_p^2 = \frac{-q\rho_o}{m \epsilon_o} \tag{2.52}$$

and

$$\omega_c = \frac{q}{m} B_o \quad . \tag{2.53}$$

We now assume, subject to consistency requirements, a linear variation of v_{ox}

$$v_{ox} = \Omega y \quad , \tag{2.54}$$

where Ω is a constant. Substitution of Eq. 2.54 into Eq. 2.51 shows $\widehat{u_y^2}$ to be a quadratic function of y. The constants of integration are

determined by the boundary conditions, Eq. 2.49, and we have

$$\widehat{u_y^2} = \frac{1}{2}(\omega_p^2-\omega_c\Omega)(y-a)(y-b) \quad . \tag{2.55}$$

The quantity $\widehat{u_x^2}$ does not appear in Eq. 2.48 since $\partial^2 u_x^2/\partial x^2 = 0$. To determine $\widehat{u_x^2}$ we make use of the conservation of energy principle, which requires of each particle that

$$\frac{-q}{m}\phi + \frac{1}{2}\bar{v}\cdot\bar{v} = 0 \quad , \tag{2.56}$$

where $\bar{v} = \bar{v}_o + \bar{u}$ is the individual particle velocity.

Averaged over the velocity distribution, Eq. 2.50 becomes

$$\frac{-2q}{m}\phi + v_{ox}^2 + \widehat{u_x^2} + \widehat{u_y^2} = 0 \quad , \tag{2.57}$$

where the potential ϕ is related to the electric field by

$$E_o = -\frac{\partial\phi}{\partial y} \quad . \tag{2.58}$$

Poisson's equation, Eq. 2.50, shows ϕ to be a quadratic function of y. The constants of integration can be calculated from Eq. 2.54 evaluated at the stream boundaries. Thus, it is found that

$$\frac{2q}{m}\phi = (\omega_p^2-\Omega^2)(y-a)(y-b) + v_{ox}^2 \quad . \tag{2.59}$$

The function $\widehat{u_x^2}$ can now be found using Eqs. 2.55, 2.57, and 2.59;

$$\widehat{u_x^2} = \frac{1}{2}(\omega_p^2+\omega_c\Omega-2\Omega^2)(y-a)(y-b) \quad . \tag{2.60}$$

We have described the various parameters of a nonlaminar stream model which are consistent with the equation of motion, Poisson's equation, and the appropriate boundary conditions. There is one further implicit restriction with very interesting consequences. This implicit restriction

is derived from the fact that $\widehat{u_x^2}$ and $\widehat{u_y^2}$ are inherently positive quantities. Since the stream is confined to the interval $a \leq y \leq b$, the product $(y-a)(y-b)$ is always negative (since $y-a \geq 0$, $y-b \leq 0$) within the stream. The coefficients of this product in the expressions for $\widehat{u_x^2}$ and $\widehat{u_y^2}$, Eqs. 2.60 and 2.55, must therefore also be negative quantities. To satisfy this requirement it is necessary that

$$\Omega \geq \left(\frac{\omega_p}{\omega_c}\right)^2 \omega_c \qquad (2.61a)$$

and

$$\Omega \geq \omega_c \quad . \qquad (2.61b)$$

The equal signs in the above inequalities correspond to the conditions for rectilinear Brillouin flow; in this case both $\widehat{u_x^2}$ and $\widehat{u_y^2}$ vanish and $\omega_p = \omega_c$.

The present stream model contains a mechanism whereby effects occurring at a given position in the stream (for example at the upper stream boundary) are distributed across the stream. We might discuss the effects of such a mechanism in the model above and expect that the discussion would provide at least a qualitative picture of similar mechanisms in actual streams. This will be done in the next chapter.

It is useful to have some idea of relative magnitudes of comparable quantities. To that end it can be noted from Eqs. 2.55 and 2.60 that

$$\frac{\widehat{u_x^2}}{\widehat{u_y^2}} = 1 + 2\,\frac{\frac{\Omega}{\omega_c}\left(\frac{\Omega}{\omega_c} - 1\right)}{\frac{\Omega}{\omega_c} - \left(\frac{\omega_p}{\omega_c}\right)^2} \geq 1 \quad . \qquad (2.62)$$

It is also found that

$$0 \leq \frac{\widehat{u_x^2}+\widehat{u_y^2}}{v_{ox}^2} = \frac{(\omega_p^2-\Omega^2)(y-a)(y-b)}{(\Omega y)^2} \leq \frac{1}{4}\left(1-\frac{\omega_p^2}{\Omega^2}\right)\frac{\left(1-\frac{a}{b}\right)^2}{a/b} \quad . \qquad (2.63)$$

This latter inequality is formed by finding the maximum value of the ratio, which occurs at $y = 2ab/(a+b)$. For thin streams ($a/b \simeq 1$), the perturbation

from the mean stream motion will be small. For thick streams ($a/b \ll 1$), the average stream motion can be a very poor description of individual particle motion.

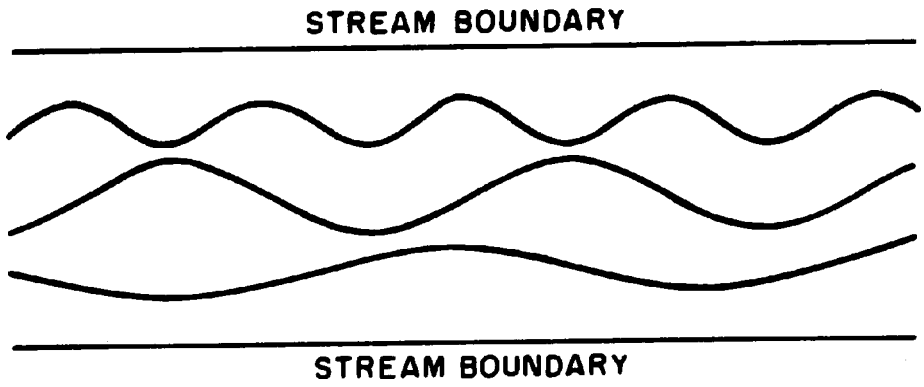
Figure 2.6 illustrates the types of motion appropriate to these two extremes. For thin streams, particle motion is restricted to the near vicinity of the average motion; for thick streams individual particles may oscillate across the entire stream. In effect there is, in the latter case, a periodic interchange of position (but not history) between electrons at the top of the stream and those at the bottom of the stream. In all cases, of course, the model requires that the electron trajectories be superimposed in such a manner that the average space-charge density across the stream is constant.

2.7.3 Axial, Nonlaminar Stream Model. An analysis, similar to the preceding one, can be carried out with relative simplicity for an axial flow. Figure 2.7 describes the geometry of an annular axial stream confined between cylindrical surfaces of radii a,b ($a < b$). A uniform magnetic field B_o, directed along the positive $\underline{z}$ direction, maintains an axially and circumferentially uniform average flow ($\partial/\partial z = \partial/\partial\theta = 0$). The space-charge density is assumed uniform throughout the stream. Subject to consistency requirements, we assume the average stream velocity is given by

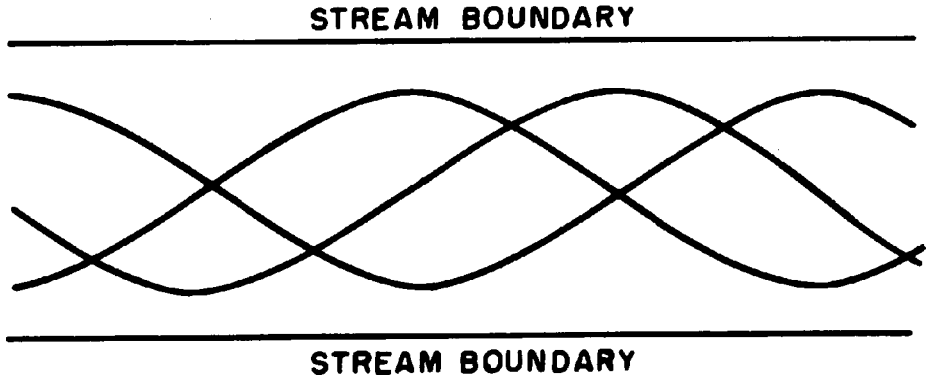
$$\overline{v}_o = v_{oz}\,\underline{\overline{z}} + r\,\Omega\,\underline{\overline{\theta}} \quad , \tag{2.64}$$

where both v_{oz} and Ω are constants of the model. There is no average radial motion.

Within the above assumptions the components of the equation of motion, Eq. 2.13, are the following:



a. THIN STREAMS. ($a/b \cong 1$)



b. THICK STREAMS. ($a/b << 1$)

FIG. 2.6 PARTICLE MOTION IN RECTILINEAR NONLAMINAR STREAM MODEL.

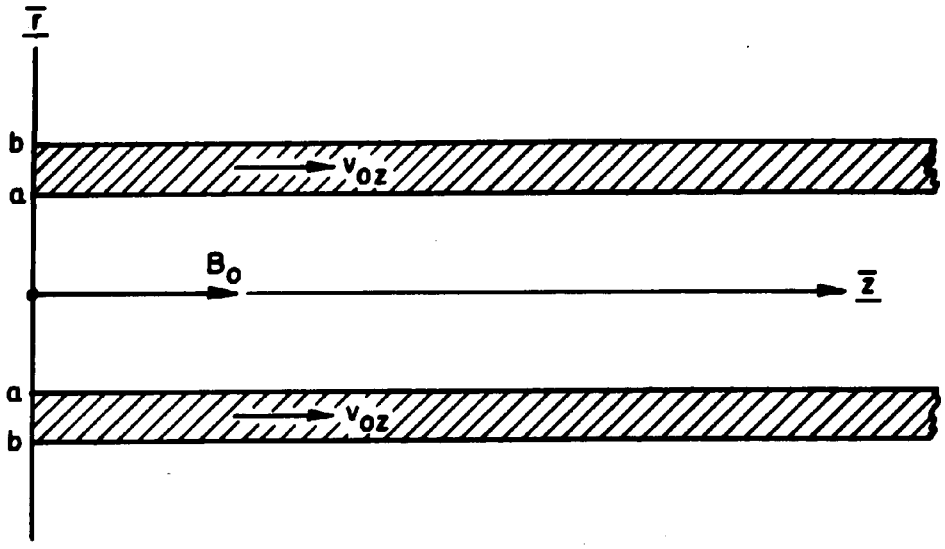


FIG. 2.7 GEOMETRY OF ANNULAR AXIAL NONLAMINAR FLOW.

$$\frac{-q}{m}\left[E_{ro} + \Omega\, r\, B_o\right] = \frac{1}{r}\frac{\partial}{\partial r}\left(r\widehat{u_r^2}\right) - r\Omega^2 \quad , \ \underline{r} \text{ component.} \tag{2.65a}$$

$$\frac{\partial}{\partial r}\left(r\,\widehat{u_r u_\theta}\right) = 0 \quad , \ \underline{\theta} \text{ component.} \tag{2.65b}$$

$$\frac{\partial}{\partial r}\left(r\,\widehat{u_r u_z}\right) = 0 \quad , \ \underline{z} \text{ component.} \tag{2.65c}$$

Since none of the stream particles has any radial velocity at the stream boundaries Eqs. 2.65b and 2.65c require that

$$\widehat{u_r u_\theta} = \widehat{u_r u_z} = 0 \quad . \tag{2.66}$$

For convenience we take the divergence of the equation of motion, Eq. 2.13, so that, by use of Poisson's equation and Eq. 2.64, we can transform Eq. 2.65a into the form

$$\omega_p^2 - 2\,\Omega\,\omega_c = \frac{1}{r}\frac{\partial^2}{\partial r^2}\left(r\,\widehat{u_r^2}\right) - 2\,\Omega^2 \quad . \tag{2.67}$$

Equation 2.67 can be easily integrated, and, on substitution of the conditions that $\widehat{u_r^2}$ vanish on the stream boundaries, we obtain

$$r\,\widehat{u_r^2} = \left(\frac{\omega_p^2 - 2\Omega\omega_c + 2\Omega^2}{6}\right)(r+a+b)(r-a)(r-b) \quad . \tag{2.68}$$

To evaluate $\widehat{u_\theta^2}$ and $\widehat{u_z^2}$ we proceed, as before, to make use of Poisson's equation, and of the conservation of energy requirements at the stream boundaries. There are, however, no restrictions in the model which require $\widehat{u_\theta^2}$ and $\widehat{u_z^2}$ to vanish on the stream boundaries in general. Instead we suppose that the partial energy, $\widehat{u_\theta^2} + \widehat{u_z^2}$, has the values $U^2(a)$ and $U^2(b)$ respectively at the indicated stream boundaries. The potential ϕ is then given by the expression

$$\frac{2q}{m}\phi - v_{oz}^2 - \Omega^2 r^2 = \widehat{u_r^2} + \widehat{u_\theta^2} + \widehat{u_z^2}$$

$$= \left(\frac{\omega_p^2}{2} - \Omega^2\right)\left[r^2 - \frac{a^2\ln(b/r) + b^2\ln(r/a)}{\ln(b/a)} \right]$$

$$+ \frac{U^2(b)\ln(r/a) + U^2(b)\ln(b/r)}{\ln(b/a)} \quad . \qquad (2.69)$$

Equation 2.68 can be used to find the quantity $\widehat{u_\theta^2} + \widehat{u_z^2}$ from Eq. 2.69. We have, as noted above, no requirements which separate these two quantities. Such a requirement can be introduced as an additional specification of the stream model. For example, if we assume $\widehat{u_r^2} = 0$ by making the coefficient in Eq.2.68 zero, we can envision this as describing a flow where electron paths lie on cylindrical surfaces about the axis. Another model can be formulated by requiring all particles to have the same vector velocity on the stream boundaries. In this case $\widehat{u_\theta^2} = \widehat{u_z^2} = 0$ on the boundaries, and hence $U^2(a) = U^2(b) = 0$. This latter case occurs when the cathode is magnetically shielded. Then, because of the circumferential symmetry, all electrons acquire the Larmor angular velocity $\omega_c/2$ and hence $\widehat{u_\theta^2} = 0$. Since $\widehat{u_r^2} = 0$ on the stream boundaries, it then follows that $\widehat{u_z^2}$ is also zero on the stream boundaries.

We can apply the above analysis to a solid stream by reconsidering the boundary conditions applied to the solution of Eq. 2.67. For a solid stream we obtain

$$\widehat{u_r^2} = \left(\frac{\omega_p^2 - 2\Omega\omega_c + 2\Omega^2}{6}\right)(r^2 - b^2) \quad . \qquad (2.70)$$

In obtaining Eq. 2.71, the conditions that $r\widehat{u_r^2}$ vanishes at $r = 0,b$ have been applied. The potential variation, calculated in the same manner as before from Poisson's equation, is

$$\frac{2q}{m}\phi - v_{oz}^2 - \Omega^2 r^2 = \widehat{u_r^2} + \widehat{u_\theta^2} + \widehat{u_z^2}$$

$$= \left(\frac{\omega_p^2}{2} - \Omega^2\right)(r^2-b^2) + U^2(b) \quad . \quad (2.71)$$

The boundary conditions used to evaluate the constants of integration involved in obtaining Eq. 2.71 are that ϕ is finite at $r = 0$ and that $\widehat{u_\theta^2} + \widehat{u_z^2} = U^2(b)$ at $r = b$. Substituting Eq. 2.70 into Eq. 71 yields

$$\widehat{u_\theta^2} + \widehat{u_z^2} = \left(\frac{\omega_p^2 - 4\Omega^2 + \Omega\omega_c}{3}\right)(r^2-b^2) + U^2(b) \quad . \quad (2.72)$$

Since the coefficient in Eq. 2.70 must be negative (for the same reasons as described for the rectilinear nonlaminar flow), the value of Ω must lie between the quadratic roots of that coefficient, i.e.,

$$\frac{\omega_c}{2} - \sqrt{\left(\frac{\omega_c}{2}\right)^2 - \frac{\omega_p^2}{2}} \leq \Omega \leq \frac{\omega_c}{2} + \sqrt{\left(\frac{\omega_c}{2}\right)^2 + \frac{\omega_p^2}{2}} \quad . \quad (2.73)$$

Since Ω must also be real, Eq. 2.73 requires that

$$\frac{\omega_c^2}{2\omega_p^2} \geq 1 \quad . \quad (2.74)$$

The equalities are appropriate for laminar, axially symmetric, Brillouin flow. In this case $\Omega = \omega_c/2$ and $2\omega_p^2 = \omega_c^2$.

If the stream is launched from a shielded cathode all electrons acquire the Larmor angular velocity $\omega_c/2$. For this case $\widehat{u_\theta^2} = 0$ and, since all the electrons will have the same velocity on the stream boundary, $U^2(b) = 0$. We have then, from Eqs. 2.70 and 2.72,

$$\widehat{u_r^2} = \left(\omega_p^2 - \frac{\omega_c^2}{2}\right)\left(\frac{r^2-b^2}{6}\right) \quad , \quad (2.75a)$$

$$\widehat{u_z^2} = \left(\omega_p^2 - \frac{\omega_c^2}{2}\right)\left(\frac{r^2-b^2}{3}\right) \quad , \quad (2.75b)$$

$$\frac{2q}{m}\phi - v_{oz}^2 - \left(\frac{\omega_c r}{2}\right)^2 = \left(\omega_p^2 - \frac{\omega_c^2}{2}\right)\left(\frac{r^2-b^2}{2}\right) . \qquad (2.75c)$$

It is interesting to compare this last nonlaminar stream model with an axially symmetric, laminar, Brillouin flow. For this comparison the two streams are assumed to have the same geometry, boundary potential, and space-charge density. The cyclotron frequency of the laminar stream is denoted by ω_{cB}. Since it has been postulated that both streams have the same space-charge density, we can substitute for ω_p^2 in Eqs. 2.75 from the relation (obtained in section 2.5.2)

$$2\,\omega_p^2 = \omega_{cB}^2 . \qquad (2.76)$$

As one index of comparison between the two streams we can use the ratio, denoted by R_c, of the partial energy $\widehat{u_r^2} + \widehat{u_z^2}$ to the total energy $2q\phi/m$ integrated over the cross-sectional area of the nonlaminar stream, i.e.,

$$R_c = \frac{\int_o^b (\widehat{u_r^2}+\widehat{u_z^2})\, 2\pi r\, dr}{\int_o^b \left(\frac{2q}{m}\phi\right) 2\pi r\, dr} = \frac{1}{1 + \dfrac{2\left(1+\dfrac{2v_{oz}^2}{\omega_c^2 b^2}\right)}{1-\left(\dfrac{\omega_{cB}}{\omega_c}\right)^2}} \qquad (2.77)$$

It should be noted that Eq. 2.76 has been used to obtain Eq. 2.77. The factor $2v_{oz}^2/\omega_c^2 b^2$ appearing on the right of Eq. 2.77 is one-half the ratio of the axial to rotational energy at the stream boundary. A not unreasonable value for this ratio might be ten. Assuming that the ratio $(\omega_{cB}/\omega_c)^2$ is 0.4, substitution in Eq. 2.77 shows that R_c is only 0.05. While the comparison of these two streams is oversimplified, the example above does illustrate the large effect a small nonlaminar motion can have on the stream characteristics (in the example, the magnetic focussing

field required). In this respect Eq. 2.75 can also be used to compare the two stream currents. The ratio of the currents will be proportional to the ratio of the axial velocities since both streams have the same geometry and space-charge density. Using Eq. 2.75c and the condition that both streams have the same boundary potential, we have

$$\left(\frac{v_{ozB}}{v_{oz}}\right)^2 = 1 - \frac{\omega_c^2 b}{4v_{oz}^2}\left(\frac{\omega_{cB}^2}{\omega_c^2} - 1\right) . \qquad (2.78)$$

The subscript B denotes the cyclotron frequency of the laminar stream. Using the same numerical order of magnitudes as in the previous calculation ($\omega_c^2 b^2/4v_{oz}^2 = 0.1$, $\omega_{cB}^2/\omega_c^2 = 0.4$), Eq. 2.78 indicates approximately a three percent lower current for the nonlaminar stream.

2.7.4 Rectilinear Flow Model Re-examined. This section describes in a different manner the rectilinear nonlaminar flow having the geometry shown in Fig. 2.5. In this case the analysis will begin with the assumption of a velocity distribution function from which the averaged parameters of the stream motion will be calculated. For simplicity the distribution function, shown in Fig. 2.8, is chosen to be symmetrical about the velocity component in the $\underline{x}$ direction. The distribution function is also assumed to be uniform over an angle of $2\psi_M$, where ψ_M is, in general, a function of position. The nature of the variation of ψ_M with position will be specified later. It is convenient to express the distribution function in terms of the angle between the velocity $\bar{v}$ and the average velocity $\bar{v}_o$, i.e., in the polar form defined by Eq. 2.12.

The distribution function can then be evaluated in terms of the average space-charge density in the following manner: from Eq. 2.8,

$$\int_{-\psi_M}^{\psi_M} F d\psi = 2\psi_M = \rho_o , \qquad (2.79)$$

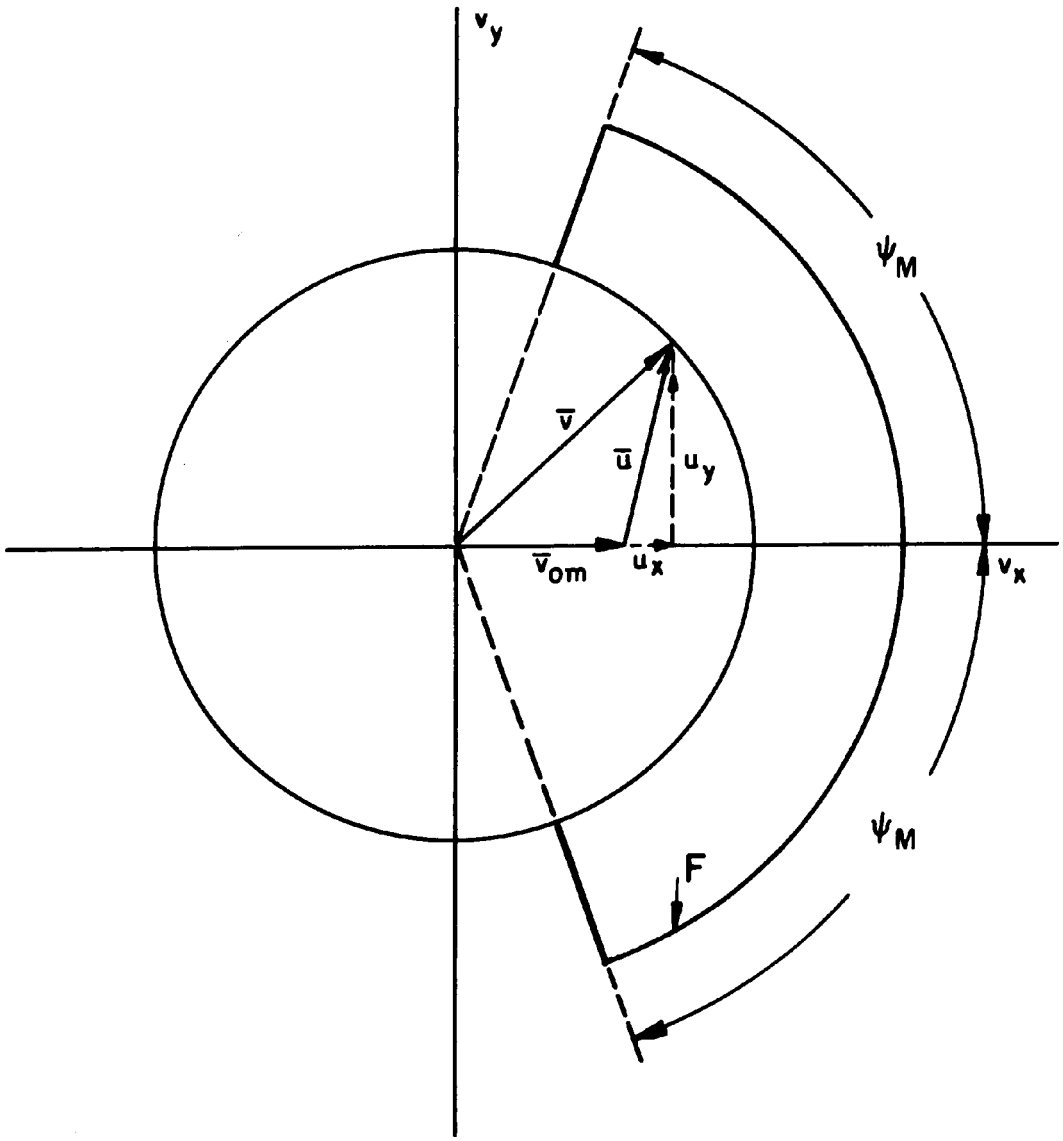


FIG. 2.8 UNIFORM SYMMETRICAL DISTRIBUTION FUNCTION FOR NONLAMINAR RECTILINEAR STREAM MODEL.

where the uniform distribution function described by Fig. 2.8 has been used. Therefore

$$F = \frac{\rho_o}{2\psi_M} \quad , \quad -\psi_M \leq \psi \leq \psi_M \quad ;$$

$$F = 0 \quad , \quad \text{elsewhere} \quad . \tag{2.80}$$

The various parameters needed to make use of Eq. 2.13 can be calculated in a straightforward manner. From Fig. 2.8 we have

$$\bar{v} = |v| \, (\cos \psi \, \bar{x} + \sin \psi \, \bar{y}) \quad , \tag{2.81}$$

and hence

$$\bar{v}_o = \frac{1}{\rho_o} \int_{-\psi_M}^{\psi_M} \bar{v} \, F d\psi$$

$$= |v| \, \frac{\sin \psi_M}{\psi_M} \, \bar{x} \quad . \tag{2.82}$$

Similarly,

$$u_x = |v| \cos \psi - v_{ox}$$

$$= |v| \left(\cos \psi - \frac{\sin \psi_M}{\psi_M} \right) \quad , \tag{2.83}$$

and

$$\widehat{u_x^2} = \frac{1}{\rho_o} \int_{-\psi_M}^{\psi_M} u_x^2 \, F d\psi$$

$$= \frac{|v^2|}{2\psi_M} \left(\psi_M - \frac{2 \sin^2 \psi_M}{\psi_M} + \frac{\sin 2\psi_M}{2} \right)$$

$$= \frac{v_{ox}^2}{2} \left[\left(\frac{\psi_M}{\sin \psi_M} \right)^2 + \psi_M \cot \psi_M - 2 \right] \quad . \tag{2.84}$$

From Fig. 2.8 we have

$$u_y = |v| \sin \psi \quad , \tag{2.85}$$

and hence

$$\widehat{u_y^2} = \frac{1}{\rho_o} \int_{-\psi_M}^{\psi_M} u_y^2 \, F d\psi$$

$$= \frac{|v^2|}{2\psi_M} \left(\psi_M - \frac{\sin 2\psi_M}{2} \right)$$

$$= \frac{v_{ox}^2}{2} \left[\left(\frac{\psi_M}{\sin \psi_M} \right)^2 - \psi_M \cot \psi_M \right] \quad . \qquad (2.86)$$

From the conservation of energy requirement averaged over the stream (Eq. 2.57), it follows that

$$\frac{2q}{m} \phi = \left(v_{ox} \frac{\psi_M}{\sin \psi_M} \right)^2 \quad . \qquad (2.87)$$

Because of the symmetry of the distribution function, the off-diagonal terms of the pressure tensor, $\widehat{u_x u_y}$, are identically zero. Substitution of the above quantities in the equation of motion, Eq. 2.13, gives

$$\omega_p^2 - \omega_c \frac{\partial v_{ox}}{\partial y} = \frac{\partial}{\partial y} \left[\frac{1}{\omega_p^2} \frac{\partial}{\partial y} (\omega_p^2 \widehat{u_y^2}) \right] \quad , \qquad (2.88)$$

where ω_p^2 and ω_c are defined in the same manner as before (Eq. 2.53). One more relation between the various stream parameters is provided by Poisson's equation

$$\frac{2q}{m} \frac{\partial^2 \phi}{\partial y^2} = 2 \omega_p^2 \quad . \qquad (2.89)$$

Equations 2.86, 2.87, 2.88, and 2.89 form a set of equations which can, at least in principle, be solved for v_{ox}^2 and ω_p^2. In this connection it should be noted that the spatial variation of ψ_M is assumed to have been given, although such a specification has not yet actually been made.

In general, solving the above set of equations involves the study of nonlinear differential equations with variable coefficients. To avoid this complication in the present illustration, we shall again make use of the technique practiced in the previous two sections. We assume the following forms for ω_p^2 and v_{ox}

$$\omega_p^2 = \text{constant} \tag{2.90a}$$

$$v_{ox} = \Omega y \quad , \tag{2.90b}$$

and solve for the form of ψ_M necessary to satisfy Eqs. 2.86 and 2.89. Substituting from Eqs. 2.86, 2.87, and 2.88 into Eq. 2.89, we obtain

$$\begin{aligned} \frac{\partial^2 \widehat{u_y^2}}{\partial y^2} &= \omega_p^2 - \omega_c \Omega \\ &= \frac{\partial^2}{\partial y^2}\left[\frac{1}{2}\left(\frac{v_{ox}\psi_M}{\sin\psi_M}\right)^2 - \frac{v_{ox}^2}{2}\ \psi_M \cot \psi_M\right] \\ &= \omega_p^2 - \frac{\partial^2}{\partial y^2}\left[\frac{v_{ox}^2}{2}\ \psi_M \cot \psi_M\right] \quad . \end{aligned} \tag{2.91}$$

Therefore

$$\frac{\partial^2}{\partial y^2}\left[\frac{v_{ox}^2}{2}\ \psi_M \cot \psi_M\right] = \omega_c \Omega \quad . \tag{2.92}$$

The bracketed quantity in Eq. 2.92 is seen to be a quadratic function of y. The constants of integration are determined from the condition that both $\widehat{u_x^2}$ and $\widehat{u_y^2}$ vanish on the stream boundaries. (See Eq. 2.50.) Equations 2.84 and 2.86 show that this requirement is equivalent to the requirement that ψ_M be zero on the stream boundaries. Applying these conditions to the solution of Eq. 2.92 we obtain

$$\psi_M \cot \psi_M = 1 + \left(\frac{\omega_c}{\Omega} - 1\right) \frac{(y-a)(y-b)}{y^2} \quad . \tag{2.93}$$

Alternatively, we can substitute Eq. 2.92 into Eq. 2.91 to obtain the equation

$$\frac{\partial^2}{\partial y^2}\left[\frac{1}{2}\left(\frac{v_{ox}\psi_M}{\sin\psi_M}\right)^2\right] = \omega_p^2 \quad . \tag{2.94}$$

The solution of Eq. 2.94, subject to the boundary conditions on ψ_M, is

$$\left(\frac{\psi_M}{\sin\psi_M}\right)^2 = 1 + \left(\frac{\omega_p^2}{r^2} - 1\right)^2 \frac{(y-a)(y-b)}{y^2} \quad . \tag{2.95}$$

On substituting Eq. 2.93 and Eq. 2.95 into the trigonometric identity

$$\psi_M^2 = \left(\frac{\psi_M}{\sin\psi_M}\right)^2 - (\psi_M \cot \psi_M)^2 \quad , \tag{2.96}$$

we obtain

$$\psi_M^2 = \frac{(y-a)(y-b)}{y^2}\left\{\frac{\omega_p^2-\omega_c^2}{\Omega^2} + \left[\frac{\omega_c}{\Omega}-1\right]^2\left[1 - \frac{(y-a)(y-b)}{y^2}\right]\right\} \quad . \tag{2.97}$$

Evaluating $\widehat{u_x^2}$, $\widehat{u_y^2}$ and ϕ as functions of y, we have

$$\widehat{u_x^2} = \frac{1}{2}(\omega_p^2 + \omega_c\Omega - 2\Omega^2)(y-a)(y-b) \quad , \tag{2.98a}$$

$$\widehat{u_y^2} = \frac{1}{2}(\omega_p^2 - \omega_c\Omega)(y-a)(y-b) \quad , \tag{2.98b}$$

$$\frac{2q}{m}\phi = (\omega_p^2 - \Omega^2)(y-a)(y-b) + v_{ox}^2 \quad . \tag{2.98c}$$

These are, of course, the equations obtained previously, since the stream model is the same as before. However, there is now available at least one distribution function which produces the flow. We are, therefore, in a better position from which to consider, for example, perturbations from the d-c flow and the effects of the pressure tensor on the perturbations.

2.8. Application of the D-C Stream Models

The purpose of this chapter, and the succeeding one, is to gain an understanding of some of the types of interaction which can occur between electrons. Certain of the d-c stream models discussed in this chapter, namely those which are mathematically relatively simple, are used in the next chapter to study wave propagation on electron streams.

CHAPTER III. WAVE PROPAGATION ON ELECTRON BEAMS

3.1 Summary

The subject matter which is discussed in this chapter is a study of general conditions under which perturbations propagate in idealized systems consisting of streams of electrons flowing in uniformly bounded media under the influence of electric and magnetic force fields.

The predominating internal stream forces are assumed to be the smoothed-out Coulomb interactions between the charged particles, and the stream flow is described in terms of the hydrodynamic analogy discussed in Chapter II.

The use of the word "perturbations" above implies a restriction of any stream disturbance to an amplitude small compared to the average motion of the stream; this restriction is stated more rigorously in the course of the discussion.

The motivation for a small-signal, greatly oversimplified theory is the hope that the results, after comparison with experimental data, may make it possible to reach a better qualitative understanding of realizable systems.

3.2 Equations of Perturbed Laminar Stream Motion

We consider, because of their relative mathematical simplicity, perturbations of laminar electron streams.

The mathematical description of the d-c stream motion is then given in terms of the Lorentz forces and Maxwell's equations[16];

$$-\frac{q}{m}\left[\bar{E}_o + \bar{v}_o \times \bar{B}_o\right] = \frac{d\bar{v}_o}{dt} \quad , \tag{3.1}$$

and

$$\nabla \times \bar{E}_o = \frac{\partial \bar{B}_o}{\partial t} , \tag{3.2a}$$

$$\nabla \times \frac{\bar{B}_o}{\mu_o} = \bar{J}_o + \epsilon_o \frac{\partial \bar{E}_o}{\partial t} , \tag{3.2b}$$

$$\nabla \cdot \bar{B}_o = 0 , \tag{3.2c}$$

$$\nabla \cdot \bar{E}_o = \rho_o/\epsilon_o , \tag{3.2d}$$

$$\nabla \cdot \bar{J}_o + \epsilon_o \frac{\partial \rho_o}{\partial t} = 0 , \tag{3.2e}$$

where

$\bar{E}_o$ = electric field intensity,

$\bar{B}_o$ = magnetic flux density,

$\bar{J}_o$ = convection current density = $\rho_o v_o$,

ρ_o = space-charge density,

$\bar{v}_o$ = stream velocity,

q/m = charge-to-mass ratio of the particles comprising the stream (a positive quantity for electrons), and

ϵ_o, μ_o = permittivity and magnetic permeability of free space, respectively.

Equations 3.2, while not all independent, are often used forms of the basic equations. The subscript zeros refer to the assumed basic d-c stream ($\partial/\partial t = 0$) satisfying Eqs. 3.1 and 3.2.

A perturbation, or departure of the stream from d-c flow, is characterized by its appropriate symbol with the subscript one. Because of their linearity, Maxwell's equations are satisfied by the perturbation quantities alone. Equations 3.2, with subscripts one, may, therefore,

be used to describe the perturbation. The equation of motion, Eq. 3.1, becomes

$$-\frac{q}{m}\left[\bar{E}_1 + \bar{v}_1 \times \bar{B}_0\right] = \frac{\partial \bar{v}_1}{\partial t} + (\bar{v}_0 \cdot \nabla)\bar{v}_1 + (\bar{v}_1 \cdot \nabla)\bar{v}_0 \qquad (3.3)$$

under the conventional assumptions

$$(\bar{v}_0 + \bar{v}_1) \times (\bar{B}_0 + \bar{B}_1) \cong \bar{v}_1 \times \bar{B}_0 + \bar{v} \times \bar{B}_0 \ , \qquad (3.4a)$$

$$[(\bar{v}_0 + \bar{v}_1) \cdot \nabla](\bar{v}_0 + \bar{v}_1) \cong (\bar{v}_0 \cdot \nabla)\bar{v}_1 + (\bar{v}_1 \cdot \nabla)\bar{v}_0 + (\bar{v}_0 \cdot \nabla)\bar{v}_0 \ . \qquad (3.4b)$$

The first assumption neglects the force effect of the perturbed magnetic field in comparison with the force due to the perturbed electric field. The second assumption neglects the change of the perturbed velocity due to the perturbation of the position at which the velocity is evaluated.

The perturbed current density, subject to similar linearizing assumptions, is

$$\bar{J}_1 = \rho_0 \bar{v}_1 + \rho_1 \bar{v}_0 \ . \qquad (3.5)$$

3.3 Perturbations of an Electron Plasma

3.3.1 Plasma-Stream Perturbations in the Absence of a Magnetic Field.[17]

A particularly simple model to analyze is one wherein the d-c stream has a single uniform velocity component, v_{0x}, constrained to the direction of axial uniformity. Such a model can be envisioned physically in terms of a completely neutralized plasma-stream. The plasma is supposed to consist of superimposed streams of ions and electrons of the same charge density. The charge-to-mass ratio of the ion stream, however, is assumed to be sufficiently small that the ions do not participate significantly in the perturbation: they simply neutralize the electric field of the d-c electron stream.

The simultaneous satisfaction of Maxwell's equations and the equation of motion leads, after appropriate mathematical manipulations, to the wave equation. In the present instance, this will be a linear differential equation with constant coefficients having simple exponential solutions. Advantage can be taken of this hindsight by initially assuming (and subsequently verifying) a solution of the form exp $j(\omega t - \alpha x - \beta y - \gamma z)$, where α, β, and γ are constants (wave numbers along the coordinate axes).

It is also convenient in discussing the equations of motion to observe the motion in a coordinate system traveling with the average stream motion. Such a transformation is implied by the substitution for

$$\frac{d}{dt} = \frac{\partial}{\partial t} + (\bar{v}_o \cdot \nabla) \quad \text{of} \quad \frac{d}{dt} = j(\omega - \alpha v_{ox}) \tag{3.6}$$

(in the stationary reference) (in the moving reference)

In the moving coordinate system the equation of motion becomes, assuming that no static magnetic field is present,

$$\omega_p^2 \, \epsilon_o \, \bar{E}_1 = j \, \omega_d \, \bar{J}_1 \, , \tag{3.7}$$

where

$$\bar{J}_1 = \rho_o \bar{v}_1 = \text{convection current density as seen in the moving reference frame,} \tag{3.8a}$$

$$\omega_p^2 = -\frac{q\rho_o}{m\epsilon_o} = \text{electron density (plasma) radian frequency, and} \tag{3.8b}$$

$$\omega_d = \omega - \alpha v_{ox} = \text{Doppler frequency, i.e., the frequency of the perturbation as seen by an observer in the moving coordinate system.} \tag{3.8c}$$

The equation of continuity, as seen in the moving coordinate system, is

$$\nabla \cdot \bar{J}_1 + j \, \omega_d \, \rho_1 = 0 \, . \tag{3.9}$$

Taking the divergence of Eq. 3.7 and substituting Eq. 3.9 we obtain

$$(\omega_p^2 - \omega_d^2)\rho_1 = 0 \quad , \tag{3.10}$$

corresponding to two possible modes of propagation

$$\omega_p^2 - \omega_d^2 = 0 \quad , \text{ [space-charge waves]} \tag{3.11a}$$

and

$$\rho_1 = 0 \qquad \text{[solenoidal waves]} \quad . \tag{3.11b}$$

The waves described by Eq. 3.11a have no net current density associated with them; i.e.,

$$\bar{J}_1 + j\,\omega_d\,\epsilon_o\,\bar{E}_1 = 0 \quad . \tag{3.12}$$

Hence $\nabla \times \bar{B}_1 = 0$ and, since no external magnetic fields have been postulated, there is no magnetic field associated with these waves. The energies involved in the perturbation alternate between the perturbed electric field and the perturbed velocity of the space charge; it is noted that

$$\frac{\text{peak electric energy storage}}{\text{peak kinetic energy storage}} = \frac{\frac{1}{2}\,\omega_d^2 |\bar{E}_1| \cdot |\bar{E}_1|}{\frac{1}{2}\,|\bar{J}_1| \cdot |\bar{E}_1|} = 1 \quad . \tag{3.13}$$

In the simplified model described above there is no convection of momentum from one region of the plasma to another. A more detailed model including a thermal velocity fluctuation accounts for such a convection coupling adjacent regions of the plasma and organizing the plasma oscillation. (In this connection, note that the group velocity is $\partial\omega/\partial\alpha = v_{ox}$; i.e., energy is transported by the average stream motion.) The effect on the dispersion relation, Eq. 3.11a, is negligible for present purposes except to provide a basis for assuming that the plasma vibrates as an organized unit.

Waves of the type given by Eq. 3.11b correspond to electromagnetic propagation as distinguished from the electrokinetic propagation described

above, and are characterized by the absence of any perturbed space-charge density in the stream; i.e., there is no bunching. For the solenoidal waves, one obtains from Maxwell's equations,

$$\begin{aligned} \nabla \times (\nabla \times \bar{E}_1) &= -\nabla^2 \bar{E}_1 = -j\omega_d \nabla \times B_1 \\ &= -j\omega_d \mu_o (\bar{J}_1 + j\omega_d \epsilon_o \bar{E}_1) \\ &= \mu_o \epsilon_o (\omega_d^2 - \omega_p^2)\bar{E}_1 \quad . \end{aligned} \tag{3.14}$$

Substituting the exponential form of the perturbation into Eq. 3.14 gives

$$\alpha^2 + \beta^2 + \gamma^2 + (\omega_p^2 - \omega_d^2)\mu_o\epsilon_o = 0 \quad . \tag{3.15}$$

Note should be taken of the special case of Eq. 3.15 which occurs when $\omega_p^2 - \omega_d^2 = 0$. This particular wave, for which the electric field is both solenoidal and irrotational, will subsequently be of interest.

Substituting appropriately, we have

$$\frac{\text{peak kinetic energy storage}}{\text{peak electric energy storage}} = \frac{|\bar{J}_1| \cdot |\bar{E}_1|}{\omega_d \epsilon_o |\bar{E}_1| \cdot |\bar{E}_1|} = \frac{\omega_p^2}{\omega_d^2} \quad . \tag{3.16}$$

The energy storage in the magnetic field is

$$\text{peak magnetic energy storage} = \frac{\omega_d}{\mu_o} |\bar{B}_1| \cdot |\bar{B}_1| = \left| 1 - \frac{\omega_p^2}{\omega_d^2} \right| \omega_d \epsilon_o |\bar{E}_1| \cdot |\bar{E}_1| \quad . \tag{3.17}$$

The propagation can, if convenient, be regarded as occurring in a medium of permittivity ϵ_o', where

$$\epsilon_o' = \left(1 - \frac{\omega_p^2}{\omega_d^2}\right) \epsilon_o \quad . \tag{3.18}$$

The energy of the electric field is greater than that of the magnetic field, with a fraction $1 - \frac{\omega_p^2}{\omega_d^2}$ contributing to the electromagnetic fields and a fraction $\frac{\omega_p^2}{\omega_d^2}$ bound to the kinetic energy of the charge.

3.3.2 Plasma Perturbation in Rectangular Coordinates. Figure 3.1 relates a Cartesian coordinate system to the geometry to be studied. Between two plane parallel admittance sheets at y = a, y = -d, a neutralized stream of electrons occupies the volume bounded by the planes y = ±h. The stream has a uniform velocity v_{ox} in the direction of the $\bar{x}$ axis.

We consider first the space-charge waves described by Eq. 3.11a, i.e., those satisfying the dispersion relation $\omega_p^2 - \omega_d^2 = 0$. Since these waves have no electromagnetic energy associated with them, it is to be expected that their influence will be restricted to the interior of the stream. The lateral boundary problem associated with the stream illustrated by Fig. 3.1 is shown in Fig. 3.2.

The boundary ripple produced by the perturbation of the space-charge density is considered to be equivalent to an alternately positive and negative charge representing the net effect of the perturbed electrons and the immobile ions. If the wavelength associated with the perturbation is considerably greater than the maximum deviation of the charge from the unperturbed stream boundary, the net effect may be regarded, to a first-order approximation, as an equivalent surface-charge density. This is the well-known approximation introduced by Hahn[18]. The height of the ripple, calculated to the first order, is

$$\Delta y = \int v_{1y} dt = \frac{v_{1y}}{j\omega_d} . \qquad (3.19)$$

The surface-charge density, corresponding to the charge enclosed under the ripple, is

$$\sigma_1 = \pm \rho_o \Delta y = \pm \frac{\rho_o v_{1y}}{j\omega_d} = \mp \epsilon_o \frac{\omega_p^2}{\omega_d^2} E_{1y} = \mp \epsilon_o E_{1y} . \qquad (3.20)$$

The surface-charge density is + $\rho_o \Delta y$ on the upper boundary, where a pos-

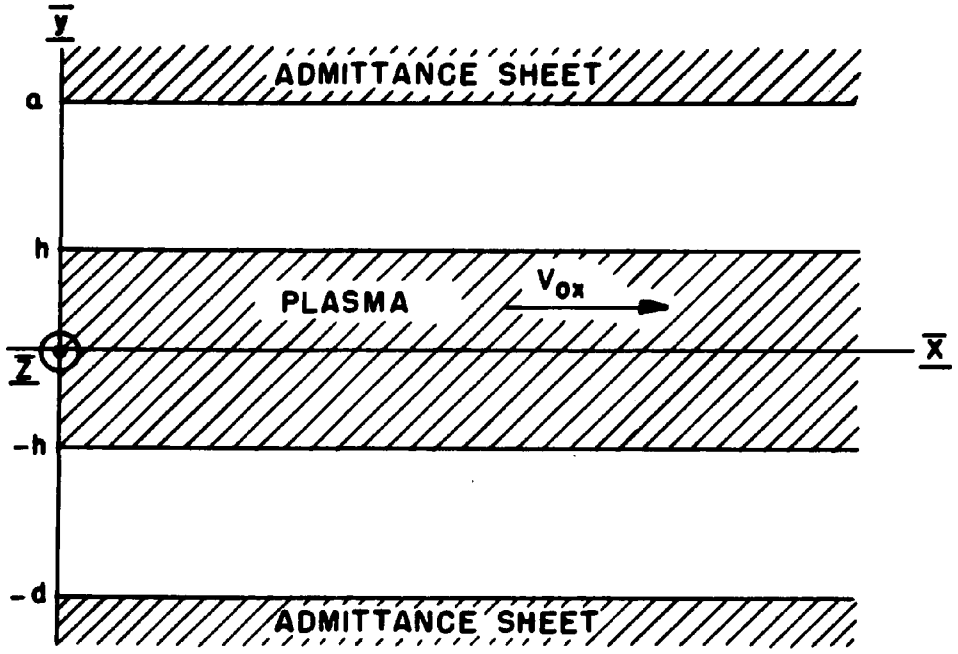


FIG. 3.1 GEOMETRY OF PLASMA PERTURBATION DESCRIBED IN SECTION 3.2.2.

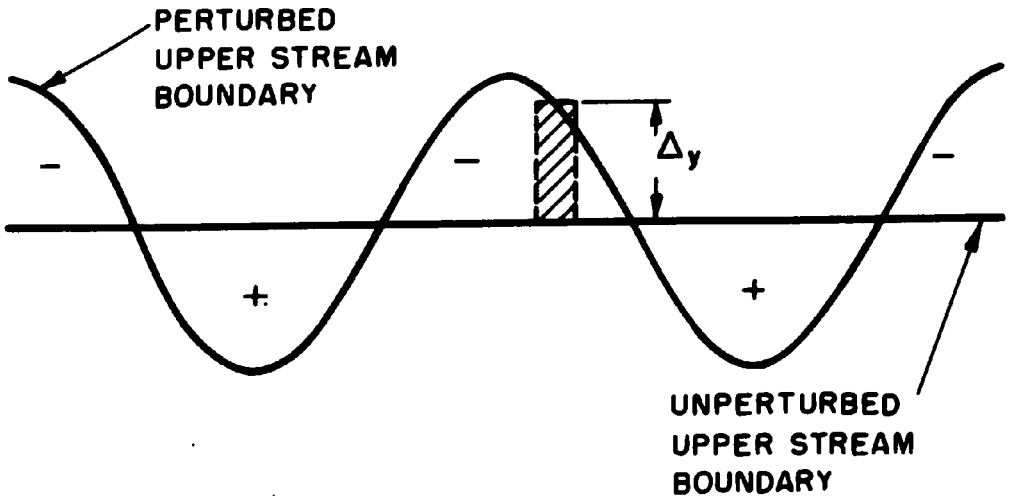


FIG. 3.2 SKETCH OF BOUNDARY PERTURBATION FOR STREAM OF FIG. 3.1.

itive perturbation of an electron's position carries it outside the stream, and hence produces an accumulation of charge. On the lower stream boundary, a positive perturbation of an electron's position carries it further into the stream, leaving behind a deficiency of charge. The surface-charge density corresponding to this decrease is therefore $-\rho_o \Delta y$.

The fields are evaluated at the unperturbed boundary position. Equation 3.20 shows that the boundary ripple terminates the internal electric field normal to the stream boundary. From the Gauss theorem it follows that the tangential field outside the stream boundary is also zero. This tangential field must be continuous across the stream boundary. In general, the space-charge waves do not have zero tangential fields at the stream boundaries. However, the continuity of any tangential component of the field at the boundary can be assured by use of that particular space-charge wave, described in connection with Eq. 3.15, whose electric field is also solenoidal. The component of this space-charge wave normal to the boundary is matched by the ripple corresponding to it, and the wave has no space charge associated with it. Its tangential component may therefore be chosen arbitrarily to satisfy any tangential boundary conditions. The presence or absence of any boundary external to the stream, therefore, does not influence the propagation of the space-charge waves. This conclusion is not restricted to the simplified geometry for which it is illustrated; it depends only on the absence of any net current in the stream ($\bar{J}_1 + j\omega_d \epsilon_o \bar{E}_1 = 0$).

The electromagnetic waves satisfying the dispersion relationship Eq. 3.15b, are, however, intimately affected by external boundaries. Consider a TM wave propagating parallel to the $\underline{x}$ axis with a phase velocity much smaller than that of light. Therefore

$$\underline{z} \cdot \nabla \times \bar{E}_1 \cong 0 \quad . \tag{3.21}$$

The impedance sheets are represented by their respective normalized transverse electric fields

$$Y = \frac{E_{1y}}{E_{1x}} \quad . \tag{3.22}$$

Since the waves considered are solenoidal in the entire space we have

$$\bar{y} \cdot \nabla \times \frac{\bar{B}_1}{\mu_o} = -\frac{\partial}{\partial x}\left(\frac{B_{1z}}{\mu_o}\right) = j\alpha \frac{B_{1z}}{\mu_o} = j\omega\epsilon_o E_{1y} \quad . \tag{3.23}$$

Therefore, the quantity Y is equal to the normalized E mode admittance,

$$Y = \frac{\alpha}{\omega\mu_o\epsilon_o} \frac{B_{1z}}{E_{1x}} \quad . \tag{3.24}$$

In rectangular coordinates, the normalized admittance of the plane at $y = a$, as seen at the plane $y = h$, is given by

$$j\, Y_h = \frac{j\, Y_a + \tanh \alpha(a-h)}{1 + j\, Y_a \tanh \alpha(a-h)} \quad . \tag{3.25}$$

The stream boundary-ripple is replaced by an equivalent normalized surface-charge density in the manner previously described;

$$\frac{\sigma_1}{\epsilon_o E_{1x}} = \pm \frac{\omega_p^2}{\omega_d^2} \frac{E_{1y}}{E_{1x}} \quad . \tag{3.26}$$

As noted previously, the ± sign corresponds to the fact that a positive perturbation of charge position on the upper side of the stream is indicative of the presence of charge, whereas on the lower stream boundary it corresponds to the absence of charge. Matching admittances at the stream boundaries, we obtain

$$Y^e_{\pm h} = Y^i_{\pm h}\left(1 - \frac{\omega_p^2}{\omega_d^2}\right) \quad , \tag{3.27}$$

where the superscript indicates the quantity is to be evaluated on the external or internal side of the stream boundary, respectively.

It is interesting to consider Eq. 3.27 in the special case of a symmetrical external admittance arrangement, i.e.,

$$Y_h^e = -Y_{-h}^e = K \quad . \tag{3.28}$$

For such a symmetrical arrangement the internal stream admittances on the boundaries can differ only by a phase shift, so that they may be described as

$$Y_h^i = A \exp(j\theta) \quad , \tag{3.29a}$$

$$Y_{-h}^i = A \exp(-j\theta) \quad . \tag{3.29b}$$

From the sum and difference of Eqs. 3.29, making use of Eqs. 3.27 and 3.28, we obtain

$$A\left(1 - \frac{\omega_p^2}{\omega_d^2}\right)\cos\theta = 0 \quad , \tag{3.30a}$$

$$A\left(1 - \frac{\omega_p^2}{\omega_d^2}\right)\sin\theta = -jK \quad . \tag{3.30b}$$

Equations 3.30 admit of two types of solutions,

$$1 - \frac{\omega_p^2}{\omega_d^2} = 0 \; ; \qquad K = 0 \quad , \tag{3.31a}$$

$$\theta = (2N+1)\pi/2 \; ; \qquad A = \frac{\pm jK}{1 - \dfrac{\omega_p^2}{\omega_d^2}} \quad , \tag{3.31b}$$

where N is any integer.

The first solution is the space-charge solution previously discussed. In general, θ can have an arbitrary value. However, it is convenient to assume the transverse field to be expanded in terms of orthogonal trigonometric functions. We can then, with complete generality, regard θ as some integral multiple of π radians. The second solution corresponds to

the propagation of solenoidal waves; the internal admittances at the stream boundaries differ only by an odd multiple of π radians in phase. Figure 3.3 illustrates the appearance of the perturbed stream for the two solutions.

In the more general case, corresponding to the geometry of Fig. 3.1, the compatibility of Eqs. 3.25 and 3.27 requires

$$\frac{\omega_p^2}{\omega_d^2} - 1 = j \frac{Y_h - Y_{-h}}{2 \tanh 2\alpha h} \left(1 \pm \sqrt{1 + \frac{4\, Y_h\, Y_{-h}}{(Y_h - Y_{-h})^2} \tanh^2 2\alpha h} \right) . \quad (3.32)$$

For the special case considered above where $Y_h^e = -Y_{-h}^e = K$, Eq. 3.32 reduces to

$$\frac{\omega_p^2}{\omega_d^2} - 1 = jK \frac{\sinh 2\alpha h}{\cosh 2\alpha h \pm 1} = jK \frac{\cosh 2\alpha h \mp 1}{\sinh 2\alpha h} . \quad (3.33)$$

If the admittance sheets are removed, i.e., if the stream is bounded by free space so that $Y_{\pm h} = \mp j$, the appropriate dispersion relation is

$$\frac{\omega_p^2}{\omega_d^2} - 1 = \frac{\sinh 2\alpha h}{\cosh 2\alpha h \pm 1} = \frac{\cosh 2\alpha h \mp 1}{\sinh 2\alpha h} . \quad (3.34)$$

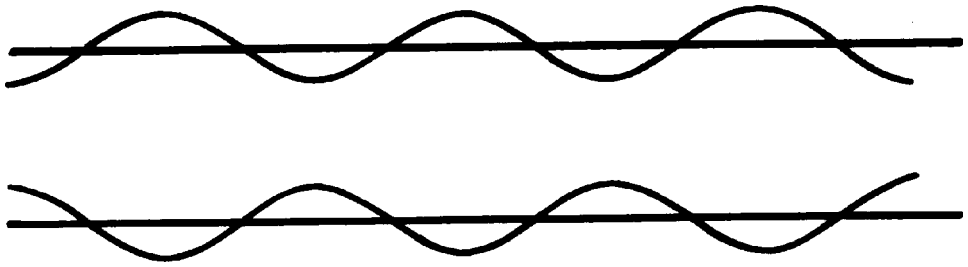
For "thick" streams ($2\alpha h \gg 0$) Eq. 3.34 reduces to

$$\frac{\omega_p^2}{1 + \coth 2\alpha h} - \omega_d^2 = 0 . \quad (3.35)$$

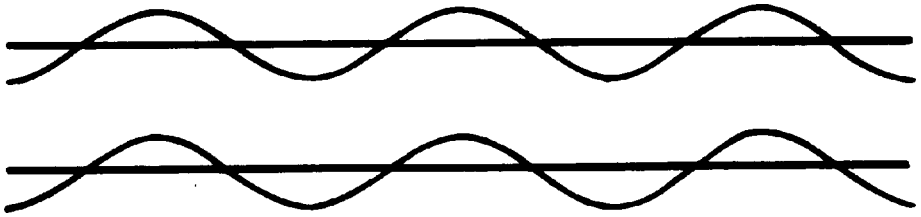
If the admittance sheets are perfectly conducting planes located at $y = \pm d$ respectively, then $Y_{\pm h}^e = \mp j \coth \alpha(d-h)$, and for "thick" streams the dispersion relation is

$$\frac{\omega_p^2}{1 + \coth \alpha(d-h) \coth 2\alpha h} - \omega_d^2 = 0 . \quad (3.36)$$

Since the normalized boundary charge perturbation is proportional to $\frac{\omega_p^2}{\omega_d^2}$, the effect of the conducting planes is seen to be one of increas-



SPACE-CHARGE WAVE PROPAGATION, $\omega_p^2 = \omega_d^2$.
(θ = EVEN MULTIPLE OF π)



SOLENOIDAL WAVE PROPAGATION, $\rho_1 = 0$
SPACE-CHARGE WAVE PROPAGATION, $\omega_p^2 = \omega_d^2$.
(θ = ODD MULTIPLE OF π)

FIG. 3.3 ILLUSTRATION OF PLASMA CONFIGURATIONS FOR THE TWO TYPES OF WAVE PROPAGATION.
—— UNPERTURBED STREAM BOUNDARY
PERTURBED STREAM BOUNDARY

ing the perturbation as the planes are brought closer to the stream. This effect can be visualized physically in terms of the image forces of the stream boundary-ripple in the conducting planes.

Equation 3.34 indicates that the stream by itself propagates an unamplified disturbance, a not unexpected result since, in the plasma system described, the disturbance is not coupled to any energy source.

3.3.3 Mutual Interaction of a Binary Plasma System. The possibilities of the mutual interaction between plasmas of different characteristics have been described by Haeff[15]. The model considered is that of two plasmas, whose characteristics are distinguished by subscripts a and b, occupying the same volume and mutually coupled through their common electric field. In view of the linearization of the equations of motion we have

$$\omega_{pa}^2 \epsilon_o \bar{E}_1 = j \omega_{da} \rho_{oa} \bar{v}_{1a} , \tag{3.37a}$$

$$\omega_{pb}^2 \epsilon_o \bar{E}_1 = j \omega_{db} \rho_{ob} \bar{v}_{1b} . \tag{3.37b}$$

From the equation of continuity we have

$$\nabla \cdot (\rho_{oa} \bar{v}_{1a} + \rho_{ob} \bar{v}_{1b}) = - j\omega_{da} \rho_{1a} - j\omega_{db} \rho_{1b} . \tag{3.38}$$

Noting that

$$\epsilon_o \nabla \cdot \bar{E}_1 = \rho_{1a} + \rho_{1b} , \tag{3.39}$$

we obtain, on substitution into Eq. 3-37,

$$\omega_{pa}^2 (\rho_{1a} + \rho_{1b}) = \omega_{da}^2 \rho_{1a} , \tag{3.40a}$$

$$\omega_{pb}^2 (\rho_{1a} + \rho_{1b}) = \omega_{db}^2 \rho_{1b} \tag{3.40b}$$

The compatibility of these homogeneous equations requires either of the

conditions

$$\frac{\omega_{pa}^2}{\omega_{da}^2} + \frac{\omega_{pb}^2}{\omega_{db}^2} = 1 \quad , \quad \begin{bmatrix}\text{space-charge} \\ \text{wave coupling}\end{bmatrix} \tag{3.41a}$$

$$\rho_{1a} = \rho_{1b} = 0 \quad , \quad \begin{bmatrix}\text{solenoidal} \\ \text{wave coupling}\end{bmatrix} \tag{3.41b}$$

corresponding in the first case to a coupling of space-charge waves and in the second case to a coupling, through the stream boundaries, of the solenoidal waves.

The coupling associated with the first case produces no fields external to the stream since the boundary-ripple equivalent charge density terminates the normal electric field; i.e.,

$$\sigma_1 = \pm\left(\frac{\rho_{oa}v_{1ya}}{j\omega_{da}} + \frac{\rho_{ob}v_{1yb}}{j\omega_{db}}\right) = \pm\left(\frac{\omega_{pa}^2}{\omega_{da}^2} + \frac{\omega_{pb}^2}{\omega_{db}^2}\right)\epsilon_o E_{1y} = \mp\,\epsilon_o E_{1y} \quad . \tag{3.42}$$

The continuity of the tangential electric fields at the stream boundaries can be assured in the same manner as described previously for the space-charge waves.

Figure 3.4 is a sketch of the nature of the variation of the two terms on the left of Eq. 3.41a as a function of the propagation constant α. This function goes to zero as α approaches $\pm\infty$ and has second-order poles at $\alpha = \beta_{ea} = \omega/v_{oxa}$ and $\alpha = \beta_{eb} = \omega/v_{oxb}$; the minimum between the poles is located at

$$\alpha = \frac{\beta_{pb}^{2/3}\,\beta_{ea} + \beta_{pa}^{2/3}\,\beta_{eb}}{\beta_{pb}^{2/3} + \beta_{pa}^{2/3}} \quad ,$$

where $\beta_{pa} = \omega_{pa}/v_{oxa}$ and $\beta_{pb} = \omega_{pb}/v_{oxb}$. The magnitude of this minimum is

$$\frac{\left[\beta_{pb}^{2/3} + \beta_{pa}^{2/3}\right]^3}{(\beta_{ea} - \beta_{eb})^2} \quad .$$

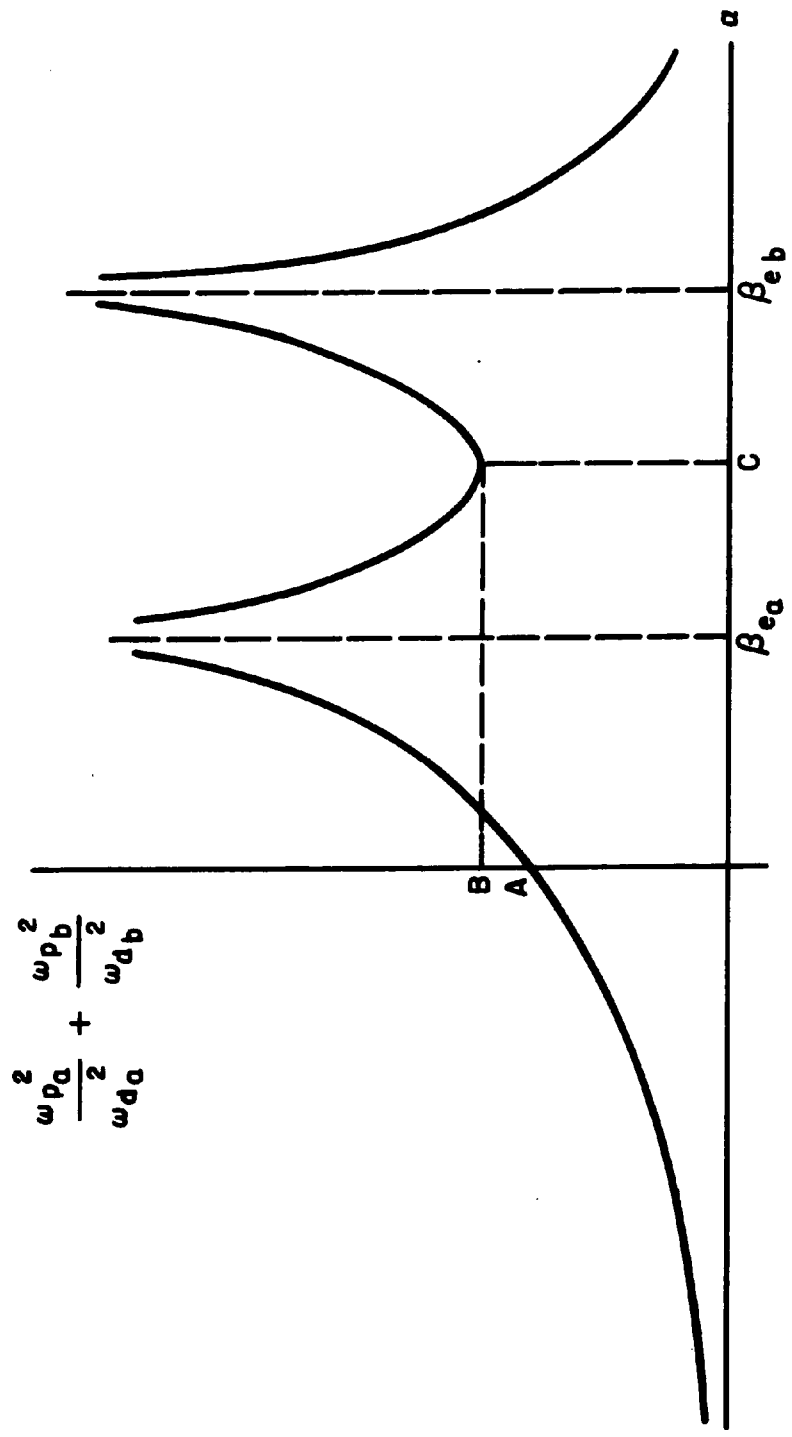


FIG. 3.4 SKETCH OF FUNCTION DISCUSSED IN RELATION TO EQUATION 3.41a

The intersections of the curve sketched in Fig. 3.4 and the ordinate unity determine the real roots of Eq. 3.41a. A pair of complex conjugate roots exist if the minimum between the poles is greater than unity, i.e., if

$$\frac{\left[\beta_{pa}^{2/3} + \beta_{pb}^{2/3}\right]^3}{(\beta_{ea} - \beta_{eb})^2} \geq 1 \quad . \tag{3.43}$$

Stated otherwise, complex roots exist in the frequency range

$$0 \leq \omega^2 \leq \frac{\left[(\omega_{pb}v_{oxa})^{2/3} + (\omega_{pa}v_{oxb})^{2/3}\right]^3}{(v_{ob} - v_{oa})^2} \quad . \tag{3.44}$$

It has been tacitly assumed that $v_{ob} - v_{oa} \neq 0$. For the degenerate case, the two poles merge, the "minimum" between the poles is infinite, and the corresponding complex roots vanish. The expressions above are symmetrical between the two plasmas so that if either plasma is stationary, e.g., $v_{ob} = 0$, the frequency range in which complex roots exist is $0 \leq \omega^2 \leq \omega_{pb}^2$, and the propagation constant is

$$\alpha = \beta_{ea} \pm j \frac{\beta_{pa}}{\sqrt{\frac{\omega_{pb}^2}{\omega^2} - 1}} \quad . \tag{3.45}$$

The intersection of the curve sketched in Fig. 3.4 with the abscissa $\alpha = 0$ occurs at

$$\left(\frac{\beta_{pa}}{\beta_{ea}}\right)^2 + \left(\frac{\beta_{pb}}{\beta_{eb}}\right)^2 = \frac{\omega_{pa}^2 + \omega_{pb}^2}{\omega^2} \quad . \tag{3.46}$$

If the value of this quantity exceeds unity one of the real roots of 3.40a occurs for negative α, which suggests a backward wave, i.e., one for which the phase and group velocities are in opposite directions. The group velocity, obtained by differentiating Eq. 3.41a, is

$$\frac{\partial\omega}{\partial\alpha} = \frac{\dfrac{\beta_{pa}^2}{(\beta_{ea}-\alpha)^2} + \dfrac{\beta_{pb}^2}{(\beta_{eb}-\alpha)^2}}{\dfrac{\beta_{pa}^2}{v_{oxa}(\beta_{ea}-\alpha)^3} + \dfrac{\beta_{pb}^2}{v_{oxb}(\beta_{eb}-\alpha)^3}} \quad . \tag{3.47}$$

For streams in the same direction, i.e., v_{oa} and $v_{ob} \geq 0$, the group velocity is positive for negative α. A special case, amenable to algebraic manipulation, occurs when $\beta_{pa} = \beta_{pb} \triangleq \beta_p$. For this case Eq. 3.41a can be written as

$$\frac{1}{\left(\dfrac{\beta_{pa}}{\beta_p} - \dfrac{\alpha}{\beta_p}\right)^2} + \frac{1}{\left(\dfrac{\beta_{eb}}{\beta_p} - \dfrac{\alpha}{\beta_p}\right)^2} = 1 \quad . \tag{3.48}$$

It is convenient to make use of the following variables:

$$\xi = \frac{1}{2}\left(\frac{\beta_{ea} + \beta_{eb}}{\beta_p}\right) - \frac{\alpha}{\beta_p} \quad , \tag{3.49a}$$

$$\zeta = \frac{1}{2}\left(\frac{\beta_{ea} - \beta_{eb}}{\beta_p}\right) \quad . \tag{3.49b}$$

Substitution of these variables in Eq. 3.48 yields

$$\xi^2 = 1 + \zeta^2 \pm \sqrt{1 + 4\zeta^2} \tag{3.50}$$

and hence

$$\frac{\alpha}{\beta_p} = \frac{\beta_{ea} + \beta_{eb}}{2\beta_p} \pm \sqrt{1 + \left(\frac{\beta_{ea}-\beta_{eb}}{2\beta_p}\right)^2} \pm \sqrt{1 + \left(\frac{\beta_{ea}-\beta_{eb}}{\beta_p}\right)^2} \quad . \tag{3.51}$$

Complex roots occur for $\left(\dfrac{\beta_{ea}-\beta_{eb}}{\beta_p}\right)^2 \leq 8$; i.e., there is a maximum velocity differential beyond which no gain occurs. It is convenient to define a velocity parameter, K, arbitrarily taken as greater than or equal to zero, as

$$\frac{v_{oxb} - v_{oxa}}{v_{oxa}} = \frac{\beta_{ea} - \beta_{eb}}{\beta_{eb}} = K \geq 0 \quad . \tag{3.52}$$

Using a superscript prime to denote normalization of a quantity with respect to β_p, we can write Eq. 3.51 in the form

$$\alpha' = \left(\frac{\beta'_{eb}K}{2}\right)\left(1 + \frac{2}{K}\right) \pm \sqrt{1 + \left(\frac{\beta'_{eb}K}{2}\right)^2 \pm \sqrt{1 + (\beta'_{eb}K)^2}} \,. \quad (3.53)$$

Figure 3.5 is a plot of the imaginary part of α' as a function of $\beta'_{eb}K$.

The coupling associated with the second case of Eq. 3.41, describing electromagnetic wave propagation, leads after matching the stream boundaries to free space, to the dispersion relation

$$\frac{\omega_{pa}^2}{\omega_{da}^2} + \frac{\omega_{pb}^2}{\omega_{db}^2} = 1 + \frac{\cosh 2\alpha h \pm 1}{\sinh 2\alpha h} \,. \quad (3.54)$$

The sketch of Fig. 3.4 applies to the equation above except that the real roots are determined by intersections with the more complicated function on the right of Eq. 3.54. For "thick" streams, i.e., $2\alpha h \gg 0$, Eq. 3.52 simplifies to

$$\frac{\omega_{pa}^2}{\omega_{da}^2} + \frac{\omega_{pb}^2}{\omega_{db}^2} \cong 2 \,. \quad (3.55)$$

Within the thick-stream approximation the previous discussion of space-charge waves carries over to the present case upon replacing the actual plasma frequencies involved with reduced, i.e., "effective," plasma frequencies equal to 0.707 the actual values. (Compare Eq. 3.41a with Eq. 3.55.)

Coupling between two plasmas does not require intermixing of the two streams. If the plasmas are spatially independent the coupling can occur through the solenoidal electromagnetic waves only and not by means of the space-charge waves. A simplified model describing such a coupling is illustrated in a succeeding section for plasmas in a uniform magnetic field.

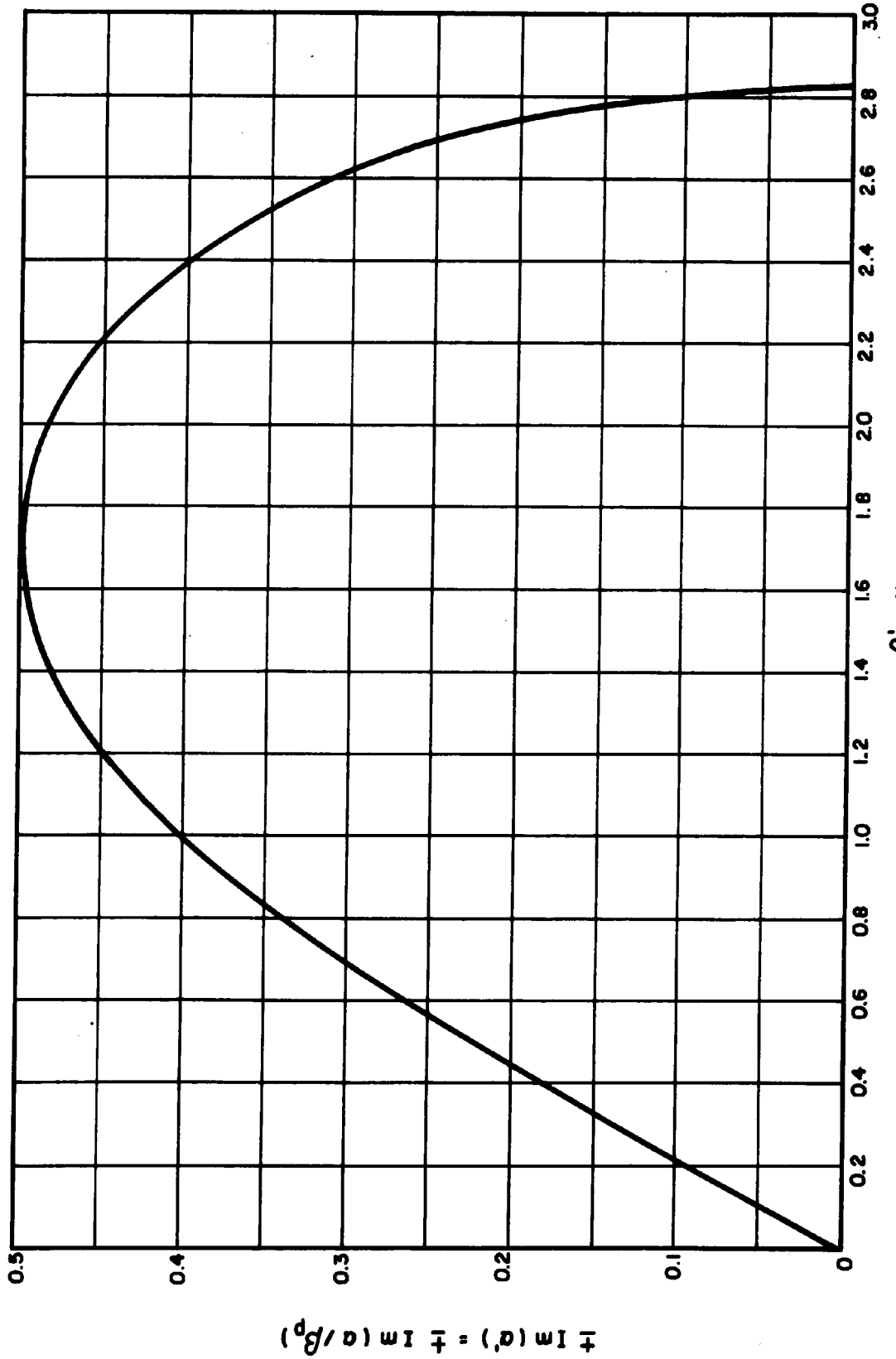


FIG. 3.5 GAIN CHARACTERISTIC FOR SPACE-CHARGE WAVE COUPLING IN A BINARY PLASMA SYSTEM.

3.3.4 Plasma Perturbation in a Static Magnetic Field. The discussion above has characterized an elementary plasma, viewed in an advancing frame of reference, as an isotropic elastic medium with a natural frequency given by the electron density frequency ω_p.

The introduction of a static magnetic field creates a spatial anisotropy by establishing an orientation of the plasma in space. The components of the velocity in a plane orthogonal to the magnetic field are coupled. This is reflected in the equation of motion, written in an advancing frame of reference,

$$\omega_p^2 \epsilon_o \bar{E}_1 = j\omega_d \bar{J}_1 - \omega_c \bar{J}_1 \times \underline{\bar{z}} \quad , \tag{3.56}$$

where $\omega_c = (q/m)B_o$ is the cyclotron frequency. The equation refers, for simplicity, to a plasma having a uniform charge density and a uniform velocity. The magnetic field B_o is parallel to the $\underline{\bar{z}}$ axis and directed negatively.

Equation 3.56 can be brought into a convenient form through the following manipulations. From the vector product of Eq. 3.56 with the unit vector $\underline{\bar{z}}$ we obtain

$$\omega_p^2 \epsilon_o \bar{E}_1 \times \underline{\bar{z}} = \omega_c \bar{J}_1 + j\omega_d \bar{J}_1 \times \underline{\bar{z}} - \omega_c J_{1z} \underline{\bar{z}} \, . \tag{3.57}$$

Elimination between the two equations formed by taking the divergence of Eqs. 3.56 and 3.57 leads to the relations

$$- \omega_c \underline{\bar{z}} \cdot \nabla \times \bar{J}_1 = \rho_1 (\omega_p^2 - \omega_d^2) \quad , \tag{3.58a}$$

$$- j\omega_d \rho_1 (\omega_p^2 + \omega_c^2 - \omega_d^2) = - \omega_c \omega_p^2 \epsilon_o \underline{\bar{z}} \cdot \nabla \times \bar{E}_1 + \omega_c^2 \frac{\partial J_{1z}}{\partial z} \, . \tag{3.58b}$$

From Maxwell's equations we have

$$\nabla \times \left(\nabla \times \frac{\bar{B}_1}{\mu_o} \right) = - \nabla^2 \frac{\bar{B}_1}{\mu_o} = \nabla \times \bar{J}_1 + j\omega_d \epsilon_o \nabla \times \bar{E}_1 = k^2 \frac{\bar{B}}{\mu_o} \, , \tag{3.59}$$

where the last expression is a consequence of the linearity of the equations and the uniform conditions assumed; k^2 is a constant equal to the sum of the squares of the propagation constants along the coordinate directions. Since

$$- j\omega_d B_{1z} = \underline{z} \cdot \nabla \times \bar{E}_1 \quad , \tag{3.60}$$

an equation relating $\underline{z} \cdot \nabla \times \bar{E}_1$ and $\underline{z} \cdot \nabla \times \bar{J}_1$ can be obtained from Eqs. 3.58 and 3.60. On substitution of this relation into Eq. 3.57a we obtain

$$\omega_c \left(j\omega_d + \frac{k^2}{j\omega_d \mu_o \epsilon_o} \right) \epsilon_o \, \underline{z} \cdot \nabla \times \bar{E}_1 = \rho_1 (\omega_p^2 - \omega_d^2) \quad . \tag{3.61}$$

On substitution of Eq. 3.61 into Eq. 3.57a we obtain

$$- j\omega_d \rho_1 \left\{ \left(1 - \frac{\omega_d^2}{\omega_p^2} \right) \left(1 + \frac{1}{\frac{k^2}{\omega_p^2 \mu_o \epsilon_o} - \frac{\omega_d^2}{\omega_p^2}} \right) + \frac{\omega_c^2}{\omega_p^2} \right\} = \frac{\omega_c^2}{\omega_p^2} \frac{\partial J_{1z}}{\partial z} \quad . \tag{3.62}$$

It will be noted that if the magnetic field vanishes the solutions reduce to those previously obtained. Also, in another limiting case, if propagation is confined to the $\underline{z}$ direction only, then, from the equation of continuity,

$$\frac{\partial J_{1z}}{\partial z} = - j\omega_d \rho_1 \quad . \tag{3.63}$$

Equation 3.62 then has the previously obtained solution for no magnetic field, since the magnetic field does not influence the motion in this case.

For simplicity we consider only propagation normal to the magnetic field ($\partial/\partial z = 0$), so that

$$\frac{\partial J_z}{\partial z} = 0 \quad . \tag{3.64}$$

Equation 3.62 indicates the solutions for this case to be

$$\left(1 - \frac{\omega_d^2}{\omega_p^2}\right)\left(1 + \frac{1}{\frac{k^2}{\omega_p^2\mu_o\epsilon_o} - \frac{\omega_d^2}{\omega_p^2}}\right) + \frac{\omega_c^2}{\omega_p^2} = 0 \quad , \tag{3.65a}$$

$$\rho_1 = 0 \quad . \tag{3.65b}$$

Substitution of the solution Eq. 3.65b into the wave equation

$$\nabla \times (\nabla \times \bar{E}_1) = -\nabla^2 \bar{E}_1 + \frac{\nabla\rho_1}{\epsilon_o} = -j\omega_d\mu_o (\bar{J}_1 + j\omega_d \epsilon_o \bar{E}_1) \quad . \tag{3.66}$$

leads to the dispersion relation

$$\frac{\omega_d^2}{\omega_p^2}\left\{1 + \frac{1}{\frac{k^2}{\omega_p^2\mu_o\epsilon_o} - \frac{\omega_d^2}{\omega_p^2}}\right\}^2 = \frac{\omega_c^2}{\omega_p^2} \quad . \tag{3.67}$$

Equation 3.65a is plotted in Fig. 3.6, which shows ω_d^2/ω_p^2 as a function of $k^2/\omega_p^2\mu_o\epsilon_o$. This figure may be interpreted as applying to a stationary plasma with the Doppler frequency ω_d as the perturbation frequency. For zero magnetic field ($\omega_c/\omega_p = 0$), Eq. 3.65a separates into the two independent solutions previously obtained,

$$\frac{\omega_d^2}{\omega_p^2} = 1 \tag{3.68a}$$

and

$$\frac{\omega_d^2}{\omega_p^2} = \frac{k^2}{\omega_p^2\mu_o\epsilon_o} + 1 \quad , \tag{3.68b}$$

which describe the longitudinal and transverse oscillations of the plasma. The effect of the magnetic field is to couple these oscillations, producing two branches to the dispersion relation corresponding to a modification of each type of oscillation. The two branches produced are asymptotic to the lines

$$\frac{\omega_d^2}{\omega_p^2} = \frac{k^2}{\omega_p^2\mu_o\epsilon_o} + 1 \tag{3.69a}$$

and

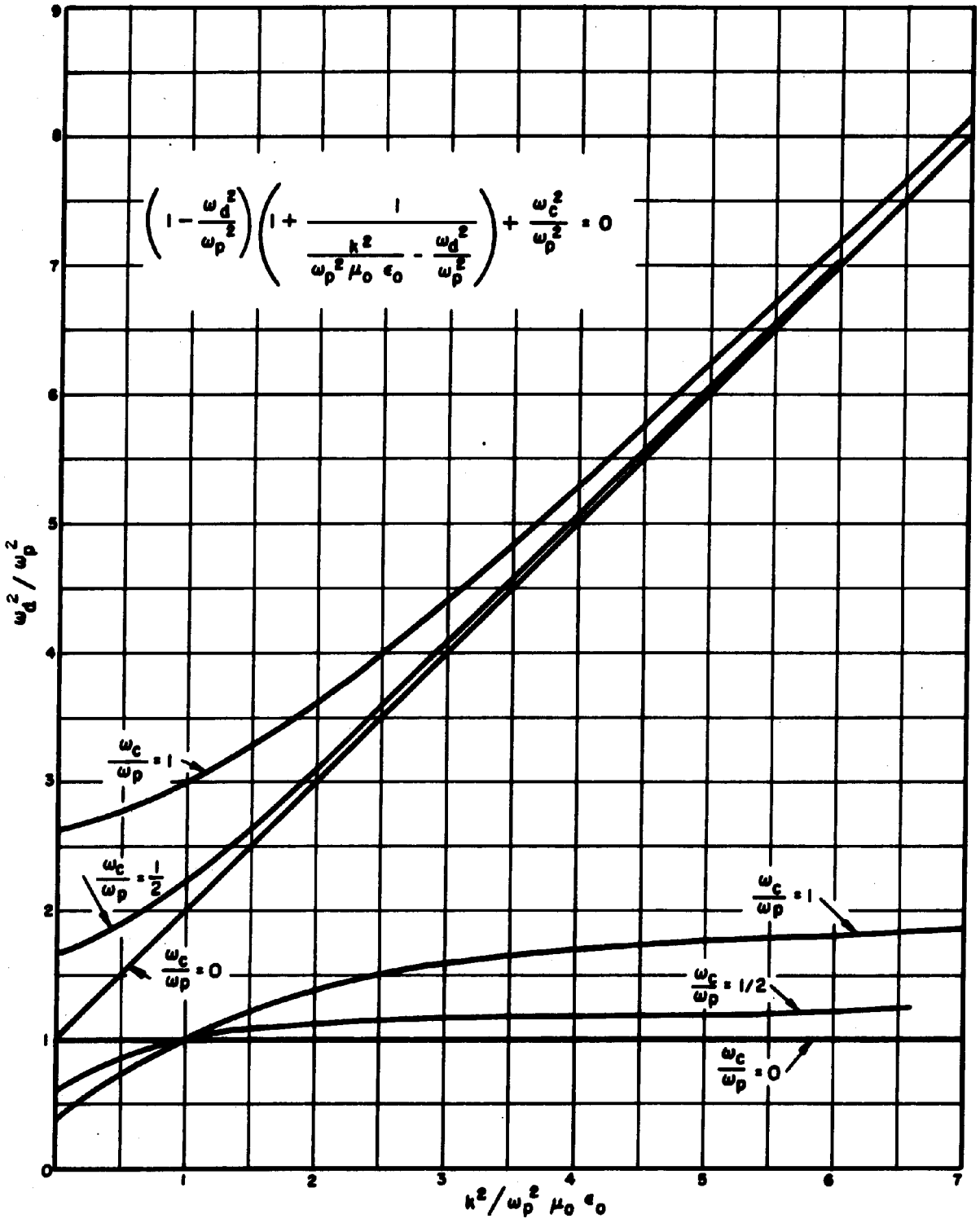


FIG. 3.6 DISPERSION RELATION FOR PROPAGATION OF SPACE-CHARGE WAVES IN A MAGNETIC FIELD, EQ. 3.63 a.

$$\frac{\omega_d^2}{\omega_p^2} = \frac{\omega_c^2}{\omega_p^2} + 1 \quad , \tag{3.69b}$$

respectively. Although we do not consider the question, it would not be surprising if the modified waves partook of the character of the longitudinal and transverse oscillations from which they are derived.

Equation 3.67, corresponding to the solution Eq. 3.65b, is plotted in Fig. 3.7 in a fashion similar to that of Fig. 3.5. For zero magnetic field the solution degenerates into the two independent branches,

$$\frac{\omega_d^2}{\omega_p^2} = \frac{k^2}{\omega_p^2 \mu_o \epsilon_o} + 1 \tag{3.70a}$$

and

$$\frac{\omega_d^2}{\omega_p^2} = 0 \quad , \tag{3.70b}$$

corresponding to a transverse oscillation and a nonpropagating disturbance of the simple plasma. In the presence of the magnetic field the dispersion relation separates into three branches, two of which are asymptotic to the line

$$\frac{\omega_d^2}{\omega_p^2} = \frac{k^2}{\omega_p^2 \mu_o \epsilon_o} + 1 \quad , \tag{3.71}$$

and one which is asymptotic to the line

$$\frac{\omega_d^2}{\omega_p^2} = \frac{\omega_c^2}{\omega_p^2} \quad . \tag{3.72}$$

The difference between the propagation characteristics of the first two modes (asymptotic to Eq. 3.71) can be found from Eq. 3.67,

$$\frac{k^2}{\omega_p^2 \mu_o \epsilon_o} = \frac{\omega_d^2}{\omega_p^2} - \frac{1}{1 \pm \frac{\omega_c}{\omega_d}} \quad , \tag{3.73}$$

and corresponds to the differential phase shift between the two modes

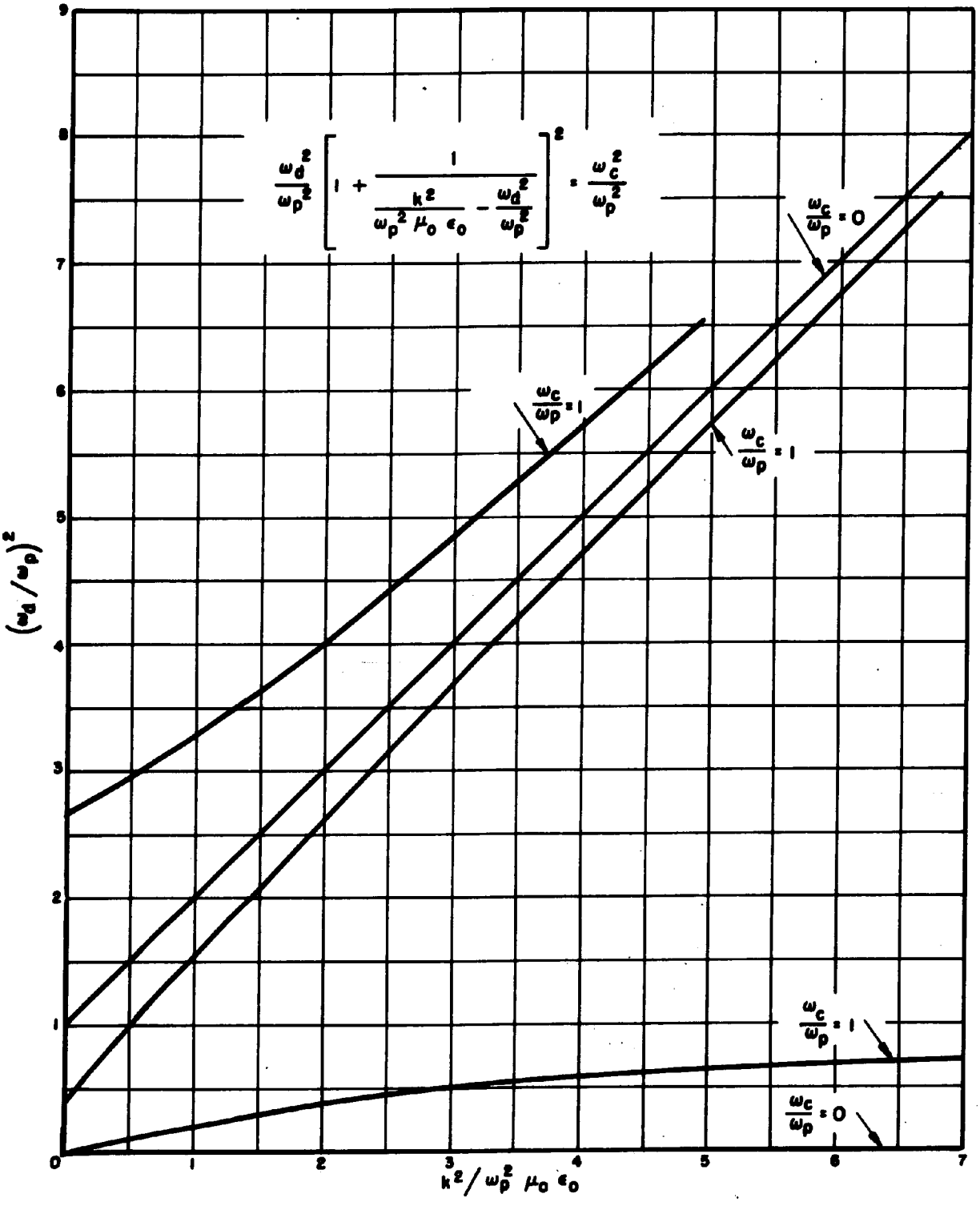


FIG. 3.7 DISPERSION RELATION FOR PROPAGATION OF SOLENOIDAL WAVES IN A MAGNETIC FIELD, EQ. 3.67.

per unit length. Propagation in a frequency range encompassing these modes permits a Faraday rotation effect similar to that observed in ferrite materials.

The mode of propagation described by Eq. 3.72 corresponds to a modification of a static perturbation due to the cyclotron rotation of a charge in the magnetic field.

The character of the motion of a unit of charge can be described in terms of a particle moving under the impress of an alternating electric field of frequency ω_d. To a first approximation we ignore the effect of the motion of the charge on the nature of the field; i.e., the nature of the motion is assumed to be consistent with the net field of the total stream. Considering the motion in a plane perpendicular to the magnetic field and denoting quantities in this plane by a subscript T (for transverse), we obtain from Eqs. 3.56 and 3.57

$$(\omega_d^2-\omega_c^2)\bar{J}_{1T} = - j\omega_d\omega_p^2\epsilon_o \bar{E}_{1T} + \omega_c\omega_p^2 \epsilon_o \bar{E}_{1T} \times \underline{\bar{z}} \quad . \qquad (3.74)$$

Since, in the advancing frame of reference, the current density is proportional to the perturbed velocity, Eq. 3.74 shows that the orthogonal components of the velocity vector in the plane transverse to the magnetic field are, in general, unequal in magnitude and $\pi/2$ radians out of space phase. This corresponds to an elliptical polarization of the velocity vector in this plane. For frequencies above the cyclotron frequency the velocity components have opposite phase relations to the electric field than they do below the cyclotron frequency.

3.3.5 Quasi-Stationary Approximations. In dealing with the interaction of streams, interest centers mainly on waves propagating with phase velocities small compared to the velocity of light. The heuristic justification for such a simplification is rooted in the fact that an

energy interchange between an electron and a wave occurs because of the motion of the electron through the electric field of the wave. For a net average energy to be exchanged the particle must, on the average, spend more time within one phase of the wave than the other and hence, the wave phase velocity and the charge velocity must be of comparable magnitudes. Stream velocities of interest here lie in a range about, roughly, one-tenth the velocity of light so that one can usually assume the above simplification when dealing with wave interaction mechanisms. The usual statement of the quasi-stationary approximation is

$$\nabla \times \bar{E}_1 \cong 0 \quad , \tag{3.75}$$

corresponding to waves propagating with a phase velocity much smaller than that of light. The corresponding form of the solutions of the wave equation are obtained by the substitution of the approximation Eq. 3.75 into Eq. 3.55b; these are

$$\frac{\omega_d^2}{\omega_p^2} = \frac{\omega_c^2}{\omega_p^2} + 1 \quad , \quad \left[\begin{matrix}\text{space-charge} \\ \text{waves}\end{matrix}\right] \tag{3.76a}$$

$$\rho_1 = 0 \quad . \quad \left[\begin{matrix}\text{solenoidal} \\ \text{waves}\end{matrix}\right] \tag{3.76b}$$

Within the quasi-stationary approximation the first solution is a modification of the simple plasma space-charge wave and the field does not extend beyond the boundary of the stream. This can be verified by noting that the normalized surface-charge density equivalent to the boundary-ripple is

$$\frac{\sigma_1}{\epsilon_o \bar{E}_{1T} \times \underline{\bar{n}} \cdot \underline{\bar{z}}} = \pm \frac{\omega_p^2}{\omega_c^2 - \omega_d^2} \left\{ \frac{-\omega_c}{j\omega_d} + \frac{\bar{E}_{1T} \cdot \underline{\bar{n}}}{\bar{E}_{1T} \times \underline{\bar{n}} \cdot \underline{\bar{z}}} \right\} , \tag{3.77}$$

where the subscript T refers, as before, to a plane transverse to the

direction of cylindrical uniformity $\underline{z}$, and $\underline{n}$ is a unit vector normal to the stream boundary. The components $\bar{E}_{1T} \cdot \underline{n}$ and $\bar{E}_{1T} \times \underline{n} \cdot \underline{z} = \bar{E}_{1T} \times \underline{z} \cdot \underline{n}$ are the normal and tangential components, respectively, of the transverse electric field on the stream boundary.

For solutions of the type described by Eq. 3.76a the above expression reduces to

$$\frac{\sigma_1}{\epsilon_o \bar{E}_{1T} \times \underline{n} \cdot \underline{z}} = \pm \frac{\omega_c}{j\omega_d} \mp \frac{\bar{E}_{1T} \cdot \underline{n}}{\bar{E}_{1T} \times \underline{n} \cdot \underline{z}} \quad . \tag{3.78}$$

The net field leaving the stream normal to the boundary is therefore

$$\frac{\sigma_1}{\epsilon_o} + \bar{E}_{1T} \cdot \underline{n} = \frac{\omega_c}{j\omega_d} \bar{E}_{1T} \times \underline{n} \cdot \underline{z} = \pm j \frac{\omega_c}{(\omega_p^2 + \omega_c^2)^{1/2}} \bar{E}_{1T} \times \underline{n} \cdot \underline{z} \quad . \tag{3.79}$$

With zero tangential field on the stream boundary, the normal field is also zero as it must be, since the dispersion relation is independent of the stream geometry.

As was done for the space-charge waves of the simple plasma, it may be noted (using Eqs. 3.56 and 3.57) that the ratio of the kinetic energy to the electric field energy stored per unit volume is

$$\frac{\text{peak kinetic energy storage}}{\text{peak electric energy storage}} = \frac{|\bar{J}_1| \cdot |\bar{E}_1|}{\omega_d \epsilon_o |\bar{E}_1| \cdot |\bar{E}_1|} = 1 \quad . \tag{3.80}$$

The second type of solution corresponds, within the quasi-stationary approximation, to a solution of Laplace's equation subject to the constraints imposed by the plasma boundary-ripple charge distribution. A solution of this type, confined entirely within the stream boundaries, and subject to the condition

$$\frac{\omega_d^2}{\omega_p^2} = \frac{\omega_c^2}{\omega_p^2} + 1 \quad ,$$

may be used as an alternative means of matching the space-charge waves

discussed above.

Figure 3.1, modified by the introduction of a static magnetic field, $-B_o\underline{z}$, affords a simplified linear geometry for which the propagation of the electromagnetic waves may be investigated. Assuming, for simplicity, that the plasma is bounded by free space (for which the normalized admittances are $\pm j$), we have from Eq. 3.79

$$\pm j = \frac{\omega_p^2}{\omega_c^2-\omega_d^2}\left\{-\frac{\omega_c}{j\omega_d} + \frac{\bar{E}_{1T}\cdot\underline{n}}{\bar{E}_{1T}\times\underline{n}\cdot\underline{z}}\right\} + \frac{\bar{E}_{1T}\cdot\underline{n}}{\bar{E}_{1T}\times\underline{n}\cdot\underline{z}}$$

$$= \left(1+\frac{\omega_p^2}{\omega_c^2-\omega_d^2}\right)\left.\frac{\bar{E}_{1y}}{\bar{E}_{1x}}\right|_{\pm h} \mp \frac{\omega_p^2}{\omega_c^2-\omega_d^2}\,\frac{\omega_c}{j\omega_d}\ , \qquad (3.81)$$

where the subscripts x and y refer to the geometry of Fig. 3.1. The normalized admittance $E_{1y}/E_{1x}|_{\pm h}$ is evaluated at the upper or lower stream boundary corresponding to the + and - sign, respectively. Since the field is Laplacian, the surface admittances are related by Eq. 3.24, obtained previously and repeated below;

$$j\left.\frac{E_{1y}}{E_{1x}}\right|_{-h} = \frac{j\left.\frac{E_{1y}}{E_{1x}}\right|_{+h} + \tanh 2\alpha h}{1 + j\left.\frac{E_{1y}}{E_{1x}}\right|_{+h}\tanh 2\alpha h}\ . \qquad (3.24)$$

Equation 3.24 supposes propagation of the form $\exp j(\omega t-\alpha x)$ and a stream thickness of 2h. On eliminating the stream admittance between Eqs. 3.81 and 3.24, the dispersion relation for electromagnetic wave propagation is obtained,

$$2\,\omega_d^2 = \omega_p^2+\omega_c^2 \pm \sqrt{(\omega_p^2+\omega_c^2)^2 - \frac{2\,\omega_p^4}{1+\coth 2\alpha h}}\ . \qquad (3.82)$$

The negative term under the radical has, for real values of α, maximum and minimum values of ω_p^4 and zero, respectively. The roots of Eq. 3.82 are then all real as they necessarily must be since the physical model precludes any coupling to a source of energy to feed a growing wave.

For "thin" streams, i.e., $2\beta h \cong 0$, the dispersion relation is

$$\omega_d^2 \cong \omega_p^2 + \omega_c^2 \quad , \tag{3.83}$$

indicating that the fields are confined to the near vicinity of the stream.

3.3.6 Coupling of Plasmas in a Static Magnetic Field. As an interesting, although greatly oversimplified, illustration of the coupling of two plasmas, we examine a system, illustrated by Fig. 3.8, consisting of two plasmas of equal space-charge density and different average velocities separated by a spacing 2h. For a pseudo-physical manifestation of such a model we can suppose the plasmas to be separated by a positive ion stream with a space-charge density equal to the plasma density and moving with the mean velocity of the two plasmas. To maintain such a laminar ion flow a static $\bar{y}$-directed electric field of magnitude

$$E_o = \left(\frac{v_{oa} + v_{ob}}{2}\right) B_o \tag{3.84}$$

is required. Subscripts a and b differentiate characteristics of the two plasmas.

To maintain the plasmas in rectilinear motion under the combined external static electric field E_o and the electric field of the positive ions it is necessary that the net transverse force on the plasmas vanish, i.e.,

$$\frac{q\,\rho_o h}{\epsilon_o} + q\left(\frac{v_{oa} + v_{ob}}{2}\right) B_o = q\,v_{oa}\,B_o \quad , \tag{3.85a}$$

$$-\frac{q\,\rho_o h}{\epsilon_o} + q\left(\frac{v_{oa} + v_{ob}}{2}\right) B_o = q\,v_{ob}\,B_o \quad . \tag{3.85b}$$

These conditions are simultaneously satisfied provided

$$v_{oa} - v_{ob} = \frac{2\,\omega_p^2}{\omega_c}\,h \quad . \tag{3.86}$$

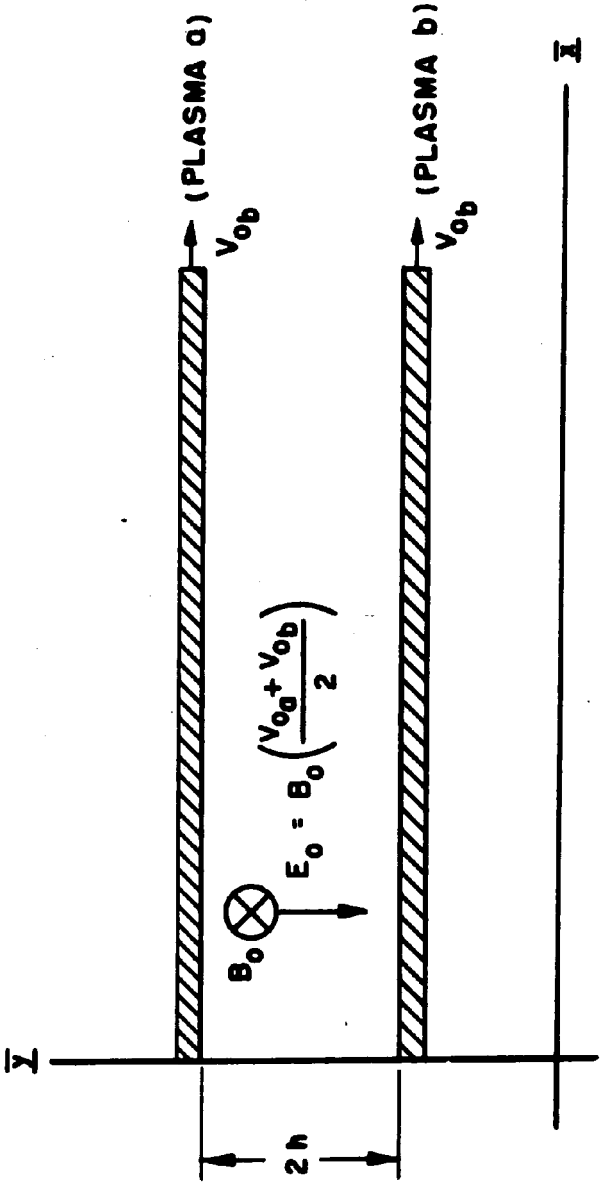


FIG. 3.8 GEOMETRY USED IN DISCUSSION OF PLASMA COUPLING IN A MAGNETIC FIELD, SECTION 3.2.5.

If the plasmas are supposed to be thin, i.e., to have transverse dimensions of a much smaller order of magnitude than the perturbations, the effect of the perturbations may be replaced by an equivalent surface-charge density distribution

$$\frac{\sigma_1}{\epsilon_o E_{1x}} = \frac{\omega_p^2}{\omega_c^2-\omega_d^2}\left\{-\frac{\omega_c}{j\omega_d} + \frac{E_{1y}}{E_{1x}}\right\} . \qquad (3.87)$$

Matching the boundary admittances to free space gives

$$-j = \left(\frac{\omega_p^2}{\omega_c^2-\omega_{da}^2}\right)\left.\frac{E_{1y}}{E_{1x}}\right|_a - \frac{\omega_p^2}{\omega_c^2-\omega_{da}^2}\,\frac{\omega_c}{j\omega_{da}} , \qquad (3.88a)$$

$$+j = \left(\frac{\omega_p^2}{\omega_c^2-\omega_{db}^2}\right)\left.\frac{E_{1y}}{E_{1x}}\right|_b - \frac{\omega_p^2}{\omega_c^2-\omega_{db}^2}\,\frac{\omega_c}{j\omega_{db}} . \qquad (3.88b)$$

Since there is no perturbed space-charge density between the plasmas, Eq. 3.24 is appropriate to transform the stream admittances between the two boundaries, i.e.,

$$j\left.\frac{E_{1y}}{E_{1x}}\right|_b = \frac{j\left.\frac{E_{1y}}{E_{1x}}\right|_a + \tanh 2\alpha h}{1 + j\left.\frac{E_{1y}}{E_{1x}}\right|_a \tanh 2\alpha h} . \qquad (3.89)$$

Elimination between Eqs. 3.88 and 3.89 leads to the dispersion relation

$$\alpha'^2(1-m^2) + (m-2\omega')\alpha' + \omega'^2 = \frac{1}{2}\,\frac{\tanh 2m\alpha'}{1 + \tanh 2m\alpha'} , \qquad (3.90)$$

where

$$\omega' = \omega/\omega_c , \qquad (3.91a)$$

$$\alpha' = \frac{\alpha}{\omega_c}\left(\frac{v_{oa} - v_{ob}}{2}\right) , \qquad (3.91b)$$

$$0 \leq m = \frac{v_{oa} - v_{ob}}{v_{oa} + v_{ob}} \leq 1 . \qquad (3.91c)$$

In obtaining Eq. 3.90 it has been assumed that

$$\left(\frac{\omega_d}{\omega_c}\right)^2 \ll 1 \quad , \tag{3.92a}$$

$$\omega_p^2 = \omega_c^2 \quad . \tag{3.92b}$$

Equation 3.91 is identical to the result obtained in a subsequent discussion of a perturbation of rectilinear Brillouin flow. Comment on it will be deferred, except for noting that the propagation constant turns out to be complex over a frequency range extending to approximately twice the cyclotron frequency. The perturbation propagates with a phase velocity approximately equal to the mean of the plasma velocities.

3.4 Perturbation of Irrotational Streams

3.4.1 The Secular Equation. The artifice of an ion-neutralized stream permits a perturbation analysis accounting for the effects of the space-charge forces on the character of the propagation of the perturbation. However, the neutralization of the d-c stream eliminates forces resulting from the space-varying d-c electric field of an unneutralized stream. In general, a perturbed electron will see an r-f force as a result of a perturbation of position in a space-varying d-c field. This field provides a coupling between the d-c energy of the stream and the energy of the perturbation. The possibility exists, under these conditions, of a self-amplifying stream perturbation feeding itself from the d-c energy of the stream.

Consider, because of the relatively simple mathematics involved, irrotational streams, for which

$$\nabla \times \bar{p}_o = \nabla \times (m\,\bar{v}_o - q\bar{A}) = 0 \quad . \tag{3.93}$$

The irrotational character of the stream is preserved under the perturbation and, neglecting the perturbed magnetic field consistent with the slow-wave approximation practiced in obtaining the equation of motion, we

have

$$\nabla \times \bar{v}_1 = 0 \quad . \tag{3.94}$$

Substitution of Eqs. 3.93 and 3.94 into the equation of motion, Eq. 3.33, leads to the result

$$\frac{\partial \bar{v}_1}{\partial t} + \nabla(\bar{v}_o \cdot \bar{v}_1) = \frac{q}{m} \bar{E}_1 \quad . \tag{3.95}$$

Use has been made of the vector identity

$$\nabla (\bar{A} \cdot \bar{B}) = \bar{A} \cdot \nabla \bar{B} + \bar{B} \cdot \nabla \bar{A} + \bar{A} \times (\nabla \times \bar{B}) + \bar{B} \times (\nabla \times \bar{A}) \tag{3.96}$$

in obtaining Eq. 3.95. Equation 3.95 may be put into the convenient form

$$\nabla \left[\frac{dS_1}{dt} + (v_o \cdot \nabla) S_1 \right] = \frac{q}{m} \bar{E}_1 \quad , \tag{3.97}$$

where the scalar stream velocity potential S_1 is defined by

$$\bar{v}_1 = - \nabla S_1 \quad . \tag{3.98}$$

Equation 3.98 is a consequence of the irrotational character of $\bar{v}_1$. From the divergence of Eq. 3.97 and Gauss' law we have

$$\nabla^2 \left\{ \frac{\partial S_1}{\partial t} + (\bar{v}_o \cdot \nabla) S_1 \right\} = \frac{-q \rho_1}{m \epsilon_o} \quad . \tag{3.99}$$

From the equation of continuity we have

$$- \frac{\partial \rho_1}{\partial t} = \nabla \cdot \rho_o \bar{v}_1 + \nabla \cdot \rho_1 \bar{v}_o = \nabla \cdot \rho_o \bar{v}_1 + (\bar{v}_o \cdot \nabla) \rho_1 \quad . \tag{3.100}$$

The last form of Eq. 3.100 requires the d-c stream velocity to be solenoidal, a condition which is verified by the equation of continuity for the d-c stream on the assumption of a uniform d-c charge density ρ_o. This assumption is justified for certain of the irrotational streams discussed in Chapter II and limits the following discussion to those streams.

Elimination of ρ_1 between Eqs. 3.99 and 3.100 yields

$$\left\{\frac{\partial}{\partial t} + (\bar{v}_o \cdot \nabla)\right\}\left\{\nabla^2\left[\frac{\partial}{\partial t} + (\bar{v}_o \cdot \nabla)\right] S_1\right\} = -\omega_p^2 \nabla^2 S_1 \quad . \tag{3.101}$$

Defining the hydrodynamic stream operation D/Dt as

$$\frac{D}{Dt} = \frac{\partial}{\partial t} + (\bar{v}_o \cdot \nabla) \tag{3.102}$$

permits Eq. 3.101 to be written in the form

$$\frac{D}{Dt}\left\{\nabla^2\left(\frac{DS_1}{Dt}\right)\right\} + \omega_p^2 \nabla^2 S_1 = 0 \quad . \tag{3.103}$$

3.4.2 Axially Symmetric Brillouin Flow. We consider Eq. 3.103 in cylindrical coordinates (r, θ, z), corresponding to axially symmetric Brillouin flow (see section 2.5.2). A perturbation of the form

$$\text{perturbation} \sim \exp j\,(\omega t - \beta\theta - \gamma z) \tag{3.104}$$

is assumed. Since the d-c velocity is

$$\bar{v}_o = \frac{\omega_c}{2} r\, \underline{\theta} + v_{oz}\, \underline{z} \quad , \tag{3.105}$$

Eq. 3.102 indicates that the hydrodynamic stream operator, operating on a scalar, is equivalent to an algebraic multiplication; i.e.,

$$\frac{D}{Dt} = j\left(\omega - \frac{\omega_c}{2}\beta - v_{oz}\,\gamma\right) = j\omega_d \quad . \tag{3.106}$$

The Doppler frequency, ω_d, is that frequency which the perturbation appears to assume for an observer traveling with the d-c motion of the stream. It is significant to note that the Doppler frequency is independent of the position of the observer in the stream. As a consequence of this, the Laplacian and hydrodynamic operators in Eq. 3.103 commute; i.e.,

$$\frac{D}{Dt}\left\{\nabla^2\left(\frac{DS_1}{Dt}\right)\right\} = \frac{D^2}{Dt^2}(\nabla^2 S_1) = \nabla^2\left(\frac{D^2 S_1}{Dt^2}\right) . \qquad (3.107)$$

Therefore Eq. 3.103 can be written as

$$\frac{D^2}{Dt^2}(\nabla^2 S_1) + \omega_p^2 (\nabla^2 S_1) = 0 , \qquad (3.108)$$

indicating that D/Dt^2 and ω_p^2 commute. Equation 3.108 therefore has the two solutions

$$\omega_p^2 - \omega_d^2 = 0 , \qquad (3.109a)$$

and

$$\nabla^2 S_1 = 0 . \qquad (3.109b)$$

As seen from the equation of continuity, Eq. 3.100, the Laplacian character of the stream velocity potential is equivalent to having zero perturbed space-charge density. The two solutions can be characterized then as

$$\omega_d^2 = \omega_p^2 , \quad \text{[space-charge waves]} \qquad (3.110a)$$

$$\rho_1 = 0 . \quad \text{[solenoidal waves]} \qquad (3.110b)$$

It should be noted in connection with Eq. 3.11a that, for axially symmetric Brillouin flow, $\omega_p^2 = \omega_c^2/2$. The two solutions above are those found by Rigrod and Lewis in their study of wave propagation on an axial Brillouin stream[18].

Since the hydrodynamic operator operating on a scalar is equivalent to multiplication by a constant in cylindrical coordinates, Eq. 3.97 becomes simply

$$j\omega_d \rho_o \bar{v}_1 = \omega_p^2 \epsilon_o \bar{E} . \qquad (3.111)$$

For waves of the type described by Eq. 3.110, Eq. 3.111 becomes

$$\rho_o \bar{v}_1 + j\omega_d \epsilon_o \bar{E}_1 = 0 , \qquad (3.112)$$

which shows that there is no total current density associated with this perturbation when viewed in a frame of reference advancing (and rotating) with the average stream motion. There is no external field from the stream since the flux terminates on the boundary equivalent surface-charge density; i.e.,

$$\frac{\sigma_1}{\epsilon_o} = \frac{\rho_o v_{1r}}{j\omega_d \epsilon_o} = \frac{J_{1r}}{j\omega_d \epsilon_o} = - E_{1r} \quad . \tag{3.113}$$

The similarity between the dynamics of a space-charge wave in the present case and the space-charge waves for a plasma-stream without magnetic field is striking. The unique balancing of the space-charge, magnetic, and centrifugal forces is maintained during the perturbation.

The second solution of Eq. 3.110 corresponds to electromagnetic wave propagation along the stream.

To simplify the mathematics we make use of the quasi-stationary hypothesis

$$\nabla \times \bar{E}_1 \cong 0 \quad , \tag{3.114}$$

and, on this basis, define a potential function ϕ_1 as

$$\bar{E}_1 = - \nabla \phi_1 \quad . \tag{3.115}$$

Because the electric field intensity for the solution being considered is solenoidal, the potential function satisfies the Laplace equation both within and without the stream, i.e.,

$$\nabla^2 \phi_1 = 0 \quad . \tag{3.116}$$

The appropriate solutions for ϕ_1 in cylindrical coordinates, omitting a factor $\exp j(\omega t - \beta\theta - \gamma z)$, are the modified Bessel functions of the first and second kind, I and K, respectively. Consider a hollow stream of radii a and b respectively ($a > b$) and, for simplicity, assume free space external to the streams. The geometry is illustrated by Fig. 3.9.

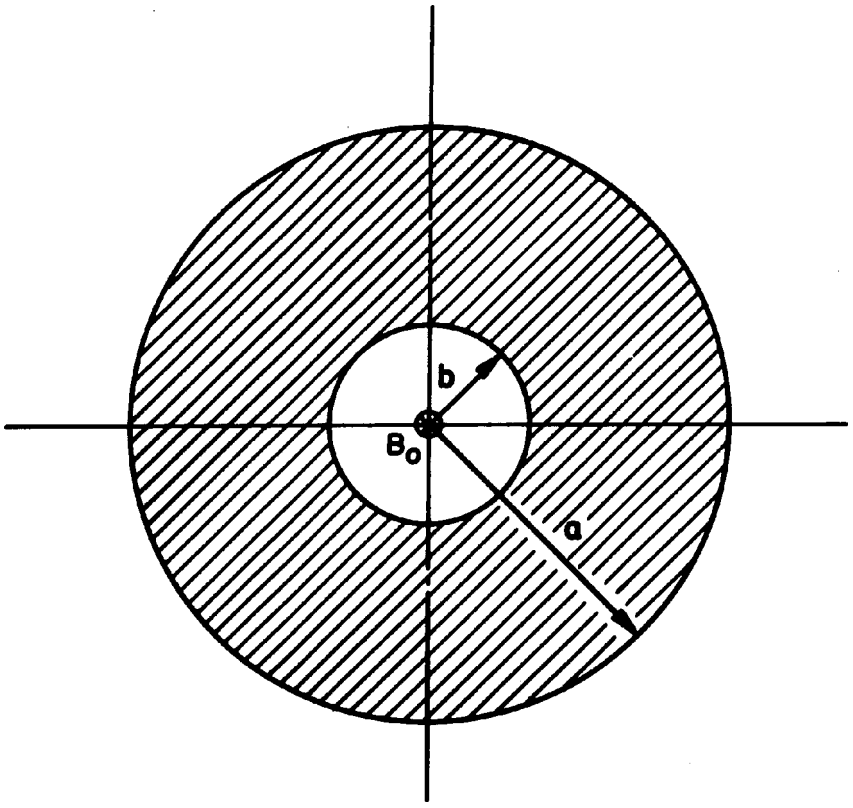


FIG. 3.9 GEOMETRY OF AXIALLY SYMMETRIC HOLLOW-STREAM FLOW DISCUSSED IN SECTION 3.3.2.

In the region for which $R = \gamma r \geq \gamma a$, the potential variation is given by

$$\phi_1 = AK_\beta(R) \quad . \tag{3.117}$$

For the region $\gamma a \geq R \geq \gamma b$, the potential variation is

$$\phi_1 = BI_\beta(R) + CK_\beta(R) \quad , \tag{3.118}$$

and for the region $R \leq \gamma b$, the potential variation is

$$\phi_1 = DI_\beta(R) \quad . \tag{3.119}$$

From the requirement of continuity of potential at the stream boundaries we obtain

$$AK_\beta^a = BI_\beta^a + CK_\beta^a \quad , \tag{3.120a}$$

$$DI_\beta^b = BI_\beta^b + CK_\beta^b \quad , \tag{3.120b}$$

where I_β^a refers to the β order of the indicated modified Bessel function with argument γa, and similarly for the other symbols.

Two additional equations are obtained from the requirement on the continuity of the normal derivatives of the potential at the stream boundaries (including the boundary surface-charge density). The boundary-ripple charge density is

$$\frac{\sigma_1}{\epsilon_o} = \frac{\rho_o v_{1r}}{j\omega_d \epsilon_o} = \frac{\omega_p^2}{\omega_d^2} \frac{\partial \phi_1}{\partial r} \quad , \tag{3.121}$$

and the equations obtained are

$$-A\left(K_{\beta+1}^a + K_{\beta-1}^a\right) = \left\{B\left(I_{\beta+1}^a + I_{\beta-1}^a\right) - C\left(K_{\beta+1}^a + K_{\beta-1}^a\right)\right\}\left\{1 - \frac{\omega_p^2}{\omega_d^2}\right\} \quad , \tag{3.122a}$$

$$D\left(I_{\beta+1}^b + I_{\beta-1}^b\right) = \left\{B\left(I_{\beta+1}^b + I_{\beta-1}^b\right) - C\left(K_{\beta+1}^b + K_{\beta-1}^b\right)\right\}\left\{1 - \frac{\omega_p^2}{\omega_d^2}\right\} \quad . \tag{3.122b}$$

Equations 3.120 and 3.122 are a set of four linear homogeneous equations

in four unknowns; their compatibility requires the determinant of the coefficients to vanish. After some algebraic manipulation of the determinant, it can be put into the form

$$\begin{vmatrix} 1 - \frac{2}{\gamma a}\frac{\omega_d^2}{\omega_p^2}\frac{1}{K_\beta^a\left(I_{\beta+1}^a + I_{\beta-1}^a\right)} & \frac{K_{\beta+1}^a + K_{\beta-1}^a}{K_{\beta+1}^b + K_{\beta-1}^b} \\ \frac{I_{\beta+1}^b + I_{\beta-1}^b}{I_{\beta+1}^a + I_{\beta-1}^a} & 1 - \frac{2}{\gamma b}\frac{\omega_d^2}{\omega_p^2}\frac{1}{I_\beta^b\left(K_{\beta+1}^b + K_{\beta-1}^b\right)} \end{vmatrix} = 0 \quad . \tag{3.123}$$

If we suppose the inner stream radius to go to zero, i.e., if we consider a solid stream, the determinental equation becomes

$$\frac{\omega_p^2}{\omega_d^2} K_\beta^a\left(I_{\beta+1}^a + I_{\beta-1}^a\right) - \frac{2}{\gamma a} = 0 \quad . \tag{3.124}$$

It should be noted that the Doppler frequency ω_d contains the axial propagation constant (see Eq. 3.106). Examination of Eq. 3.124 shows that the axial propagation constant is real, and no growing waves exist on the solid Brillouin stream.

As another relatively simple case we consider a hollow stream and a perturbation for which there is no circumferential variation, i.e., $\beta = 0$. The determinental equation, Eq. 3.123, reduces to

$$\begin{vmatrix} I_1^a K_o^a - \frac{\omega_d^2}{\gamma a\, \omega_p^2} & I_o^b K_1^a \\ I_1^b K_o^a & I_o^b K_1^b - \frac{\omega_d^2}{\gamma b\, \omega_p^2} \end{vmatrix} = 0 \quad , \tag{3.125}$$

and leads to the following expression:

$$\frac{2\omega_d^2}{\gamma\,\omega_p^2} = aI_1^a K_0^a + bI_0^b K_1^b \pm \sqrt{\left(aI_1^a K_0^a + bI_0^b K_1^b\right)^2 - 4abI_0^b K_0^a \left(I_1^a K_1^b - I_1^b K_1^a\right)}$$

$$= aI_1^a K_0^a + bI_0^b K_1^b \pm \sqrt{\left(aI_1^a K_0^a - bI_0^b K_1^b\right)^2 + 4abI_0^b K_0^a I_1^b K_1^a} \quad . \tag{3.126}$$

The second form of the right-hand side of Eq. 3.126 shows the radical to be a real quantity under the tentative assumption of real γ. On noting that

$$I_1^a K_1^b - I_1^b K_1^a \geq 0 \quad , \tag{3.127}$$

the first form of the right-hand side of Eq. 3.126 is identified as a positive real quantity. Comparison of the left-hand side of Eq. 3.126 with the conclusions above indicates their compatibility. It seems reasonable to conclude that Eq. 3.126 has only real roots which are of significance.

For a more general perturbation of a hollow cylindrical stream the determinant, Eq. 3.123, becomes more difficult to interpret. It appears probable, however, that a similar conclusion will be reached upon critical examination, i.e., that growing waves do not exist on the perturbed hollow axial stream. Such a conclusion is apparently in contradiction to the experimentally observed phenomenon of hollow-stream breakup[6]. This discrepancy is discussed subsequently. For the present we consider only why, experimental evidence to the contrary, a lack of instability is plausible for the model considered. To provide an instability a source of energy must be coupled to the perturbation; this coupling is generally attributed to the "slipping stream" nature of the flow. Actually an axial Brillouin flow does <u>not</u> slip; all the electrons have the same axial

velocity and the same angular velocity. A sector (wedge-shaped slice of the stream) maintains its identity throughout the flow. Since no one segment of electrons "slips" past any other, there is no coupling between electrons. If we assume that a significant perturbation (in the present discussion) is carried along by the perturbed electrons at approximately the electron axial velocity we implicitly also assume that none of the electrons move through the perturbation.

As a preliminary to reconciling the above discussion with the incontrovertible experimental observations we consider a different model of a hollow-stream perturbation: a so-called "thin" stream model.

In this model the hollow stream is assumed to be sufficiently limited in thickness that the various fields can be approximated by the average of the fields on either side of the hollow stream. A perturbation of the stream is now assumed to be of a much larger order of magnitude than the stream thickness Δ. The resulting boundary value problem is illustrated in Fig. 3.10. The discussion of the first few paragraphs of section 3.3.2 remains valid for this model in that, for electromagnetic wave propagation, the perturbed space-charge density is zero. As a first-order approximation the r-f boundary conditions at the stream may be obtained by superimposing on the unperturbed stream position a similar stream of positive ions. This artifice provides a convenient method of subtracting the d-c field from the total field of the perturbed stream. The d-c volume charge density ρ_o can be replaced for the "thin"-stream analysis by an equivalent surface-charge density, σ_o, given by the expression

$$\frac{-q\,\sigma_o}{m\,\epsilon_o\Delta} = \omega_p^2 \quad . \tag{3.128}$$

As illustrated in Fig. 3.10, the resulting configuration, to a first-

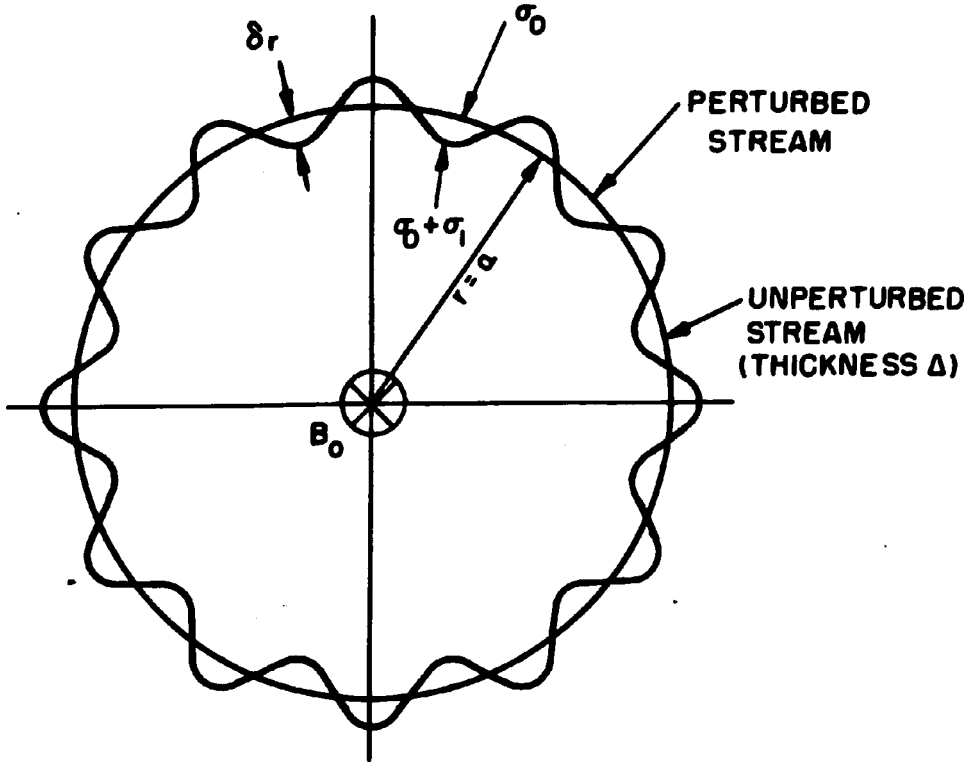


FIG. 3.10 PERTURBATION OF A "THIN" AXIALLY SYMMETRIC HOLLOW STREAM.

order approximation, is equivalent to a surface dipole moment distribution. This dipole layer causes a discontinuity in potential given by

$$\phi_{1u} - \phi_{1\ell} = \frac{\sigma_o \, \delta r}{\epsilon_o} \quad , \tag{3.129}$$

where the subscript u applies to quantities evaluated just above the stream and the subscript ℓ refers to quantities evaluated just below the stream. In accordance with the initial assumptions above,

$$\phi_{1u} + \phi_{1\ell} = 2 \, \phi_s \quad , \tag{3.130}$$

where the subscript s refers to quantities evaluated within the stream. Making use of Eq. 3.11, we have

$$\phi_u - \phi_\ell = \frac{\sigma_o \, v_{1r}}{j\omega_d \, \epsilon_o} = \frac{\omega_p^2}{\omega_d^2} \, \Delta \, \frac{\partial}{\partial r} \left(\frac{\phi_u + \phi_\ell}{2} \right) \quad . \tag{3.131}$$

As before, the potential functions describing the perturbation are solutions of Laplace's equation in cylindrical coordinates, i.e.,

$$\phi_1 = A \, K_\beta(\gamma r) \quad \text{(above the stream)} \quad , \tag{3.132a}$$

$$\phi_1 = B \, I_\beta(\gamma r) \quad \text{(below the stream)} \quad . \tag{3.132b}$$

Since there is no space-charge bunching in the stream, we have, at the stream,

$$\frac{\partial \phi_u}{\partial n} = \frac{\partial \phi_\ell}{\partial n} \quad . \tag{3.133}$$

Substituting Eq. 3.132 into Eq. 3.133 gives

$$\frac{A}{B} = - \frac{I^a_{\beta+1} + I^a_{\beta-1}}{K^a_{\beta+1} + K^a_{\beta-1}} \quad , \tag{3.134}$$

where the quantities have been evaluated at the mean stream radius, a. Applying this result to Eq. 3.132 we have

$$-\frac{\omega_p^2}{\omega_d^2}\,\frac{\Delta\gamma}{2} = \frac{K_\beta^a}{K_{\beta+1}^a + K_{\beta-1}^a} + \frac{I_\beta^a}{I_{\beta+1}^a + I_{\beta-1}^a}$$

$$= \frac{2}{\gamma a\left(I_{\beta+1}^a + I_{\beta-1}^a\right)\left(K_{\beta+1}^a + K_{\beta-1}^a\right)}\,, \qquad (3.135)$$

where use has been made of the Wronskian

$$I_\beta^a\, K_{\beta+1}^a + I_{\beta+1}^a\, K_\beta^a = \frac{1}{\gamma a}\,. \qquad (3.136)$$

It is convenient to make use of the relation between the plasma and cyclotron frequencies, and the definition of the Doppler frequency, to write Eq. 3.135 as

$$\left(\frac{2\gamma\, v_{oz}}{\omega_c} + \beta - \frac{2\omega}{\omega_c}\right)^2 = -\frac{1}{2}\,\frac{\Delta}{a}\,(\gamma a)^2\left(I_{\beta+1}^a + I_{\beta-1}^a\right)\left(K_{\beta+1}^a + K_{\beta-1}^a\right). \qquad (3.137)$$

Since the stream has been assumed "thin," i.e., $\Delta/a \ll 1$, the value of γ obtained by setting the left side of Eq. 3.136 equal to zero can be substituted for the γ appearing on the right side, as a first-order approximation. The resulting equation is

$$\gamma = \left(\gamma_e - \frac{\gamma_c\beta}{2}\right)\left\{1 \pm j\,\frac{\gamma_c}{2}\sqrt{\frac{\Delta a}{2}\left(I_{\beta+1}^a + I_{\beta-1}^a\right)\left(K_{\beta+1}^a + K_{\beta-1}^a\right)}\right\}, \qquad (3.138$$

where

$$\gamma_e = \frac{\omega}{v_{oz}}\,, \qquad (3.139a)$$

$$\gamma_c = \frac{\omega_c}{v_{oz}}\,. \qquad (3.139b)$$

The "thin"-stream analysis thus shows an instability to be present in the stream. However, the "thin" stream represents a <u>different</u> model from that considered previously. In this connection we can study the determinental equation, Eq. 3.123, in the limiting case where a approaches b. We set

$$b - a = \Delta \ , \tag{3.140}$$

and assume that the Bessel functions have essentially the same value at b as at a for small Δ. Equation 3.123 then reduces to

$$\frac{\omega_d^2}{\omega_p^2} = 1 + \frac{\Delta\gamma}{2} I_\beta^a \left(K_{\beta+1}^a + K_{\beta-1}^a \right) . \tag{3.141}$$

This result is considerably different from the "thin"-stream result, Eq. 3.135.

This apparent contradiction is also encountered in the more easily visualized case of circular Brillouin flow discussed below.

3.4.3 Circular Brillouin Flow. A somewhat simpler model to analyze than the preceding case, and one which exhibits similar apparent contradictions, is that corresponding to circular Brillouin flow. As far as the d-c stream behavior is concerned, circular Brillouin flow can be regarded as the special case of axially symmetric Brillouin flow which results when the stream has zero axial velocity. Figure 3.11 illustrates the geometry of a circular Brillouin flow. A perturbation is assumed to propagate circumferentially. As in axial Brillouin flow the perturbation propagates either as a space-charge wave for which the total current density as viewed in a frame of reference rotating with the electrons is zero, or as an electromagnetic wave for which the space-charge density of the perturbation is zero. The general discussion of the space-charge waves of an axially symmetric Brillouin flow is applicable to the space-charge waves of the present case and need not be repeated; the solenoidal waves are discussed below.

Within the quasi-stationary hypothesis, the two-dimensional Laplace equation in cylindrical coordinates describes the fields in the circular Brillouin flow model (illustrated by Fig. 3.11) by a potential function

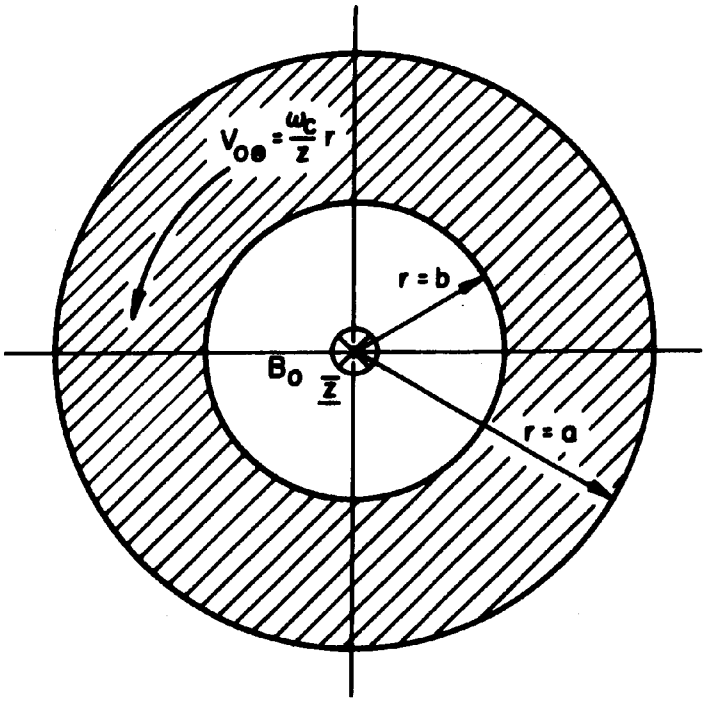


FIG. 3.11 GEOMETRY OF CIRCULAR BRILLOUIN FLOW.

ϕ_1, such that

$$\phi_1 = Ar^{-\beta} \quad , \quad r \geq a \quad , \tag{3.142a}$$

$$\phi_1 = Br^{\beta} + Cr^{-\beta} \quad , \quad a \geq r \geq b \quad , \tag{3.142b}$$

$$\phi_1 = Dr^{\beta} \quad , \quad b \geq r \quad . \tag{3.142c}$$

The above solutions correspond to a stream confined between radii a and b, $a > b$, and bounded externally by free space. A common factor, exp $j(\omega t - \beta\theta)$, is omitted in Eqs. 3.142. In the same manner as before, the boundary conditions on the potential and potential gradient evaluated at the stream boundaries lead to four linear homogeneous equations in four unknowns:

$$Aa^{-\beta} = Ba^{\beta} + Ca^{-\beta} \quad , \tag{3.143a}$$

$$Db^{\beta} = Bb^{\beta} + Cb^{-\beta} \quad , \tag{3.143b}$$

$$-\beta Aa^{-\beta-1} = \left(\beta Ba^{\beta-1} - \beta Ca^{-\beta-1}\right)\left(1 - \frac{\omega_p^2}{\omega_d^2}\right) \quad , \tag{3.143c}$$

$$\beta Db^{\beta-1} = \left(\beta Bb^{\beta-1} - \beta Cb^{-\beta-1}\right)\left(1 - \frac{\omega_p^2}{\omega_d^2}\right) \quad . \tag{3.143d}$$

The requirement that the determinant formed from Eq. 3.143 vanish leads to the result

$$\left(\beta - 2\frac{\omega}{\omega_c}\right)^2 = 1 \pm \left(\frac{b}{a}\right)^{\beta} \quad . \tag{3.144}$$

We now make use of the power series representation

$$\left(\frac{b}{a}\right)^{\beta} = \sum_{n=0}^{\infty} \frac{\left(\beta \ln \frac{b}{a}\right)^n}{n!} \quad . \tag{3.145}$$

On the assumption

$$\frac{b}{a} \cong 1 \quad , \tag{3.146}$$

the first two terms of the series provide an adequate approximation so

that we have

$$\left(\beta - 2\frac{\omega}{\omega_c}\right)^2 \cong 1 \pm \left(1 + \beta \ln \frac{b}{a}\right) \quad . \qquad (3.147)$$

The quadratic equation above has the solutions

$$\beta = 2\frac{\omega}{\omega_c} + \frac{1}{2}\ln\frac{b}{a} \pm \sqrt{2\left[1 + \frac{\omega}{\omega_c}\ln\left(\frac{b}{a}\right)\right] + \left(\frac{1}{2}\ln\frac{b}{a}\right)^2} \quad , \qquad (3.148a)$$

$$\beta = 2\frac{\omega}{\omega_c} - \frac{1}{2}\ln\frac{b}{a} \pm \sqrt{-2\frac{\omega}{\omega_c}\ln\frac{b}{a} + \left(\frac{1}{2}\ln\frac{b}{a}\right)^2} \quad . \qquad (3.148b)$$

Neither solution indicates the existence of growing waves consistent with the approximations made in obtaining them.

The field solution above may be compared with a "thin"-stream solution as was done in the case of an axially symmetric Brillouin flow. Equations 3.131 and 3.132 are also appropriate in the present case. The fields are described in terms of a potential function obtained from Laplace's equation in polar coordinates. Assuming free space external to the stream we have

$$\phi_1 = Ar^{-\beta} \quad , \quad r \geq a \quad , \qquad (3.149a)$$

$$\phi_1 = Br^{\beta} \quad , \quad r \leq a \quad , \qquad (3.149b)$$

where a is the mean radius of the stream. On eliminating between the equations obtained from satisfying the boundary conditions in the same manner as before, we obtain

$$\beta = 2\frac{\omega}{\omega_c} - \frac{\Delta}{2a} \pm \sqrt{-2\frac{\omega}{\omega_c}\frac{\Delta}{a} + \left(\frac{\Delta}{2a}\right)^2} \quad . \qquad (3.150)$$

Here also the existence of growing waves is predicted in contrast to the conclusions of the previous field analysis of a "thick" stream.

3.4.4 Rectilinear Brillouin Flow. In further consideration of the discrepancy between a "thick"- and "thin"-stream analysis, we apply Eq.

3.103 to the rectilinear Brillouin flow described in Section 2.5.1.

If a plane wave perturbation varying as exp j ($\omega t - \alpha x - \gamma z$) is assumed, the hydrodynamic stream operator becomes

$$\frac{D}{Dt} = j(\omega - \alpha v_{ox} - \gamma v_{oz}) = j\omega_d \quad . \qquad (3.151)$$

When propagation is confined to a direction parallel to the magnetic field ($\alpha = 0$) the hydrodynamic operator becomes independent of position. Equation 3.103 then leads, as in the case of axial Brillouin flow, to the two solutions

$$\omega_p^2 = \omega_d^2 \quad , \qquad (3.152a)$$

$$\rho_1 = 0 \quad . \qquad (3.152b)$$

The discussion of a plasma perturbation in rectangular coordinates (section 3.2.2) describes these solutions also. The space-charge neutralization mechanism of the plasma is replaced, in the present case, by a balancing between the electric and magnetic field forces.

In general, however, the hydrodynamic stream operator is not independent of position ($\gamma \neq 0$). Substitution in Eq. 3.103 leads to the general equation

$$\frac{\partial^2 v_{1x}}{\partial \xi^2} + \frac{2\xi}{\xi^2 - 1} \frac{\partial v_{1x}}{\partial \xi} - \frac{\gamma^2 + \alpha^2}{\alpha^2} v_{1x} = 0 \quad , \qquad (3.153)$$

where $\xi = \omega_d/\omega_c$ and $\omega_d = \omega - \alpha v_{ox} - \gamma v_{oz}$. The same equation is obtained for v_{1z}. The remaining velocity component v_{1y} is related to v_{1x} and v_{1z} by the condition that the velocity is irrotational. For simplicity, only the case where propagation is normal to the magnetic field is considered ($\gamma = 0$). Equation 3.153 then reduces to the differential equation studied by Buneman[20], and by MacFarlane and Hay[21],

$$\frac{\partial^2 v_{1x}}{\partial \xi^2} + \frac{2\xi}{\xi^2+1} \frac{\partial v_{1x}}{\partial \xi} - v_{1x} = 0 \quad . \tag{3.154}$$

Particular interest concerns wave solutions of Eq. 3.154 with a phase velocity approximately equal to the d-c stream velocity, i.e., waves for which

$$\xi^2 \ll 1 \quad . \tag{3.155}$$

Subject to this approximation, and with the hindsight afforded by the previous studies of Eq. 3.154, we neglect the second term in that equation. An approximate solution to Eq. 3.154 is, therefore,

$$v_{1z} = A \cosh \alpha y + B \sinh \alpha y \quad , \tag{3.156}$$

where A and B are constants and the space variation is stated directly in terms of y, rather than the normalized variable ξ, for convenience. Since the perturbed velocity is irrotational we have

$$v_{1y} = \frac{j}{\alpha} \frac{\partial v_{1z}}{\partial y} = j (A \sinh \alpha y + B \cosh \alpha y) \quad . \tag{3.157}$$

The normalized surface-charge density equivalent of the stream boundary-ripple is

$$\frac{\sigma_1}{\epsilon_o E_{1z}} = \frac{\rho_o v_{1y}}{j\omega_d \epsilon_o E_{1z}} = -\frac{\omega_c^2}{\omega_d^2} \frac{v_{1y}}{v_{1z}} = -\frac{1}{\xi^2} \frac{v_{1y}}{v_{1z}} \quad . \tag{3.158}$$

If free space external to the stream boundaries is assumed, matching of the fields at the stream boundaries requires

$$\frac{v_{1y}}{v_{1z}} = \frac{-j\xi}{1+\xi} \quad \text{at the upper stream boundary} \quad , \tag{3.159a}$$

$$\frac{v_{1y}}{v_{1z}} = \frac{-j\xi}{1-\xi} \quad \text{at the lower stream boundary} \quad . \tag{3.159b}$$

Compatibility of Eqs. 3.154, 3.155, and 3.159 requires

$$\xi_+ \xi_- + \frac{\xi_- - \xi_+}{2} - \frac{1}{2} \frac{\tanh 2\alpha h}{1 + \tanh 2\alpha h} = 0 \quad , \tag{3.160}$$

where subscripts + and - are used to distinguish between quantities evaluated at the upper and lower stream boundaries, respectively, and where 2h is the stream thickness.

Equation 3.160 can be put into a convenient form by defining the normalized variables

$$\alpha' = \frac{\alpha}{2\omega_c} (v_{o+} + v_{o-}) \quad , \tag{3.161a}$$

$$\omega' = \omega/\omega_c \quad , \tag{3.161b}$$

$$0 \leq m = \frac{v_{o+} - v_{o-}}{v_{o+} + v_{o-}} \leq 1 \quad . \tag{3.161c}$$

Substitution of these variables into Eq. 3.160 allows it to be rewritten as

$$(1-m^2)\alpha'^2 + \alpha'(m-2\omega') + \omega'^2 - \frac{1}{2} \frac{\tanh 2m\alpha'}{1 + \tanh 2m\alpha'} = 0 \quad . \tag{3.162}$$

Under the assumption that $2m\alpha'$ is sufficiently small, the hyperbolic tangent functions in Eq. 3.162 can be replaced by their arguments and Eq. 3.162 rewritten as

$$(1+m^2)\alpha' - 2\omega'\alpha' + \omega'^2 = 0 \quad . \tag{3.163}$$

The roots of Eq. 3.163 are

$$\alpha' = \frac{\omega'}{1+m^2} (1 \pm jm) \quad . \tag{3.164}$$

In interpreting Eq. 3.164 it is useful to note that the parameter m is

$$m = \frac{v_{o+} - v_{o-}}{v_{o+} + v_{o-}} = \frac{b-a}{b+a} \quad , \tag{3.165}$$

where b and a are the coordinate locations of the upper and lower stream boundaries. Equation 3.165 describes a pair of waves propagating with approximately the mean velocity of the stream. One of the waves is

a growing wave and the other is a declining wave.

A more detailed investigation shows that Eq. 3.163 is valid only for small values of ω'. Figure 3.12 is a plot of more accurate solutions of Eq. 3.162 for m = 0.25. Also shown is the corresponding plot obtained by MacFarlane and Hay[21] using a more precise series approximation to the solution of the differential equation, Eq. 3.154.

As before, the solution above can be compared with the solution for a "thin"-stream model of rectilinear flow. Figure 3.13 represents the geometry of the stream model considered. The stream is assumed to have a thickness Δ sufficiently small that the perturbation quantities do not vary appreciably across the stream. As before, space-charge effects are accounted for by replacing the d-c volume-charge density by an equivalent surface-charge density σ_o defined by

$$\frac{-q\sigma_o}{m\,\epsilon_o\Delta} = \omega_p^2 \quad . \tag{3.166}$$

The average d-c stream velocity is

$$\bar{v}_o = v_{ox}\,\underline{\bar{x}} = \omega_c\, b\,\underline{\bar{x}} \quad , \tag{3.167}$$

where b is the average stream position.

Solutions of Laplace's equation, describing the transverse variation of the perturbed potential field outside the stream, are

$$\phi_1 = A\,\epsilon^{-\alpha(y-b)} \quad , \quad y \geq 0 \quad , \tag{3.168a}$$

$$\phi_1 = B\,\epsilon^{\alpha(y-b)} \quad , \quad y \leq 0 \quad , \tag{3.168b}$$

where waves are assumed to propagate as exp $j(\omega t - \alpha x)$. It is assumed that there is a negligible error in evaluating quantities at the mean position of the stream rather than at, for example, the stream boundaries $b \pm \Delta$. In the same manner as was described for the case of axial streams, r-f boundary conditions are determined by superimposing a positive ion

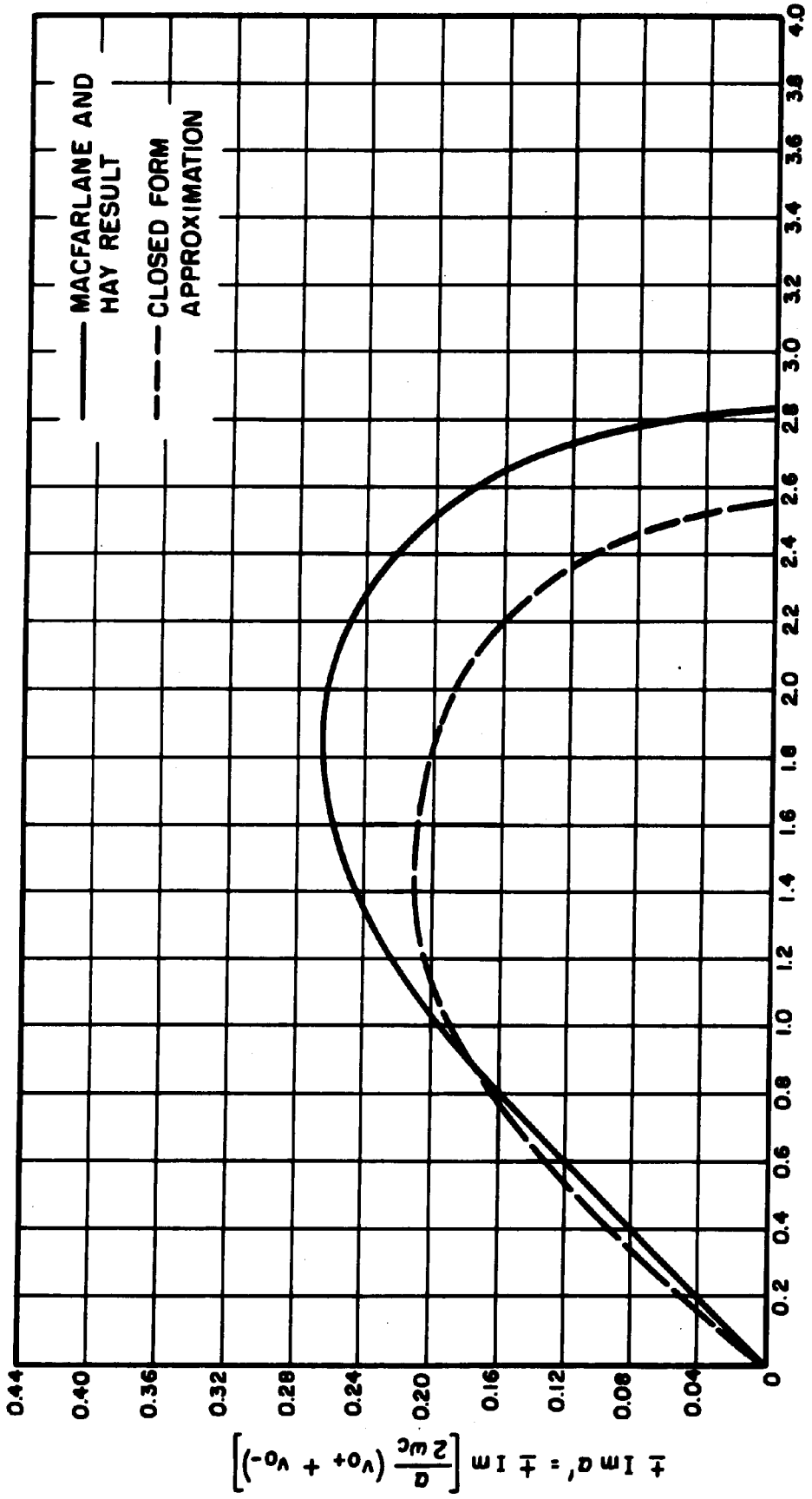


FIG. 3.12 GAIN VS. FREQUENCY FOR AN UNCONFINED SLIPPING STREAM. (m = 0.25)

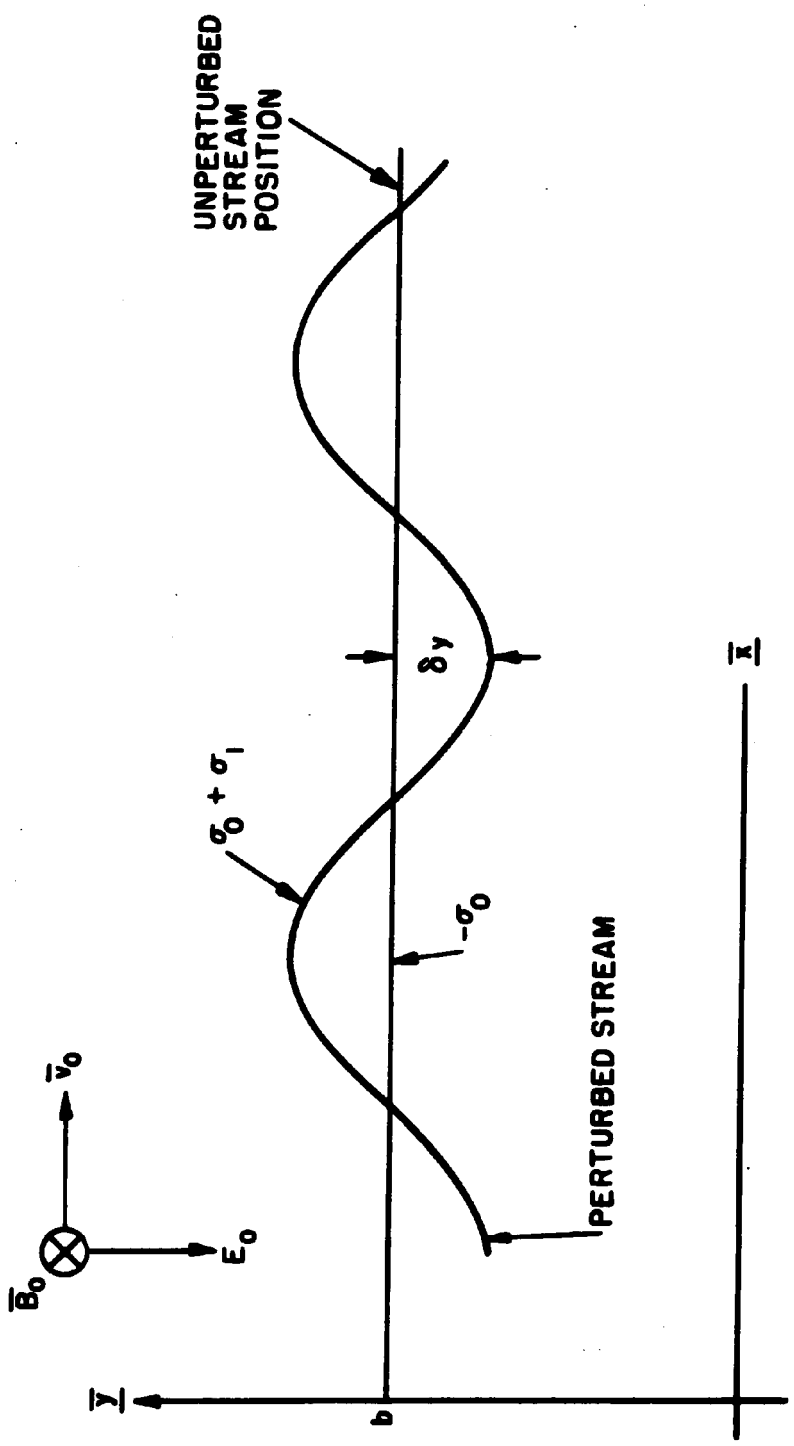


FIG. 3.13 GEOMETRY OF "THIN" STREAM RECTILINEAR FLOW MODEL.

stream on the unperturbed stream position. This is the physical equivalent of subtracting the d-c field of the unperturbed stream from the total fields of the perturbed stream. The resulting dipole layer, illustrated in Fig. 3.13, causes a discontinuity in potential

$$\phi_u - \phi_\ell = \frac{\sigma_o \delta_y}{\epsilon_o} = \frac{\sigma_o v_{1y}}{j\omega_d \epsilon_o} , \qquad (3.169)$$

where the subscripts indicate the potential is to be evaluated at the upper and lower edges of the stream respectively. The normal electric field (potential gradient) is discontinuous across the stream by an amount equal to the perturbed surface-charge density σ_1, i.e.,

$$- \frac{d\phi_u}{dy} + \frac{d\phi_\ell}{dy} = \frac{\sigma_1}{\epsilon_o} . \qquad (3.170)$$

The surface-charge density σ_1 is the "thin"-stream equivalent of the perturbed volume-charge density ρ_1, i.e.,

$$\sigma_1 = \rho_1 \Delta . \qquad (3.171)$$

From Eq. 3.95 we have

$$j\omega_d v_{1x} = \frac{q}{m} \frac{\partial \phi_s}{\partial x} , \qquad (3.172a)$$

$$\omega_c v_{1x} + j\omega_d v_{1y} = \frac{q}{m} \frac{\partial \phi_s}{\partial y} , \qquad (3.172b)$$

where the subscript s refers to a quantity evaluated within the stream. From the equation of continuity we have

$$\nabla \cdot \sigma_o \bar{v}_1 + j\omega_d \sigma = 0 . \qquad (3.173)$$

Elimination between the above equations, taking note of the fact that $\omega_p^2 = \omega_c^2$, leads to the equation

$$\frac{1}{\Delta\alpha} \left(\frac{\omega_d}{\omega_c}\right)^4 - \frac{1}{2} \left(\frac{\omega_d}{\omega_c}\right)^2 - 1 = 0 . \qquad (3.174)$$

Equation 3.174 has roots for $\Delta\alpha \ll 1$ which are

$$\frac{\omega_d}{\omega_c} = \pm \left(\frac{\Delta\omega}{v_{ox}}\right)^{1/4} , \tag{3.175a}$$

$$\frac{\omega_d}{\omega_c} = \pm j\left(\frac{\Delta\omega}{v_{ox}}\right)^{1/4} , \tag{3.175b}$$

Using the parameters defined by Eq. 3.161, we have as corresponding quantities

$$\begin{aligned} m &\rightarrow \frac{\Delta}{2b} , \\ \Delta\alpha &\rightarrow 2m\alpha' . \end{aligned} \tag{3.176}$$

Substituting these expressions into Eq. 3.175b we have for the growing (and decaying) wave

$$\alpha' = \omega' \left[1 \pm j\left(\frac{2m}{\omega'^3}\right)^{1/4}\right] . \tag{3.177}$$

There is another stream model which has appeared in the literature as a description of rectilinear Brillouin flow[22]. This is a one-dimensional thin-stream model. Figure 3.14 and the boundary conditions described in that figure are appropriate to this model. It is usually assumed, without specific justification, that the d-c stream velocity does not vary across the stream and also that the perturbation quantities inside the stream do not vary in the y direction. Because of these assumptions Eqs. 3.172 are replaced by

$$j\omega_d v_{1x} - \omega_c v_{1y} = \frac{q}{m} \frac{\partial \phi_s}{\partial x} , \tag{3.178a}$$

$$\omega_c v_{1x} + j\omega_c v_{1y} = \frac{q}{m} \frac{\partial \phi_s}{\partial y} . \tag{3.178b}$$

The equation of continuity, Eq. 3.173, is replaced by its one-dimensional counterpart

$$\frac{\partial (\sigma_o v_{1x})}{\partial x} + j\omega_d \sigma_1 = 0 . \tag{3.179}$$

Elimination between Eqs. 3.178 and 3.179, and application of the boundary conditions leads to the result

$$\alpha' = \omega' (1 \pm jm) \quad . \tag{3.180}$$

This solution is obtained under the approximation $(\omega_d/\omega_c)^2 \ll 1$ and corresponds to the field solution as given by Eq. 3.164.

This last model, however, is not representative of rectilinear Brillouin flow. Rather, it describes a perturbation of a thin plasma stream. It is under the condition of a neutralized d-c electric field that the d-c velocity gradient across the stream can be made zero and hence Eqs. 3.178, rather than Eqs. 3.172, applied. There is, nevertheless, a correlation between the mechanism by which growing waves occur in this plasma model and the mechanism by which waves grow in the "thick"-stream model. This is discussed in the following section.

3.5 Energy Exchange Mechanisms Between Electrons

In this section the mechanisms by which electrons can exchange energy are discussed. In particular the distinctions between the mechanisms acting, or not acting, in the stream models described above are brought out.

We consider a system consisting of an electron stream flowing in crossed d-c electric and magnetic fields. Collisions between electrons are assumed to be of negligible effect. The system is also considered to be closed, in the sense that the only "external" energy source which may be present is a d-c electric field which results from potentials on an electrode configuration bounding the system; in particular, no r-f energy source introduces power into the system.

To simplify the following discussion it is assumed that such "internal" r-f fields as arise are describable within the quasi-stationary

hypothesis $\nabla \times \bar{E}_1 \cong 0$. This assumption is basically a limitation of the discussion to waves which have a phase velocity much less than the speed of light. As a result of this condition, the r-f magnetic field is ordinarily of negligible effect in comparison to the electric field. The effect of a change in the energy density of the electric field is instantaneously communicated everywhere. Physically this means that the electric field distribution can be viewed as a sequence of steady states; at any instant the field pattern resulting from a distribution of r-f charge is the same as that of an identical distribution of d-c charge.

With the above simplification in mind, consider the transfer of energy between the electrons comprising the stream of the system described above. In particular, consider two volume elements of the stream chosen at random. The volume elements are assumed to be sufficiently small so that the space-charge density, velocity, etc., associated with each element does not vary spatially within the element. Because Maxwell's equations are linear, we can discuss the part of the total electric field due to the space charge in any one volume element separately from all the other volume elements comprising the total stream; i.e., we apply the principle of superposition. Further, we can say the partial electric field associated with one volume element moves with the average velocity associated with that volume element. This is in accordance with the quasi-stationary hypothesis made above. It then follows that the electrons in one volume element experience an electric field force, due to the charge in the other volume element, which moves past them with the relative average velocity of the two volume elements. If this relative velocity is zero there can be no energy exchange between the electrons in each volume element which uses the d-c kinetic energy of the electrons as a source.

In a neutralized electron stream (plasma flow) having a uniform velocity none of the electrons move relative to each other. Hence there is no coupling to an energy source in such a flow and there can be no growing waves. On the other hand the double-stream plasma model described previously has two distinct velocity components in the flow. Growing waves are possible in such a model and, indeed, they do exist. The mechanism of the energy exchange in this case is the transfer of energy from the d-c stream motion into the r-f field of the perturbation in a manner similar to that occurring in a traveling-wave tube. As a matter of fact, there is a double transfer of energy in this case. The slower stream extracts energy from the r-f wave as in a linear accelerator. The faster stream is the source of energy for the perturbation.

There has been a tacit assumption made in the preceding paragraphs about the nature of the perturbation. It has been assumed that the stream boundaries are not disturbed significantly by the perturbation. (Using Hahn's equivalent surface-charge density concept, the stream boundary is not affected by the perturbation. Only the charge distribution on the <u>same</u> boundary as the unperturbed stream is affected.) If this constraint is relaxed, there is a source of energy available to a perturbation of even a single velocity stream. This source is the potential energy involved in the relative positioning of electrons in the stream.

The type of perturbation referred to is exemplified by the second type of thin-stream model described in section 3.4 for a rectilinear Brillouin stream. (Figure 3.13 is a sketch of the model.) This model is actually not appropriate as a description of the Brillouin stream since it assumes a uniform velocity across the unperturbed stream. It is actually a model of a <u>boundary</u> perturbation of a plasma flow. More

accurately, since the ion stream is assumed immobile, the boundary of only the electron stream is perturbed. As a result of the stream perturbation the space-charge forces are no longer balanced, and they act in such a way as to enhance the perturbation. If no magnetic field is present the perturbation is evidently simply a failure of the focusing mechanism. This is also true, although perhaps less evident, when a magnetic field is present. The action of the magnetic field is to limit the rate of increase of the electron separation.

This last energy exchange mechanism is basically different from the first mechanism described.

Consider now the axially symmetric stream models discussed in this chapter. First consider perturbations under the constraint that the stream boundaries do not change. Since, in the axially symmetric stream models considered, electrons do not move relative to each other, a perturbation is not coupled to the d-c kinetic energy of the stream. There can be no growing waves depending on this energy source.

If we now allow a boundary perturbation as in a "thin" hollow stream we encounter, as described in section 3.3.2, a failure of the stream focusing mechanism. The space-charge field is not balanced by the magnetic field when the perturbation is present and the stream defocuses. The energy source is, in this case also, the d-c potential energy associated with the relative positions of the electrons.

The reason for the apparent anomaly in the results of "thick"- and "thin"-stream perturbation analyses is now clear. These analyses consider different kinds of perturbations. There is no reason to expect similar results. It is reasonable to expect that the "thick"-stream analysis would, in the limit, pass over to the "thin" stream analysis. Unfortunately, the boundary conditions which are applied in the two types

of analysis are basically different, and must be reconsidered on passing, in the limit, from a "thick" to a "thin" stream.

The same conclusion as above applies to the consideration of the rectilinear Brillouin stream models. First, we consider perturbations within fixed stream boundaries. There is, because of the velocity slip across the stream, a coupling of a perturbation to the d-c kinetic energy of the stream. There is also an indirect coupling to the d-c electric field. When the perturbation extracts energy from the d-c stream velocity, the focusing system forces the electrons to regain this energy from the d-c electric field established by the electrode potentials. In this somewhat complicated process, the d-c kinetic energy of the stream acts only as an energy dispenser. Actually there is a two-way energy exchange. Electrons at the top of the stream extract energy from the perturbation and return this energy to the d-c electric field. Electrons at the bottom of the stream act in just the opposite fashion.

The rectilinear Brillouin stream is also unstable under a boundary perturbation. This again is a failure of the focusing system.

The discussion of this section has been thus far confined to laminar stream. When the possibility of nonlaminar streams is entertained, the entire discussion must be reconsidered. Unfortunately the problem is quite complex both from a physical and from a mathematical point of view. If we return to the introductory discussion of this section, and again consider two volume elements of an electron stream, it is not true that the d-c kinetic energy of volume elements having no average relative velocity is not coupled to a perturbation. Individual electrons in the volume may have a relative velocity even though there is no average motion between volume elements. Other complex effects are possible. For example, in rectilinear flow electrons near the top of the stream give

energy to the d-c electric field whereas electrons near the bottom of the stream extract energy from this field. In a possible nonlaminar stream a given electron may, at different times, be in both positions. That is, a given electron might move across the stream. The effects of various degrees of nonlaminar motion under different focusing systems have not, as yet, received adequate attention. Since essentially all electron streams obtained in practice are unavoidably nonlaminar, the consequences and importance of nonlaminar motion should certainly be investigated.

CHAPTER IV. THE CROSSED-FIELD STREAM ANALYZER

4.1 The Purpose of the Crossed-Field Stream Analyzer

As noted in section 1.3, the usual interpretation of the diocotron effect as a manifestation of a "slipping-stream" amplification process does not account for the order of magnitude of the negative-sole currents observed. For the further study of the diocotron phenomena it was necessary to extend the limited data available in the literature. For this reason an experimental crossed-field stream analyzer was designed and built.

The stream analyzer is specifically designed to study the characteristics of the negative sole current as a function of distance along the sole. To do this the sole is divided into a number of electrically insulated segments each of which can be individually monitored.

4.2 Description of the Stream Analyzer and Experimental Setup

4.2.1 Over-All Geometry of the Stream Analyzer. Figure 4.1 is an assembly drawing of the crossed-field stream analyzer. The active portion of the stream analyzer is of the same general geometry as illustrated in Fig. 1.1. The vacuum envelope is fashioned in the form of a box; each wall and the two ends of the box constitute a subassembly on which various parts of the internal structure are mounted. In Section B-B of Fig. 4.1, two of the walls (number 3) are copper-plated hot-rolled steel. These walls are the magnetic pole pieces for an external electromagnet. In addition, these walls are used to space the electrodes on the other two walls properly. Both the remaining walls are OFHC copper. One of these walls (number 2) is the base plate on which the anode assembly is mounted. The anode consists of four copper segments, each mechanically

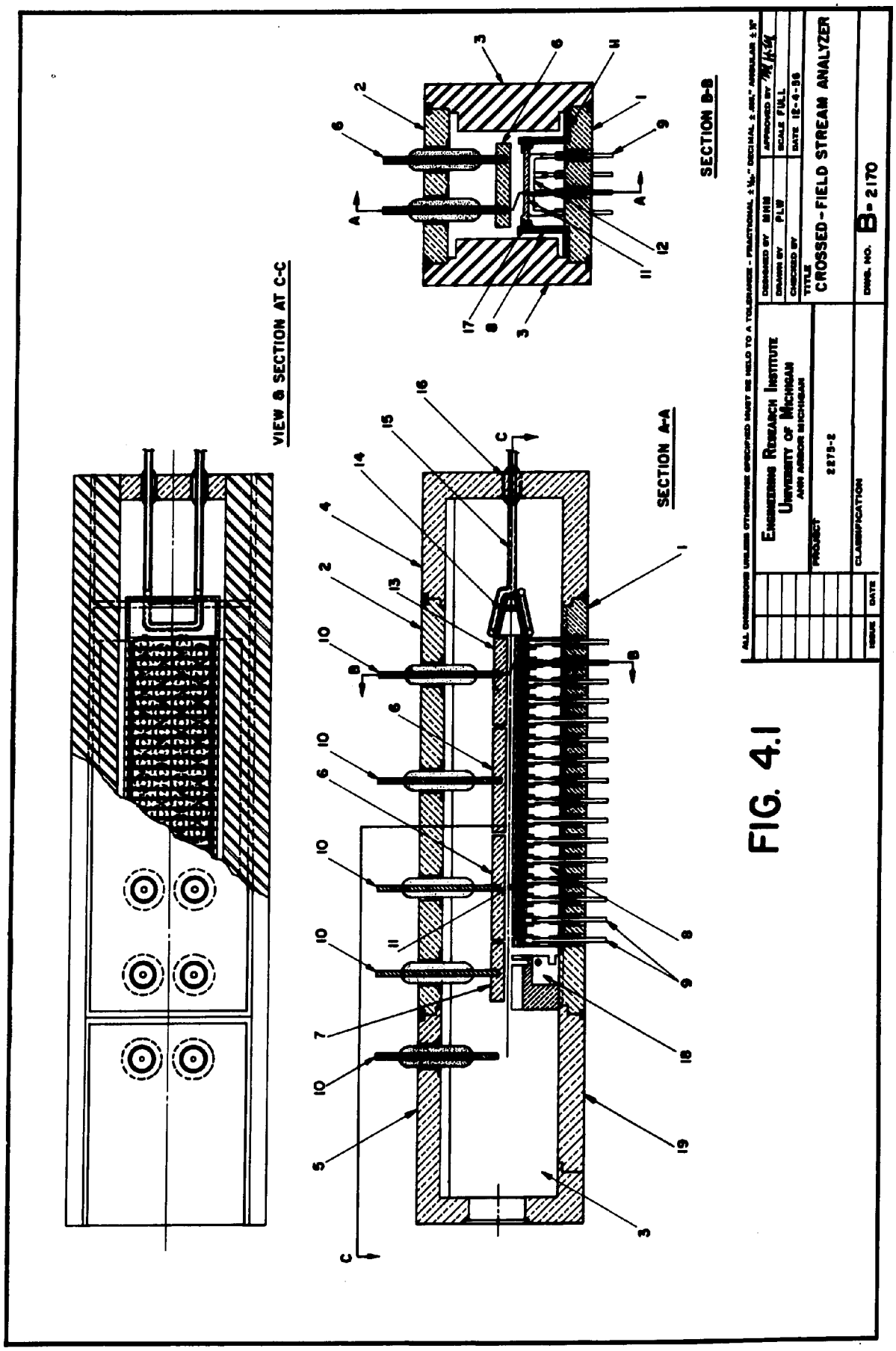

VIEW B SECTION AT C-C
SECTION B-B
SECTION A-A
ENGINEERING RESEARCH INSTITUTE
UNIVERSITY OF MICHIGAN
ANN ARBOR MICHIGAN
PROJECT 2273-2
CLASSIFICATION
DRAWN BY PLB
CHECKED BY
SCALE FULL
DATE 12-4-56
TITLE
CROSSED-FIELD STREAM ANALYZER
DWG. NO. B-2170

FIG. 4.1

supported by two Stupakoff vacuum feedthroughs. The segments are insulated from one another and from the base plate. Figure 4.2 shows photographs of the entire anode subassembly.

The other wall is the mounting for the sole and cathode (number 1 in Fig. 4.1). The sole consists of thirty-one copper segments (or probes) electrically insulated from one another and from the base plate. Each segment can be water-cooled; the cooling pipes also serve as electrical connections to the segment. Figure 4.3 is an assembly drawing of a sole segment and its associated cooling pipes. The segments are mechanically supported by two "L"-shaped side pieces (number 8 in Fig. 4.1). Corresponding notches in the sides of the segments and the L supports serve as guides for sapphire rods which provide the mechanical constraint and maintain the electrical isolation of the probes. The sole segments are spaced from one another by ground pyrex washers hung on the sapphire rods. Figure 4.4 is a photograph (prior to assembly) of the stream analyzer cross section corresponding to section B-B of Fig. 4.1. Figure 4.5 shows photographs of the completed sole assembly. One of the L supports has been removed so as to exhibit greater detail of the structure. (This has produced some distortion of the assembly. With both L supports present, however, the maximum variation in height along the sole is less than 0.005 inch. The plate-sole spacing is 0.20 inch.)

Figure 4.5 also shows the cathode assembly which is mounted on one end of the sole base-plate. Figure 4.6 is an isometric view of the cathode block and the filament. The block is copper and is mechanically fastened to the sole base-plate. The filament is a tungsten tape fastened to the cathode block at one end and riding in a trough flush with the upper surface of the block. The other end of the filament rides free in a notch cut in an insulated molybdenum plate. This plate is used as a

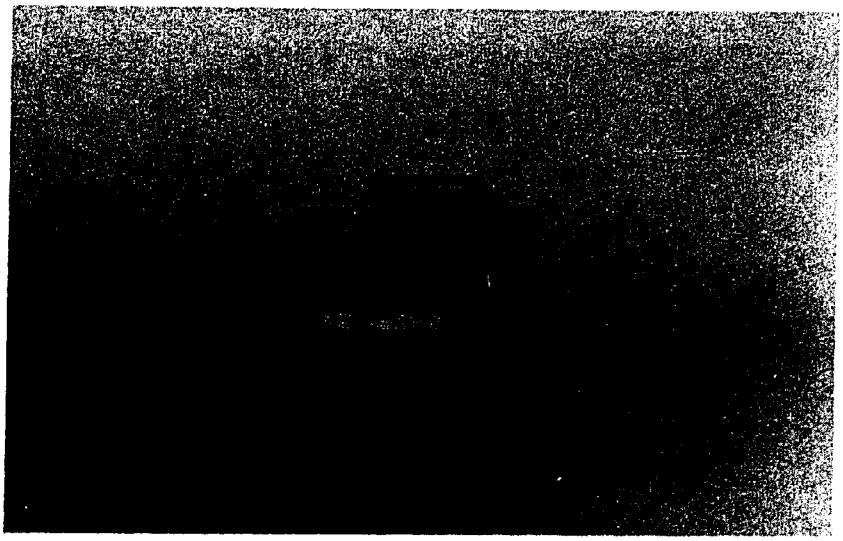




FIG. 4.2 STREAM ANALYZER ANODE SUBASSEMBLY.

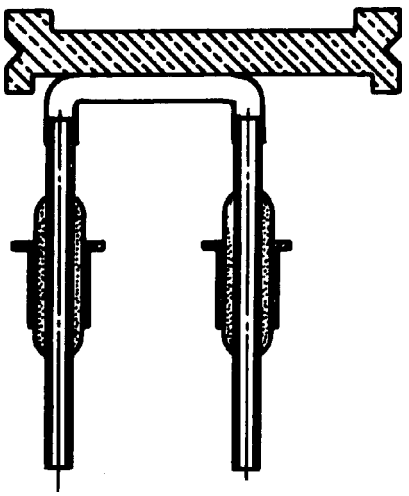


FIG. 4.3

SOLE SEGMENT SUBASSEMBLY

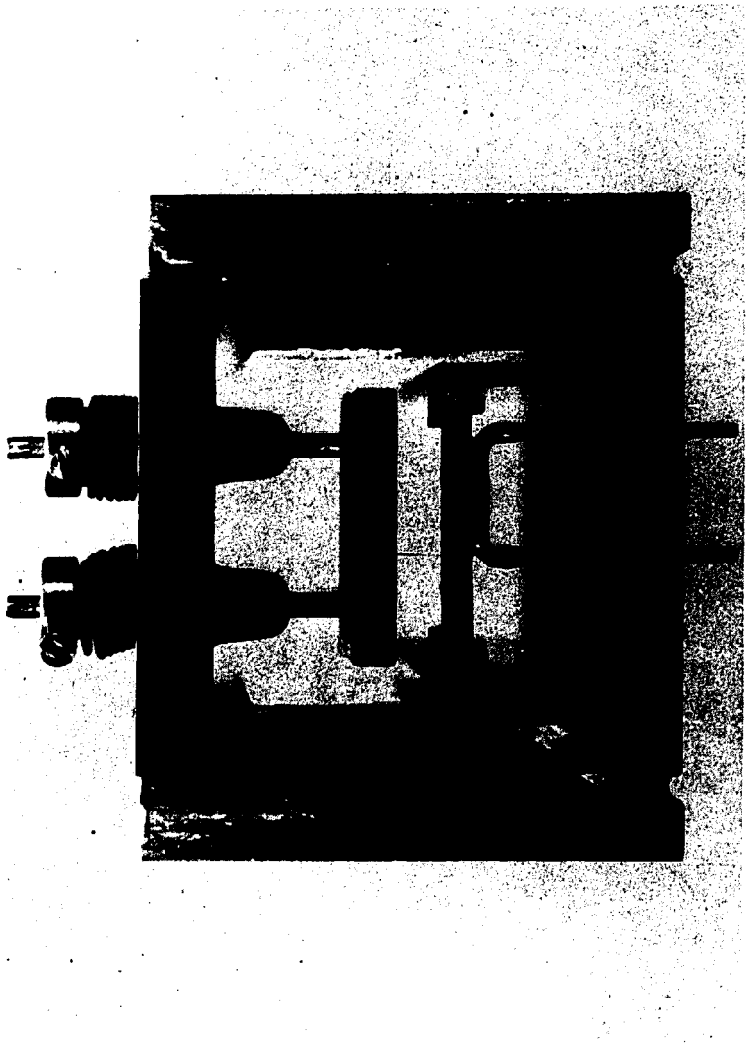
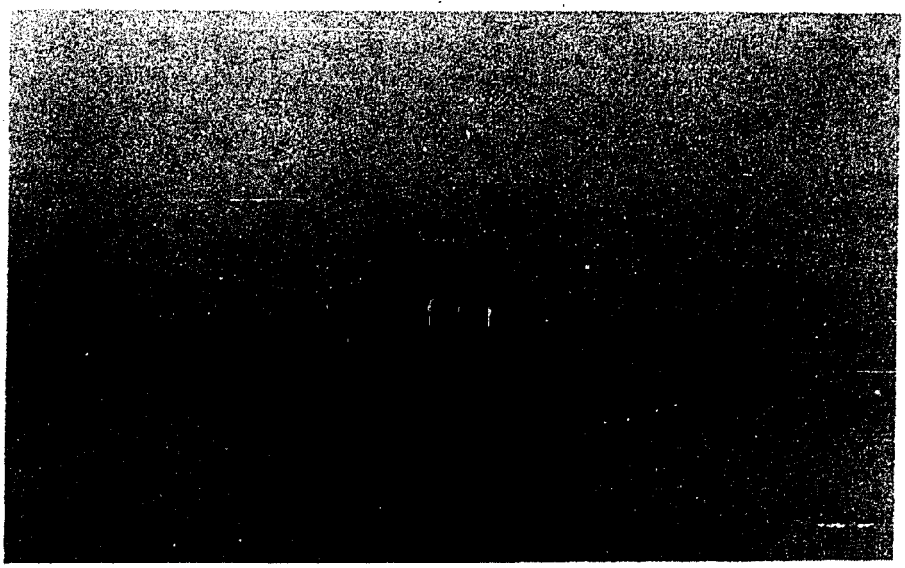
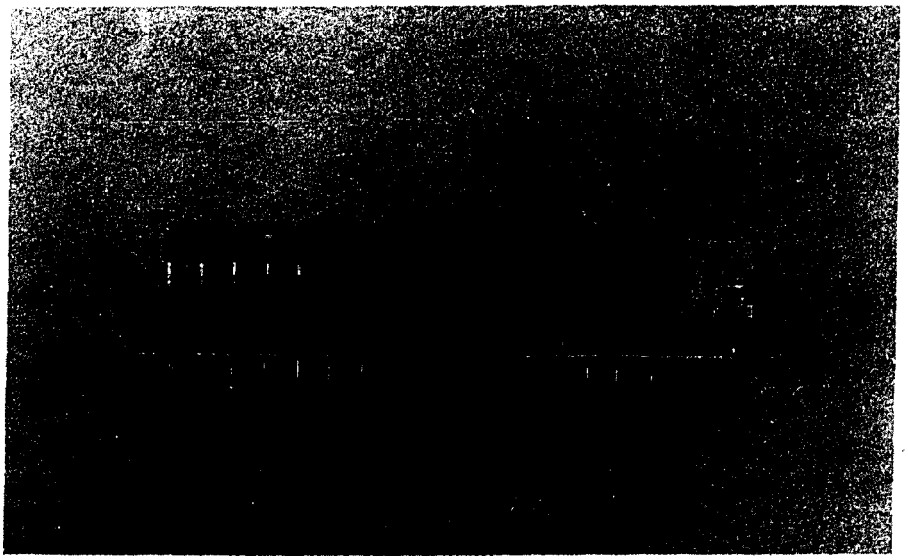


FIG. 4.4 CROSS SECTION OF STREAM ANALYZER GEOMETRY.
(SEE SECTION B-B OF FIG. 4.1)



a. END VIEW OF SOLE AND BASE PLATE.



b. FRONT VIEW OF SOLE AND BASE PLATE.

FIG. 4.5 CROSSED-FIELD STREAM ANALYZER.

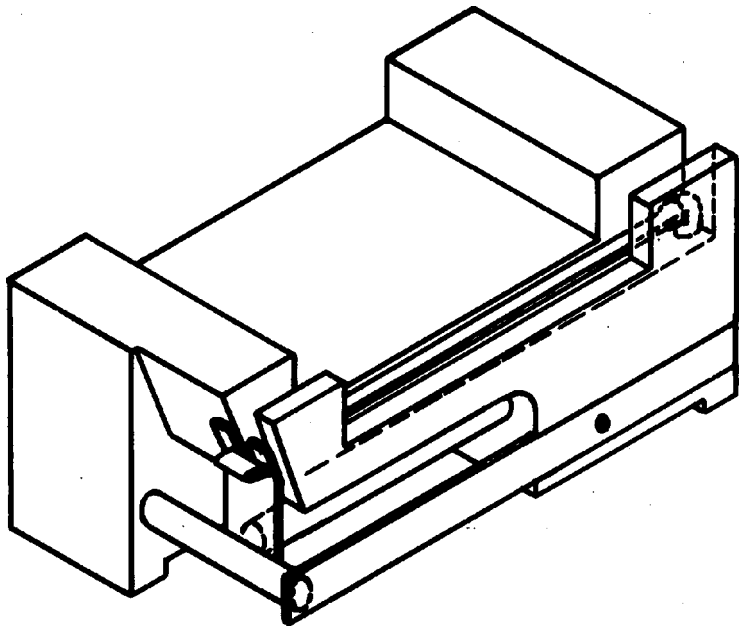


FIG. 4.6 CATHODE BLOCK AND FILAMENT ASSEMBLY.

flat spring to maintain tension on the filament. The vacuum envelope of the stream analyzer is one terminal of the filament and a lead brought from the spring through the rear of the cathode block is the other filament terminal. The spring itself is brazed to a sapphire rod which is supported by the cathode block (see Fig. 4.6).

One of the two ends of the vacuum envelope houses the collector (numbers 14 and 15 in Fig. 4.1). The collector is water-cooled; the cooling pipes are also used as electrical connections to the otherwise insulated collector. The other end of the vacuum envelope mounts the vacuum feedthroughs for bringing out the filament lead fastened to the filament spring, and the exhaust port (number 5 in Fig. 4.1).

The ends of the box and the magnetic pole pieces are silver-soldered together to form a frame on which the anode and sole base plates are mounted. Figure 4.7a is a photograph of the several stream analyzer subassemblies prior to final assembly. (The collector is soft-soldered into place as a part of the frame of the box.) The plate and sole subassemblies are indium-soldered onto the frame so that they can be independently removed.

4.2.2 Experimental Test Setup. Figures 4.8a and 4.8b are photographs of the stream analyzer mounted in its electromagnet, and some of the associated wiring. The pipe coming out of the end of the stream analyzer is the exhaust tubulation leading to the vacuum station. The sole-segment cooling pipes and the electrical connections to them are visible in the center of Fig. 4.8a. The sole segments were not water-cooled for the experiments described subsequently in this dissertation. Figure 4.9 is a photograph of the entire experimental setup (except for auxiliary measuring equipment on a movable table.) The metering and switching panel can be seen directly in front of the stream analyzer. On the far

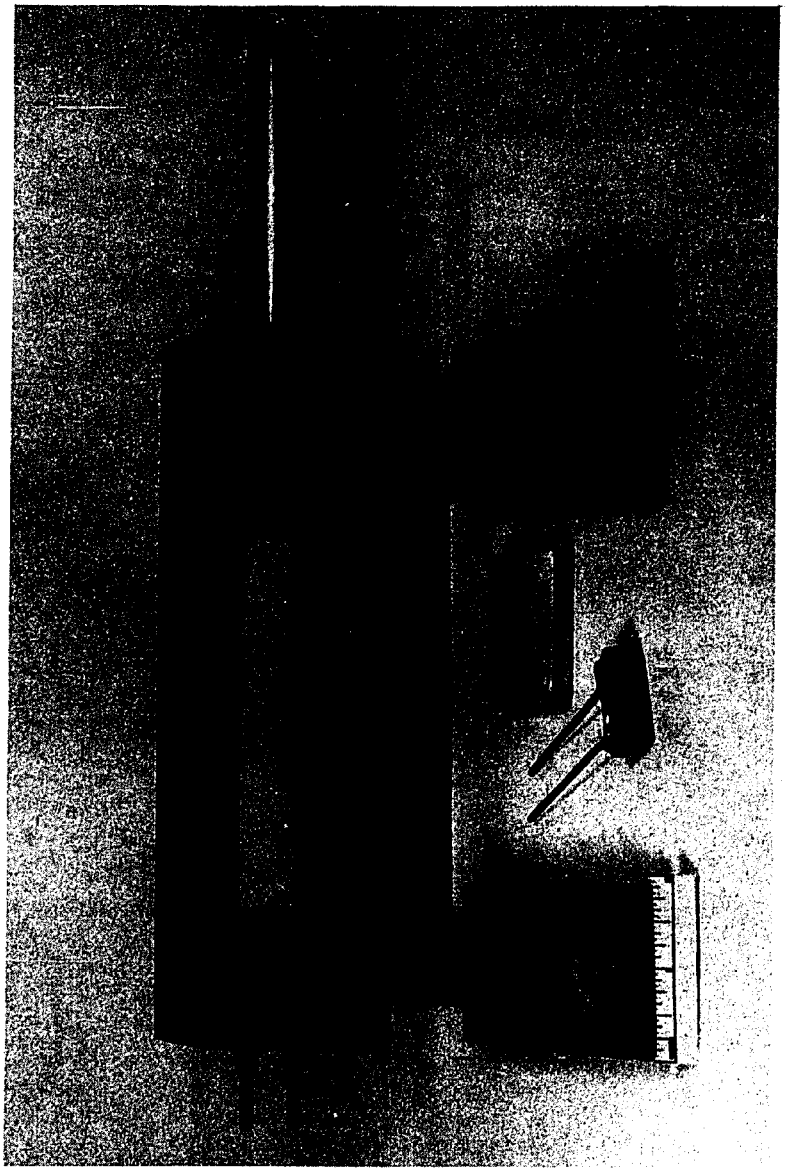
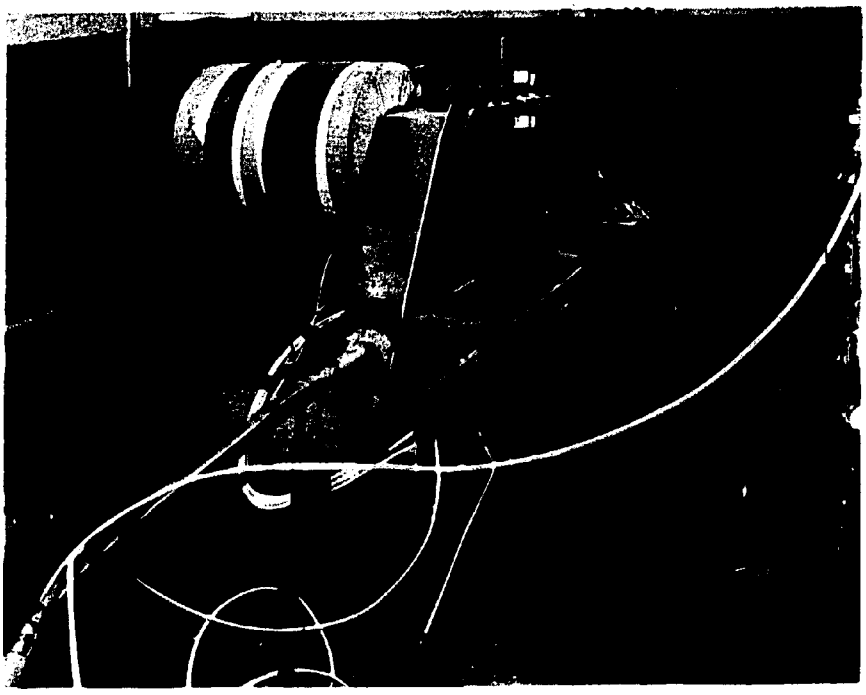
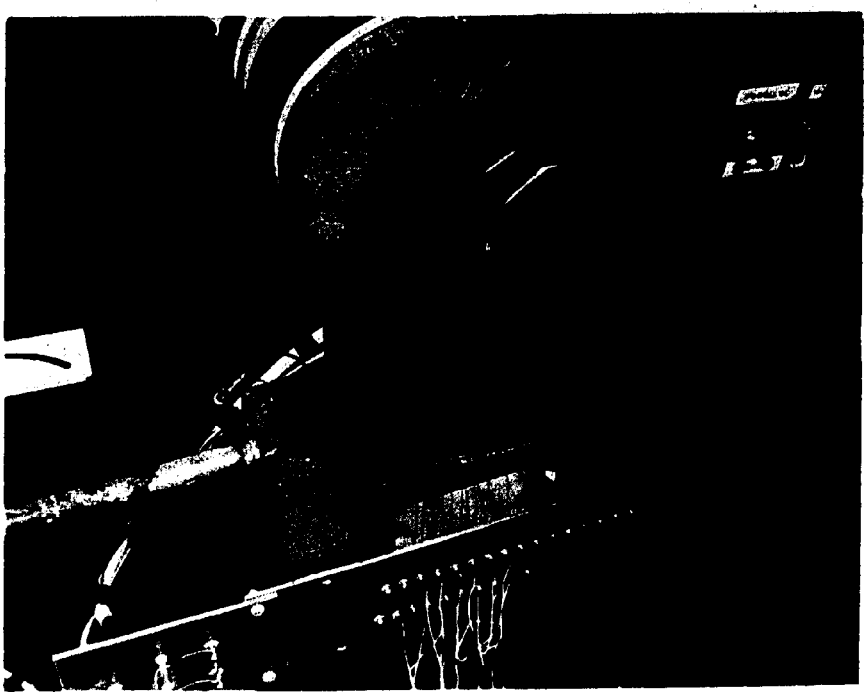


FIG. 4.7 STREAM ANALYZER COMPONENTS.



a. STREAM ANALYZER IN MAGNET.



b. CLOSE-UP OF STREAM ANALYZER IN MAGNET

FIG. 4.8 STREAM ANALYZER EXPERIMENTAL SETUP.

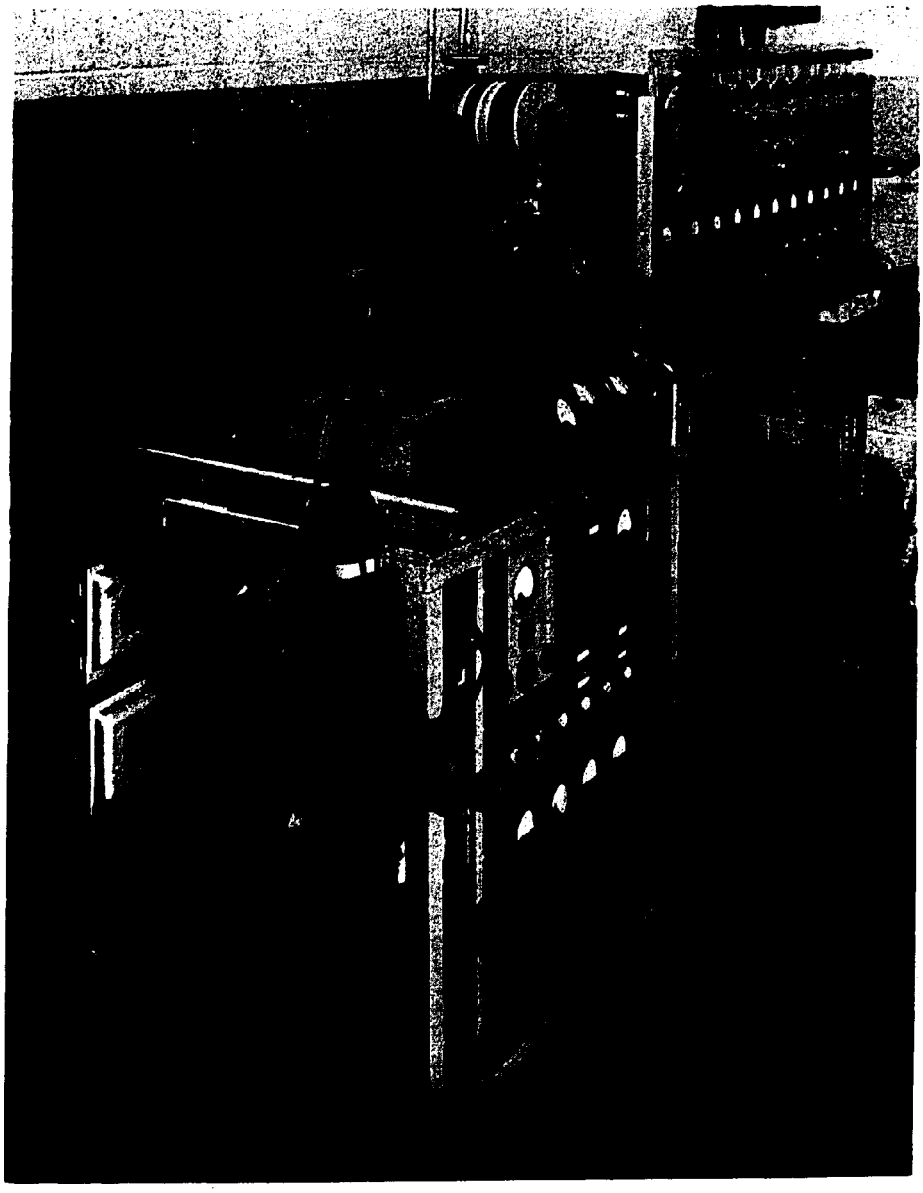


FIG. 4.9 EXPERIMENTAL TEST SETUP.

right, below the table, the cooling hose for the collector is wrapped around a wood support. Ann Arbor tap water has a year-round resistivity of about 5000 ohms per centimeter cube. Six feet of cooling hose suffice to keep leakage currents negligible relative to the collector currents involved in the measurements.

4.3 Uniformity and Calibration of the Magnetic Field

It is necessary to maintain a uniform magnetic field in the region in which the electron stream flows. This was accomplished simply by making the pole pieces much larger than the electron stream region. For example, where the pole pieces had a width of 1.968 inches, the corresponding dimension of the stream region, the plate-sole spacing, is 0.20 inch. The pole pieces are 9.0 inches long; the distance from cathode to collector is somewhat under 5.20 inches. Of course, it is desirable to keep the spacing between the pole pieces small to maintain field uniformity and to minimize the magnet current needed to produce a given field. The spacing between pole pieces is 1.175 inches and the nominal stream width, the stream dimension corresponding to this, is 0.75 inch. The magnetic field, measured with a Hall effect gaussmeter, varies less than five percent along the direction of the stream motion and less than two percent across the stream width. There is negligible variation of the magnetic field between the plate and sole.

Since the stream analyzer is completely enclosed during operation it was necessary to precalibrate the magnetic field produced by the pole pieces against the current to the magnet. This was done after the frame of the vacuum envelope of the tube was soldered together so that the magnetic field geometry was fixed. There is a small amount of hysteresis in the pole pieces, which leads to an uncertainty in the magnetic field for

a given current setting of about ten percent at 400 gauss, six percent at 1000 gauss, and three percent at 1500 gauss.

4.4 Geometry of the Interaction Space

Figure 4.10 is a sketch showing the dimensioning of the plate-sole space and the cathode region. The design of the stream analyzer developed basically in two steps; first, the plate-sole region was designed, and then, the cathode system for injecting the electron stream into the plate-sole space was designed.

4.4.1 Design of the Plate-Sole Space. The first dimension chosen was the plate-sole spacing of 0.2 inch. Such a spacing would not be unusual in a crossed-field oscillator or amplifier designed for L or S-band operation. The diocotron phenomenon has been observed in such tubes. The remaining dimensions were then chosen to obtain a wide range of operating conditions. A useful criterion of "wide range" is the cycloidal motion of a single electron in uniform crossed electric and magnetic fields.

In section 2.2, it is shown that, in general, electron motion in uniform crossed fields consists of a superposition of a linear motion at a velocity $\frac{\bar{E}_o \times \bar{B}_o}{\bar{B}_o \cdot \bar{B}_o}$, and a circular motion at an angular radian frequency $\frac{q}{m}\bar{B}_o$. The sketch shown in Fig. 4.11 represents a uniform crossed-field environment. A difference of potential ϕ_{oa} exists between two parallel planes a distance d apart. A uniform magnetic field B_o is directed into the page. For this environment the linear motion of an electron is in the $\bar{x}$ direction and has a magnitude given by

$$\text{linear velocity component} = \frac{\phi_{oa}}{dB_o} \quad . \tag{4.1}$$

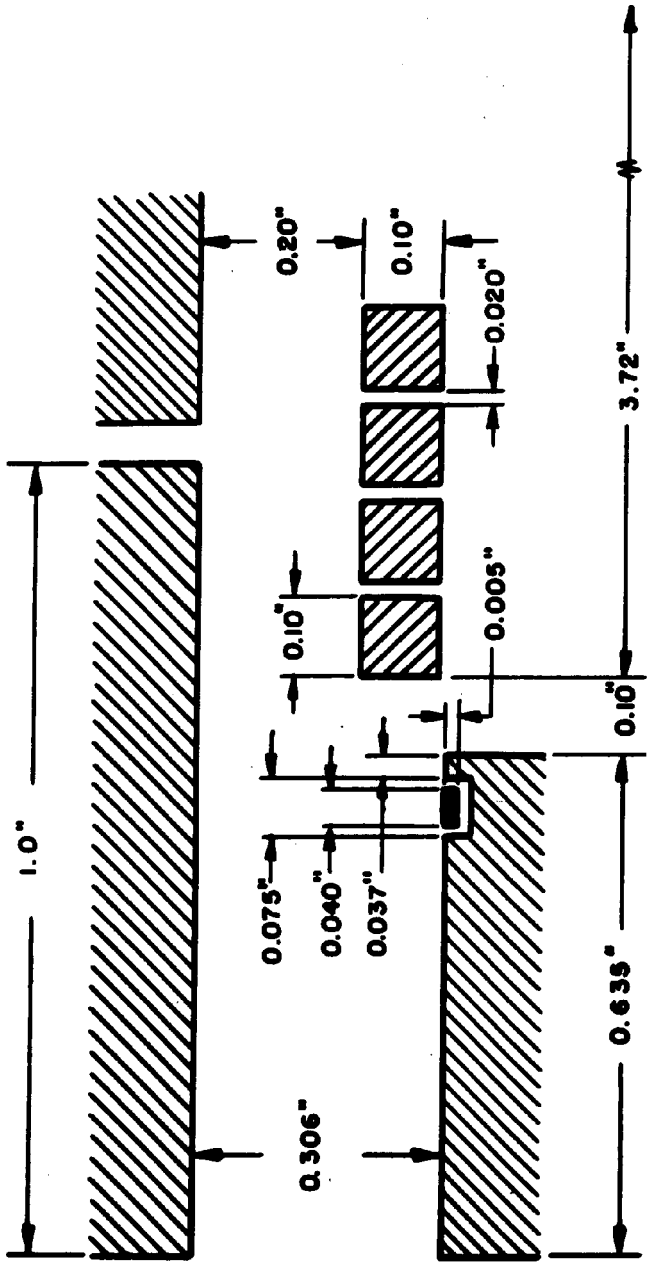


FIG. 4.10 DIMENSIONING OF PLATE-SOLE SPACE AND CATHODE REGION.

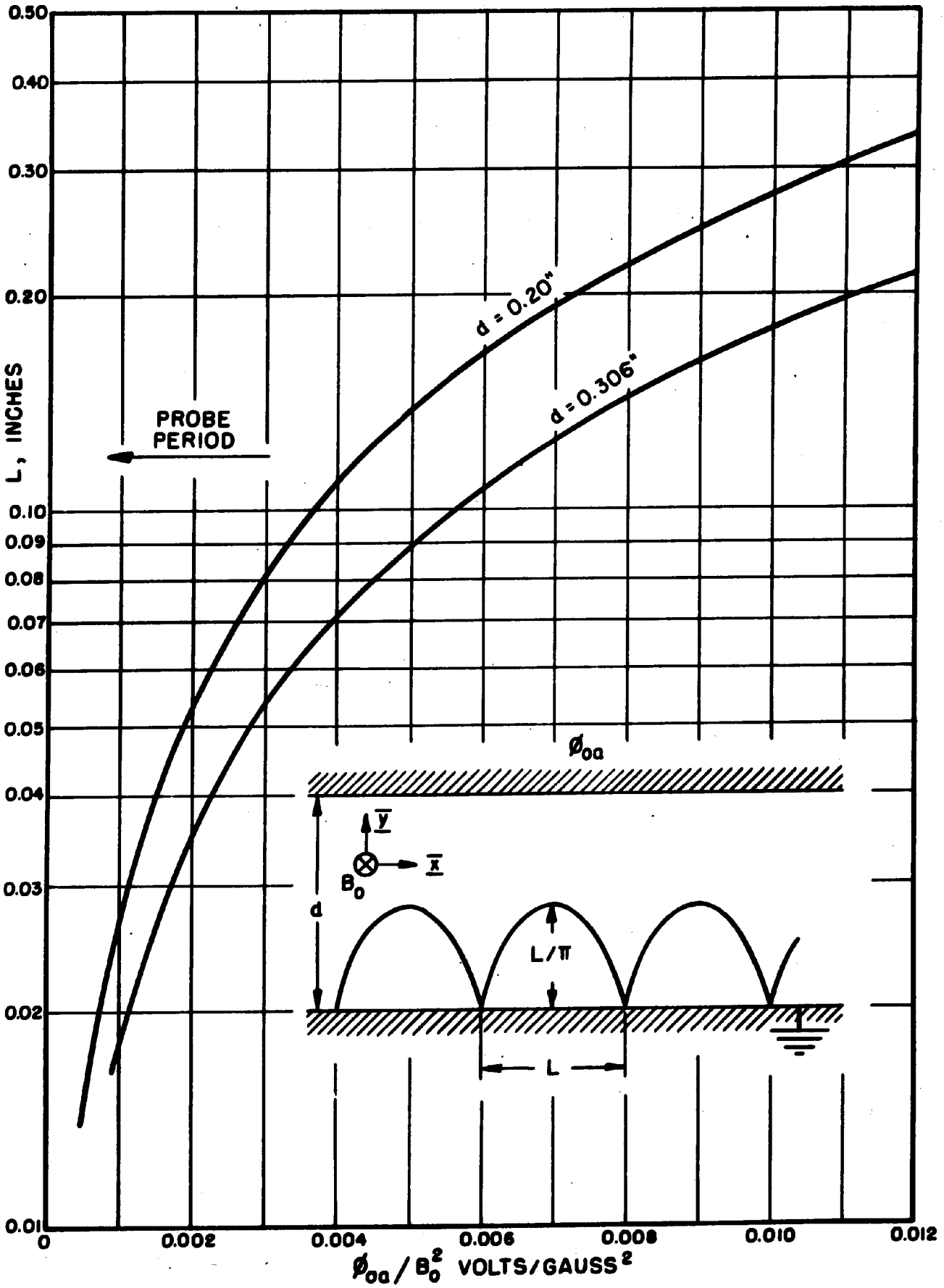


FIG. 4.11 CYCLOIDAL MOTION IN UNIFORM CROSSED FIELDS.

The angular frequency of rotation around the magnetic flux lines is

$$\text{angular frequency of rotation} = \omega_c = \frac{q}{m} B_o \quad . \tag{4.2}$$

An important property of the motion is suggested by Eq. 4.1 and 4.2. The time to complete one cycle or period of the motion is a function only of the magnetic field. The velocity at which the electron advances is, for a given geometry, a function only of ϕ_{oa}/B_o. Hence the distance advanced by an electron in the course of one cycle is a function of the ratio ϕ_{oa}/B_o^2. It can be shown, in fact, that the shape of any trajectory traced by an electron in a fixed geometry of any configuration is a function only of the ratio ϕ_{oa}/B_o^2.[8] The time taken for a particular electron to trace out a given portion of a trajectory is, however, inversely proportional to the magnetic field. A relatively simple possible electron motion is the cycloidal motion of an electron released from a zero-potential plane with zero initial velocity. The trajectory traced by such an electron is described by the parametric equations

$$x = \frac{\phi_{oa}}{\omega_c B_o d} (\omega_c t - \sin \omega_c t) \quad , \tag{4.3a}$$

$$y = \frac{\phi_{oa}}{\omega_c B_o d} (1 - \cos \omega_c t) \quad . \tag{4.3b}$$

The length of one period of this cycloidal motion, L, is

$$L = \frac{2\pi m}{qd} \frac{\phi_{oa}}{B_o^2} \quad , \tag{4.4}$$

and the height of the cycloid is simply $1/\pi$ of the length of one period of the motion. The cycloidal period corresponding to electrode spacings of 0.2 inch and 0.306 inch are plotted in Fig. 4.11 as functions of the scaling ratio ϕ_{oa}/B_o^2. (These spacings correspond to the plate-sole and plate-cathode spacings, respectively, of the stream analyzer.)

The conditions under which an electron, leaving the lower plate in Fig. 4.10, just grazes the upper plate are useful in design considerations. These conditions can be obtained by setting y in Eq. 4.3 equal to the electrode spacing d, i.e.,

$$\frac{\phi_{oa}}{\omega_c B_o d^2} = 1 \quad \text{(grazing condition)} \quad . \tag{4.5}$$

For electrode spacings of 0.2 inch and 0.306 inch, the scaling parameters for a grazing trajectory are 0.0226, and 0.0529 volt/gauss^2, respectively. The corresponding period lengths are π times the electrode spacings. The grazing trajectory conditions represent a measure of the limits of possible operating conditions (as specified by the scaling parameter ϕ_{oa}/B_o^2).

The sole, as described above, consists of thirty-one segments. The period of the sole segmentation was chosen so that operating conditions could be obtained involving cycloidal periods both less than and greater than the sole segment period. The segment period is 0.12 inch. Comparison with the cycloidal period as a function of the scaling parameter can be made on Fig. 4.10. The segment itself is 0.10 inch wide and the spacing between segments accounts for the remaining 0.020 inch. The length of the sole was chosen so that several cycloidal periods, even at high values of the scaling parameter (0.02 to 0.03 volt/gauss^2), would be completed before collection at the end of the plate-sole space. The length of the sole is 3.72 inches. Actually, the presence of the collector at the end of the sole distorts the electric field in its immediate vicinity. The last few sole segments are therefore in a different environment than the other sole segments. This, however, is not an important problem, as the measurements described later show.

The anode in the stream analyzer is formed by four copper segments.

This was done so that operating conditions could be separately adjusted in different sections of the stream analyzer.

4.4.2 The Electron Stream Injection System. The electron gun is a Charles gun, a type frequently used in rectilinear crossed-field tubes. It is based on the idealized cycloidal injection system illustrated by Fig. 4.12. The plane in which the cathode is located (in the idealized system) is twice as far from the plate as is the sole. It is assumed that the electric field is uniform in both the cathode region and the plate-sole space, i.e., that the transition field between the two regions is concentrated in a very narrow band as indicated by the dotted line in Fig. 4.12. The cathode is located at a distance from the entrance plane of the plate-sole space that corresponds to one-half the cycloidal period of the space-charge-free motion of an electron in the fields of the cathode region. An electron originating in the cathode will therefore enter the plate-sole space normally at the end of one-half a cycloidal period. Its entrance height above the sole, obtained from Eq. 4.3, is shown in Fig. 4.12. Differentiation of Eq. 4.3a shows that the entrance velocity is $\phi_{oa}/B_o d$. This is exactly the velocity for which the trajectory in the plate-sole space is rectilinear.

There are various omissions which make the ideal injection system above academic for the purposes of the present investigation. Neglect of space-charge forces is, at least for low-current-density streams, not too serious an omission. There will be a broadening of the stream because of emission along a cathode of finite width. However, cathodes of small widths can be used for low-current-density streams. In addition, there is a certain degree of convergence of trajectories originating from different points along the cathode. This can be seen by sketching several cycloidal trajectories. The transition of the fields between the

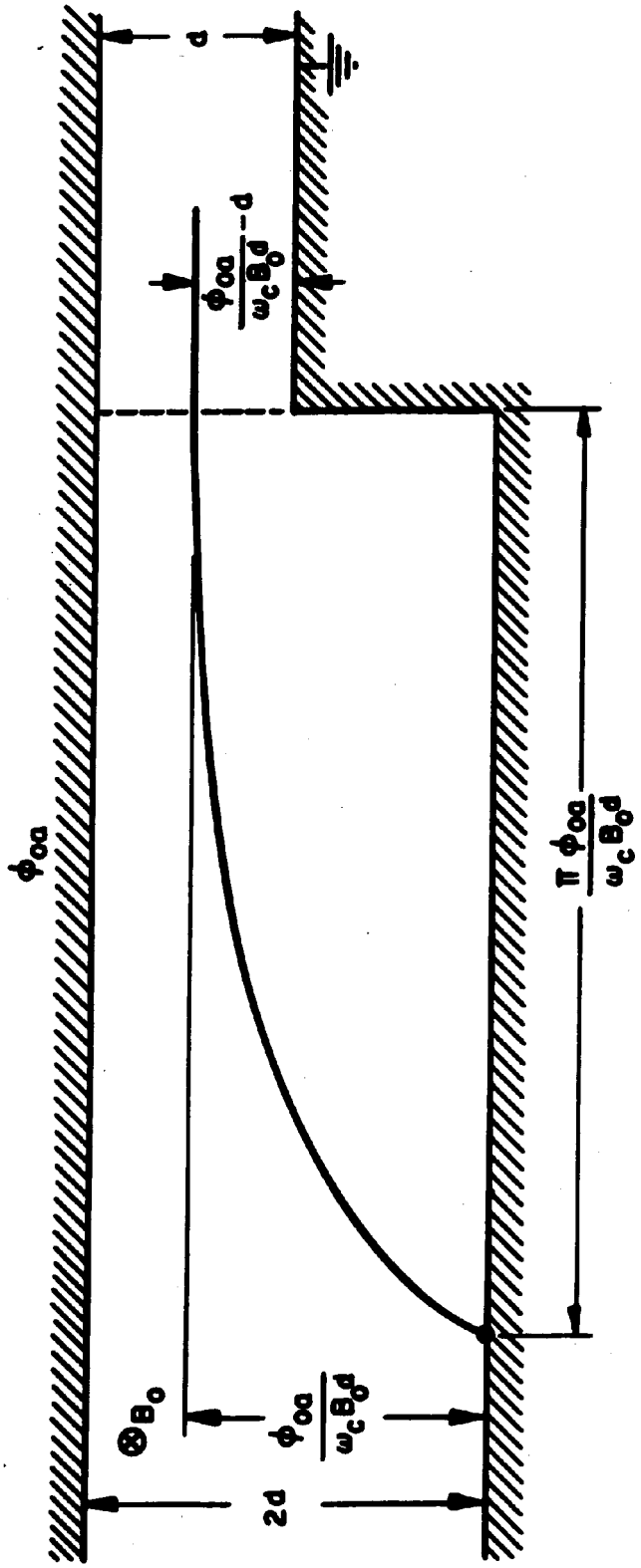


FIG. 4.12 IDEALIZED ELECTRON STREAM INJECTION SYSTEM.

cathode region and the plate-sole space will, in general, occur over a significant distance. However, several trial designs using the actual electric fields in the design geometry to compute electron trajectories can produce a reasonable approximation to the ideal injection system.

From the point of view of the purpose for which the stream analyzer is designed the most serious difficulty with the ideal system is that the cathode location is proportional to the scaling parameter ϕ_{oa}/B_o^2. Since the stream tester is to be operated over a wide range of values of the scaling parameter, the cathode will, for the most part, be in the "wrong" position. However, focussing of the stream can be maintained at the expense of having electrons move along trochoidal rather than rectilinear trajectories in the plate-sole space. If operating conditions (as measured by ϕ_{oa}/B_o^2) are limited to the range for which the height of the trochoidal trajectory is much less than the plate-sole spacing the stream will traverse the plate-sole space in the general fashion illustrated by Fig. 4.13. Electrons will "roll" uphill into the plate-sole space along an equipotential (approximately). If the sole potential is less than the cathode potential, no electrons can reach the sole. Hence almost any value of scaling parameter for which the amplitude of the trochoid-like electron motion is much less than the plate-sole spacing will focus the stream.

A number of electron trajectories for various geometries were calculated by hand. On the basis of these calculations the cathode dimensions shown in Fig. 4.10 were chosen. It might be noted that the cathode assembly is easily removable from the base plate. Except for the delay following from losing the vacuum in the stream analyzer, there is no difficulty in changing cathode dimensions without altering the remainder of the geometry.

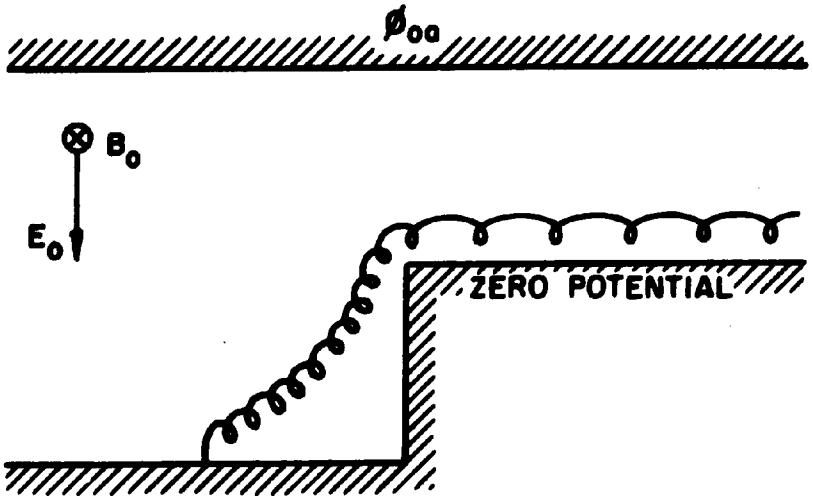


FIG. 4.13 TROCHOIDAL STREAM FOCUSSING.

4.5 Space-Charge-Free Electron Trajectories in the Stream Analyzer

Subsequent to the design and construction of the stream analyzer an electron trajectory computer developed by Rowe and Martin[23] became available for computation of electron trajectories. The equations describing the motion of a single electron normal to a uniform magnetic field were programmed on an analogue computer. A conducting film analogue of the stream analyzer geometry was constructed to obtain the equipotential pattern. Information on the electric field components and potential is taken off the analogue by means of a four-contact traveling probe and fed into the computer. The computer output (coordinate position of the electron) is then used to control the movement of the probe. The probe, starting from an initial position corresponding to a point on the cathode, then follows a trajectory which is the analogue of the electron motion. An auxiliary recorder duplicates the probe motion to form a permanent record of the motion.

Before the results of the computer computations are presented the general characteristics of the motion will be described. Figure 4.14 is a sketch of the stream analyzer geometry with several representative electron trajectories (for different values of the electrode potentials and magnetic field) superimposed. The dotted lines in the figure illustrate the general configuration of the equipotential lines. The electric field is essentially uniform after the first sole segment and also, it is uniform in the immediate vicinity of the cathode. Due to the uniform conditions in the plate-sole space all trajectories in this region will describe some sort of trochoidal motion. The details of the motion in this region will depend on the direction and magnitude of the electron velocity as it enters. Because of this, attention can be directed primarily to the characteristics of trajectories in the cathode region.

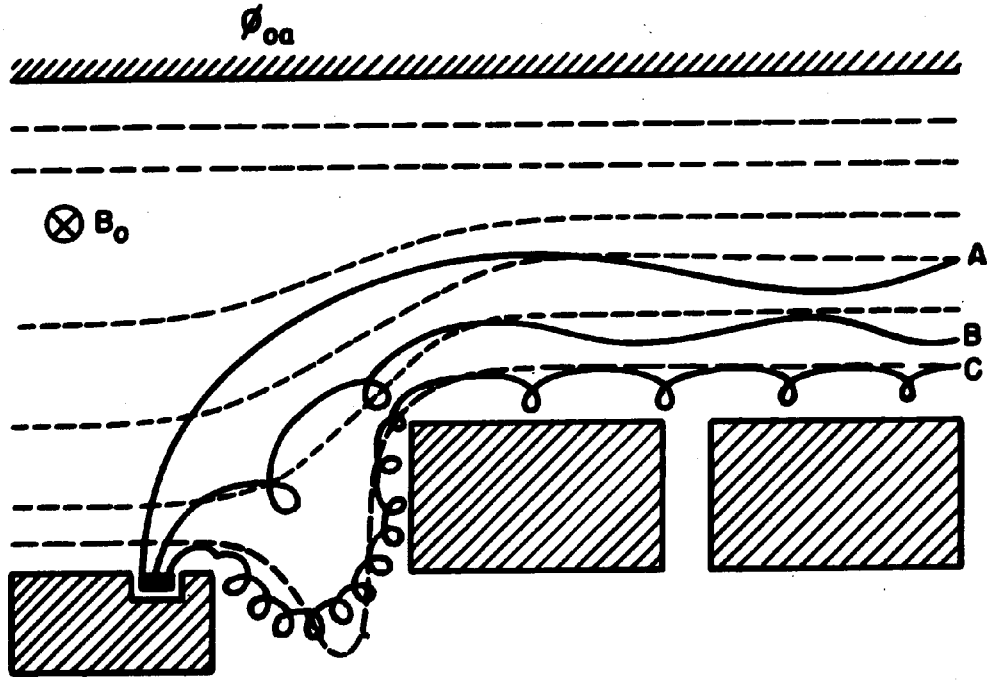


FIG. 4.14

SKETCH ILLUSTRATING THE NATURE OF SPACE-CHARGE-FREE TRAJECTORIES AND EQUIPOTENTIALS IN THE STREAM ANALYZER.

Since the electric field is also uniform in the immediate vicinity of the cathode, the initial part of a trajectory will be cycloidal in nature.

It is convenient, in describing the nature of the electron trajectories, to imagine the electrode potentials to be held fixed and the magnetic field to be increased, in steps, from zero. For no magnetic field the trajectory would be more or less straight up into the anode. As the magnetic field is increased a trajectory such as illustrated by curve A in Fig. 4.14 is obtained. The electron moves relatively rapidly into the plate-sole space through a region of slowly space-varying electric fields. This sort of trajectory is an approximation to the ideal injection system described previously.

As the magnetic field is increased further the electron is forced into the region where the equipotentials have a steep slope (curve B). This is a region of lower potential than that traversed by the first curve; hence, in general, a longer transit time is involved in going from the cathode into the plate-sole region. Another result of the lower potentials along the trajectory is the appearance of loops in the trajectory. This corresponds to the electron having a rotational velocity greater than its translational velocity. As described previously, the general character of the trajectory can be approximated in a series of increments. Each increment of the motion is taken over a relatively uniform section of the electric field. The initial conditions of one increment are taken as the final conditions of the previous increment.

For a sufficiently strong magnetic field, an electron will be forced into the potential valley between the cathode and the first sole segment. If the potential difference between the cathode and sole is small compared to the potential difference between the anode and cathode,

the potentials in the valley will be relatively quite low and the electric field intensity will also be very low. As a result, an electron will tend to follow an equipotential line (approximately the zero equipotential), executing a series of tight loops. This is illustrated by curve C in Fig. 4.14. The transit time from the cathode to the plate-sole region becomes extremely long. (In one case, the computer time to accomplish this transit was eight minutes compared to about eight seconds for a transit by electrons following curves such as A or B.)

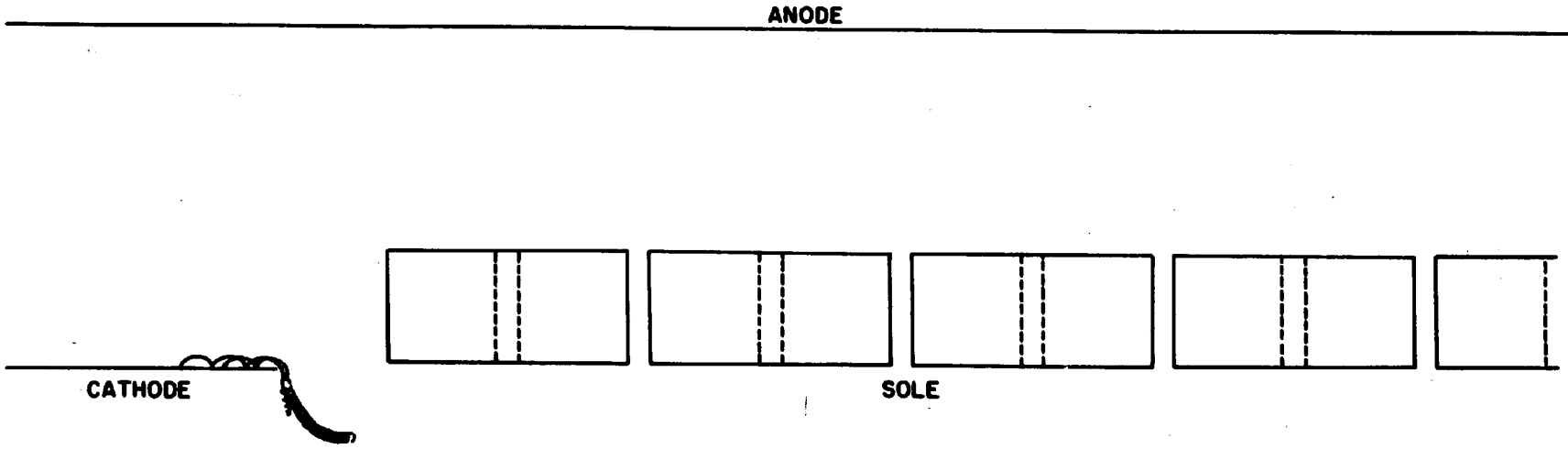
The transition from one curve to another, as the magnetic field is increased, is not as smooth as might be inferred from the discussion above. In the immediate neighborhood of the edge of the cathode block, and, also, of the first sole segment, there is a strong electric field. If the magnetic field is such as to force an electron close to these corners some rather striking changes in the character of the motion occur abruptly. This will be evident from some of the computed trajectories.

Figures 4.15 to 4.23 present the results of the computer study. Each trajectory is characterized by the value of the scaling parameter, ϕ_{oa}/B_o^2, for which it was computed. In addition the value of the magnetic field used to obtain a given value of scaling parameter is noted. Two trajectories are shown for each value of scaling parameter. These correspond to emission from either edge of the filament. For all the trajectories the cathode and sole are at the same potential.

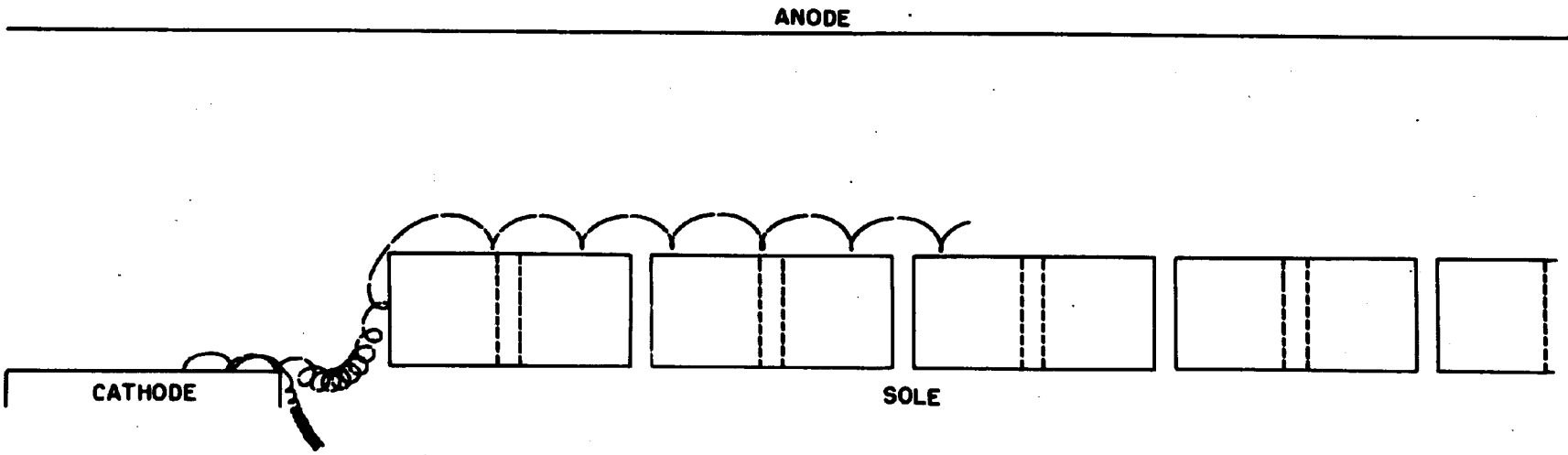
For trajectories of type C in Fig. 4.14, the computation was discontinued usually soon after the electron entered the potential valley. The buildup of error in the computer during the extremely long transit of the electron through the valley made the continuation of the trajectory into the plate-sole space difficult to interpret.

Figure 4.19a is an example of the anomaly which occurs in the neighborhood of the edge of the cathode. The motion of one electron is such that it is carried away from the valley by the edge fields. The other electron is carried further into the valley.

A more detailed discussion of the trajectory computations is deferred until Chapter V. The discussion is carried further there in correlation with the experimental measurements of the negative-sole current phenomenon.

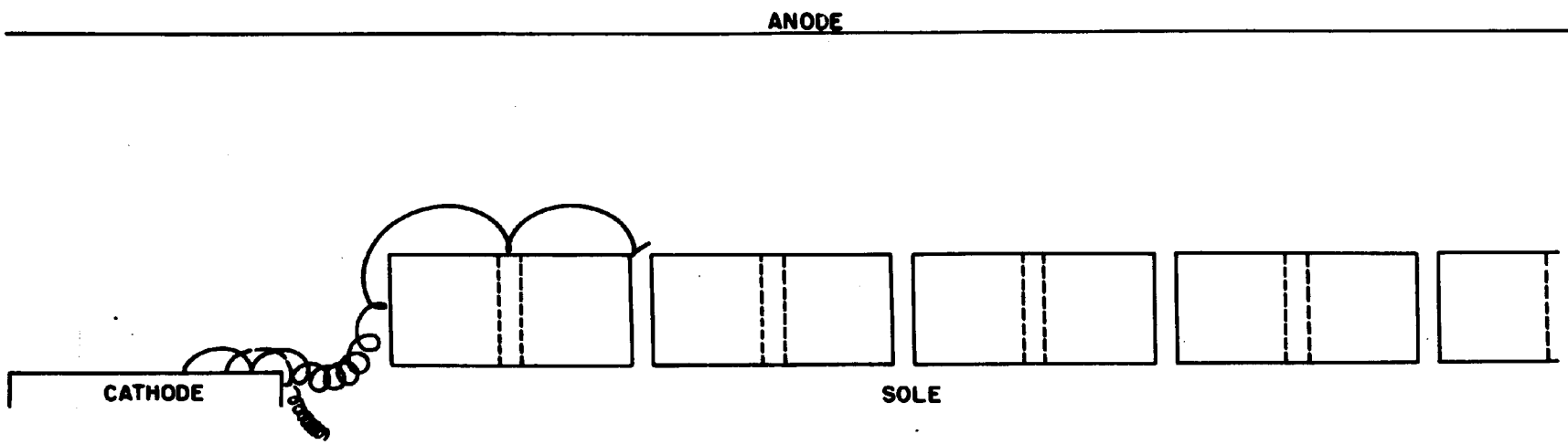


a. $\phi_{0a}/B_0^2 = 2.00 \times 10^{-3}$ VOLTS/GAUSS^2, $\phi_{0s} = 0$, $B_0 = 1000$ GAUSS.

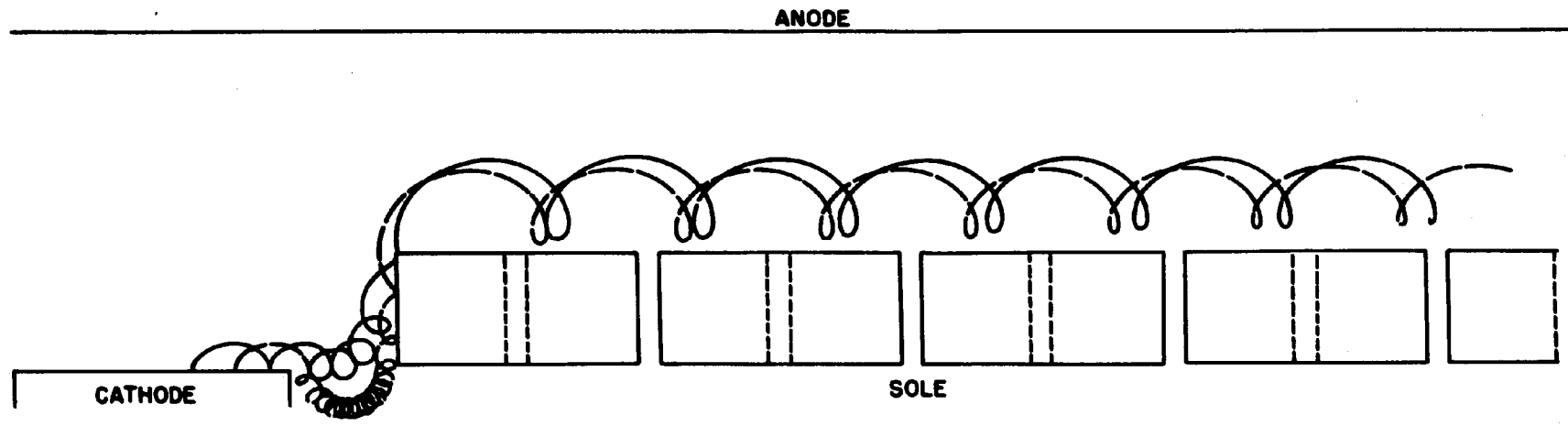


b. $\phi_{0a}/B_0^2 = 2.94 \times 10^{-3}$ VOLTS/GAUSS^2, $\phi_{0s} = 0$, $B_0 = 700$ GAUSS.

FIG. 4.15 SPACE-CHARGE-FREE ELECTRON TRAJECTORIES IN STREAM ANALYZER GEOMETRY.

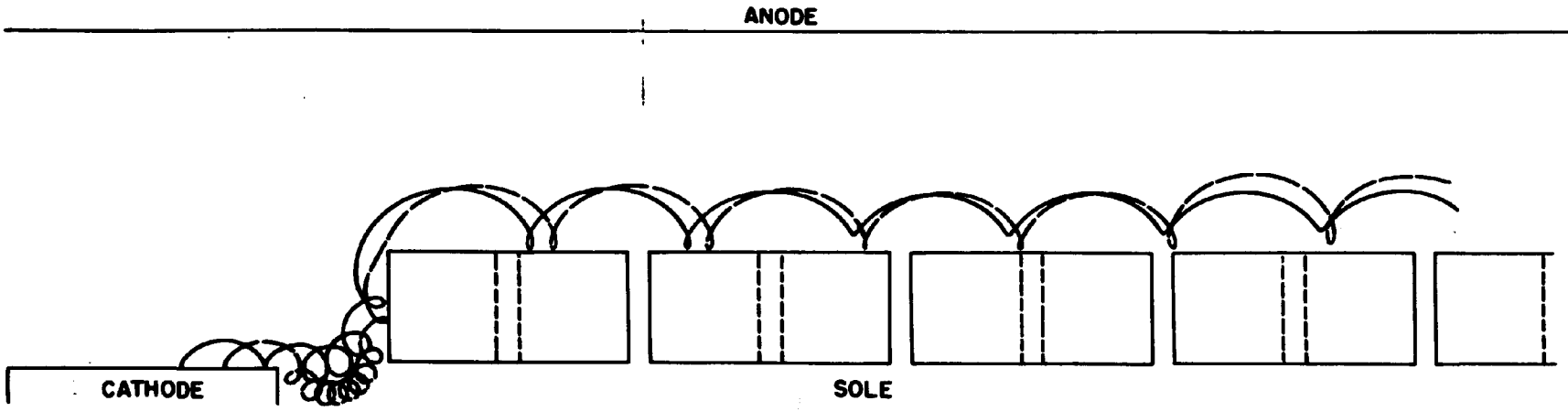


a. $\phi_{oa}/B_0^2 = 4.08 \times 10^{-3}$ VOLTS/GAUSS^2, $\phi_{os} = 0$, $B_0 = 700$ GAUSS.

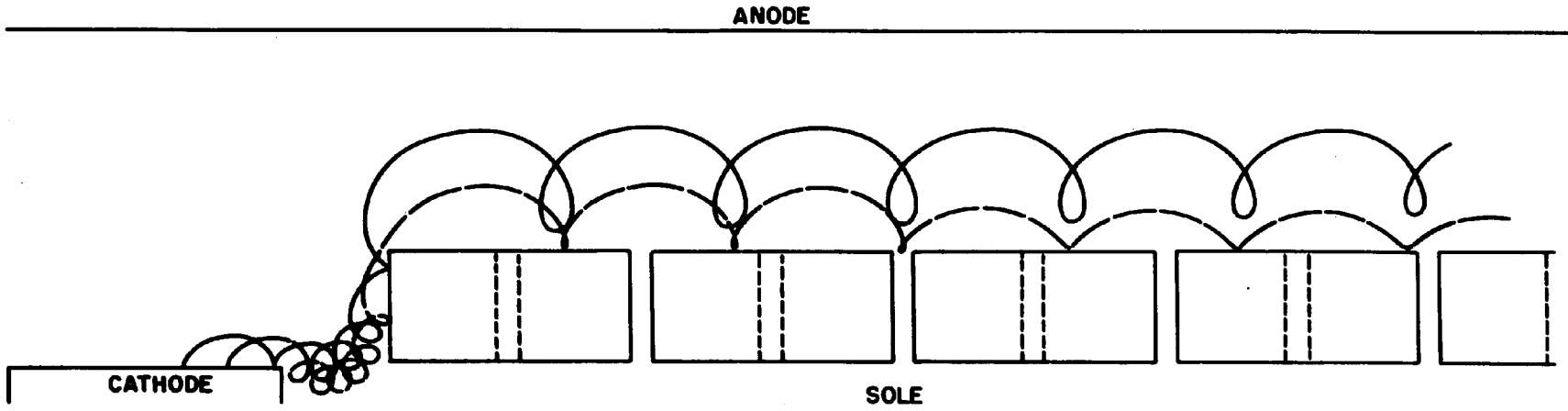


b. $\phi_{oa}/B_0^2 = 5.12 \times 10^{-3}$ VOLTS/GAUSS^2, $\phi_{os} = 0$, $B_0 = 625$ GAUSS.

FIG. 4.16 SPACE-CHARGE-FREE ELECTRON TRAJECTORIES IN STREAM ANALYZER GEOMETRY.

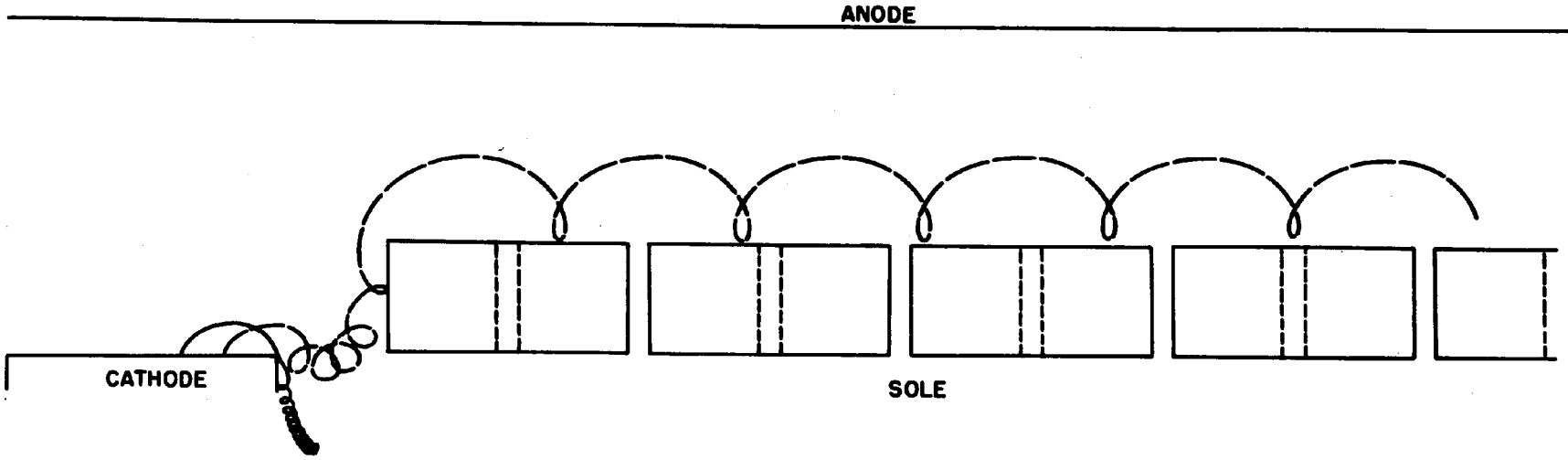


a. $\phi_{oa}/B_0^2 = 5.12 \times 10^{-3}$ VOLTS/GAUSS^2, $\phi_{os} = 0$, $B_0 = 625$ GAUSS.

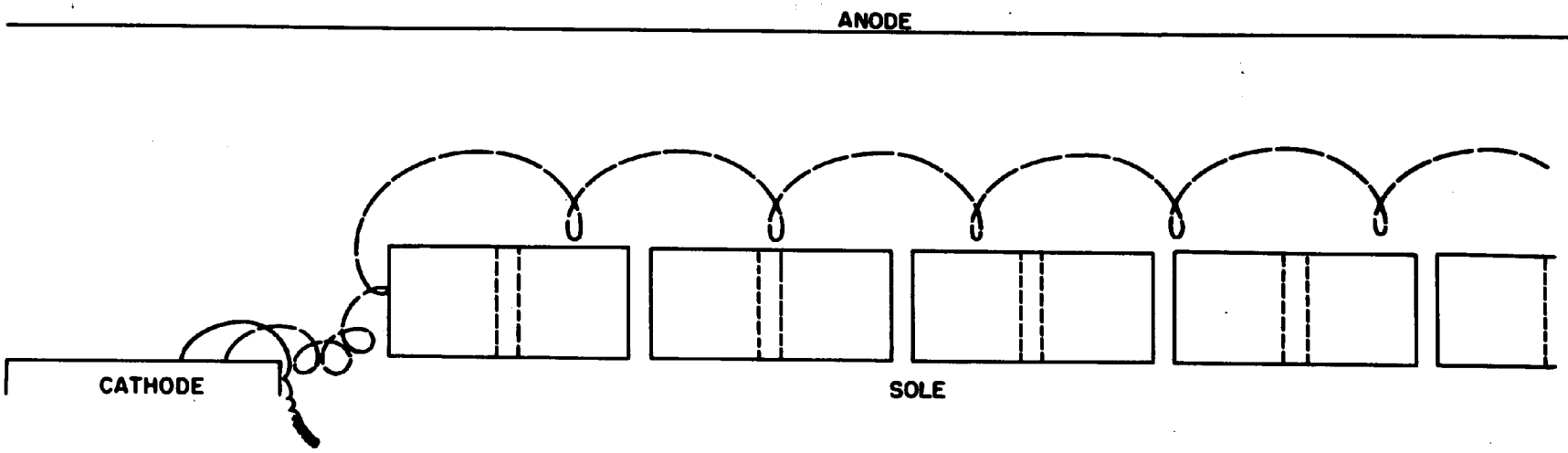


b. $\phi_{oa}/B_0^2 = 5.56 \times 10^{-3}$ VOLTS/GAUSS^2, $\phi_{os} = 0$, $B_0 = 600$ GAUSS.

FIG. 4.17 SPACE-CHARGE-FREE ELECTRON TRAJECTORIES IN STREAM ANALYZER GEOMETRY.

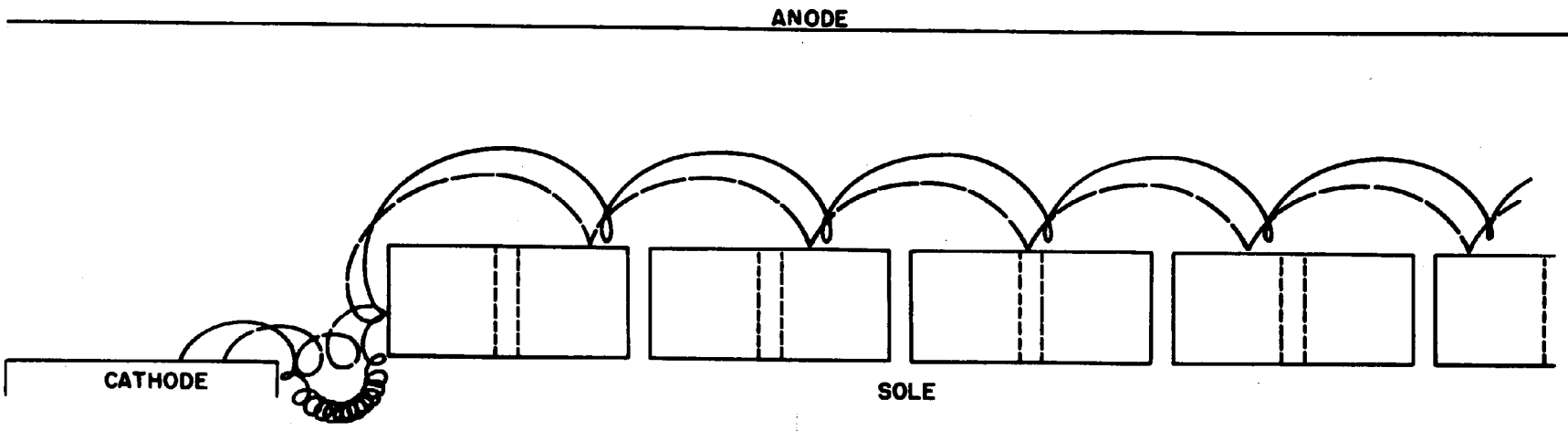


a. $\phi_{oa} / B_o^2 = 6.05 \times 10^{-3}$ VOLTS/GAUSS^2, $\phi_{os} = 0$, $B_o = 575$ GAUSS.

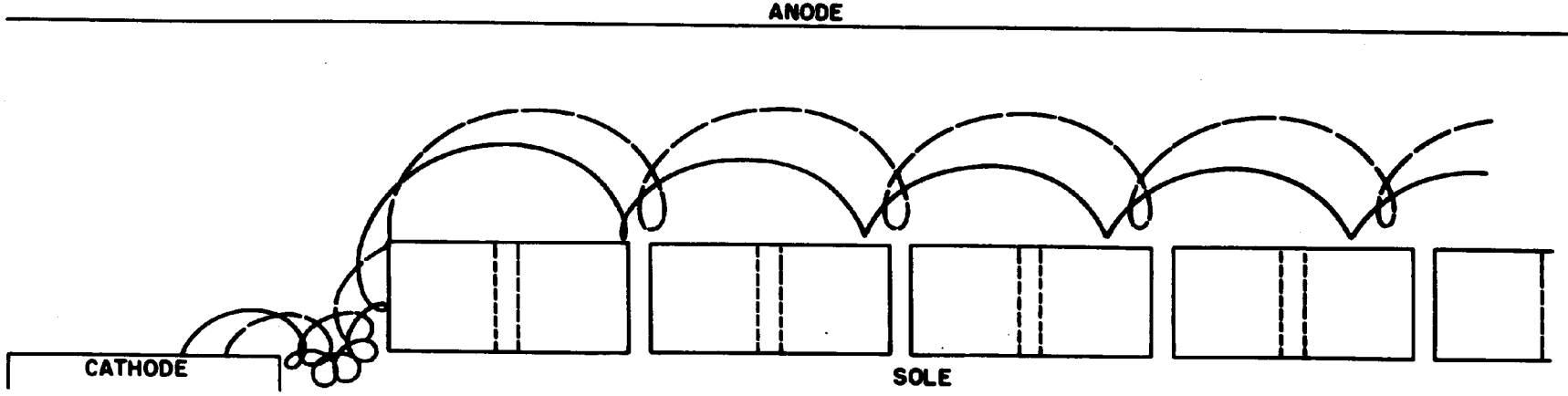


b. $\phi_{oa} / B_o^2 = 6.61 \times 10^{-3}$ VOLTS/GAUSS^2, $\phi_{os} = 0$, $B_o = 550$ GAUSS.

FIG. 4.18 SPACE-CHARGE-FREE ELECTRON TRAJECTORIES IN STREAM ANALYZER GEOMETRY.

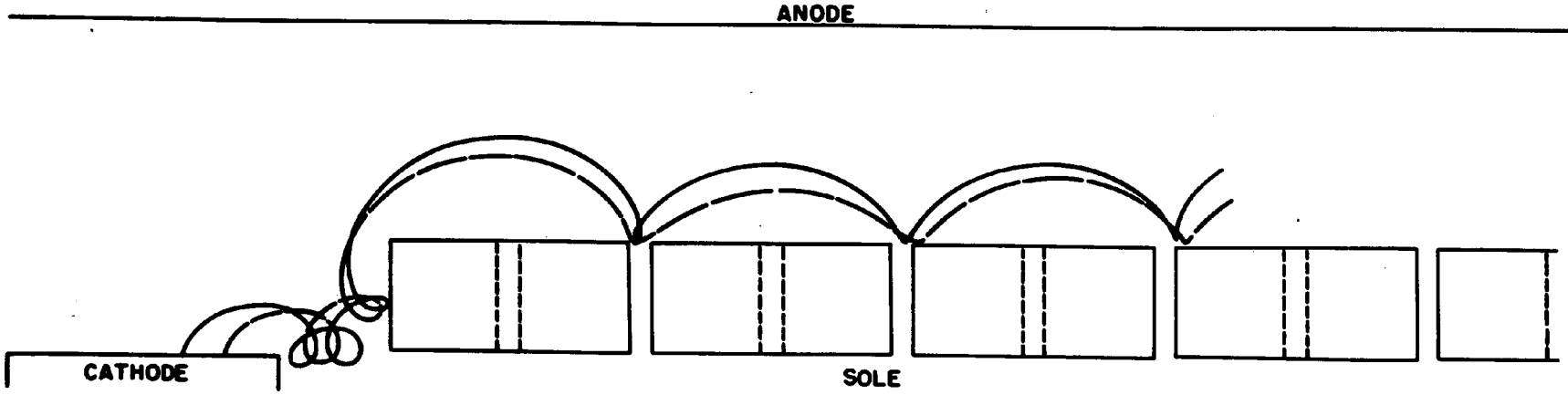


a. $\phi_{oa}/B_o^2 = 7.26 \times 10^{-3}$ VOLTS/GAUSS^2, $\phi_{os} = 0$, $B_o = 525$ GAUSS.

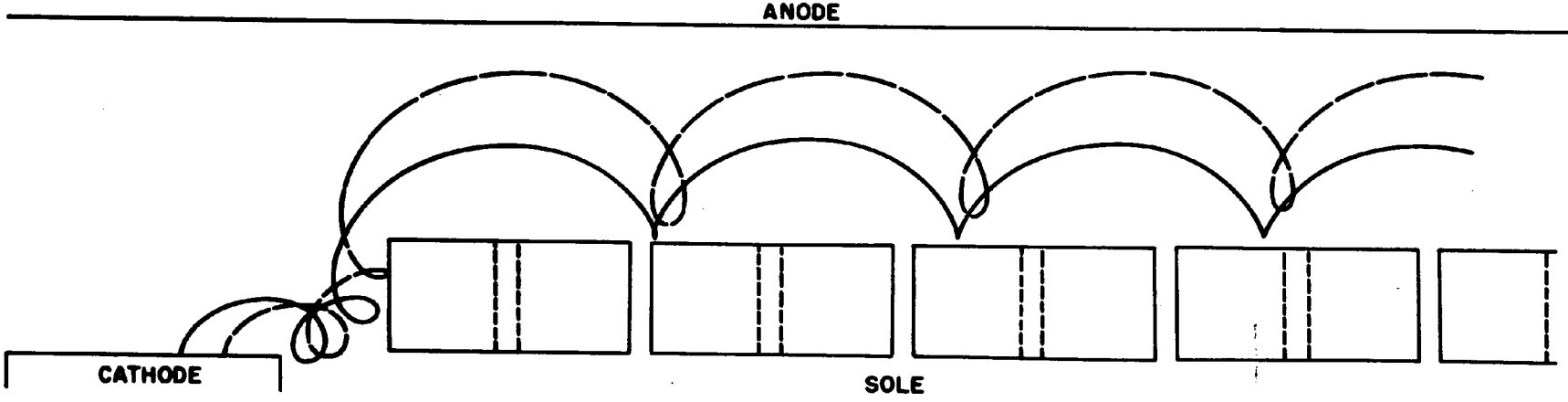


b. $\phi_{oa}/B_o^2 = 8.00 \times 10^{-3}$ VOLTS/GAUSS^2, $\phi_{os} = 0$, $B_o = 500$ GAUSS.

FIG. 4.19 SPACE-CHARGE-FREE ELECTRON TRAJECTORIES IN STREAM ANALYZER GEOMETRY.

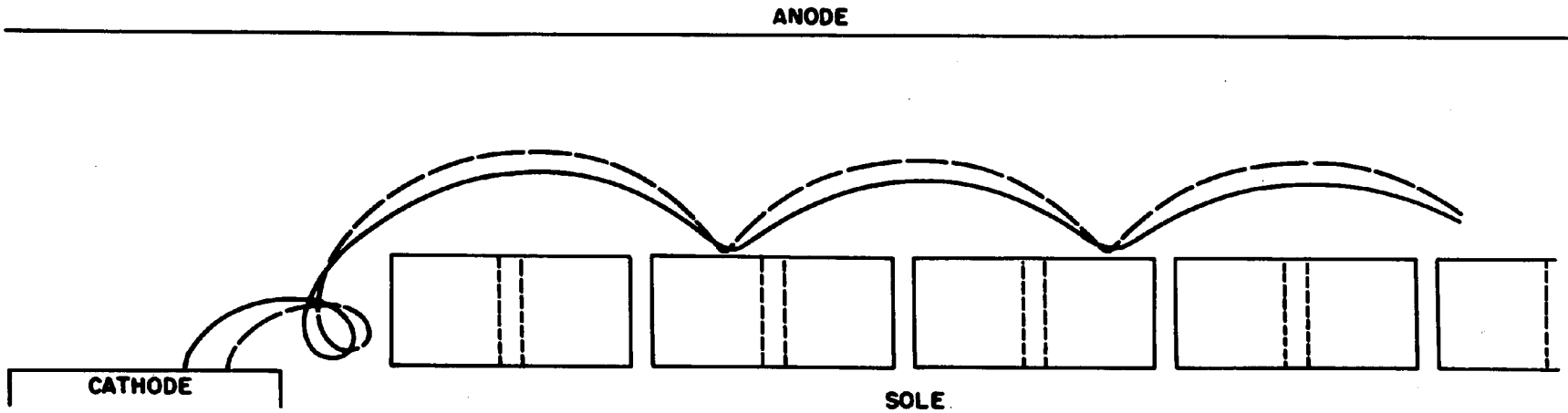


a. $\phi_{oa}/B_o^2 = 8.86 \times 10^{-3}$ VOLTS/GAUSS^2, $\phi_{os} = 0$, $B_o = 475$ GAUSS.

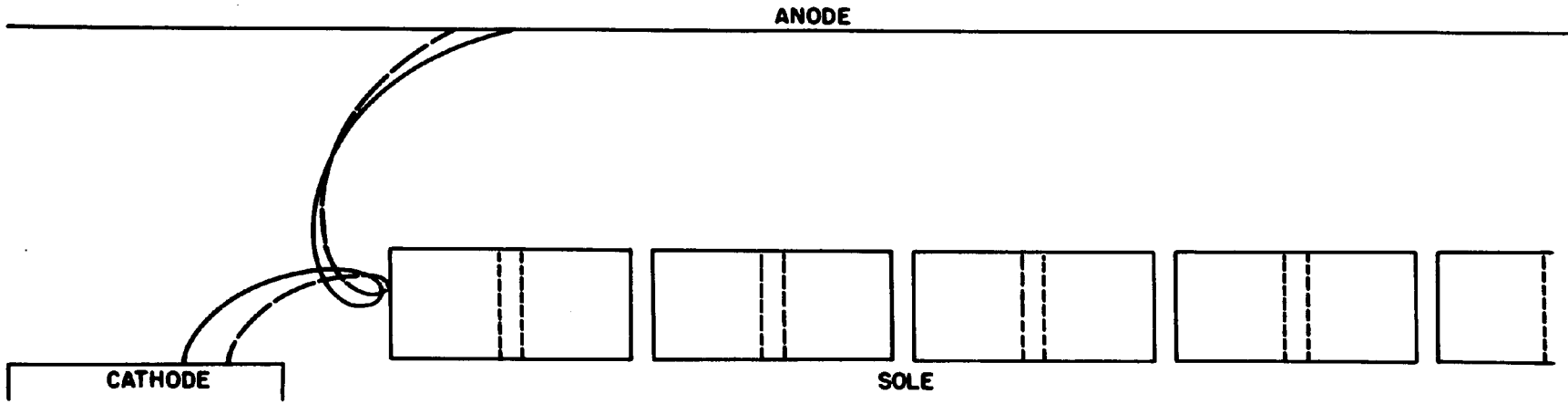


b. $\phi_{oa}/B_o^2 = 9.88 \times 10^{-3}$ VOLTS/GAUSS^2, $\phi_{os} = 0$, $B_o = 450$ GAUSS.

FIG. 4.20 SPACE-CHARGE-FREE ELECTRON TRAJECTORIES IN STREAM ANALYZER GEOMETRY.

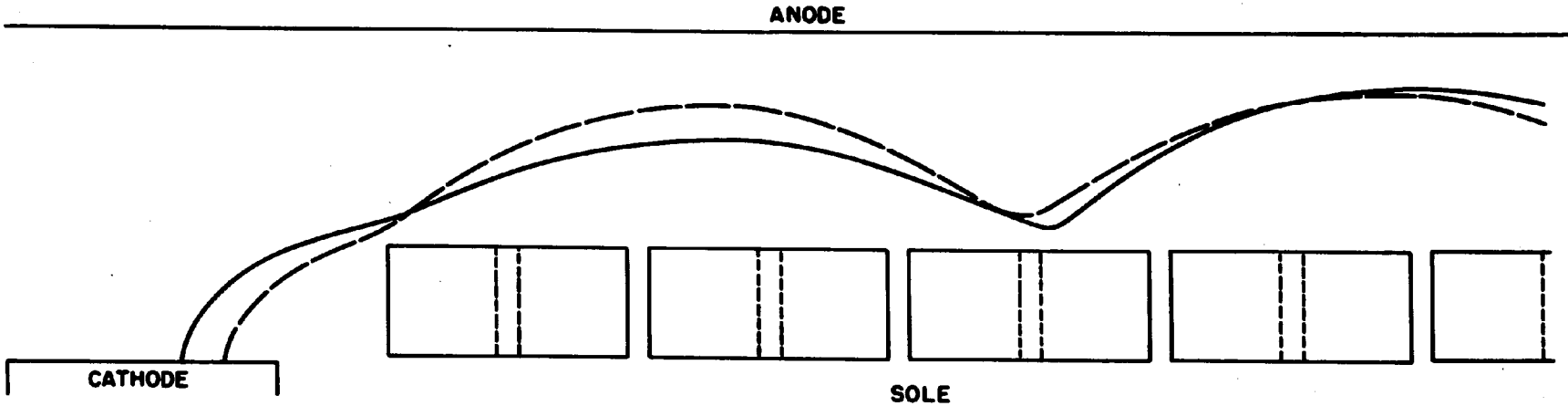


a. $\phi_{oa}/B_o^2 = 12.5 \times 10^{-3}$ VOLTS/GAUSS^2, $\phi_{os} = 0$, $B_o = 400$ GAUSS.

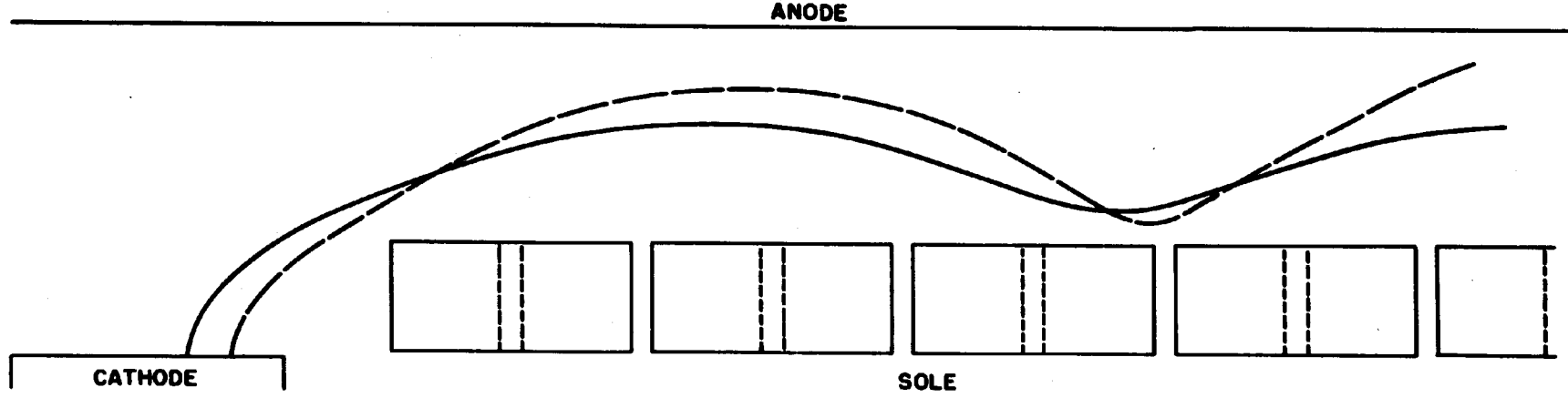


b. $\phi_{oa}/B_o^2 = 16.33 \times 10^{-3}$ VOLTS/GAUSS^2, $\phi_{os} = 0$, $B_o = 350$ GAUSS.

FIG. 4.21 SPACE-CHARGE-FREE ELECTRON TRAJECTORIES IN STREAM ANALYZER GEOMETRY.



a. $\phi_{oa}/B_0^2 = 22.22 \times 10^{-3}$ VOLTS/GAUSS^2, $\phi_{os}=0$, $B_0 = 300$ GAUSS.



b. $\phi_{oa}/B_0^2 = 26.45 \times 10^{-3}$ VOLTS/GAUSS^2, $\phi_{os} = 0$, $B_0 = 275$ GAUSS.

FIG. 4.22 SPACE-CHARGE-FREE ELECTRON TRAJECTORIES IN STREAM ANALYZER GEOMETRY.

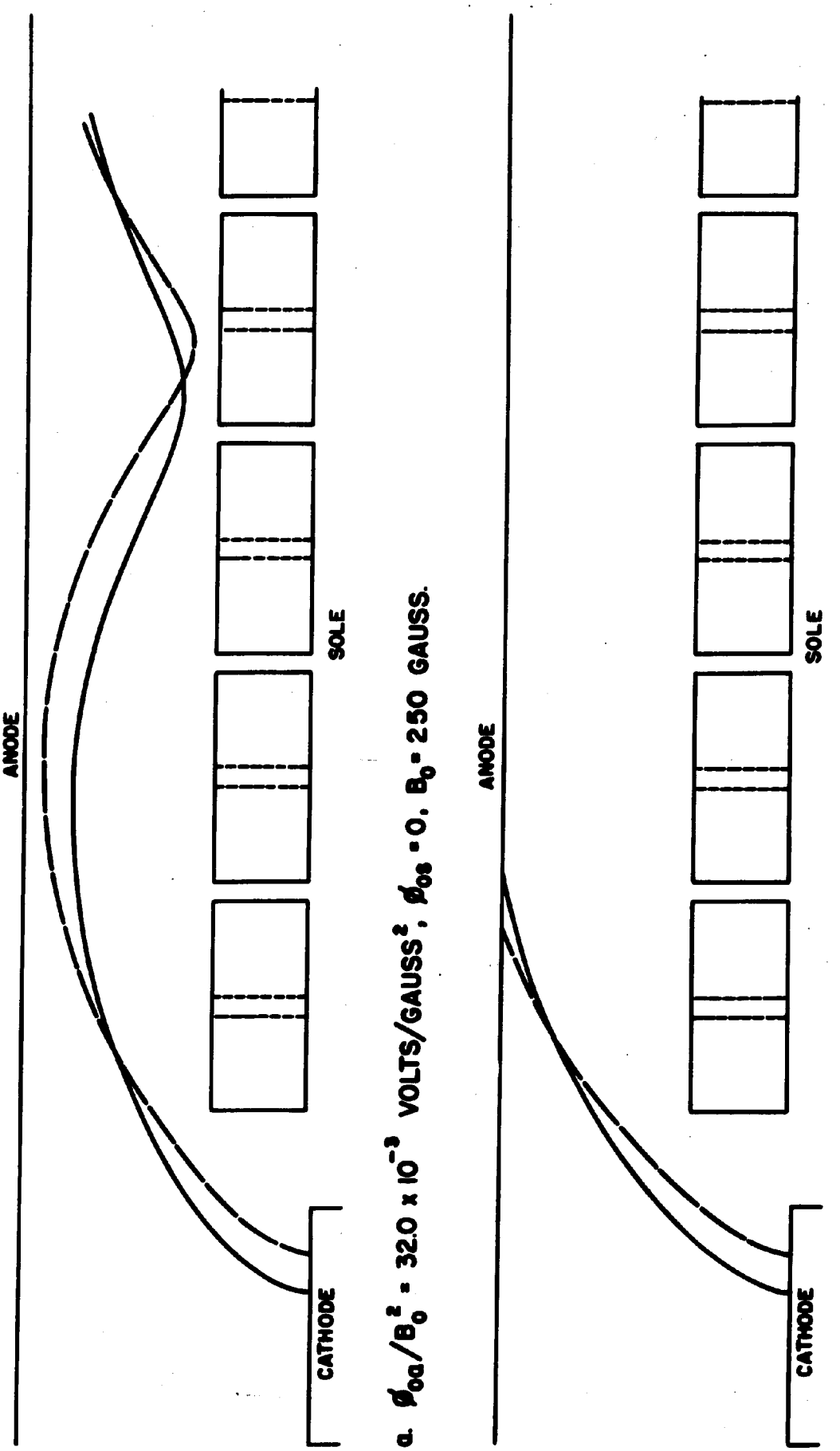


FIG. 4.23 SPACE-CHARGE-FREE ELECTRON TRAJECTORIES IN STREAM ANALYZER GEOMETRY.

CHAPTER V. EXPERIMENTAL INVESTIGATION OF THE DIOCOTRON PHENOMENON

5.1 Introduction

The crossed-field stream analyzer was designed principally for the purpose of determining the characteristics of the negative-sole current phenomenon as a function of distance along the sole. In addition to measurements of this type, data were obtained concerning r-f signals generated as an additional manifestation of the process causing the diocotron effect.

The following types of measurements were made:

(a) Preliminary measurements were made, more or less at random, to establish the existence of the phenomenon in the stream analyzer and to determine the general range of parameters (voltage, current, magnetic field) over which it occurred. With this information as a guide, data were obtained on the gross nature of the negative-sole-current phenomenon. In particular, the total current to the sole as a function of various parameters was measured.

(b) Detailed measurements of the distribution of current along the sole were then made over the range of parameters which the previous measurements had shown to be significant.

(c) With one of the sole segments being used as a probe, the energy distribution in the stream as it passed over this probe was measured. Also, the effect of a modification of the stream as it passed over one probe on the properties of the stream as it passed over subsequent probes was investigated.

(d) In addition to the above d-c measurements, r-f data were obtained from a coaxial probe (electric) inserted just behind the filament.

For all the measurements reported, the cathode of the stream analyzer was operated space-charge-limited.

The data are presented in the order described above. To a certain extent, data are interpreted when presented. However, because of the complexity of the phenomenon, the principal discussion of the data is deferred until after all the measurements have been presented.

5.2 Definition of Certain Symbols

For convenience, the symbols used to denote the principal voltages and currents measured are defined below. Additional symbols of less frequent occurrence are defined in the text. All potentials are measured relative to the cathode.

ϕ_{oa} = d-c anode potential. All the anode segments were operated at the same potential for all the measurements reported here.

ϕ_{os} = d-c sole potential. This refers to the potential of the sole when all the segments have the same potential, or when only one or two specifically noted segments have different potentials from the remaining segments.

ϕ_{osn} = d-c potential of the nth sole segment. The sole segments are numbered one to thirty beginning with the segment adjacent to the cathode block.

ϕ_{oc} = d-c collector potential. For all the measurements here reported $\phi_{oc} = \phi_{oa}$.

I_{oa} = d-c current to all the anodes.

I_{oc} = d-c current to the collector.

I_{os} = d-c current to the entire sole.

I_{osn} = d-c current to the nth sole segment.

$$I_{os} = \sum_{n=1}^{30} I_{osn} \quad . \tag{5.1}$$

I_{ok} = d-c cathode current. $I_{ok} = I_{oa} + I_{oc} + I_{os}$. It is possible, and even likely, that some current from the cathode is collected on the cathode support structure. Since the cathode and its supporting structure are internally connected, this current is not measurable. Cathode current, as used here, refers to current which returns to the cathode through external circuitry.

I_{otn} = d-c current remaining in the stream <u>after</u> it has passed over the nth sole segment and <u>before</u> it passes over the (n+1)st sole segment.

Figure 5.1 is a sketch illustrating the measuring circuitry employed and the symbols defined above.

5.3 D-C Characteristics of the Electron Gun

Since the stream analyzer construction does not permit actually viewing the electron stream it is necessary to rely on indirect measurements to obtain some idea of the stream geometry. One such type of measurement is a study of the characteristics of the electron gun.

It is quite difficult to predict the detailed performance of the electron gun. Part of the difficulty lies in the fact that there is no analytic model of the stream flow which is a satisfactory approximation of the actual stream flow. Calculations based on a rectilinear Brillouin stream model, for example, give quite different results from measured values.

Nevertheless, it is possible to establish the limiting behavior of the electron gun and to obtain some idea of its behavior. A good index

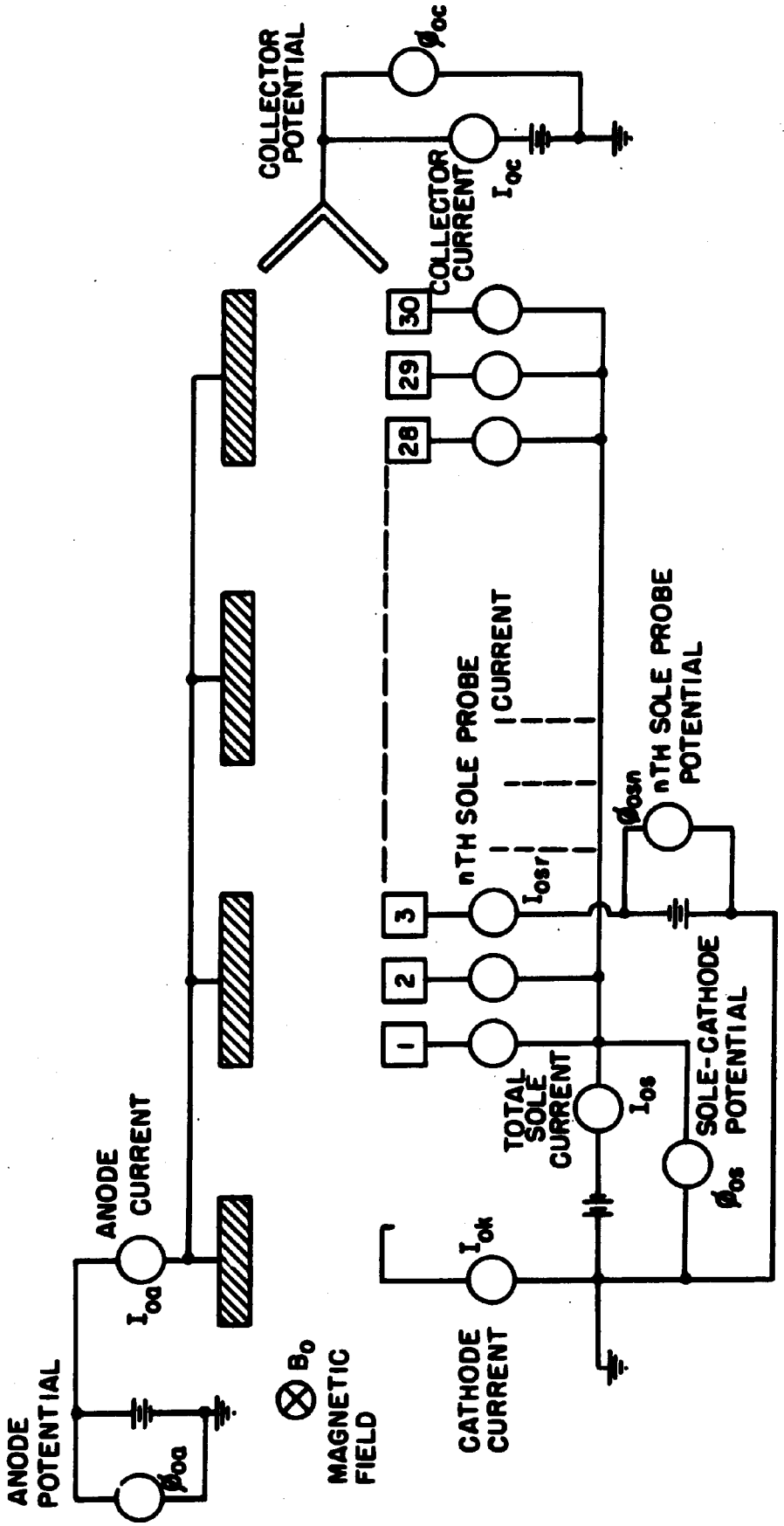


FIG. 5.1 SCHEMATIC OF MEASURING CIRCUITRY AND DEFINITION OF SYMBOLS.

of the performance of the electron gun is the perveance $I_{ok}/\phi_{oa}^{3/2}$. It can be shown that in a fixed geometry, and for space-charge-limited operation, the perveance is a function only of the scaling parameter ϕ_{oa}/B_o^2 discussed in section 4.4. (This assumes that the ratio ϕ_{oa}/ϕ_{os} is constant, i.e., the shape of the electrical equipotential lines is unchanged.) As one extreme, we can calculate the value of perveance for an infinite value of scaling ratio, i.e., when there is no magnetic field. In this case the electron gun is, except for end effects, essentially a parallel-plane diode. Applying the Child-Langmuir diode current law we have, for the dimensions of the stream analyzer,

$$\frac{I_{ok}}{\phi_{oa}^{3/2}} = 2.33 \times 10^{-6} \frac{w \times \ell}{s^2}$$

$$= 0.647 \times 10^{-6} \text{ pervs} \quad , \qquad (5.2)$$

where

w = filament width = 0.040 inch,

ℓ = active filament length = 0.65 inch, and

s = anode-filament spacing = 0.306 inch.

As another extreme, we have for a value of scaling parameter equal to zero, e.g., for zero ϕ_{oa}, a value of perveance equal to zero. For intermediate values of the scaling parameter we can say, not altogether tritely, that the perveance will generally increase. Physically, the effect of increasing the magnetic field (or, specifically, decreasing the scaling parameter) is, in general, to bend electron paths into lower-potential, and hence, lower-velocity regions. For space-charge-limited operation this results in a higher space-charge density in the vicinity of the cathode and hence in a lowered cathode current. Figure 5.2 is a plot of the measured gun perveance as a function of the scaling parameter. For the data shown, the sole potential ϕ_{os} was zero. Superimposed on the

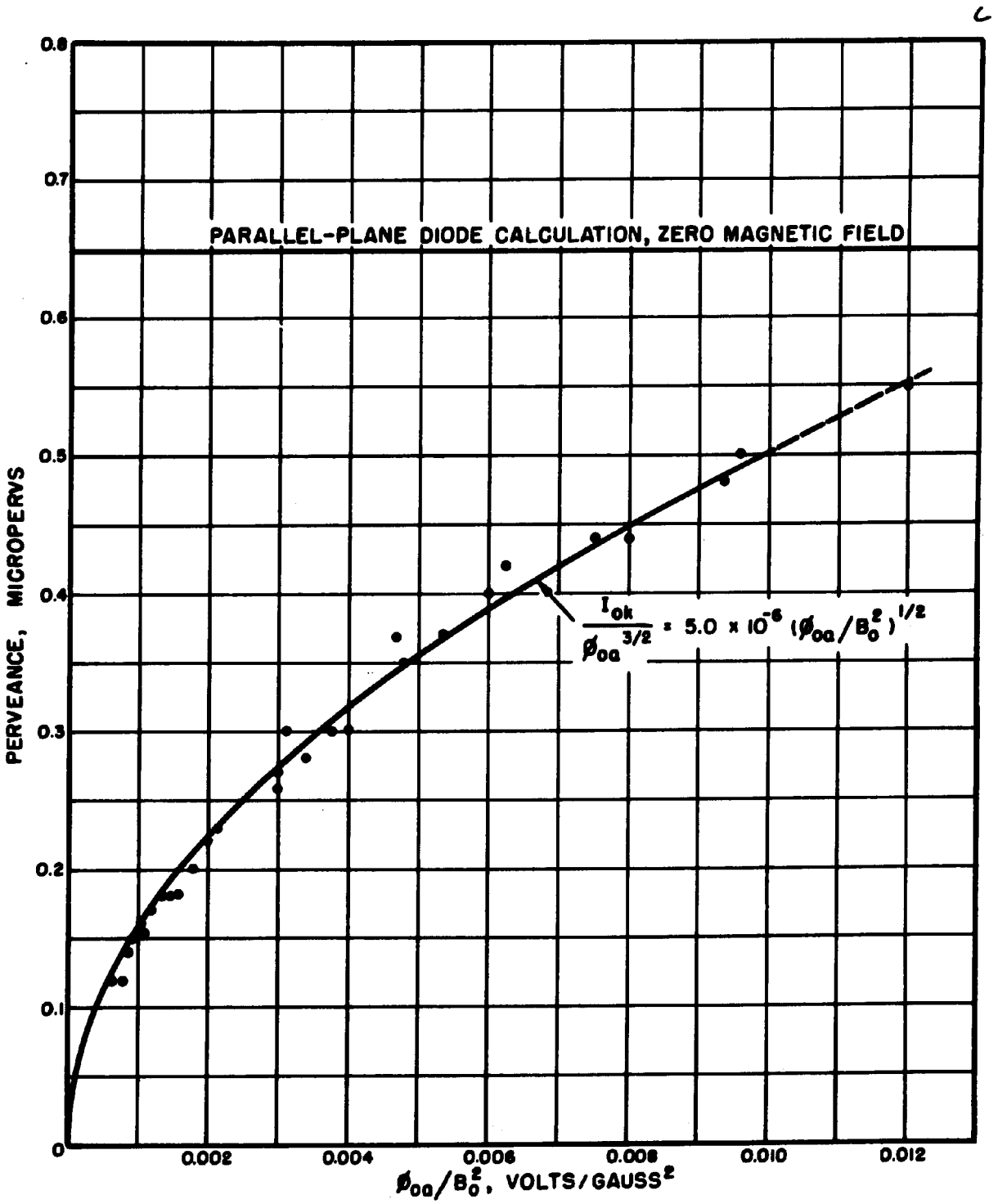


FIG. 5.2 PERVEANCE OF STREAM ANALYZER ELECTRON GUN.
($\phi_{os} = 0$. CATHODE NO. 1)

plotted points is the curve given by

$$\frac{I_{ok}}{\phi_{oa}^{3/2}} = 5 \times 10^{-6} \left(\frac{\phi_{oa}}{B_o^2}\right)^{1/2} . \qquad (5.3)$$

Over the range of the scaling parameter for which data were taken, this curve fits the data extremely well. It is not applicable, of course, for all values of the scaling parameter since the perveance has an upper limit.

In the course of making measurements, a high-voltage breakdown of one of the anode feedthroughs led to a loss of the filament. While the nominal dimensions of the replacement parts were the same as for the original parts, it was not possible to duplicate the original geometry exactly. For example, the heat capacity of the filament assembly was not the same as in the first construction. Hence, because of less efficient heat conduction, the effective filament length changed significantly (from 0.65 to 0.70 inch). Also the geometrical position of the filament relative to the sole was somewhat different. Figure 5.3 is a plot of the perveance characteristics of the second cathode. The superimposed curve is given by

$$\frac{I_{ok}}{\phi_{oa}^{3/2}} = 7.25 \times 10^{-6} \left(\frac{\phi_{oa}}{B_o^2}\right)^{1/2} . \qquad (5.4)$$

The calculated value of perveance for $\phi_{oa}/B_o^2 = \infty$, shown in Fig. 5.3, is obtained from Eq. 5.2, using an effective cathode length of 0.70 inch. The data shown in Fig. 5.3 were taken for three scalings of the sole potential, that is, three values of the ratio ϕ_{oa}/ϕ_{os}. For anode potentials of 1000 volts, these would correspond to sole potentials of 0, -20, and -40 volts, respectively.

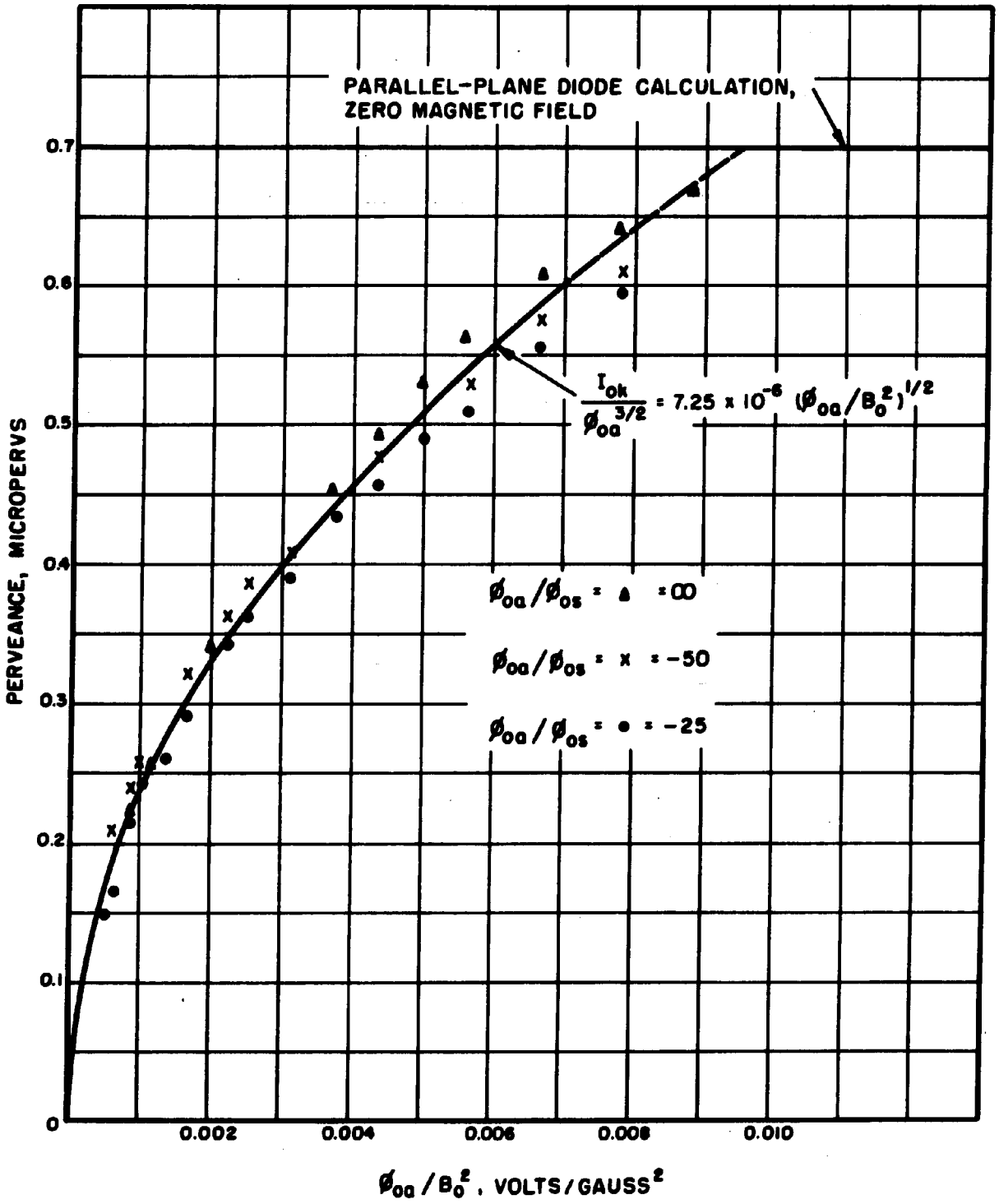


FIG. 5.3 PERVEANCE OF STREAM ANALYZER ELECTRON GUN.
(CATHODE NO. 2)

It is seen from Fig. 5.3 that the perveance is relatively insensitive to small changes in sole potential.

To differentiate data taken with the original cathode from those taken with the replacement assembly, the former are labeled "cathode No. 1" and the latter, "cathode No. 2."

Figure 5.4 is a plot of the volt-ampere characteristics of cathode No. 1 for zero sole potential. This figure shows the general range of voltages, currents, and magnetic fields used in obtaining data.

With the help of the trajectory plots of Chapter IV (Figs. 4.15 to 4.23) we can, in a general way, interpret the perveance characteristics of Figs. 5.2 and 5.3. For high values of the scaling parameter $\phi_{oa}/B_o^2 > 9 \times 10^{-3}$ volts/gauss^2), electrons are drawn away from the filament relatively rapidly and the limiting perveance is (approximately) obtained. As the scaling parameter is made smaller $\phi_{oa}/B_o^2 < 6 \times 10^{-3}$ volts/gauss^2) the space-charge density near the cathode increases, and causes a reduction of cathode current.

5.4 Gross Characteristics of the Negative-Sole Current

Preliminary measurements of the negative-sole current were made primarily for the purpose of obtaining general information about the order of magnitude of the effect under various operating conditions. Gross measurements of the negative-sole current were made, i.e., data were taken in the following fashion: for a given measurement the stream analyzer was operated with fixed voltages and magnetic field, and the total currents to the sole, anode, and collector (I_{os}, I_{oa}, and I_{oc}, respectively) were individually measured. In addition, the cathode current, I_{ok}, was measured as a running check on the other currents.

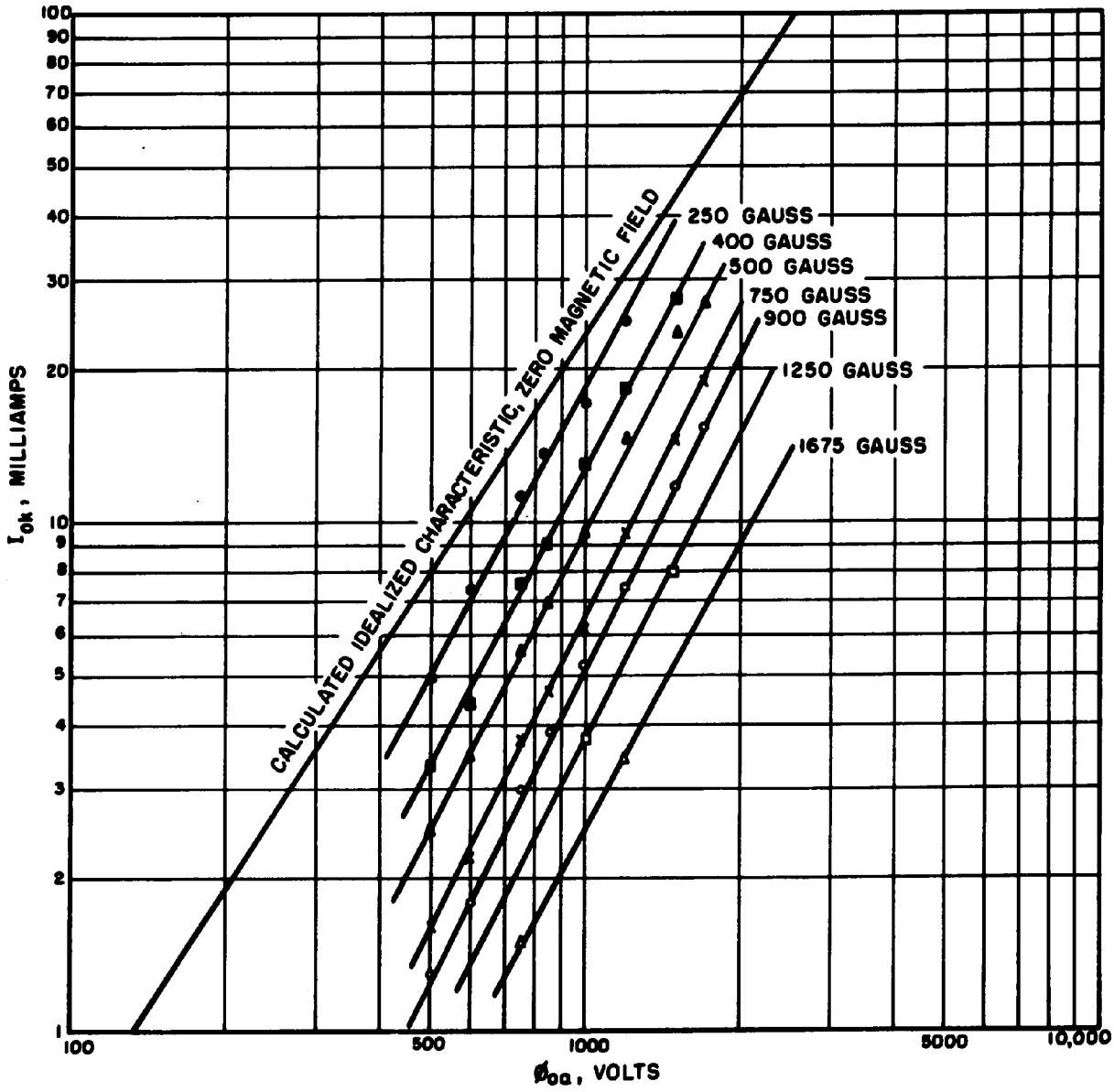


FIG. 5.4 VOLT-AMPERE CHARACTERISTIC OF STREAM ANALYZER ELECTRON GUN. (ϕ_{os} = 0. CATHODE NO. 1)

Significantly, it was found that all the data could be summarized by plotting the fraction of the cathode current going to the sole as a function of the scaling ratio ϕ_{oa}/B_o^2. Figure 5.5 is a plot of data obtained with cathode No. 1. The sole potential was zero for all the data shown. In interpreting these data, it should be kept in mind that no anode current was observed for any of the data. As shown on Fig. 5.5, the data were obtained by varying the anode voltage at a fixed magnetic field. This was done for several values of magnetic field.

Similar data were obtained for cathode No. 2. Moreover, in addition to data for zero sole potential, data were also obtained for two scaled values of sole potential, $\phi_{oa}/\phi_{os} = -50$ and -25. (These values correspond to sole potentials of -20 and -40 volts, respectively, when the anode potential is 1000 volts.) These data are plotted in Fig. 5.6.

Some data on gross sole-current magnitudes were obtained from a C.S.F. report on the development of carcinotrons. These data were taken with the sole at cathode potential and, for a fixed anode voltage, over a range of magnetic field strengths. These data are replotted in Fig. 5.7 in the same fashion as the previous two figures. It is seen from the figure that these data are also scaleable.

The fact that the data are scaleable implies that the diocotron effect is not significantly associated with the r-f properties of the stream analyzer geometry. Rather, it implies that the negative-sole current is associated with the geometry of the stream trajectory. We will therefore seek to associate the nature of the electron trajectories described in Chapter IV with the nature of the data presented by Figs. 5.5 and 5.6.

Figures 5.5 and 5.6 show that the negative-sole current is a sizeable fraction of the cathode current up to a value of scaling parameter

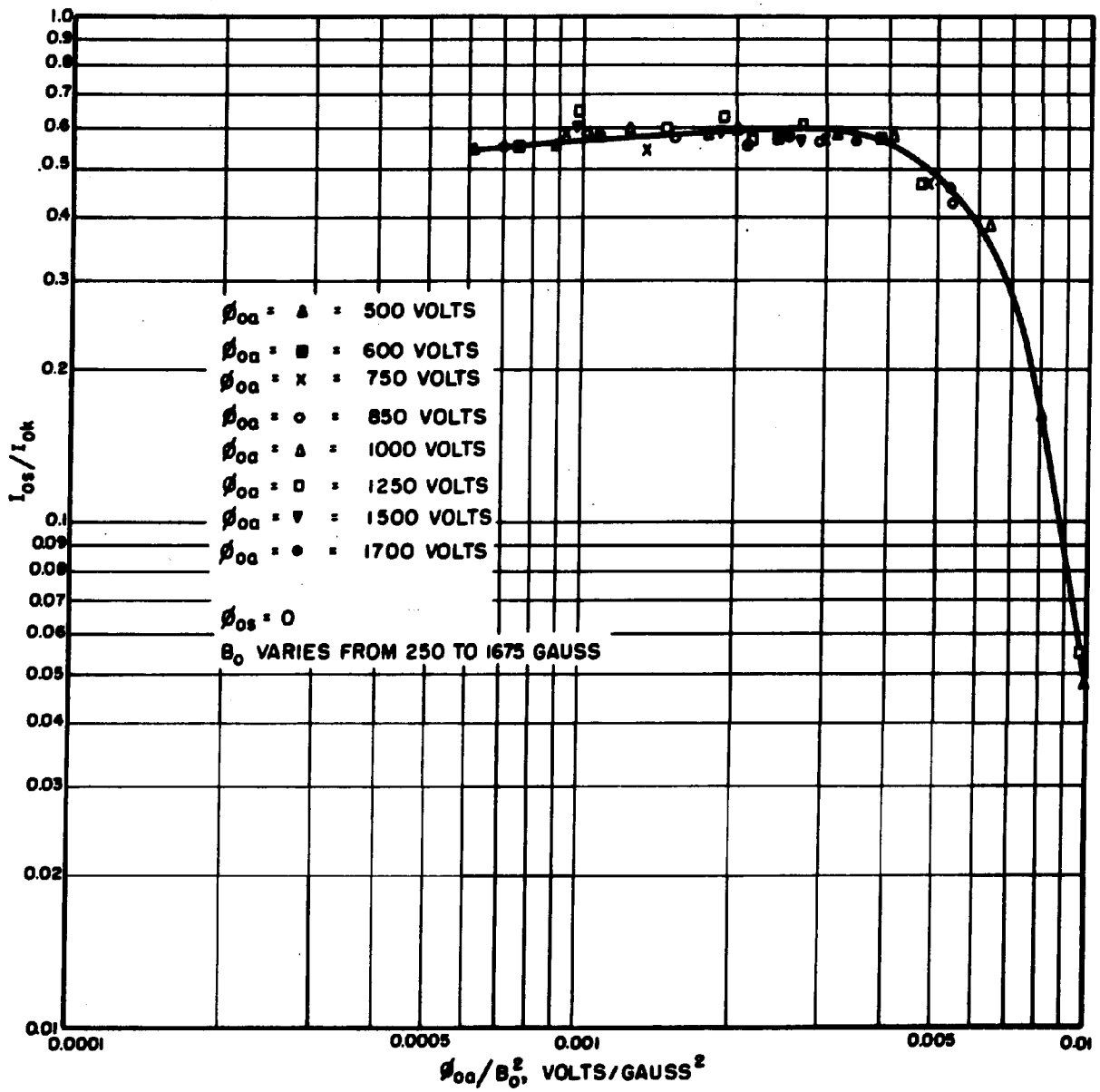


FIG. 5.5 GROSS SOLE CURRENT CHARACTERISTIC. (CATHODE NO. 1.)

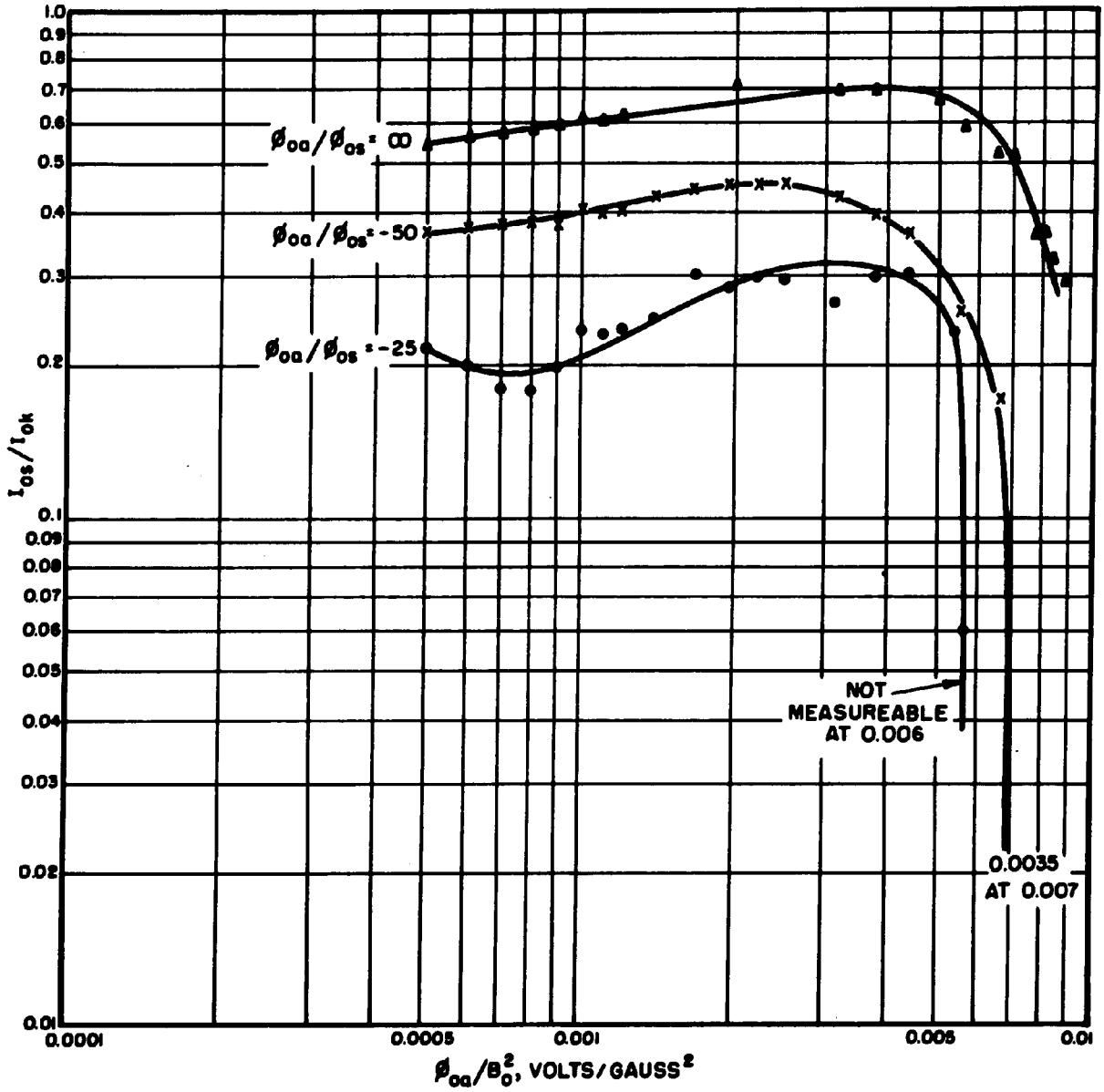


FIG. 5.6 GROSS SOLE CURRENT CHARACTERISTIC. (CATHODE NO. 2)

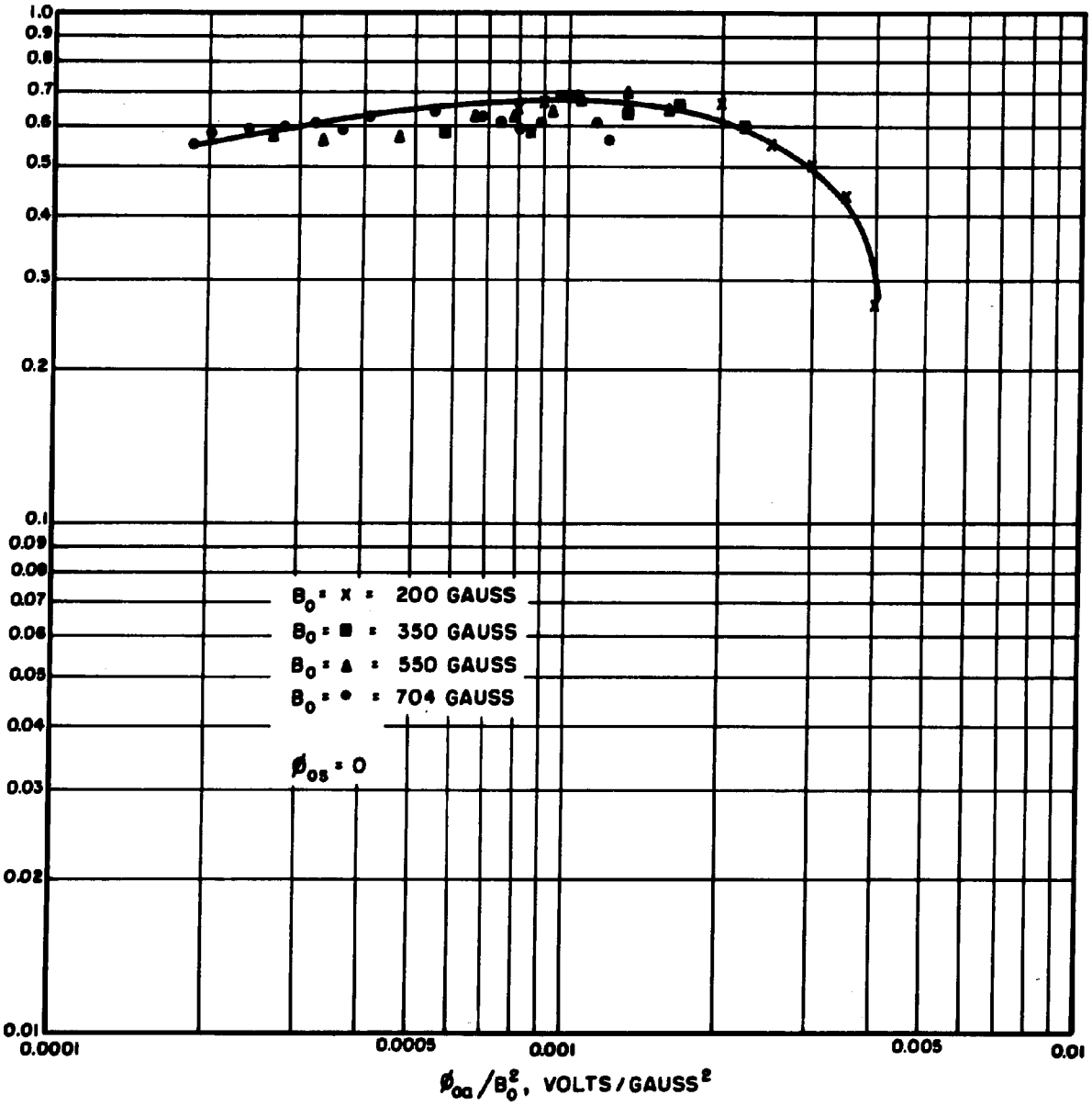


FIG. 5.7 GROSS SOLE CURRENT CHARACTERISTIC, C.S.F. DATA.

of about 0.006 volt/gauss^2. Above (about) this value, there is an extremely sharp reduction in the magnitude of the effect. Figure 5.6 shows the same type of behavior even for negative sole potentials.

There are two requirements to be met before an electron can reach a negative sole. One requirement is that the electron must necessarily have gained extra energy corresponding, at least, to the potential difference between the cathode and sole. This, however, is not sufficient to insure its being collected on the sole. In addition to having sufficient energy to permit collection by the sole, the electron must also follow a trajectory which intercepts the plane of the sole. The space-charge-free trajectory plots (Figs. 4.15 to 4.23) do not indicate any radical change in the nature of the trajectories in the plate-sole space which might account for a sharp reduction in sole current. There is, on the other hand, a significant change in the nature of the trajectories in the cathode region. For values of the scaling parameter less than about 0.007 volt/gauss^2 electrons become trapped in the potential valley between the cathode block and the first sole segment.

Figure 4.19a (for $\phi_{oa}/B_o^2 = 0.00726$ volt/gauss^2) can serve to show some order of magnitudes. The transit time from the cathode into the plate-sole space can be computed approximately by counting the number of trochoidal loops in a trajectory. Each loop represents, roughly, a time interval equal to the period of the cyclotron frequency ω_c. The trajectory (in Fig. 4.19a) which is forced into the potential valley has about five times as long a transit time into the plate-sole space as the other trajectory. For lower values of scaling parameter the differences in transit times are further emphasized. For example, the trajectories shown in Fig. 4.15b ($\phi_{oa}/B_o^2 = 0.00294$ volt/gauss^2) indicate

that the lower trajectory requires a transit time about fifty times as long as the upper trajectory.

One interesting aspect of the near trapping of electrons between the cathode block and the first sole segment can be observed in Figs. 4.15 to 4.19. For low values of the scaling parameter, electrons originating from the left-hand side of the cathode are trapped. As the value of the scaling parameter is increased, the trapped electrons are those originating on the right-hand side of the filament. As the value of the scaling parameter is increased further, electrons emitted from the left-hand side of the cathode are trapped again.

The trajectory plots are, of course, computed without space charge present. However, even at very high current densities the actual stream behavior will be of the general nature shown by the space-charge-free computations.

The above discussion has, of course, presented no direct evidence linking the electron trapping with the negative-sole current. There is, however, in the data presented, a strong indication of a correlation between the two effects.

5.5 Distribution of the Sole Current Along the Sole

Because the diocotron phenomenon is scaleable, a concise set of measurements of the distribution of current along the sole can be made. Measurements were made in the following manner:

(a) For a given measurement, the stream analyzer was operated at a fixed value of the scaling parameter ϕ_{oa}/B_o^2, i.e., at a fixed anode voltage and magnetic field.

(b) The sole was held at a fixed potential, and the currents to

all the electrodes were measured. The current to each sole segment was measured separately. Current measurements were made with a number of values of sole potential for each value of the scaling parameter.

(c) The measurements were made, as described above, over a range of values of the scaling parameter.

For all the data presented there was no anode current. Hence the cathode current was collected either by the sole or by the collector. (Actually it is possible, and even likely, that a small fraction of the emitted current was collected on the cathode block. Since the cathode is internally connected to the cathode block, it was not possible to measure such a current. Cathode current, as used here, refers to current which returns to the cathode through external circuitry.)

It is convenient, particularly because of the division of cathode current between only the sole and collector, to present the data in the form of an integrated distribution curve, i.e., in the form of a plot of I_{otn}/I_{ok} as a function of distance along the sole. The stream current loss factor, I_{otn}/I_{ok}, is the fraction of the cathode current remaining in the stream after it has passed over the nth sole segment, but before it has reached the(n+1)st segment. Since there is no anode current, I_{otn} is related to the sole segment current by the equation

$$\frac{I_{otn}}{I_{ok}} = 1 - \sum_{m=1}^{n} \frac{I_{osm}}{I_{ok}} \quad . \tag{5.5}$$

(See section 5.2 for definition of all current symbols.) Distance along the sole is measured in terms of "probe units," i.e., intervals of distance corresponding to the period of the sole segmentation (0.120 inch).

The data are presented in Figs. 5.8 to 5.21. All the data shown are for cathode No. 2. Similar, although less complete, data were obtained with cathode No. 1.

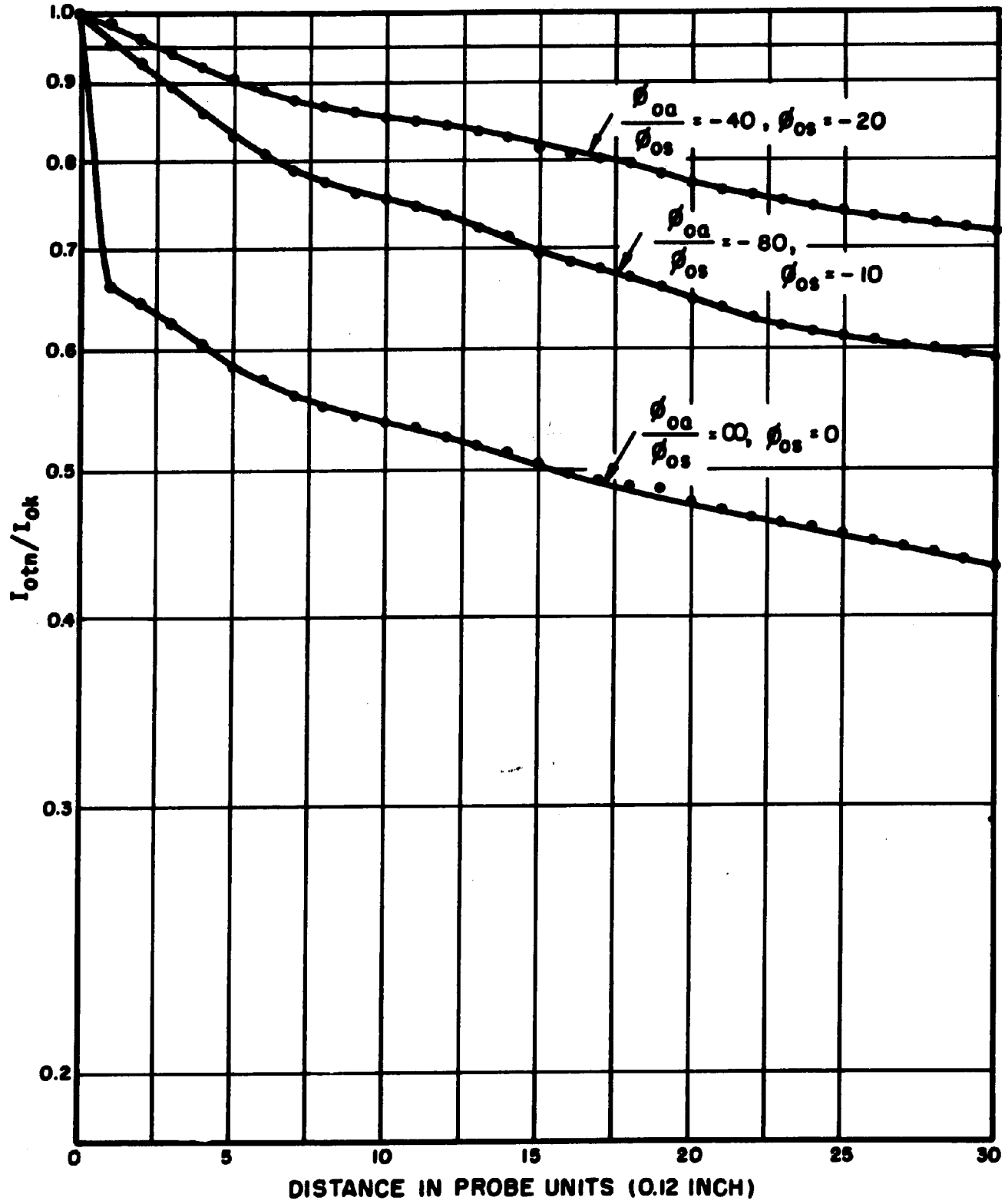


FIG. 5.8 DISTRIBUTION OF SOLE CURRENT ALONG THE SOLE. (ϕ_{oa} = 800 VOLTS, B_o = 1000 GAUSS, ϕ_{oa}/B_o^2 = 0.8 x 10^{-3} VOLTS/GAUSS^2. CATHODE NO. 2)

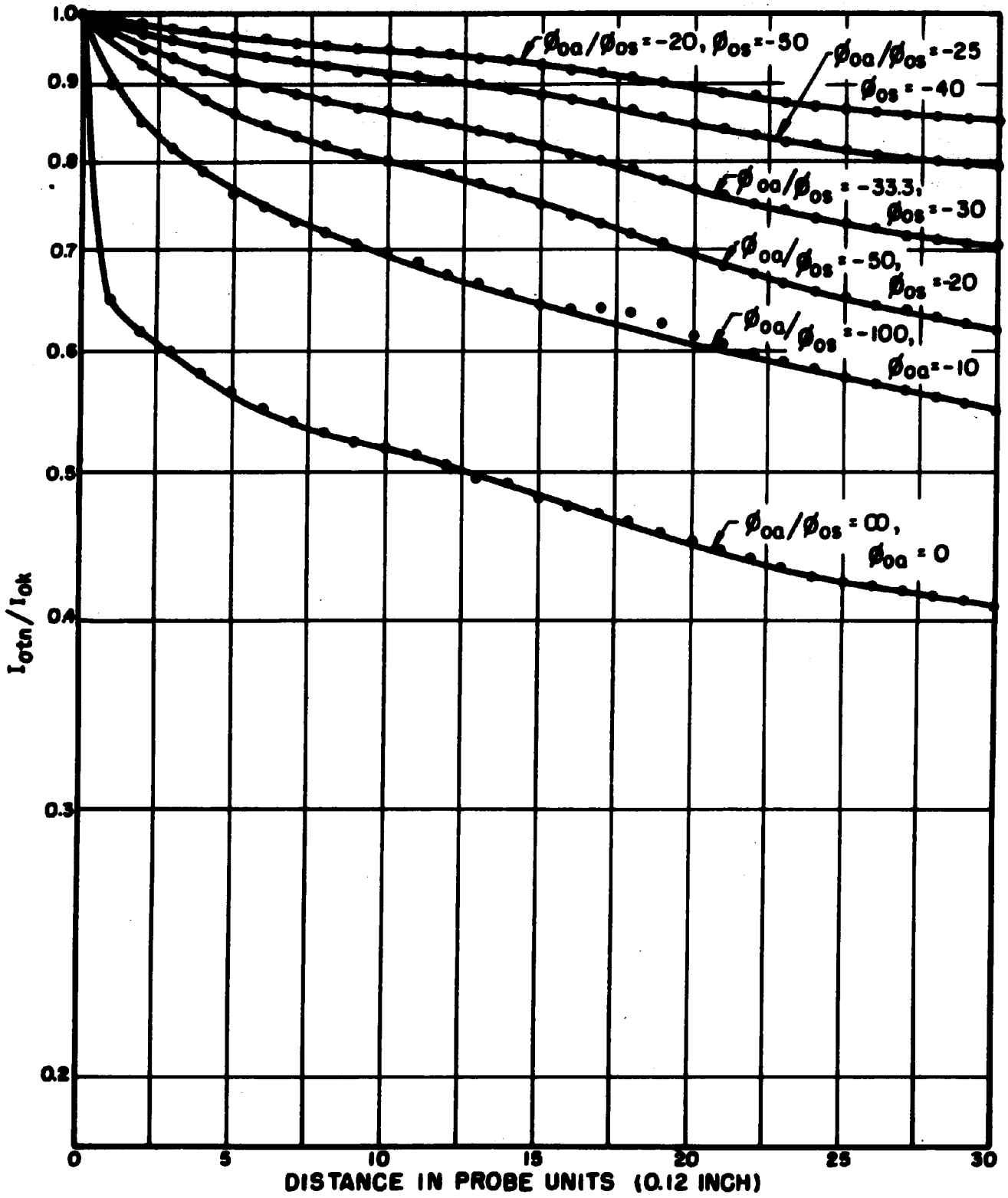


FIG. 5.9 DISTRIBUTION OF SOLE CURRENT ALONG THE SOLE. (ϕ_{oa} = 1000 VOLTS, B_0 = 1000 GAUSS, ϕ_{oa}/B_0^2 = 1.0 x 10^{-3} VOLTS/GAUSS^2. CATHODE NO. 2)

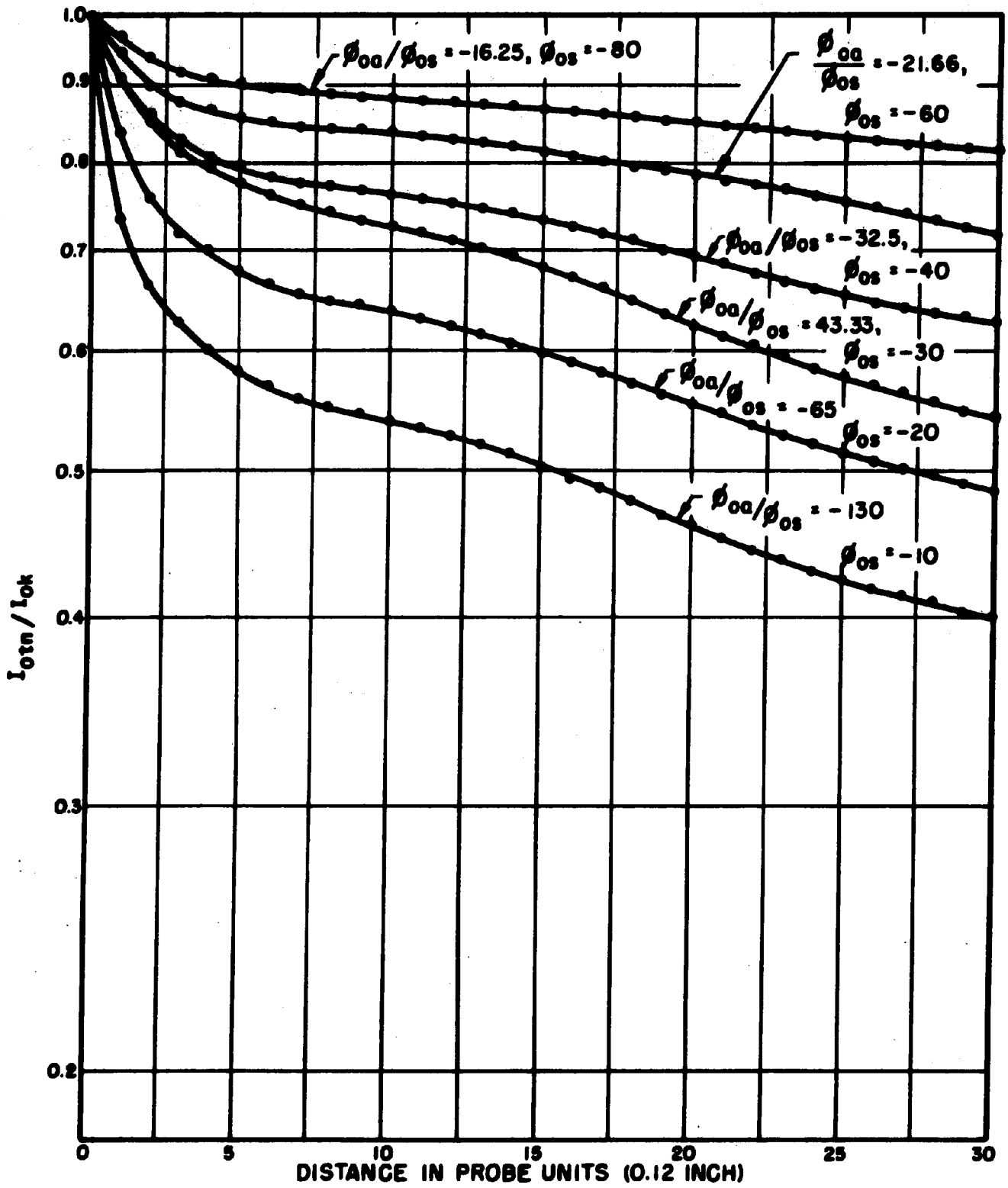


FIG. 5.10 DISTRIBUTION OF SOLE CURRENT ALONG THE SOLE. (ϕ_{oa} = 1300 VOLTS, B_o = 1000 GAUSS, ϕ_{oa}/B_o^2 = 1.3 x 10^{-3} VOLTS/GAUSS^2. CATHODE NO. 2)

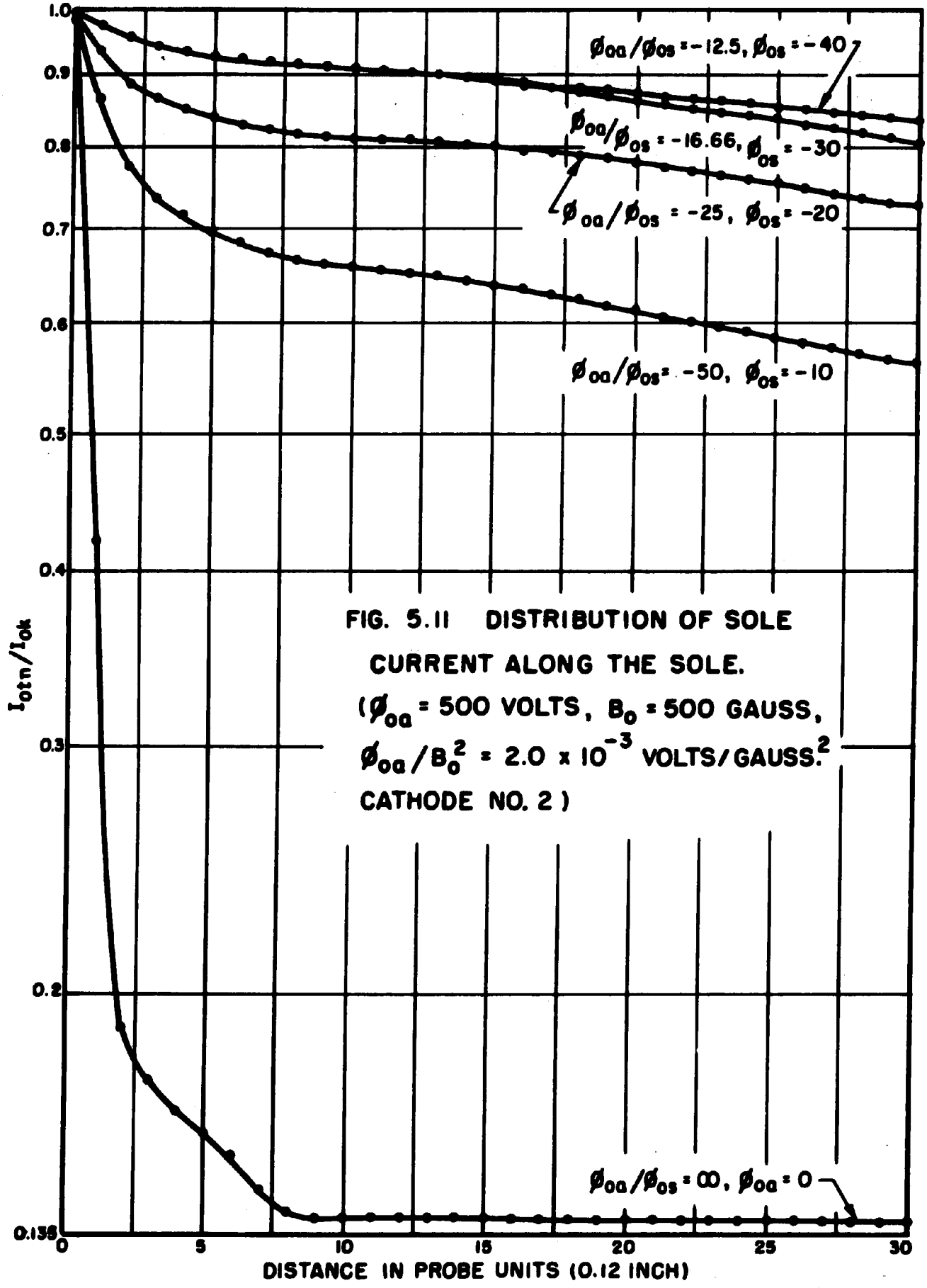


FIG. 5.11 DISTRIBUTION OF SOLE CURRENT ALONG THE SOLE.
(ϕ_{oa} = 500 VOLTS, B_0 = 500 GAUSS, $\phi_{oa}/B_0^2 = 2.0 \times 10^{-3}$ VOLTS/GAUSS.^{2} CATHODE NO. 2)

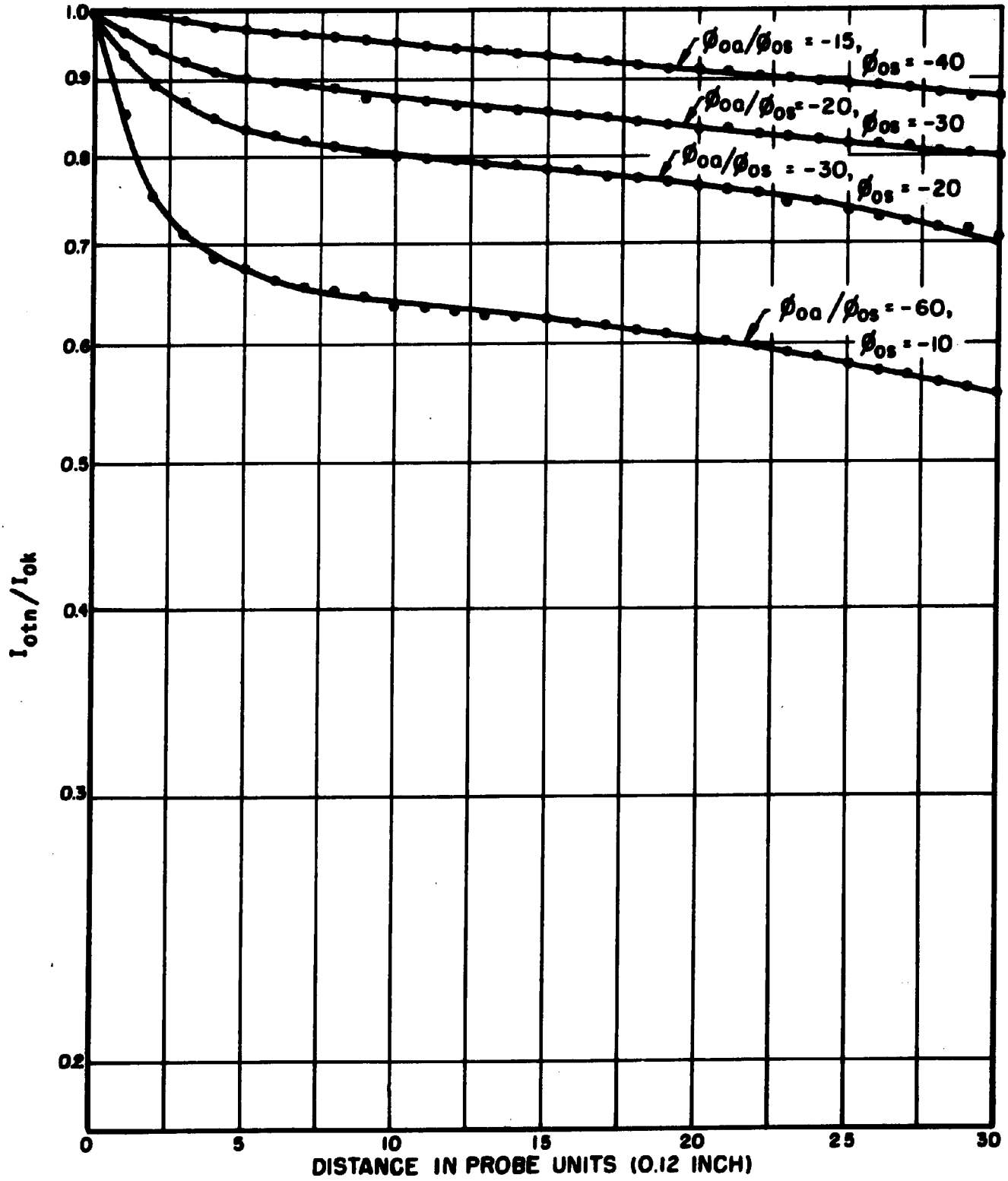


FIG. 5.12 DISTRIBUTION OF SOLE CURRENT ALONG THE SOLE. (ϕ_{oa} = 600 VOLTS, B_o = 500 GAUSS, ϕ_{oa}/B_o^2 = 2.4 x 10^{-3} VOLTS/GAUSS^2 CATHODE NO. 2)

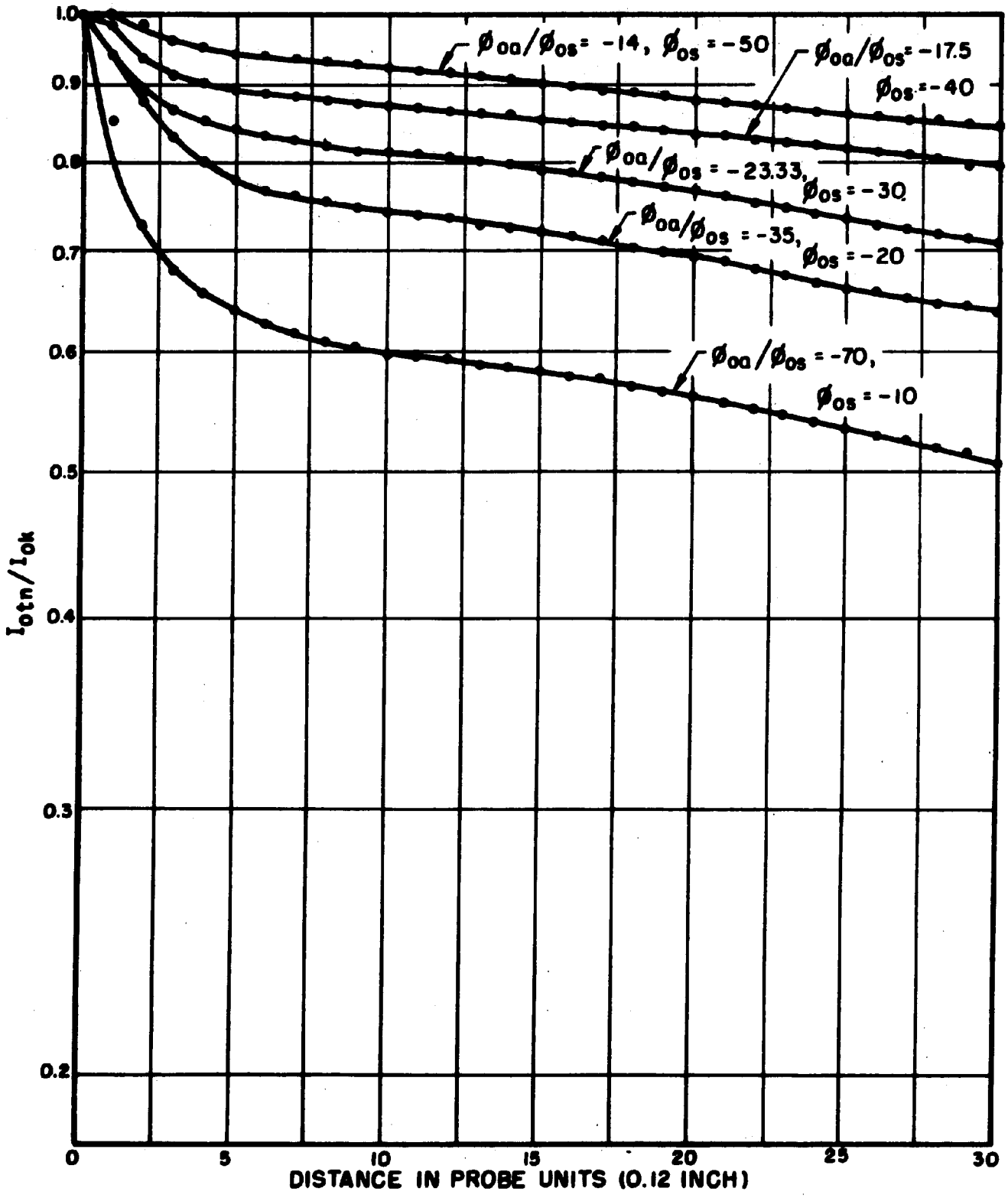


FIG. 5.13 DISTRIBUTION OF SOLE CURRENT ALONG THE SOLE. (ϕ_{oa} = 700 VOLTS, B_o = 500 GAUSS, ϕ_{oa}/B_o^2 = 2.8 x 10^{-3} VOLTS/GAUSS^2. CATHODE NO. 2)

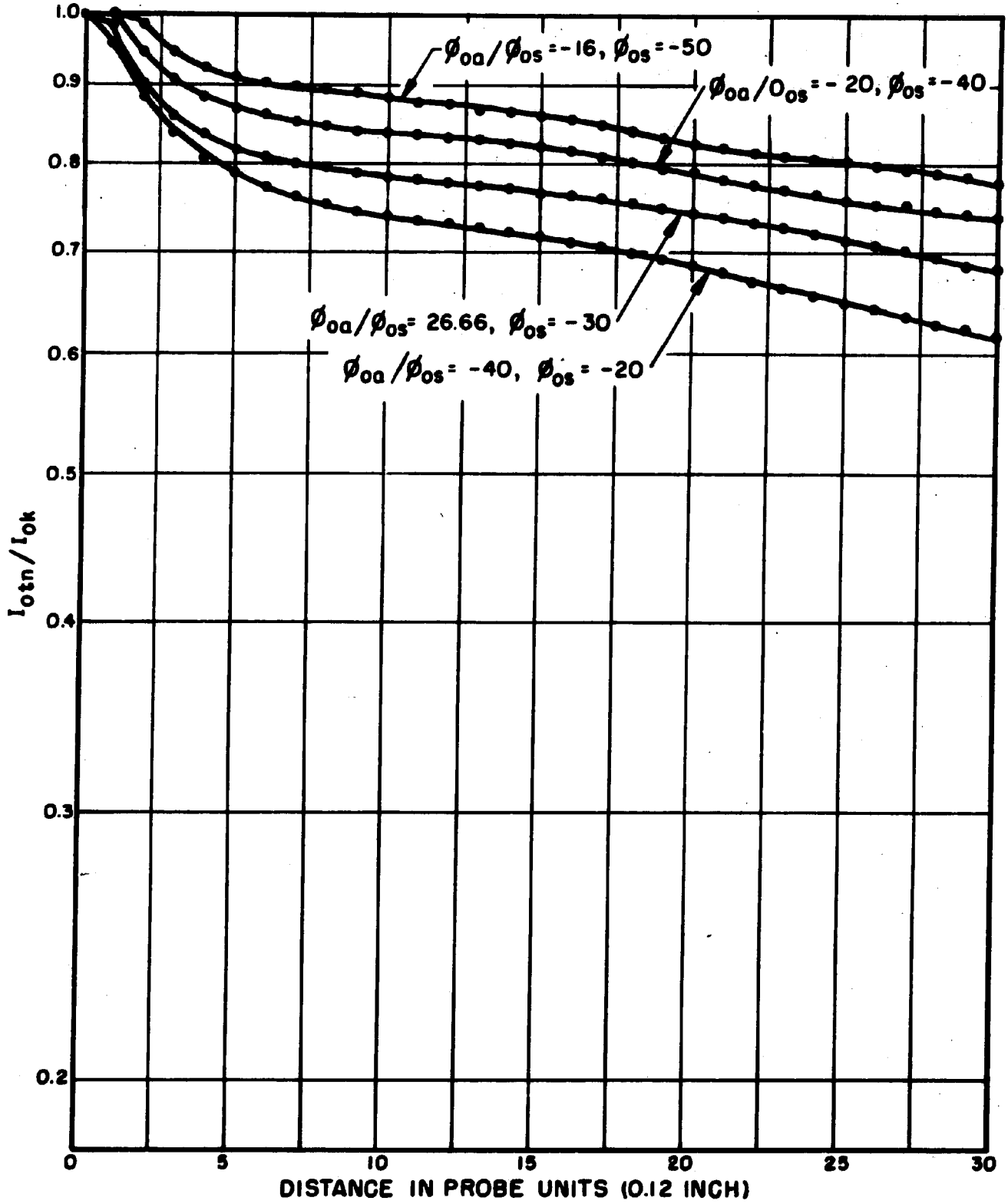


FIG. 5.14 DISTRIBUTION OF SOLE CURRENT ALONG THE SOLE.
(ϕ_{oa} = 800 VOLTS, B_0 = 500 GAUSS, ϕ_{oa}/B_0^2 = 3.2 x 10^{-3} VOLTS/GAUSS.^{2} CATHODE NO. 2)

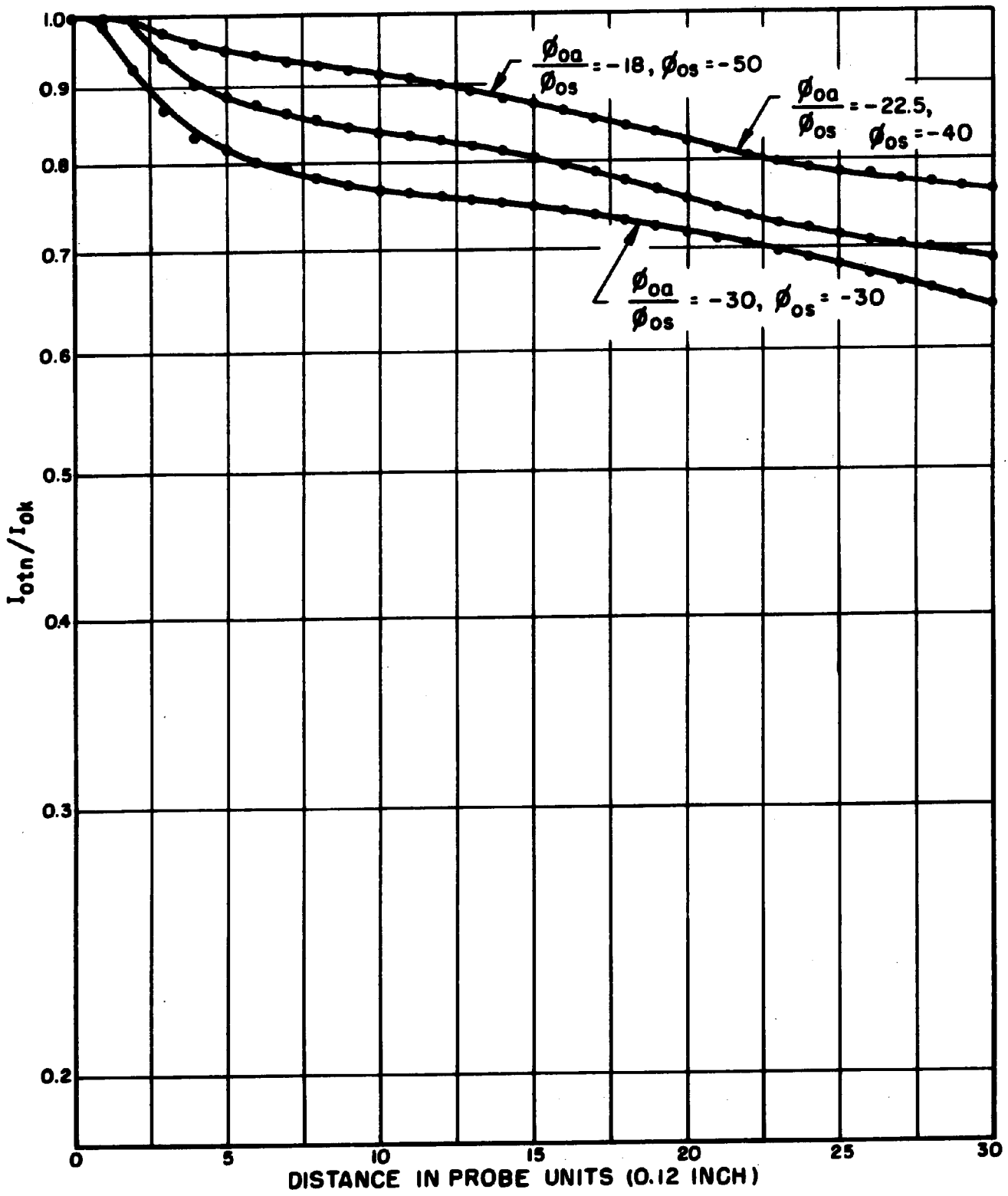


FIG. 5.15 DISTRIBUTION OF SOLE CURRENT ALONG THE SOLE. (ϕ_{oa} = 900 VOLTS, B_o = 500 GAUSS, $\phi_{oa}/B_o^2 = 3.6 \times 10^{-3}$ VOLTS/GAUSS^2. CATHODE NO. 2)

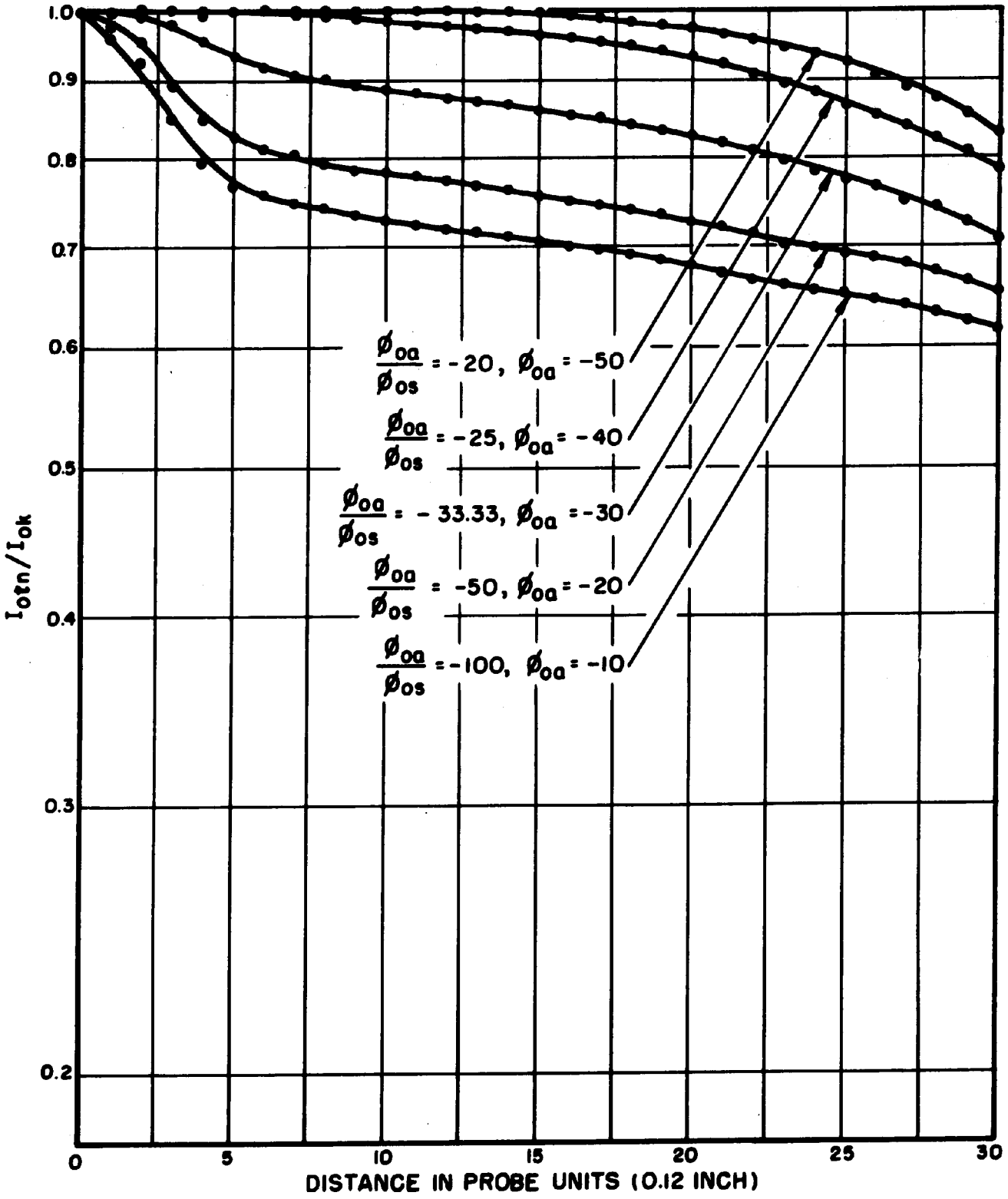


FIG. 5.16 DISTRIBUTION OF SOLE CURRENT ALONG THE SOLE. (ϕ_{oa} = 1000 VOLTS, B_o = 500 GAUSS, $\phi_{oa}/B_o^2 = 4.0 \times 10^{-3}$ VOLTS/GAUSS^2. CATHODE NO. 2)

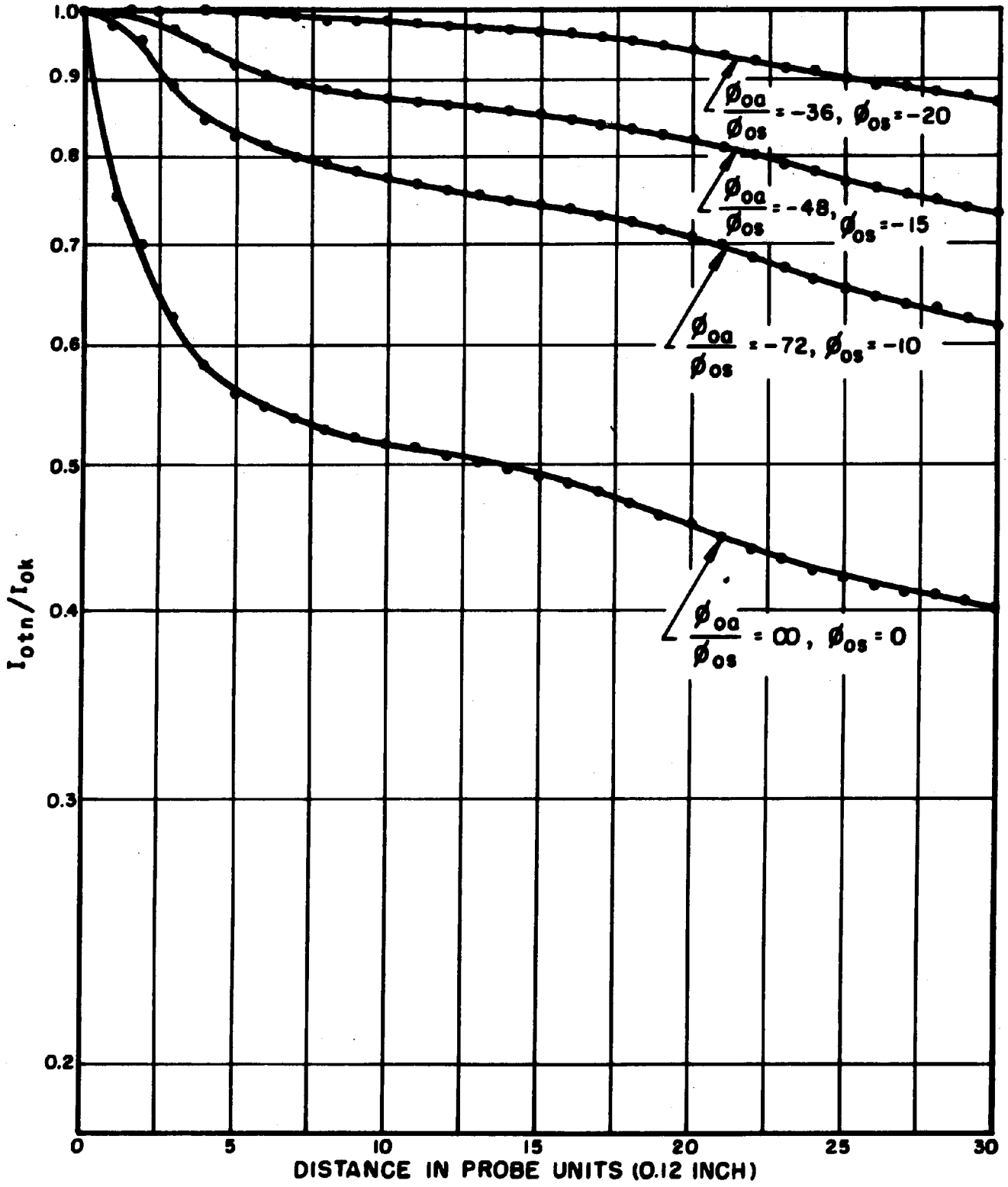


FIG. 5.17 DISTRIBUTION OF SOLE CURRENT ALONG THE SOLE. (ϕ_{oa} = 720 VOLTS, B_0 = 400 GAUSS, ϕ_{oa}/B_0^2 = 4.5 x 10^{-3} VOLTS/GAUSS^2. CATHODE NO. 2)

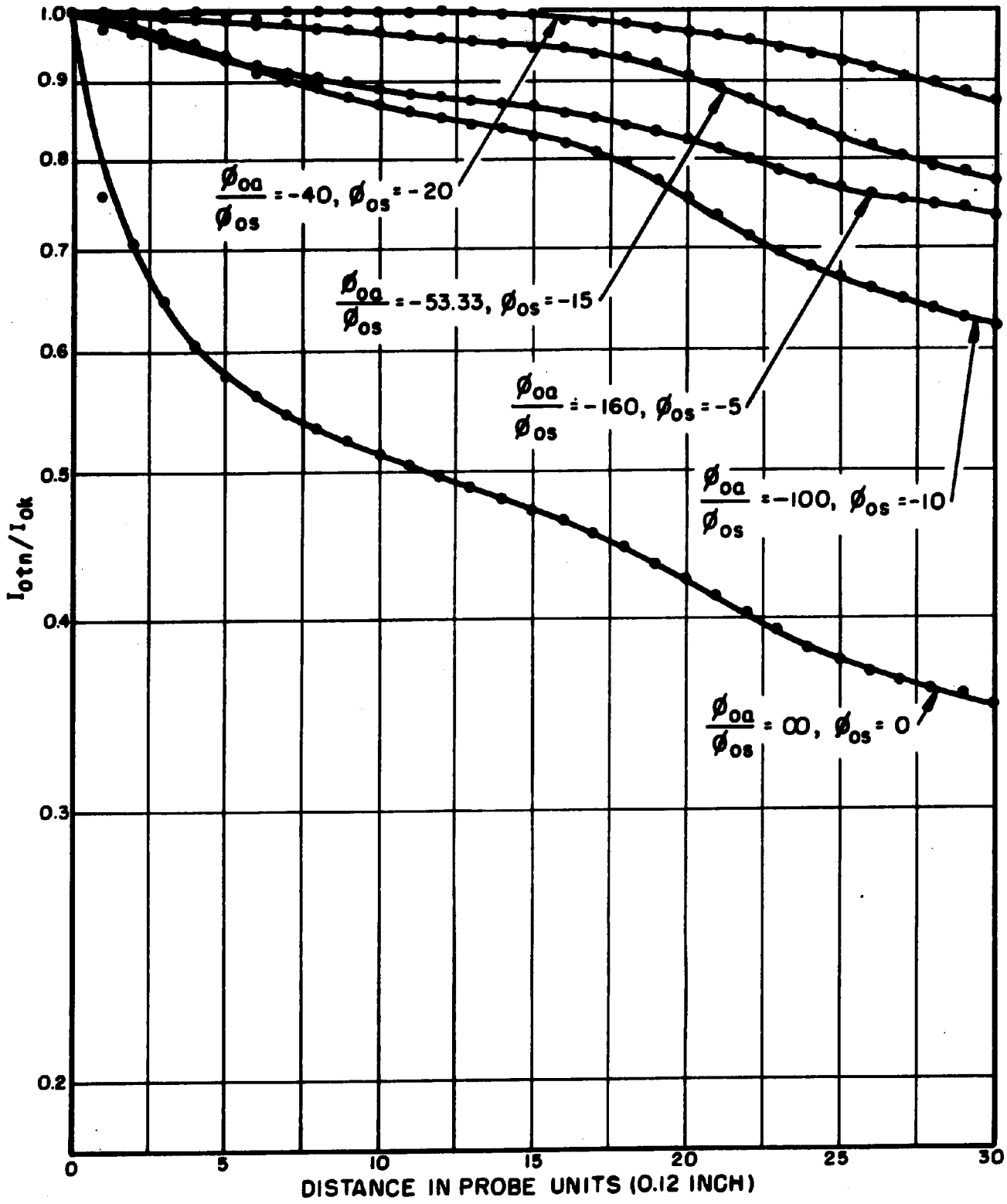


FIG. 5.18 DISTRIBUTION OF SOLE CURRENT ALONG THE SOLE.
(ϕ_{oa} = 800 VOLTS, B_0 = 400 GAUSS, $\phi_{oa}/B_0^2 = 5.0 \times 10^{-3}$ VOLTS/GAUSS.^{2} CATHODE NO. 2)

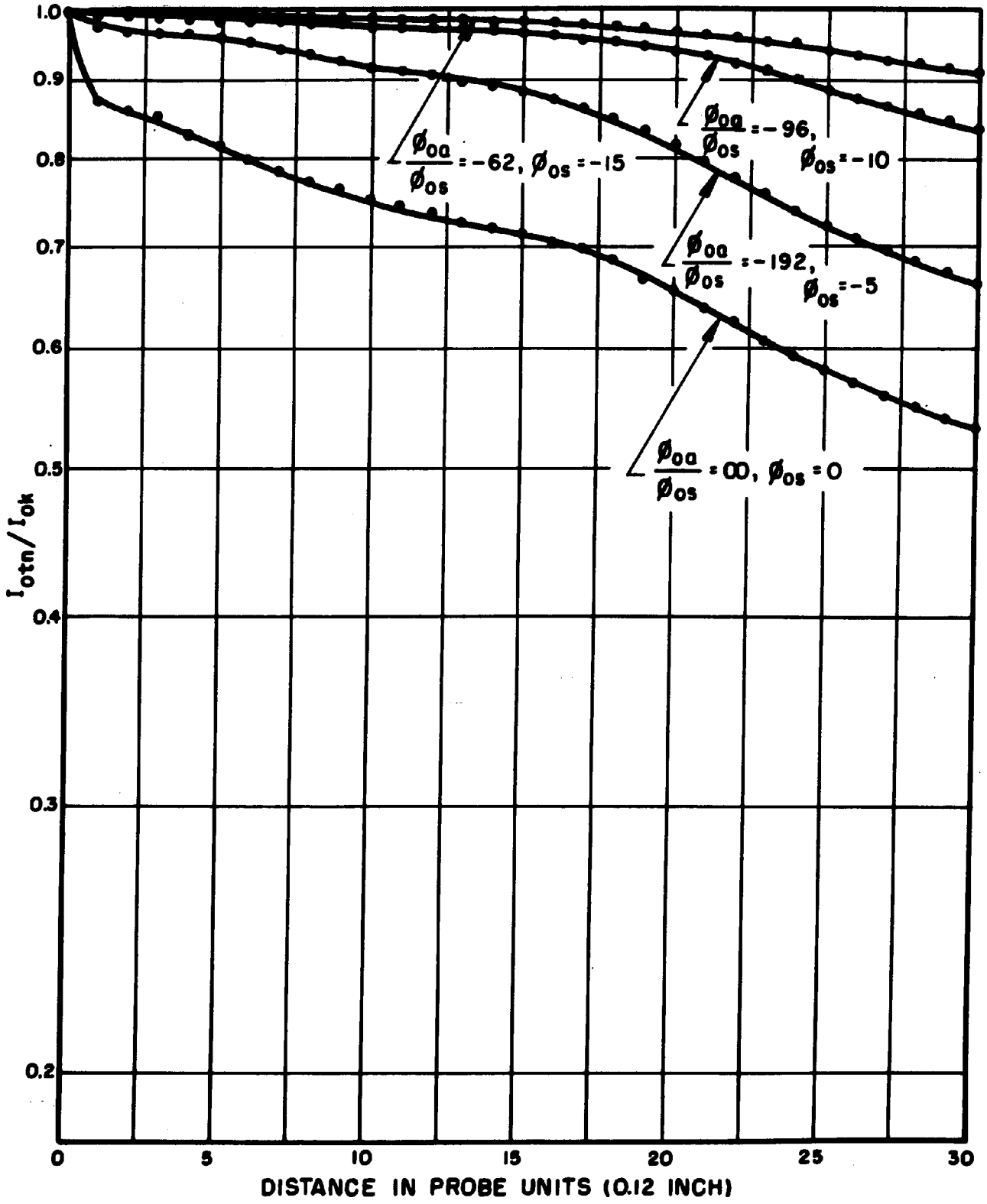


FIG. 5.19 DISTRIBUTION OF SOLE CURRENT ALONG THE SOLE. (ϕ_{oa} = 960 VOLTS, B_0 = 400 GAUSS, ϕ_{oa}/B_0^2 = 6.0 x 10^{-3} VOLTS/GAUSS.^{2} CATHODE NO. 2)

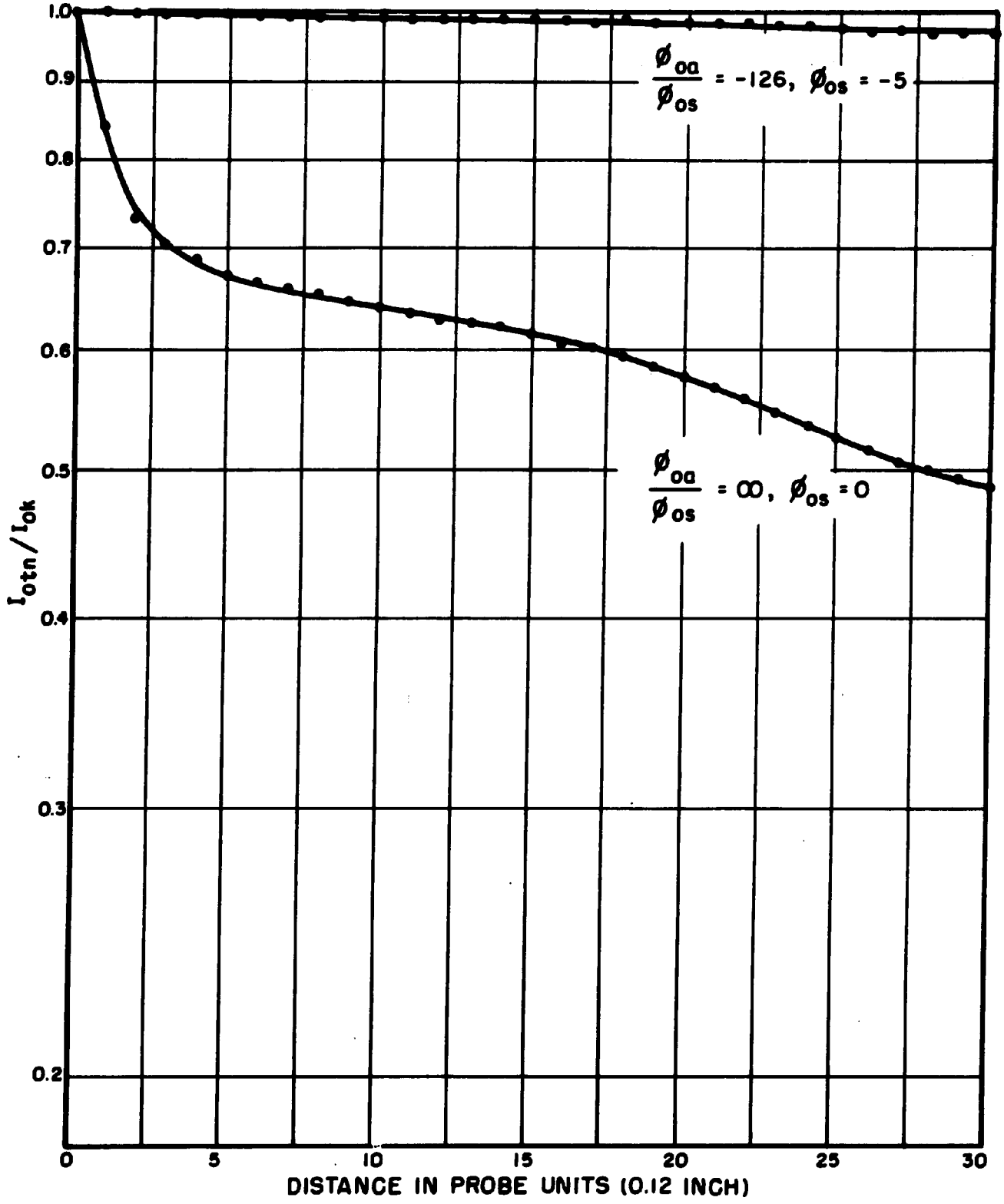


FIG. 5.20 DISTRIBUTION OF SOLE CURRENT ALONG THE SOLE. (ϕ_{oa} = 630 VOLTS, B_0 = 300 GAUSS, ϕ_{oa}/B_0^2 = 7.0 x 10^{-3} VOLTS/GAUSS^2. CATHODE NO. 2)

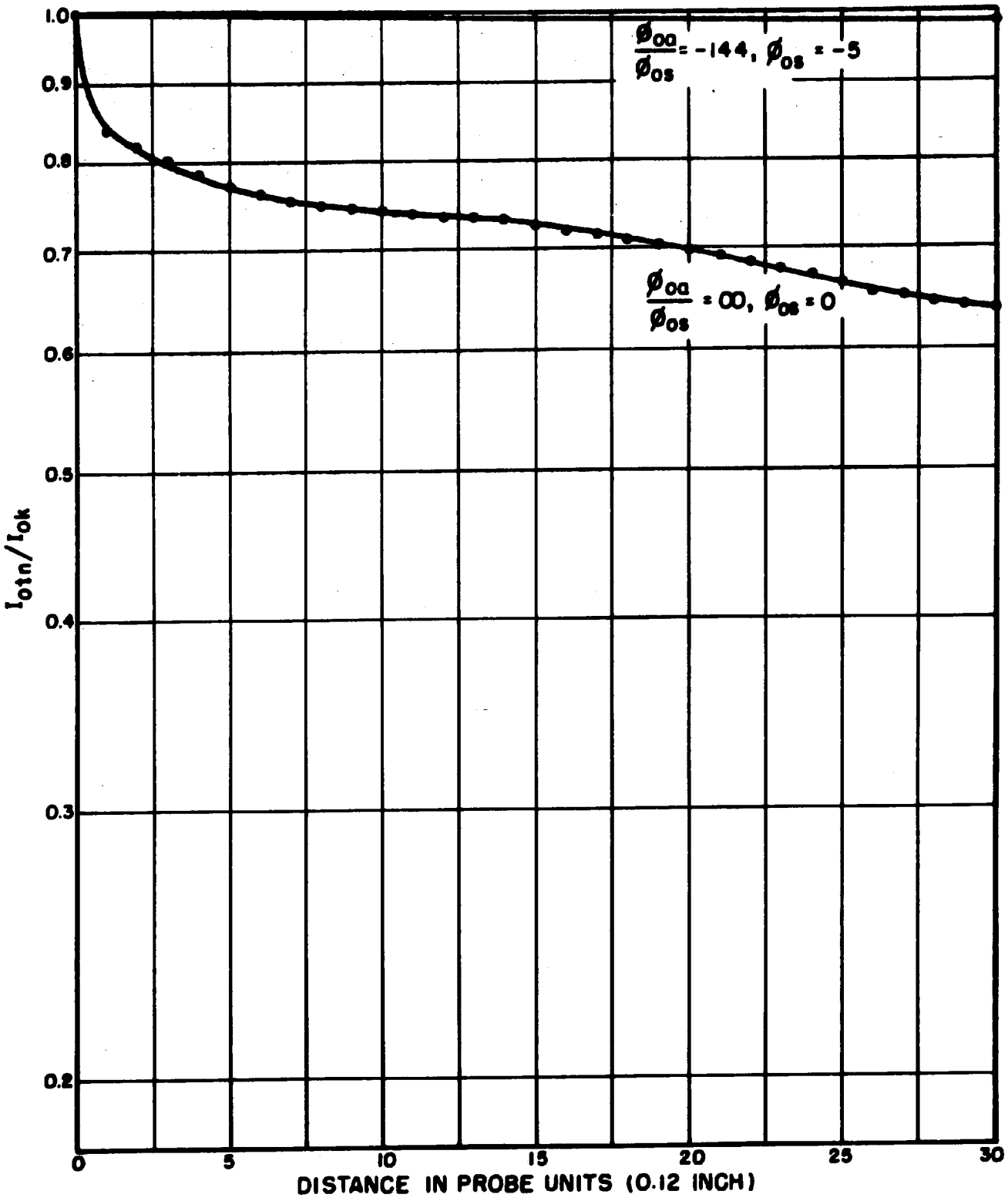


FIG. 5.21 DISTRIBUTION OF SOLE CURRENT ALONG THE SOLE. (ϕ_{oa} = 720 VOLTS, B_o = 300 GAUSS, ϕ_{oa}/B_o^2 = 8.0 x 10^{-3} VOLTS / GAUSS^2 CATHODE NO. 2)

The anode voltage and the magnetic field used to obtain a given value of ϕ_{oa}/B_o^2 are indicated on each figure. Also shown on each curve is the value of sole potential for which the data were taken. To scale the data to other values of ϕ_{oa} and B_o, it is necessary also to scale the sole potential so as to keep the ratio ϕ_{oa}/ϕ_{os} constant. This scaling requirement should be kept in mind also when comparing one figure with another. (The appropriate value of the ratio ϕ_{oa}/ϕ_{os} is shown for each curve.)

One very interesting characteristic of the data, exhibited strikingly by most of the curves, is the large change in slope of the curves after one third or less of the sole has been traversed. Most of the current collected by the sole is collected almost immediately after the stream enters the plate-sole space. This is true even when the sole has a considerably negative potential. It is evident from these data that a considerable part of the cathode current acquires the energy necessary to reach a negative sole before the stream enters the plate-sole space. There is therefore a significant energy exchange mechanism functioning in the cathode region.

Another characteristic of the data is the fact that all the sole current is not collected on the first few sole segments. Essentially, uniform field conditions exist in the plate-sole space after the first one or two sole segments. It would ordinarily be expected that if an electron had sufficient energy to reach the sole it would be collected the first time its trajectory intercepted the sole. In Fig. 4.11, it is seen that the period of trochoidal motion in the plate-sole space, even at the highest values of the scaling parameter for which data are shown, is less than two probe periods. It is, therefore, interesting that a small current is collected by sole segments relatively far from the cathode.

5.6 Energy Distribution Measurements

In the measurements described in the previous section, the sole segments were used to make passive measurements, i.e., the entire sole was an actual part of the stream analyzer environment. In contrast, the sole segments can be used actively to sample certain characteristics of the stream. One such type of measurement is to examine the various sole-segment currents as a function of the potential of one sole segment, all other potentials and the magnetic field remaining fixed. Figures 5.22 to 5.24 show the results of such a measurement made with cathode No. 1. These figures correspond to data taken by varying the potential on sole segments 4, 7, and 13, respectively. Figures 5.25 and 5.26 show similar data taken with cathode No. 2.

Since all the figures exhibit similar characteristics, the discussion of the data will be illustrated by particular reference to Fig. 5.22; the general observations made will be applicable to all the figures. Figure 5.22 presents data taken for a value of the scaling parameter of 2.133×10^{-3} volts/gauss^2 (ϕ_{oa} = 1200 volts, B_o = 750 gauss), and with a sole potential (except for the fourth sole segment) of -20 volts. The curves show the variation of current of the first twelve sole segments as a function of the potential of the fourth sole segment. Also shown is the variation of the total sole current (including the current to the fourth sole segment).

Before referring specifically to the data, it is useful to consider the effect of varying the potential of a single sole segment on the stream analyzer environment. Consider first the case when the segment has a potential less negative than the remainder of the sole. For this condition the equipotentials are depressed in the neighborhood of the segment,

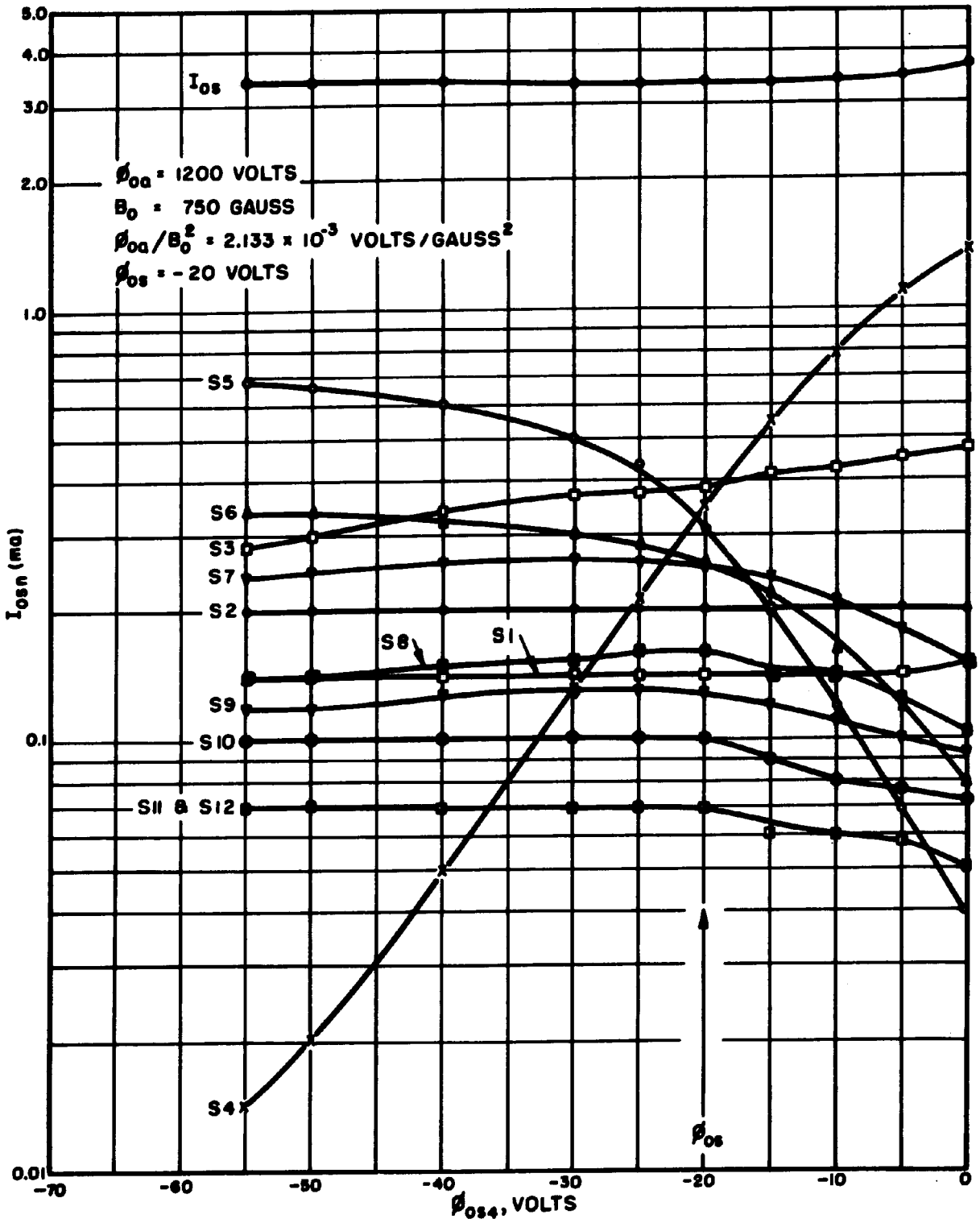


FIG. 5.22 ENERGY DISTRIBUTION CURVES, SOLE SEGMENT NO. 4. (CATHODE NO. 1)

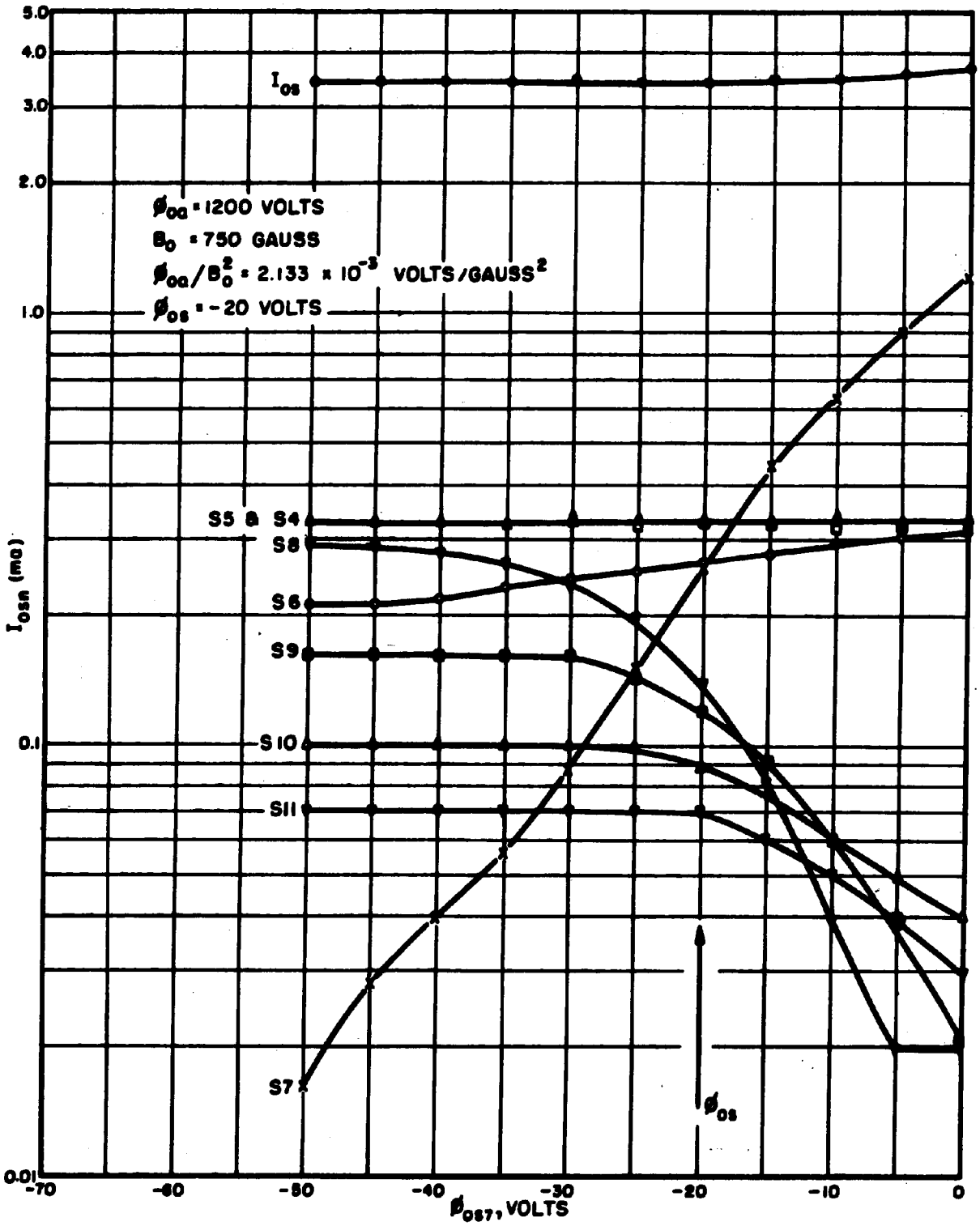


FIG. 5.23 ENERGY DISTRIBUTION CURVES, SOLE SEGMENT NO. 7. (CATHODE NO. 1)

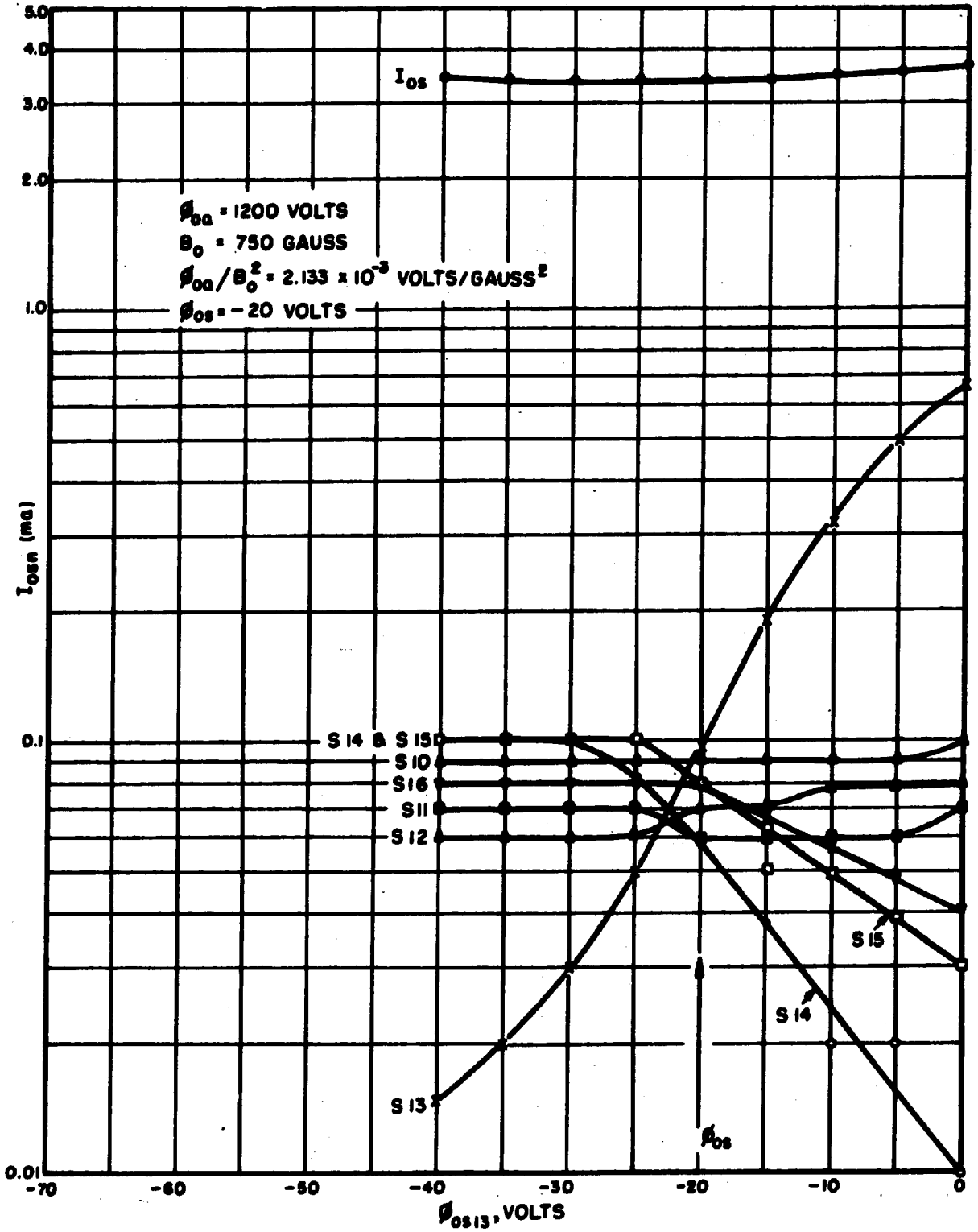


FIG. 5.24 ENERGY DISTRIBUTION CURVES, SOLE SEGMENT NO. 13. (CATHODE NO. 1)

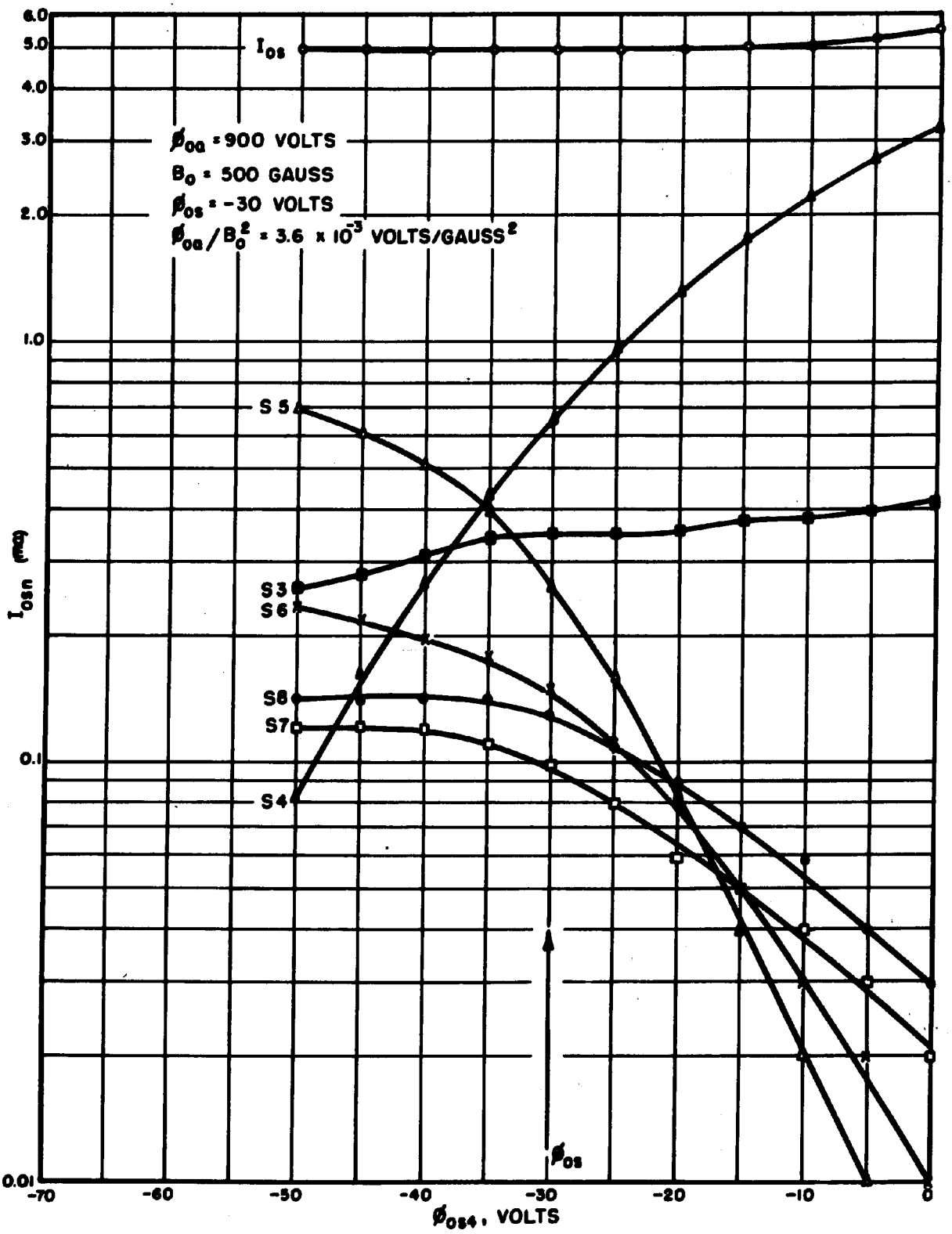


FIG. 5.25 ENERGY DISTRIBUTION CURVES, SOLE SEGMENT NO. 4 (CATHODE NO. 2)

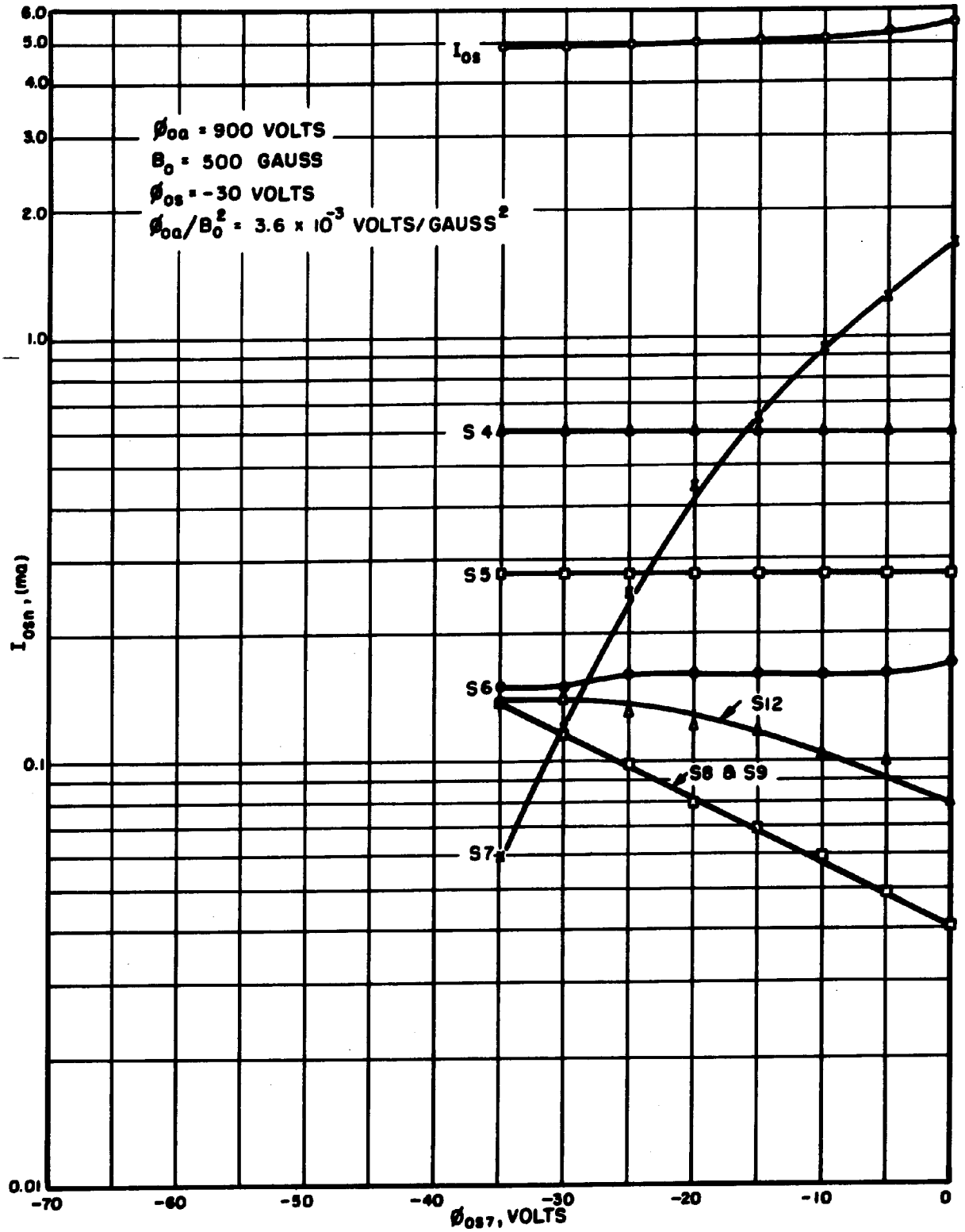


FIG. 5.26 ENERGY DISTRIBUTION CURVES, SOLE SEGMENT NO. 7. (CATHODE NO. 2)

forming a trough. Because of the tendency of the electrons to follow the equipotential lines, the stream is brought closer to the segment by the potential depression. To a lesser extent, depending on how strong a depression is formed, the stream is brought closer to segments adjacent to the particular segment whose potential is being varied. Bringing the stream closer to the sole causes some electron trajectories to intercept the sole whereas normally they would not do so. Consequently the currents intercepted by those sole segments in the vicinity of the potential depression will increase as the depression is increased. In addition, of course, raising the potential of a sole segment allows it to collect electrons of lower energy. The converse situation occurs when the segment has a more negative potential than the remainder of the sole. In this case a potential hump forms in the neighborhood of the segment.

Referring now to Fig. 5.22, we see that there are significant changes in the distribution of current along the sole as a result of varying the potential of the fourth sole segment. However, the total sole current is unaffected. Also, the currents to the first two sole segments do not vary. The curve for the current to the third sole segment, however, has a small positive slope; this is what is expected on the basis of the effect of the alteration of the shape of the equipotentials as described above. The current variation of the fourth sole segment is approximately linear, which (since Fig. 5.22 is a semi-log plot) is characteristic of a Maxwellian energy distribution. It is seen that current to the fourth sole segment increases at the expense of current to succeeding segments, particularly the immediately succeeding segments. The further a segment is from the fourth segment the less it is affected. Conversely, raising

the energy requirement for collection of current by the fourth sole segment increases the current to the immediately succeeding segments.

The data support the previous conclusion that nearly all of the energy exchange occurs in the cathode region. If current, which would ordinarily be intercepted by the fourth segment, is denied access to that segment (by making $\phi_{os4} < \phi_{os}$), it is then collected by the next few segments. On the other hand, if is withdrawn prematurely (by making $\phi_{os4} > \phi_{os}$) there is no energy exchange mechanism of sufficient influence to cause it to be replaced.

Since the current characteristic for the segment whose potential is being varied (ϕ_{os4} in Fig. 5.22) is approximately Maxwellian, the slope of the curve is approximately the voltage equivalent of the temperature of the electrons collected by the segment, and is half the average energy of the electrons. In Fig. 5.22 the voltage equivalent of temperature is 23 electron-volts, corresponding to an average energy of 46 electron-volts. Actually, the average energy is somewhat lower than this because of the deficiency of low-energy electrons in the distribution; i.e., the distribution is not exactly Maxwellian.

The average energy, calculated in the approximate manner described above, does not change to any great extent as a function of distance along the sole. This can be seen from Fig. 5.27, which is a plot of the energy distribution for a number of sole segments, using the same voltages and magnetic field as were used to obtain the data of Fig. 5.22. Another interesting fact shown by these data is that not all the current corresponding to electrons which have gained extra energy is collected by the sole. For example the curve for the last sole segment (No. 30) shows that an appreciable number of electrons, which would ordinarily not be

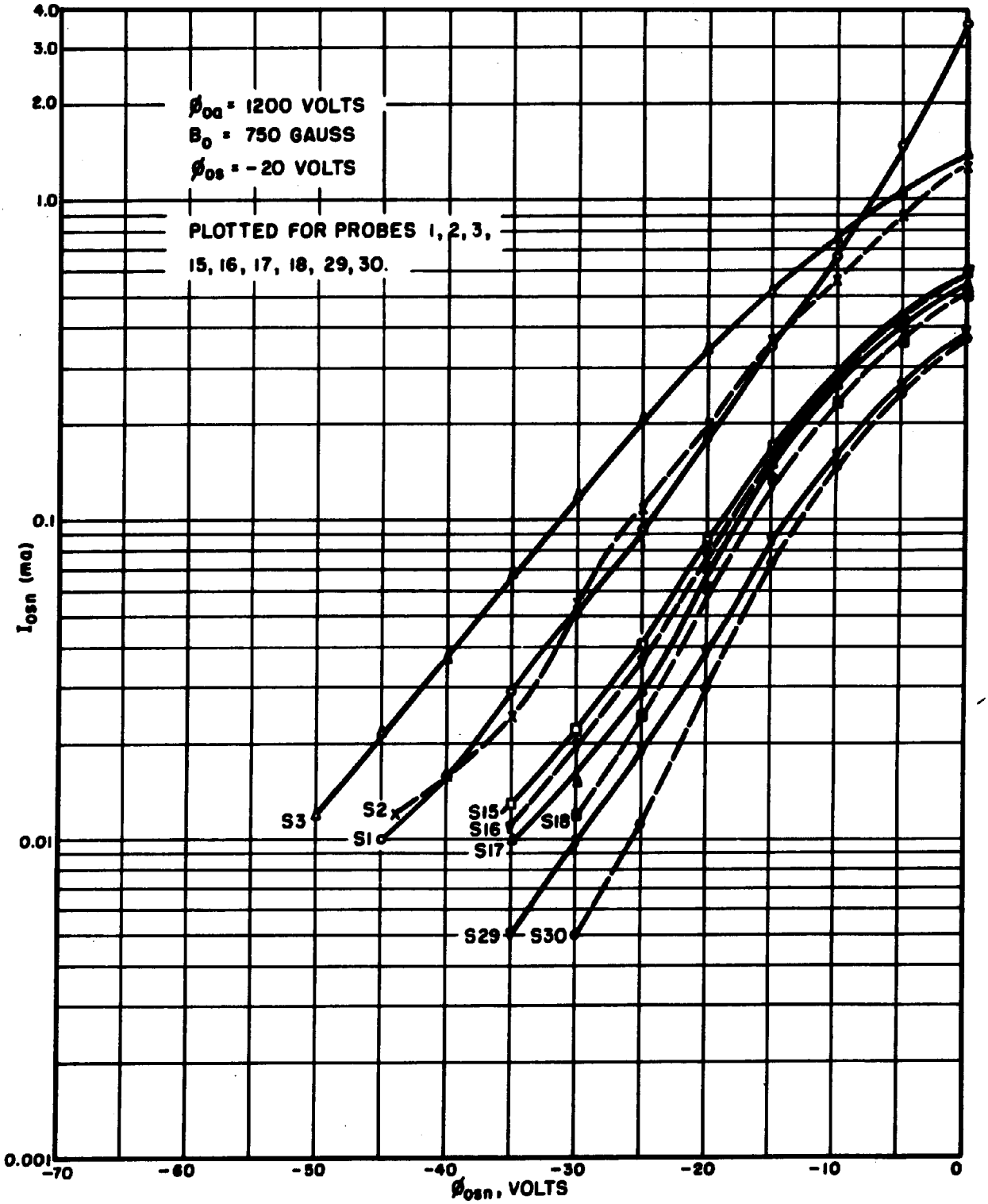


FIG. 5.27 ENERGY DISTRIBUTION CURVES, SOLE SEGMENTS 1, 2, 3, 15, 16, 17, 18, 29, 30. (CATHODE NO. 1)

collected by the negative sole, had considerable excess energy.

This last point was explored further with reference to the data presented in Figs. 5.25 and 5.26. Under the same operating conditions as used for these data (ϕ_{oa} = 900 volts, ϕ_{os} = -30 volts, B_o = 500 gauss), measurements were made in the following fashion: for the above operating conditions the potential of the fourth sole segment was set at a given value (not, in general, the same as ϕ_{os}), and the current to the seventh sole segment was measured as a function of the potential of the seventh sole segment. Measurements were made with several different values of potential on the fourth sole segment. The data obtained are shown in Fig. 5.28.

It is seen that when part of the excess energy of the stream on the fourth probe is withdrawn (by making ϕ_{os4} less negative), there is a consequent reduction of excess energy in the stream at the seventh probe; i.e., the energy loss is not replaced during the transit of the stream between the probes. On the other hand, if the fourth probe is made sufficiently negative so that it no longer collects a significant amount of current, then a further decrease in its potential has little effect at the seventh probe.

It is interesting that the average energy of the electrons collected by the seventh probe is, roughly speaking, the same for all values of the potential of the fourth probe. Consideration of this point will be postponed until later, when an overall evaluation of the measurement is made.

5.7 R-F Measurements

In the course of replacing the cathode No. 1 assembly, advantage was taken of the opportunity to insert an r-f probe between the anode

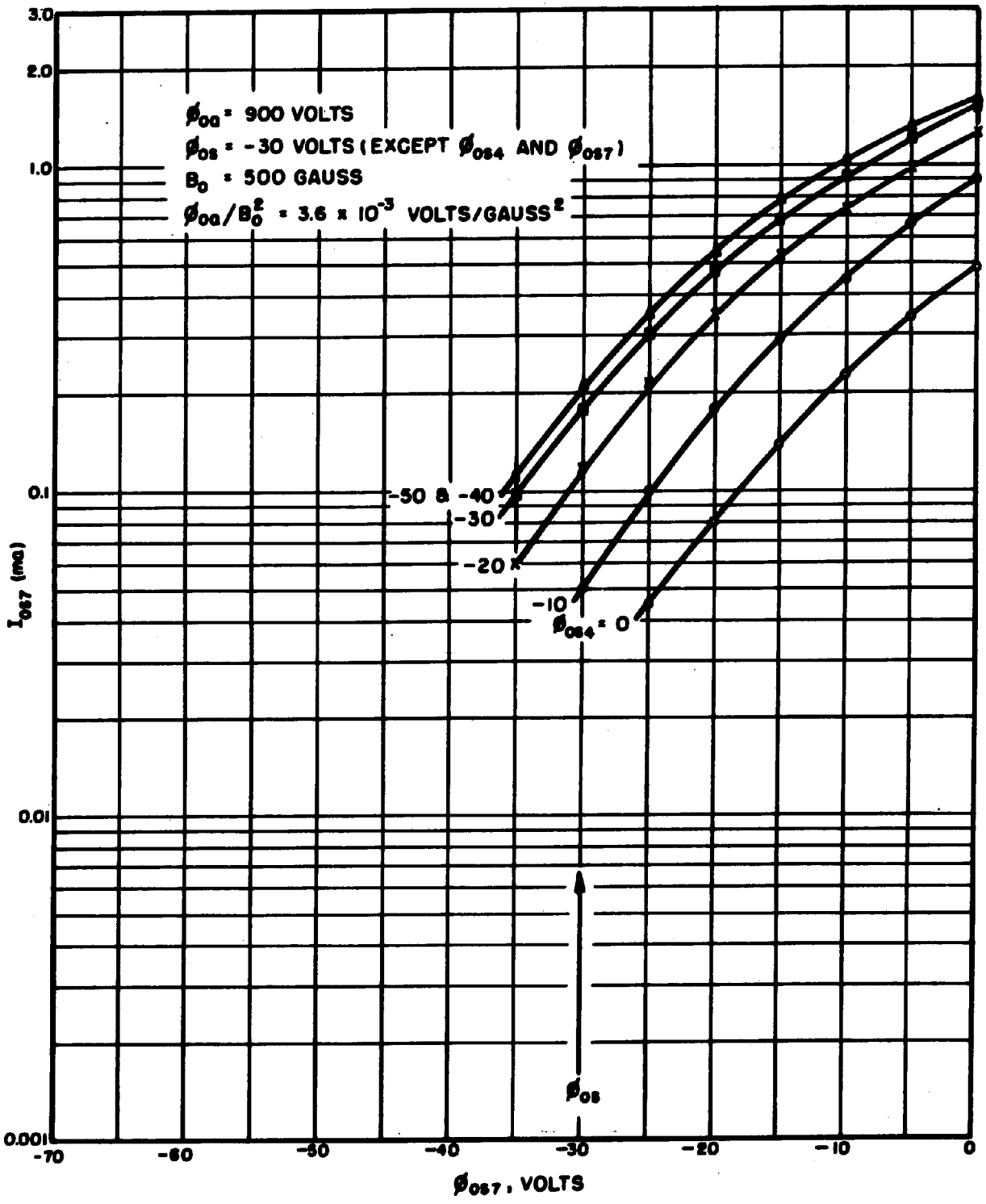


FIG. 5.28 ENERGY DISTRIBUTION CURVES, SOLE SEGMENT NO. 7. (CATHODE NO. 2)

and cathode block. The probe is actually an extension of the center conductor of a coaxial line. The coaxial line consists of a copper outer conductor concentric with a tungsten inner conductor. The inner conductor is supported by two glass beads; the beads also serve as vacuum seals. Figure 5.29 is a sketch of r-f probe assembly, showing its dimensions and its location relative to the geometry of the stream analyzer. While the location and orientation of the probe are not the most desirable, they have the merit of not requiring any modification of the stream analyzer geometry.

It was obvious from the rather large energy involved with the negative-sole current that there must exist strong r-f fields inside the stream analyzer, as only by such fields could the energy exchange between electrons take place. The r-f probe was inserted for the purpose of obtaining information about the nature and frequency of the spectrum of the r-f fields. The voltage standing-wave ratio (with the stream analyzer "cold"), looking into the stream analyzer through the probe, is less than 3:1 from about 2 to 4 kilomegacycles/second. This, however, provides scant information about the coupling of the probe to r-f signals generated inside the stream analyzer.

Relatively weak signals (estimated to be fractions of a microwatt) were detected in the range of values of the scaling parameter corresponding to high sole current. Depending on particular operating conditions, the frequency of the observed signals was in the range of 2 to 3 kilomegacycles/second, typically about 2.5 kilomegacycles/second.

The frequency was observed to be sensitive to the value of the scaling parameter. A ten percent change in the value of the scaling parameter produced, roughly, a 10-megacycle/second frequency change. Similarly,

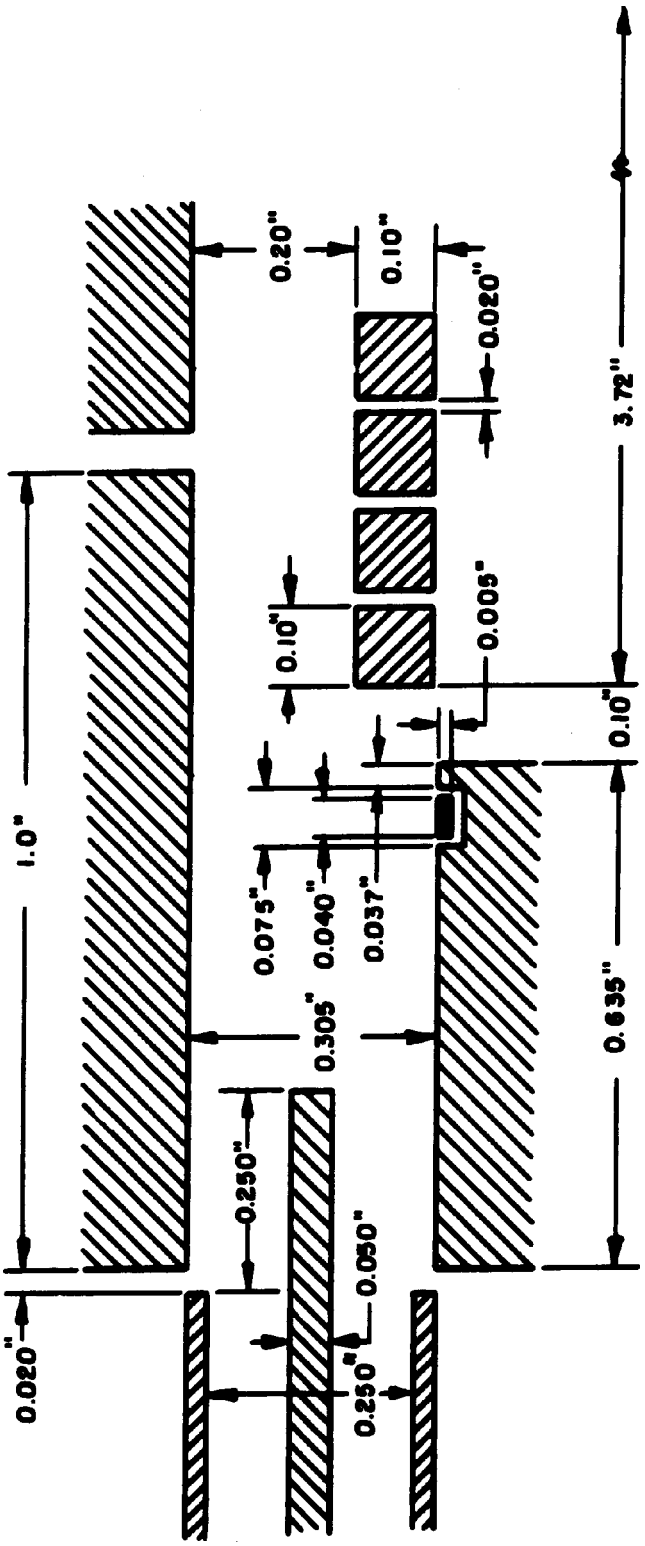


FIG. 5.29 LOCATION OF R-F PROBE IN THE CATHODE REGION.

the frequency of the observed signal is sensitive to the potential on the first sole segment. It was noted that a change in the potential of the second sole segment, or any other but the first sole segment, had no effect on the detected signal. This last observation lends emphasis to the conclusions drawn from the previously presented data; i.e., the behavior of the electron stream in the region between the cathode and the first sole segment is the key to understanding the diocotron effect.

Another interesting observation was made by introducing a 1-watt signal (from an external generator) of approximately the same frequency as the signal emanating from the stream analyzer. Depending on the frequency of the applied signal, the negative-sole current could be significantly increased or decreased compared with the sole current for no applied signal. This variation occurred over a frequency range of about 100 megacycles/second.

The frequency spectrum of the observed signal was investigated by displaying it on a spectrum analyzer (Polarad Model TSA, R-F Tuning Unit STU-2A), after the signal was first amplified by an S-band traveling-wave tube (Hewlett-Packard 490B). Because of the observed sensitivity of the signal to variations of sole potential and magnetic field, both these quantities were obtained using batteries as sources. The high-voltage anode and collector power supply is quite well filtered. The cathode supply (d-c generator) had some ripple; however, no change in source was made for the cathode. Figure 5.30 shows typical photographs of the spectra observed. The particular photographs shown are for the following conditions: ϕ_{oa} = 700 volts, ϕ_{os} = -35.5 volts, I_{oc} = 6 ma, I_{os} = 1.8 ma, B_o = 500 gauss, $\phi_{oa}/B_o^2 = 2.8 \times 10^{-3}$ volts/gauss^2. Figure

5.30a was taken with the spectrum analyzer sweep speed adjusted to obtain a stationary pattern on the screen. Figure 5.30b is a trace obtained with a single sweep of the spectrum analyzer beam.

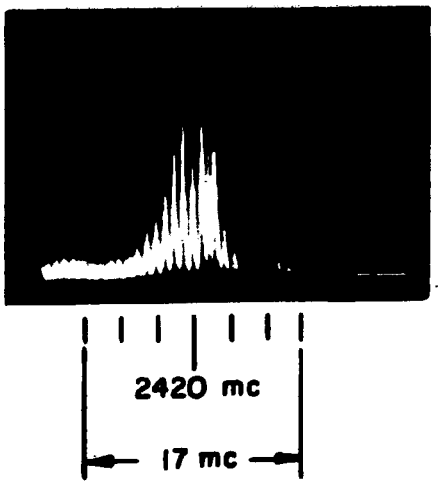
The spectrum shown in Fig. 5.30 is characteristic of a frequency-modulated signal. Because of the sensitivity of the pattern to sweep speed, it is likely that some 60-cycle modulation is occurring in addition to that evidenced in the photographs. However, it is clear that the signal is a very narrow-band one, and further that it is not an incoherent oscillation. (In this last respect, note that the spectrum analyzer resolution is approximately 25 kilocycles/second.)

It was difficult to extend the frequency measurements with the present experimental setup because of the extreme sensitivity of the signal to voltage and magnetic field. Also, the magnetic field strength is uncertain to within about ± five percent due to hysteresis in the pole pieces. As noted above, this represents a comparatively large frequency shift. The most significant aspect of the measurements made is the qualitative observation of a narrow-band coherent signal which is sensitive to the potential of the first, and only the first, sole segment.

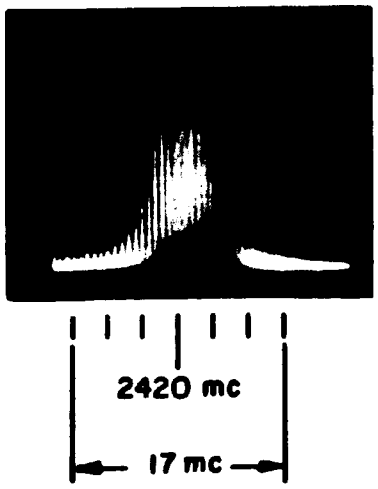
5.8 Further Interpretation of the Experimental Evidence

In this section we shall develop a theory, based on the experimental evidence, which is able to account for the observed phenomena. The theory is not able to provide a complete quantitative description of the diocotron effect; its purpose is primarily to provide a coherent interpretation of the data from which further, more refined, experiments can be devised.

The data have shown that nearly all of the energy exchange implied by the appearance of a negative-sole current occurs in the cathode region



A. SYNCHRONIZED SWEEP.



B. SINGLE SWEEP.

FIG. 5.30 SPECTRUM OF OBSERVED R-F SIGNAL. (ϕ_{oa} = 700 VOLTS, ϕ_{os} = -35.5 VOLTS, B_o = 500 GAUSS, $\phi_{oa}/B_o^2 = 2.8 \times 10^{-3}$ VOLTS/GAUSS^2, CATHODE NO. 2)

prior to the entrance of the electron stream into the plate-sole space. Since this energy exchange forms the prelude to the diocotron effect, we shall consider it first.

5.8.1 The Cathode Region. We have, as a basis on which to initiate a study of the energy exchange mechanism in the cathode region, three important experimental facts. These are:

(a) the diocotron phenomenon is scaleable,

(b) a narrow-band, coherent, r-f signal is generated as a part of the diocotron effect, and

(c) the energy distribution of the sole current is approximately Maxwellian, with a temperature on the order of 300,000°C.

Because of the scaleability of the phenomena, we can deduce that the r-f properties of the geometry of the structure (vacuum envelope, electrodes, etc.) are not a significant aspect of the diocotron effect. This deduction follows from the fact that the r-f properties of the structure are not changed in the scaling process; i.e., the geometry of the stream analyzer is fixed. Further, the scaling property suggests that the phenomenon is associated not merely with the electron stream as a whole, but, in particular, with the trajectories of the electrons comprising the stream. It is rather difficult to determine electron trajectories in crossed electric and magnetic fields taking space-charge forces into account. On the other hand, space-charge-free trajectories are not likely to correspond in detail with the corresponding trajectories computed with space-charge forces accounted for. However, the general trends of the trajectories computed with and without space charge as a function of, say, the scaling parameter ϕ_{oa}/B_o^2 should be very similar. We shall, therefore, continue to make use of the trajectory computations presented in Figs. 4.15 to 4.23 as a guide to a

qualitative understanding of the actual trajectories in the stream analyzer.

In correlating these trajectories with the diocotron effect we note that the negative-sole current falls off extremely rapidly when the scaling parameter ϕ_{oa}/B_o^2 exceeds a certain critical value. It is therefore interesting to observe a similar critical behavior of the space-charge-free trajectories. Up to a certain value of scaling parameter, which is very nearly the same as the experimentally observed value referred to above, electrons are nearly trapped in a potential valley between the cathode block and the first sole segment. It is tempting to associate the negative-sole current with the near trapping of the electrons; this is just what we do.

Trajectories of electrons passing through the slow-drift region between the cathode block and the first sole segment are characterized by very long transit times. Therefore, a large space-charge density builds up in this region. The order of magnitude of this space-charge density can be estimated fairly easily. As an illustration, consider the trajectories shown in Fig. 4.16b. The transit time from the cathode into the plate-sole space can be estimated by counting the number of trochoidal loops in the trajectory. Each loop corresponds, roughly, to a time interval equal to the cyclotron period. From Fig. 4.16b, it is seen that one trajectory takes about six cyclotron periods and the other about fifteen. For an order-of-magnitude figure, we will use ten cyclotron periods as an average transit time. We shall want to compute the average drift velocity of an electron between the cathode and the first sole segment. To do so, the length of the path along which the electron drifts is needed. We shall take the path length as the length of the trajectory along which

the electron moves in the above transit time (ignoring, however, the trochoidal looping of the trajectory; i.e., we use the distance along the path in the direction of the average forward motion of the electron). We shall use an average path length of 6 millimeters. This number is obtained by measuring off the path length on Fig. 4.16b. (To scale dimensions in Fig. 4.16b note that the length of a sole segment is 0.10 inch.) From the experimental data we have the following measurements (cathode No. 2):

$$\begin{aligned} \phi_{oa}/B_o^2 &= 0.005 \text{ volt/gauss}^2, \\ \phi_{oa} &= 800 \text{ volts}, \\ \phi_{os} &= 0 \text{ volts}, \\ B_o &= 400 \text{ gauss}, \ (\omega_c = 7 \times 10^9 \text{ radians/second}), \text{ and} \\ I_{ok} &= 12.9 \text{ milliamperes}. \end{aligned} \tag{5.6}$$

Then, approximately,

$$\begin{aligned} \text{average transit time} &= \left(\begin{matrix}\text{number of} \\ \text{cyclotron periods}\end{matrix}\right)\left(\begin{matrix}\text{cyclotron} \\ \text{period}\end{matrix}\right) \\ &= (10)\ (2\pi/\omega) \\ &= 8.9 \times 10^{-9} \text{ seconds}. \end{aligned} \tag{5.7}$$

The average velocity with which the electrons drift along their trajectories is, therefore,

$$\begin{aligned} \text{average drift velocity} &= \frac{\text{average path length}}{\text{average transit time}}, \\ &= \frac{6 \times 10^{-3}}{8.9 \times 10^{-9}} \\ &= 6.74 \times 10^5 \text{ meters/second}. \end{aligned} \tag{5.8}$$

This drift velocity corresponds to about 1.1 electron-volts.

We shall need some idea of the cross-sectional area of the stream. For the width of the stream we use the value 0.7 inch. This is the effective width of the cathode. From Fig. 4.16b, we estimate an average stream thickness of 1.5 millimeter. The average space-charge density can now be calculated from

$$\rho_o = \frac{\text{stream current}}{\text{average drift velocity x stream cross-sectional area}} ,$$

$$= \frac{12.9 \times 10^{-3}}{6.74 \times 10^5 \times 0.7 \times 2.54 \times 10^{-2} \times 1.5 \times 10^{-3}} ,$$

$$= 7.17 \times 10^{-4} \ \frac{\text{coulomb}}{\text{meter}^3} .$$

It is convenient to state the space-charge density in terms of a corresponding electron density radian frequency; the electron density radian frequency corresponding to the above space-charge density is

$$\omega_p = \left(\frac{-q\ \rho_o}{m\epsilon_o}\right)^{1/2} = 3.78 \times 10^9 \text{ radians/second} . \qquad (5.10)$$

The above calculation provides an approximation to the space-charge density (or equivalently, the electron density radian frequency) in the slow-drift region.

The point of computing the space-charge density in the slow-drift region is to discover whether there is a correlation between the plasma oscillation frequency and the r-f signal observed experimentally. However, because of the presence of the magnetic field, we must modify the concept of a simple plasma oscillation. As shown in section 3.3.5, in the presence of a magnetic field the dispersion relation for space-charge wave propagation is

$$\omega_d^2 = \omega_p^2 + \omega_c^2 . \qquad (5.11)$$

For the calculation above, this leads to a value for ω_d of

$$\omega_d = 8 \times 10^9 \text{ radians/second.} \qquad (5.12)$$

The Doppler frequency ω_d (the electron oscillation frequency as seen by an observer advancing with the average drift velocity of the stream) is related to the frequency as seen by a stationary observer through the formula

$$\omega_d^2 = (\omega - \alpha v_o)^2 \quad , \qquad (5.13)$$

where α is the propagation constant of the electron oscillation and v_o is the average electron drift velocity. We can estimate a value of α by noting that the high space-charge density is concentrated in a length approximately equal to the average path length as defined above. Since there is a large change in space-charge density in the stream as it passes out of the cathode region in the plate-sole space, it is reasonable to assume that the electron oscillation has a wavelength in some way related to the dimensions of the stream in the cathode region. In order to facilitate an energy exchange the wavelength would presumably be of the same order of magnitude as the average path length. Hence, approximately,

$$\alpha = \frac{2\pi}{\lambda} \approx \frac{2\pi}{6 \times 10^{-3}} = 1.05 \times 10^3 \text{ meter}^{-1} \quad . \qquad (5.14)$$

The factor αv_o appearing in Eq. 5.13 is therefore equal to 0.7×10^9 radian/second. Since this is small in comparison to ω_d, the observed frequency should be approximately equal to the calculated value of ω_d.

This very rough estimate of frequency is within a factor of two of the experimentally observed frequency reported in section 5.7.

In the simple model used for the above calculation it was assumed that it is permissible to view the crossed-field electron flow in the slow-drift region as being similar to an ion-neutralized electron flow in a magnetic field. This assumption is justified in the following manner: the presence of positive ions in a plasma flow cancels the space-charge forces of the electrons. This same effect can be achieved without positive ions by balancing the space-charge forces against external d-c focussing fields. Axially symmetric Brillouin flow, described in Chapters II and III, is a good example of this. For this type of flow, the d-c force balance is maintained during the perturbation. Rectilinear Brillouin flow, to which the flow in the stream analyzer may be likened, is another example of a balanced flow. However, the d-c force balance is not maintained in a perturbation of rectilinear flow. Nevertheless, if the velocity difference across the stream is small enough, the unbalancing of the d-c forces is small (see section 3.3.4). We are assuming this to be the case in our discussion. Therefore, an observer advancing with the average velocity of the electrons in the slow-drift region would see much the same electron oscillation as if the stream were neutralized by positive ions. On this basis we can apply, as an approximation, the dispersion relation used to calculate ω_q above.

Thus far we have advanced the hypothesis that an electron oscillation occurs in the cathode region with a space wavelength comparable to the dimensions of the stream in this region. We will now relate such an oscillation to a mechanism of energy exchange.

While, of course, electron trajectories in the slow-drift region will not correspond in detail to the space-charge-free trajectories, the motion will be grossly similar; i.e., electrons will have a more or less looping motion superimposed on an average forward drift. The fact that

a large energy exchange is accomplished in a very short distance suggests some sort of synchronization effect. In particular, it suggests that the loop-like motion of the electrons is (approximately) synchronous with the space-charge oscillation described above; i.e., the energy exchange occurs through a cyclotron resonance of the d-c stream motion with the electron oscillation. In this way an electron could maintain the proper phase to extract energy from the electron oscillation for a relatively long time interval.

It is useful to have some idea of the order of magnitude of the electric field of the electron oscillation which would be necessary to account for the observed energy exchange. To estimate this field, we examine a system consisting of an electron rotating with a uniform d-c angular velocity (at radius r) in an r-f electric field of the same frequency. The field and the electron motion are assumed to be in phase; this will provide the maximum energy exchange. The energy exchange during one cycle of the r-f field (or one revolution of the electron) is proportional to the integral of the product of the velocity and the electric field; i.e.,

$$\text{Energy Exchange} = \int_{\omega_c t=0}^{2\pi} q\,(r\omega_c \sin \omega_c t)\,(E \sin \omega_c t)\,dt \,.$$

$$= q\pi r E \,. \qquad (5.15)$$

In this expression the electric field is assumed to be of the form $E \sin \omega_c t$. We now calculate the electric field which would lead to an energy exchange of 40 electron-volts. (This is the general magnitude of the average energy exchange measured.) As a value for the radius, we use 0.2 millimeter; this value corresponds to the smallest loops measured in Figs. 4.15 to 4.23 in the cathode region. The electric field

is then

$$E = \frac{20}{2\pi \times 10^{-4}} = 6.36 \times 10^{4} \frac{\text{volts}}{\text{meter}}$$

$$= 636 \frac{\text{volts}}{\text{centimeter}} \quad . \tag{5.16}$$

Of course, if the angular frequency of rotation of the electron and the frequency of the electric field are not synchronous, a stronger electric field than that calculated above would be necessary to account for the observed energy exchange. On the other hand, it was supposed that the entire energy exchange occurred during one r-f cycle. It is much more likely that the energy exchange occurs over considerably more than one cycle. Thus, an electric field strength significantly smaller than the value calculated above would account for the observed energy exchange; we can roughly estimate the field strength to be between, say, 60 and 600 volts/centimeter. A field strength of this order of magnitude is not unreasonable. In this respect it is interesting to estimate the magnitude of the transverse d-c electric field in the slow-drift region. This can be done by noting that the average drift velocity in this region is approximately equal to the ratio of the transverse d-c electric field to the d-c magnetic field. Using the value of the average drift velocity calculated by Eq. 5.8, we have

$$\begin{aligned} E_o &= \text{average drift velocity} \times B_o \\ &= 6.74 \times 10^{5} \times .04 \\ &= 2.7 \times 10^{4} \text{ volts/meter} \\ &= 270 \text{ volts/centimeter} \quad . \end{aligned} \tag{5.17}$$

Hence the strength of the r-f field calculated above is, roughly speaking, of the same order of magnitude as the d-c electric field.

The prediction that a strong coherent r-f field exists in the slow-

drift region appears, at first, to be at variance with the experimentally observed facts that only weak signals were detected with the r-f probe, and that a near-random distribution of energy among the electrons was measured. It is not difficult, however, to see, at least qualitatively, why there is actually no inconsistency.

As pointed out earlier, the electron stream in the slow-drift region can be regarded as being similar in behavior to an ion-neutralized stream. The discussion presented in Chapter III showed that the fields associated with the space-charge oscillations of an ion-neutralized stream are confined entirely within the boundaries of the stream. Hence, it is not unreasonable to expect that a probe outside the stream would detect only relatively weak signals.

The fact that a near-random energy distribution is measured can be attributed to the nature of the electron interaction. The nature of the electron trajectories indicates the highly nonlaminar motion of the stream as it enters the slow-drift region. Following along the lines of the discussion of nonlaminar motion in Chapter II, we might expect the electrons in a given volume element to have a distribution of velocity directions. It would not be surprising if the distribution itself were near-Maxwellian with a mean velocity in the direction of the average stream motion. The distribution in direction produces a distribution in phase between the space-charge oscillation and the electron motion, which leads to a distribution in the amount of energy exchange undergone by electrons originating in the same volume element. In addition to this initial tendency toward randomization there is another, probably more significant, randomizing mechanism. This mechanism is the energy exchange itself, which produces a strong scattering of electron trajectories. As a result, the phasing between the electron motion and the space-

charge oscillation is further randomized. It has been suggested by W. G. Dow that as a result of the energy exchange electrons are temporarily "kicked" outside the stream. Since the space-charge oscillation fields are essentially confined within the stream, this means that electrons would "dip" into the space-charge oscillation in a random fashion.

The environment of the slow-drift region is sufficiently chaotic that, rather than it being remarkable that a random energy distribution is obtained, it would be remarkable if one were not obtained.

The theory*, thus far, describes the phenomenon in the cathode region. We now extend the analysis into the plate-sole space.

5.8.2 The Plate-Sole Space. We have thus far described a mechanism by which electrons exchange large amounts of energy in the cathode region. Related to this process, and depending on it, is the collection of current by a negative-potential sole. However, while an increase in energy is a necessary condition for an electron to reach the sole, it is not a sufficient condition. In addition, the trajectory followed by the electron must be such as to intercept the sole. Therefore, much of the plate-sole space phenomenon must be related to the electron trajectories in this region.

A simple explanation of the distribution of current collected by the sole would be to say that electrons travel uninterrupted along some trochoid-like trajectory in the uniform fields of the plate-sole space;

*It has been recently reported[24] that a carcinotron operated with a temperature-limited cathode produced significantly less sole current than when it was operated space-charge-limited. This is what would be expected in terms of the theory presented above. Under temperature-limited conditions the potential minimum in front of the cathode would vanish and electrons would be accelerated out of the cathode region with less likelihood of passing through a slow-drift region. Of course, if the scaling parameter were made sufficiently small the conditions for an energy exchange in the cathode region could be obtained even with temperature-limited operation.

those electrons following trajectories intercepting the sole constitute the sole current. Unfortunately the data show this cannot be more than a partial description. The period of a trochoid-like trajectory in the plate-sole space, for the values of scaling parameter entering into the data, would be about two sole segments or less in length. Hence, if an electron trajectory were going to intercept the sole, it would do so in a distance less than the length of, say, the first four sole segments. While the data (Figs. 5.8-5.21) show a generally high current to the first few sole segments, there is, in addition, a significant current collected along the rest of the sole (at least, for certain values of the scaling parameter).

This anomaly suggests that the electron trajectories are not as simple as described above, i.e., that an additional energy exchange occurs in the plate-sole space, altering the electron trajectories.

An additional energy exchange process is also suggested by the data obtained in the energy distribution measurements, Figs. 5.27 and 5.28. Figure 5.27 shows that the near-randomness of the energy distribution is maintained along the entire sole. Figure 5.28 shows that the energy distribution of the current collected by one sole segment remains approximately random even when the stream is strongly perturbed by a preceding sole segment. Two possibilities suggest themselves:

a) the current collected by a sole segment is a small fraction of the total current, or

b) the electrons are continuously randomized.

With respect to the first possibility, the measurements show the energy distribution to be approximately Maxwellian at, say, the fifteenth or twentieth sole segment even though a considerable fraction of the cathode current has already been collected. Moreover, Fig. 5.27 shows that the

temperature is roughly the same for all of the sole segments. For these reasons the second possibility is the more likely one. We are thus led to the conclusion that an energy exchange process continuously randomizes the energy distribution of the electrons.

However, the energy exchange process does not add a significant amount of energy to the stream. In the measurements illustrated by Figs. 5.22 to 5.26, the total sole current remains constant even though the distribution of sole current along the sole is radically altered by varying the potential of one of the sole segments. For example, consider Fig. 5.25, which presents data taken for the same value of scaling parameter as the current distribution curves shown in Fig. 5.15. Figure 5.25 shows that the sole current is not dependent on the potential (in this figure) of the fourth sole segment. This segment was used because it is sufficiently far from the cathode region so that the initial stream current loss to the sole has already been collected, and not so far but that a significant amount of current remains to be collected (see Fig. 5.15). Figure 5.26 shows the same behavior for the seventh sole segment, which is definitely not receiving a significant amount of the initial sole current. The fact that the total sole current remains constant suggests that the energy exchange process in the plate-sole region is primarily a randomizing process, i.e., that the fraction of the cathode current which will reach the sole is determined in the cathode region.

It is not unlikely that the energy exchange process in the plate-sole space is related to the "slipping stream" amplification described in Chapter III, although significantly modified by the nonlaminar nature of the electron motion. To illustrate the process we have in mind, we can make use of the nonlaminar stream model described in section 2.7.2. By analogy to the laminar Brillouin stream model, we can say that energy

is transferred from electrons on the faster side of the stream to electrons in the slower side of the stream. However, in the case of a non-laminar stream, the same electron can, at different times, be on both sides of the stream. It is possible to visualize a situation where there is a large energy exchange between electrons, and yet where not very much energy is added to the stream; in other words, a situation where the energy exchange process simply reshuffles energy among the electrons.

An energy exchange process of the sort described above could very easily account for the sole-current characteristics observed. It is more than likely that a reshuffling process would randomize the energy distribution; the more so if the initial energy distribution is already approximately random.

The above discussion leads to the following description of the phenomena occurring in the plate-sole space:

a) As a result of an energy exchange process in the cathode region electrons enter the plate-sole space with a near-Maxwellian energy distribution. A temperature on the order of 300,000°C is attained.

b) The excess energy of these electrons allows a certain fraction of them to be collected on the first few sole segments. The number of electrons collected by a sole segment is determined by two factors: how many electrons have sufficient energy to overcome the negative bias of the sole segment, and how many of these are directed so as to intercept the sole segment.

c) Because of the continuous loss of high-energy electrons to the sole, the energy distribution of the electrons tends to lose its randomness. However, an additional energy exchange process in the plate-sole space rerandomizes the electrons. This rerandomization is accomplished

without significantly increasing the total amount of energy.

This process continues as the stream progresses along the sole.

5.9 Summary

We have, in this chapter, presented and interpreted data obtained from a crossed-field stream analyzer pertaining to the diocotron effect. In addition a phenomenological theory, explaining the measurements, has been presented.

In reviewing the contents of this chapter, the subject matter can be divided into two parts. First, there are the experimentally observed facts. Perhaps the single most important point which the data show is the incontrovertible fact that the significant energy exchange between electrons occurs in the cathode region. Two other most interesting observations are the appearance of a narrow-band r-f signal, and the near-Maxwellian energy distribution of electrons collected by the sole. In addition to these general observations, detailed measurements of the negative-sole current characteristics over a wide range of operating conditions were obtained.

The second part of the subject matter of this chapter is the presentation of a theory which provides a reasonable explanation of the measurements, and is qualitatively in agreement with their general behavior. We believe the theory provides a framework within which further experimental and theoretical investigation can be developed. The basis for this belief is the opinion that any theory which ties together a broad range of phenomena in a consistant manner is bound to be reasonably closely related to the observed phenomena.

The next step in the study of the diocotron effect would be to verify and extend the theory. The next section discusses several ways in which this can be done.

5.10 Suggestions for the Continuation of the Investigation

The most straightforward extension of the present investigation is an experimental one. The present investigation has shown the importance of the cathode region in the energy exchange process. It would be useful to have a more detailed knowledge of the behavior of the electrons in the slow-drift region than was obtained with the present stream analyzer design. A modification of the present design so as to provide a slow-drift region about, say, halfway down the sole would allow investigation of the characteristics of the stream both before and after it passed through the slow-drift space. In addition, provision could be made for probing the stream in the slow-drift space itself. At the same time, the r-f signals associated with the energy exchange could be studied, and also the effect of an injected signal could be studied.

A separate phenomenon from that involved above is the energy exchange process occurring in the plate-sole space. It is, however, difficult to isolate this phenomenon from the cathode region phenomena which determine the state of the stream as it enters the plate-sole space. Nevertheless it would be interesting to study the propagation of r-f signals along the stream in the plate-sole space. Such r-f signals could include, in addition to signals generated in the cathode region, externally applied r-f signals.

There are a number of theoretical problems associated with the above experimental studies. The formulation of a more precise model to describe the energy exchange in the cathode region would be most desirable. Such a model would necessarily be a most complex one, involving the concept of nonlaminar streams. The formulation of d-c nonlaminar-stream models is a formidable undertaking. The study of the propagation of

perturbations on nonlaminar streams is even more formidable. Nevertheless, such a study would be most revealing in understanding many anomalous effects in devices utilizing electron streams.

BIBLIOGRAPHY

1. Alfven, H., Lindberg, L., Malfors, K. G., Wallmark, T., and Åström, E., "Theory and Applications of Trochotrons," Trans. Roy. Inst. Techn., Stockholm; 1948.

2. Klemperer, O., Electron Optics, Cambridge University Press; 1939.

3. Warnecke, R., Huber, H., Guenard, P., et Doehler, O., "Amplification par ondes de charge d'espace dans un faisceau électronique se déplacant dans des champs électrique et magnétique croisés," C. R. Acad. Sc., Vol. 235, pp. 470-472; 1952.

4. Guenard, P., et Huber, H., "Étude expérimentale de l'interaction par ondes de charge d'espace au sein d'un faisceau électronique se déplacant dans des champs électrique et magnétique croises," Annales de Radioelectricite, Vol. VII, No. 30, pp. 252-278; October, 1952.

5. Peterson, W. W., "The Trajectron--An Experimental DC Magnetron," Ph. D. dissertation, The University of Michigan; 1954.

6. Kyhl, R. L., and Webster, H. F., "Breakup of Hollow Cylindrical Electron Beams," Trans. PGED-IRE, Vol. ED-3, pp. 172-183; October, 1956.

7. Dow, W. G., Fundamentals of Engineering Electronics, Wiley; 1952.

8. Pierce, J. R., Theory and Design of Electron Beams, Van Nostrand; 1954.

9. Spangenberg, K. R., Vacuum Tubes, McGraw-Hill; 1948.

10. Goldstein, H., Classical Mechanics, Addison-Wesley; 1951.

11. Chapman, S., and Cowling, T. G., Mathematical Theory of Non-Uniform Gases, Cambridge University Press; 1952.

12. Mayer, J. E., and Mayer, M. G., Statistical Mechanics, Wiley; 1948.

13. Gabor, D., Colloquium Talks, Massachusetts Institute of Technology, 1951.

14. Kluver, J. W., "Backward Wave-Interaction in Magnetron Amplifiers," Ph. D. dissertation, University of California; 1957.

15. Haeff, A. V., "The Electron-Wave Tube. A Novel Method of Generation and Amplification of Microwave Energy," Proc. IRE, Vol. 37, pp. 4-10; January, 1949.

16. Stratton, J. A., Electromagnetic Theory, McGraw-Hill; 1941.

17. Hok, G., "The Noise Factor of Traveling Wave Tubes," Letter Proc. IRE, Vol. 44, No. 8, p. 1016; August, 1956.

18. Hahn, W. C., "Small Signal Theory of Velocity-Modulated Electron Streams, General Electric Review, Vol. 6, p. 258; June, 1939.

19. Rigrod, W. W., and Lewis, A., "Wave Propagation along a Magnetically Focussed Cylindrical Electron Beam," B.S.T.J., Vol. 33, pp. 399-416; March, 1954.

20. Buneman, O., "Generation and Amplification of Waves in Dense Charged Beams under Crossed Fields," Nature, Vol. 165, pp. 474-476; March, 1950.

21. MacFarlane, G. G., and Hay, H. G., "Wave Propagation in a Slipping Stream of Electrons: Small Amplitude Theory," Proc. Phys. Soc., Vol. 63, Sect. 6-B, pp. 407-427; 1950.

22. Gould, R., "Space Charge Effects in Beam-Type Magnetrons," J.A.P. Vol. 28, pp. 599-605; May, 1957.

23. Rowe, J. E., and Martin, R. J., "The Study of Electron Interaction in Crossed-Field Electron Devices," Quarterly Progress Reports, The University of Michigan Electron Tube Laboratory; 1957.

24. Doehler, O., Dubois, A., and Maillart, D., "An M-Type Pulsed Amplifier," paper presented before International Convention on Microwave Valves, London; May, 1958.

LIST OF SYMBOLS

In choosing the various symbols, certain general principles have been followed. A vector is denoted by a bar placed over the symbol for the physical quantity. The components of a vector are denoted by the symbol for the vector without the bar, and with subscripts to distinguish between different components. The subscripts used most often are the following:

a) o denotes a d-c quantity,
b) 1 denotes an r-f quantity, and
c) x,y,z,r,θ refer, respectively, to coordinate directions in rectangular and cylindrical coordinates.

Thus E_{or} is the magnitude of the radial component of the d-c electric field intensity.

The following list of symbols includes the most important symbols, and those which may possibly give rise to ambiguity.

$\bar{A}$ vector potential

A coefficient used in the representation of r-f potential

a particular value of a space coordinate

$\bar{B}$ (also with subscripts) magnetic flux density vector

B (with subscripts) component of $\bar{B}$

B coefficient used in the representation of r-f potential

b particular value of a space coordinate

C coefficient used in the representation of r-f potential

c velocity of light in free space

D coefficient used in the representation of r-f potential

d anode-sole spacing

$\bar{E}$ (also with subscripts) electric intensity vector

E (with subscripts) component of $\bar{E}$

e superscript indicating a quantity is evaluated outside the electron stream

F velocity distribution function

H Hamiltonian function

h particular value of a space coordinate

I_{oa} d-c anode current

I_{oc} d-c collector current

I_{ok} d-c cathode current

I_{os} d-c sole current

I_{osn} d-c current to the nth sole segment

I_{otn} d-c current remaining in the stream <u>after</u> it has passed over the nth sole segment and <u>before</u> it passes over the (n+1)st sole segment

I_β^a modified Bessel function of the first kind, of order β with argument γa

i superscript indicating a quantity is evaluated inside the electron stream

$\bar{J}$ (also with subscripts) convection current density vector

J (with subscripts) component of $\bar{J}$

j $\sqrt{-1}$

K normalized surface immittance

K_β^a modified Bessel function of the second kind, of order β with argument γa

k wave number of a plane wave in free space

ℓ subscript indicating a quantity is evaluated at the lower (or inner) stream boundary

m mass of an electron

$\underline{\bar{n}}$ unit vector normal to stream boundary

o subscript indicating a d-c quantity

$\tilde{P}$ pressure tensor

$\bar{p}$ generalized momentum

q electron charge magnitude

$\bar{r}$ vector location of a volume element

$\underline{\bar{r}}$ radial unit vector in cylindrical coordinates

r radial space coordinate, cylindrical coordinates

r subscript indicating a quantity associated with the $\underline{\bar{r}}$ component of a vector

$\bar{s}$ arbitrary vector

S scalar velocity potential

T subscript denoting the part of a vector in a plane transverse to the d-c magnetic field

t time coordinate

U root-mean-square excess velocity of electrons at stream boundary

u subscript denoting a quantity which is evaluated at the upper (or outer) stream boundary

$\bar{u}$ excess over average velocity of an electron (vector)

$u_\alpha u_\beta$ $\alpha\beta$ component of pressure tensor

$\bar{v}$ (also with subscripts) electron velocity vector

$\bar{v}_{om}$ mean d-c vector velocity associated with a volume element of a nonlaminar stream

$\bar{v}_o$ d-c vector velocity of a laminar stream

v (with subscripts) component of $\bar{v}$

$\underline{\bar{x}}$ unit vector, rectangular coordinates

x space coordinate, rectangular coordinates

x	subscript indicating a quantity associated with the $\bar{x}$ component of a vector
Y	normalized surface immittance
$\bar{y}$	unit vector, rectangular coordinates
y	space coordinate, rectangular coordinates
y	subscript indicating a quantity associated with the $\bar{y}$ component of a vector
Δy	an incremental change in y
$\bar{z}$	unit vector, rectangular or cylindrical coordinates
z	space coordinate, rectangular or cylindrical coordinates
z	subscript indicating a quantity associated with the $\bar{z}$ component of a vector
α	wave number in $\bar{x}$ or $\bar{r}$ direction
β	wave number in $\bar{y}$ or $\bar{\theta}$ direction
γ	wave number in $\bar{z}$ direction
Δ	thickness of "thin" stream
ϵ_o	permittivity of free space
$\bar{\theta}$	angular unit vector in cylindrical coordinates
θ	angular space coordinate, cylindrical coordinates
θ	subscript indicating a quantity associated with the $\bar{\theta}$ component of a vector
μ_o	permeability of free space
ρ	(with subscripts) space-charge density
σ	(with subscripts) surface-charge density
ϕ	(also with subscripts) scalar potential
ϕ_{oa}	d-c anode potential

ϕ_{oc} d-c collector potential

ϕ_{os} d-c sole potential

ϕ_{osn} d-c potential of the n th sole segment

ψ angle between the d-c vector velocity of a single electron and the average d-c vector velocity associated with a volume element

ψ_M maximum value of ψ

Ω constant of proportionality used in describing d-c stream velocity

ω radian frequency

ω_c cyclotron frequency

ω_d Doppler frequency

ω_p electron density (plasma) frequency

$\nabla_{\bar{p}}$ momentum gradient operator in momentum phase space

1 subscript denoting an r-f quantity